

# Predicting polymer drag reduction in turbulent pipe flows from rheological characteristics

by

Satyajit Singh

A thesis submitted in partial fulfillment of the requirements for the degree of

Master of Science

Department of Mechanical Engineering

University of Alberta

© Satyajit Singh, 2023

# Abstract

Predicting polymer drag reduction from polymer solution rheology can be potentially achieved by developing a model between friction factor and rheological characteristics. The model's foundation depends on establishing a correlation between these parameters, and its robustness depends on the size of the data utilized. To establish this relation for hydrocarbon-based polymer solutions, the present work demonstrates friction factor tests with water-based polymer solution as preliminary results and parallelly presents the design, fabrication and commissioning of a flow facility that can operate with diesel fuel as the flow medium. The water-based polymer solution analysis includes extensive pipe flow tests for three different pipe sizes (1-inch, 1.5-inch, and 2-inch inner diameter) and several drag reduction percentages, to gather pressure drop data from the pipe flow facility to further calculate the skin friction coefficient ( $C_f$ ). For each pressure drop, a fluid sample from the pipe flow setup is tested for shear viscosity and extensional viscosity measurements. The shear viscosity ( $\mu$ ) measurements, along with the known fluid density ( $\rho$ ), flow velocity ( $V$ ) and pipe inner diameter ( $D$ ) were utilized to calculate the Reynold's number ( $Re$ ) of the flow through the relation  $Re = (\rho V D) / \mu$  and the extensional viscosity data provides the relaxation time ( $t_r$ ) of the sample which was utilized along with the shear rate ( $\gamma$ ) to calculate the Weissenberg number ( $Wi$ ), given by  $Wi = t_r \cdot \gamma$ . These values of  $C_f$ ,  $Re$  and  $Wi$  for each sample point when projected together, exhibit good correlation, and presents strong clues towards understanding the dependence of  $C_f$  on  $Wi$  and  $Re$ . The extensive data for water-based polymer

solution test and its analysis are presented. This will be used as foundational work for similar pipe flow tests planned with diesel-based polymer solution, to be conducted in a separate flow facility for diesel.

Based on the concept of the water flow loop, the diesel flow facility with a 1-inch pipe size was designed with consideration on safety and ventilation around the loop. The detailed component level design is presented, and the fabrication and commissioning of the loop was completed. Similar to the water-based tests, three preliminary tests with diesel fuel were conducted at six different  $Re$  values (5000, 10000, 15000, 20000, 25000, and 30000) to confirm the alignment with the Newtonian friction factor values. The results showed close and consistent alignment with the Newtonian  $C_f-Re$  curve, confirming the diesel flow loop's readiness for polymer solution tests.

# Preface

For the water-based tests, all the pressure drop measurements and shear viscosity measurements were taken by me. The extensional viscosity measurement was a collaborative work, with the dripping test setup's design and commissioning completed by Lucas Warwaruk and Joel Fenske, and all subsequent relaxation time measurements performed by me.

I solely worked on the design of the new diesel flow loop under guidance of Dr. Sina Ghaemi and Lucas Warwaruk. The component level fabrication was a collaboration between the machine shop and a third-party welding company for certified welding for pressurized components for use with diesel. Post fabrication, the assembly and commissioning of the diesel flow loop was a collaborative effort between me, the machine shop, and the electrical department under the machine shop.



# Acknowledgement

I would like to express my heartfelt gratitude to Dr. Sina Ghaemi, for his unwavering support, guidance, and mentorship throughout my academic journey. Your profound knowledge, dedication, and enthusiasm have been instrumental in shaping my research skills and nurturing my intellectual growth.

I would also like to extend my appreciation to Lucas Warwaruk, whose invaluable assistance and collaboration have played a pivotal role in the success of this research. Your patience, expertise, and willingness to share your knowledge have been a source of inspiration.

I wish to extend my sincere thanks to Liam Abrams, Les Dean and Wade Parker for all their help in setting up the test facility.

I would like to acknowledge the generous support of Enbridge Inc., whose funding made this project possible. I am genuinely grateful for your confidence in my work and your commitment to fostering innovation.

Lastly, I want to express my heartfelt thanks to my family and friends for their unwavering understanding and support throughout this challenging journey. Your encouragement, patience, and belief in me have been my driving force.

# Contents

Abstract	ii
Preface	iv
Acknowledgement	v
Content	vi
List of tables	ix
List of figures	x
Nomenclature	xii
List of abbreviations	xiii
Chapter 1. Introduction.....	1
1.1 Motivation.....	1
1.2 Thesis overview.....	2
Chapter 2. Literature review.....	4
2.1 Shear viscosity.....	4
2.2 Extensional viscosity.....	9

2.3 Friction in pipe flow.....	13
2.4 Polymer drag reduction.....	18
Chapter 3. Water-based polymer solution tests.....	23
3.1 Details of the pipe flow facility.....	23
3.2 Preparation of the polymer solution.....	26
3.3 Test preparation and procedure.....	27
3.3.1 Calculation of mass flow rate.....	27
3.3.2 Pressure transducer calibration.....	28
3.3.3 De-airing and transducer bleeding procedure.....	28
3.3.4 Test procedure for baseline water test.....	30
3.3.5 Polymer degradation test.....	32
3.3.6 Polymer solution test.....	37
3.4 Calculation of skin friction coefficient.....	39
3.5 Shear viscosity measurements.....	41
3.6 Extensional viscosity measurements.....	44
3.7 Uncertainty analysis for $C_f$ , $Re$ and $Wi$ .....	48
Chapter 4. Results.....	51
4.1 Friction Factor.....	51

4.2 Relation between $C_f$ , $Re$ and $Wi$ .....	58
4.3 $Wi$ calculated from bulk shear rate ( $\dot{\gamma}_b$ ).....	63
Chapter 5. Design and commissioning of a hydrocarbon flow loop.....	67
5.1 Calculation of mass flow rate.....	71
5.2 De-airing and transducer bleeding procedure.....	71
5.3 Test procedure for baseline diesel test.....	73
5.4 Measurements.....	74
Chapter 6. Conclusion and future work.....	78
6.1 Conclusion.....	78
6.2 Future work.....	80
References.....	81
Appendices.....	86
Appendix A: Engineering drawings for diesel flow loop.....	86
Appendix B : Pressure-drop ( $\Delta P$ ) versus time ( $t$ ) plots.....	121
Appendix C: Shear viscosity data.....	126
Appendix D: Extensional viscosity data.....	135
Appendix E: Safe operating procedure for diesel flow loop.....	167
Appendix F: NETZSCH PC pump drawing and curve.....	172

# List of tables

1	Mass flow rate calculations for pipe flow test with water.....	27
2	Step-by-step procedure for water baseline test.....	31
3	Step-by-step procedure for water-based polymer degradation test.....	35
4	Step-by-step procedure for water-based polymer test.....	38
5	Percentage uncertainty calculations for $C_f$ , $Re$ and $Wi$ .....	50
6	%DR for water-based test in 1-inch pipe size.....	53
7	%DR for water-based test in 1.5-inch pipe size.....	55
8	%DR for water-based test in 2-inch pipe size.....	57
9	Mass flow rate calculations for pipe flow test with diesel.....	71
10	Step-by-step procedure for diesel baseline test.....	74

# List of figures

1	Velocity profile and shear stress versus gradient of velocity profile .....	5
2	Newtonian and non-Newtonian fluid categorizations.....	6
3	The Moody plot for Darcy friction factor versus Reynolds number.....	17
4	Pipe flow setup overview for water-based test.....	24
5	Pipe flow setup valve configuration.....	24
6	Test section details for water-based test.....	26
7	$\Delta P$ versus time plot for polymer degradation test in 1.5-inch pipe size.....	36
8	%DR versus degradation time, for polymer degradation test in 1.5-inch pipe size...36	
9	$\Delta P$ versus time plot example for polymer solution test.....	39
10	Discovery hybrid rheometer and double gap concentric cylinder geometry.....	41
11	Viscosity versus shear rate plot example for water-based polymer solution.....	42
12	Dripping test setup and high-speed camera frame.....	44
13	Evolution of filament minimum diameter with respect to time.....	45
14	Minimum diameter of the filament versus time plot for water-based test .....	46
15	$C_f$ versus $Re$ plot for baseline water test.....	52
16	$C_f$ versus $Re$ plot for water-based polymer solution test in 1-inch pipe size.....	54
17	$C_f$ versus $Re$ plot for water-based polymer solution test in 1.5-inch pipe size.....	56

18	$C_f$ versus $Re$ plot for water-based polymer solution test in 2-inch pipe size.....	57
19	$C_f$ versus $Re$ plot color mapped with $Wi$ for 1-inch pipe size.....	59
20	$C_f$ versus $Re$ plot contour mapped with $Wi$ for 1-inch pipe size.....	59
21	$C_f$ versus $Re$ plot color mapped with $Wi$ for 1.5-inch pipe size.....	60
22	$C_f$ versus $Re$ plot contour mapped with $Wi$ for 1.5-inch pipe size.....	60
23	$C_f$ versus $Re$ plot color mapped with $Wi$ for 2-inch pipe size.....	61
24	$C_f$ versus $Re$ plot contour mapped with $Wi$ for 2-inch pipe size.....	61
25	$C_f$ versus $Re$ plot contour mapped with $Wi_c$ for 1-inch pipe size.....	64
26	$C_f$ versus $Re$ plot contour mapped with $Wi_c$ for 1.5-inch pipe size.....	64
27	$C_f$ versus $Re$ plot contour mapped with $Wi_c$ for 2-inch pipe size.....	65
28	$C_f$ versus $Wi_c$ for all three pipe size.....	66
29	Pipe flow setup overview for diesel-based test.....	69
30	$\Delta P$ versus time plot for diesel baseline test.....	75
31	$C_f$ versus $Re$ plot for diesel baseline test.....	76

# Nomenclature

$A$	Cross section area	$n$	Rate index
$D$	Pipe inner diameter	$t_r$	Relaxation time
$D_l$	Minimum diameter at start of elastic regime	$t_f$	Time scale of the flow
$D_{min}$	Minimum diameter of the filament	$t_{dg}$	Degradation time
$D_0$	Nozzle diameter	$\tau$	Shear stress
$L$	Characteristic length	$\tau_w$	Shear stress at the wall
$V$	Velocity	$\gamma$	Wall shear rate
$Q$	Volumetric flow rate	$\gamma_b$	Bulk shear rate
$C_f$	Skin friction coefficient	$\sigma$	Surface tension
$De$	Deborah number	$\Delta P$	Pressure drop
$Tr$	Trouton ration	$\mu$	Viscosity
$Wi$	Weissenberg number (wall shear rate)	$\mu_s$	Viscosity (polymer solution)
$Wi_c$	Weissenberg number (bulk shear rate)	$\mu_0$	Zero rate viscosity
$V_b$	Bulk velocity	$\mu_\infty$	Infinite rate viscosity
$m$	Slope	$\lambda$	Extensional viscosity
$b$	Intercept (vertical axis)	$\epsilon$	Strain rate
$c$	Consistency	$\epsilon$	Pipe roughness (absolute)
$f$	Friction factor	$\rho$	Density
$f_s$	Friction factor (smooth pipes)	$\rho_w$	Density (water)
$f_r$	Friction factor (rough pipes)	$\rho_s$	Density (polymer solution)
$k$	Relative pipe roughness	$\eta_p$	Polymer contribution to viscosity



# List of abbreviations

DR	-	Drag reduction.
MDR	-	Maximum drag reduction.
RPM	-	Rotation per minute.
PIV	-	Particle image velocimetry.
DNS	-	Direct numerical simulations.
VFD	-	Variable frequency drive.
ID	-	Inner diameter.
PID	-	Proportional integral derivative.

# Chapter 1

## Introduction

### 1.1 Motivation

Frictional losses in pipe flow play a crucial role in various engineering applications, such as fluid transport, pipeline design and energy distribution. Understanding the factors influencing friction in pipe flow and minimizing these frictional losses is essential for optimizing system performance and minimizing energy consumption. In hydrocarbon pipelines, the fluid is transported over very long distances at high flow rates, this implies turbulent flow and thus higher frictional losses causing a significant decrease in throughput, requiring increased energy consumption and higher operating costs.

Drag reduction (DR) through the addition of small amounts of high molecular weight polymers is a well-known phenomenon, first observed by Toms (1948). It has proven to be an effective method in minimizing flow turbulence and increasing throughput. This was successfully demonstrated for crude oil pipelines by Lescarbourea et al. (1971) in both laboratory and field testing and was first commercially implemented in the Trans Alaskan pipeline system in 1979 (Burger et al., 1982).

Quantifying this drag reduction requires extensive testing of the polymer solution in a pipe flow system, which becomes impractical for a large-scale oil transport operation. The present work aims

to understand the relationship between the DR percentage and the rheological properties of water-based polymer solution by testing these parameters for three different pipe sizes, each with five different Reynold's number flow for 6-8 different DR percentages and utilizing these 30-40 data points for each pipe diameter to understand the trend and develop a robust model to predict the DR percentage using polymer solution rheology. The current work was focused on the water-based polymer solutions because a functioning water flow facility was already available to start testing immediately and results from these tests can be utilized as a proof of concept, but to provide a scalable prediction model for hydrocarbons, similar work was required to be done with diesel-based polymer solution, because the drag reducing polymers used for hydrocarbons are different from the one used for water in terms of molecular weight, solubility and drag reducing capabilities, this requires a separate diesel flow facility. To address this requirement, the design and commissioning of a diesel flow loop is scoped in this work, and successful commissioning and baseline tests are presented, confirming the loop readiness for future polymer-solution tests. The choice of using diesel was based on the facts that, firstly, diesel has a higher flash point ( $> 52$  °C) and low volatility, making it safer to handle at room temperature compared to other easily available hydrocarbons like gasoline and kerosine, and secondly, it has a much lower viscosity than crude oil, making the flow loop design simpler, manageable pump requirements and easier drainage of the loop for repeating tests.

## 1.2 Thesis overview

This report starts with a discussion on the background work and fundamental concepts related to this field to set the stage, followed by the detailed account of the water-based polymer solution

tests. It then goes over the rheological analysis for water-based solutions and discusses the results and observations from these tests. The discussion then pivots to the details of the diesel flow facility, followed by its preliminary testing, results and observations. Conclusion and future work are discussed henceforth. Below is a chapter wise breakdown of this overview.

Chapter 2 provides the background and current state of research in this field, and dives into a few conceptual topics that are used as framework for this study.

Chapter 3 discusses the pipe flow facility for water-polymer test and details the test procedures, followed by the calculations of  $C_f$ . Furthermore, it details the shear viscosity and extensional viscosity measurement setup and data processing to calculate  $Re$  and  $Wi$ , concluding with a section for the analysis of uncertainty in the measurements for  $C_f$ ,  $Re$  and  $Wi$ .

Chapter 4 examines the results for the water-based polymer solution tests and talks about the observations.

Chapter 5 discusses the pipe flow facility for diesel-polymer test and details the baseline test procedures and discusses the preliminary results.

Chapter 6 summarizes the findings of water-polymer test and provides details on the future work.

## Chapter 2

# Literature review

This chapter will first discuss two fundamental properties of fluid, shear viscosity and extensional viscosity, understanding of which is important in laying the foundation for discussing the next topics like friction in pipe flow and polymer drag reduction that are key in understanding the background work, the current state of research in this field and the current work presented.

### 2.1 Shear viscosity

The shear viscosity of a fluid is a fundamental property which is governed by the strength of the intermolecular cohesive forces of the fluid and characterizes its resistance to flow. To understand it better, consider a fluid flow over a flat surface. In this flow condition, due to high intermolecular attraction between the fluid and the solid surface molecules, the fluid layer in contact with the surface gets stuck to it, leading to zero velocity (no slip condition) and as this resistance is transferred to the fluid layers adjacent to this contact layer, the flow velocity progressively decreases near the solid surface, this result in a typical velocity profile as shown in figure 1(a). This relative velocities between fluid layers leads to the development of shear stress ( $\tau$ ) acting coplanar, between two adjacent layers. For Newtonian fluids, at constant temperature and pressure

conditions the magnitude of shear stress ( $\tau$ ) is directly proportional to the gradient of the velocity profile ( $dV/dy$ ). Here,  $y$  is the vertical axis described in figure 1 and  $dV/dy$  can also be equated to shear rate ( $\gamma$ ). As shown in figure 1(a), towards the free stream the difference in velocity between layers is very small (Slope-1), resulting in lower shear stress and as we go closer to the surface the velocity changes much more rapidly (Slope-2), causing higher shear stress. This relation is called the newton's law of viscosity,

$$\tau = \mu \cdot \left( \frac{dV}{dy} \right) \quad (1)$$

or

$$\tau = \mu \cdot \gamma, \quad (1.1)$$

where the fluid's viscosity ( $\mu$ ) is the proportionality constant. The higher the intermolecular cohesion in a fluid, higher will be the shear stress developed for a given shear rate and thus higher will be the value of viscosity for that fluid.

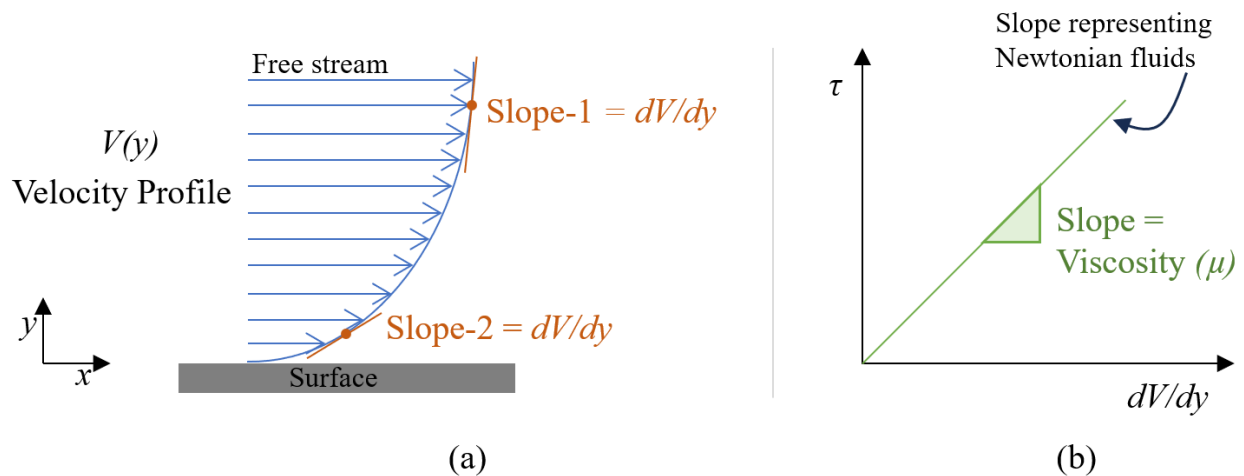


Figure 1: (a) Velocity profile of fluid flow over a surface. (b) Shear Stress ( $\tau$ ) versus gradient of velocity profile ( $dV/dy$ ) plot showing the slope which represents the viscosity.

Viscosity is highly dependent on the temperature; it decreases with the increase in temperature. As the temperature of the fluid increases, its molecules attain a higher energy level, making it easier to overcome the cohesive forces between them and thus reducing the shear stresses for a given shear rate, resulting in lower viscosity. When the temperature is reduced, the intermolecular cohesive forces dominate again, causing viscosity to increase. The effect of pressure on viscosity is opposite, viscosity increases with the increase in pressure. This effect is comparatively much smaller and is usually neglected.

It can be summarized that for Newtonian fluids the relation between  $\tau$  and  $\gamma$  at constant temperature and pressure is linear and the  $\tau$ - $\gamma$  curve crosses through zero. There is a class of fluids that does not follow either or both of the above two conditions, these fluids are categorized as non-Newtonian fluids. In general, these fluids can be sub categorized as detailed in figure 2 (Chhabra et al., 2010).

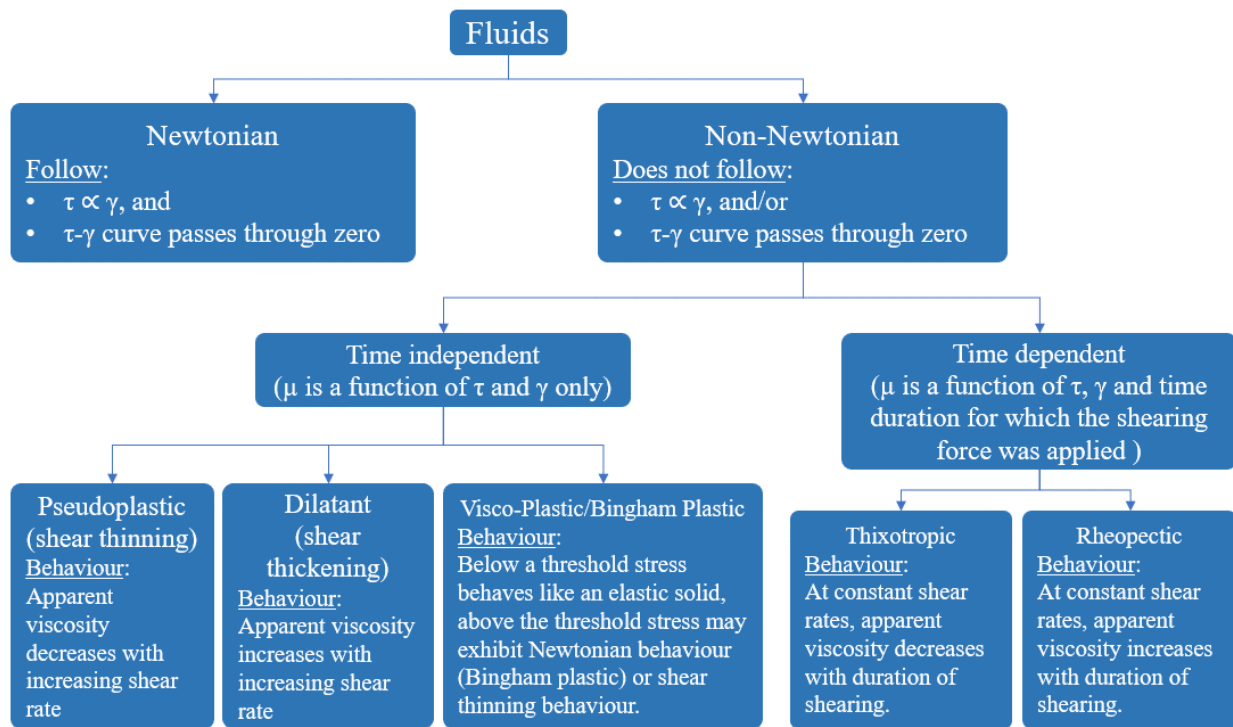


Figure 2: Fluid categories showing Newtonian and non-Newtonian properties and expanding on the further categorization of non-Newtonian fluids with their behavioral properties.

We will further elaborate on the pseudoplastic (shear thinning) fluids which is among the most common non-Newtonian fluids and represents the dilute polymer solutions that we will study extensively in the report. In shear thinning fluids the apparent viscosity decreases with the increase in shear rate. Specifically, for polymer solutions, at very low shear rates ( $< 10^{-2}$  1/s) the apparent viscosity approaches a constant value and becomes independent of shear rates, exhibiting Newtonian behaviour, this is termed as zero-rate viscosity ( $\mu_0$ ). Similarly, at very high shear rates the apparent viscosity plateaus towards a constant value of infinite-rate viscosity ( $\mu_\infty$ ).

There have been many mathematical models and experimental fits proposed to approximate this behaviour for polymer solutions, the two most notable are elaborated below (Chhabra et al., 2010).

1. The power law model (Ostwald de Waele equation):

This model is represented as

$$\mu = c (\dot{\gamma})^{n-1} , \quad (2)$$

where,  $c$  is the consistency, and  $n$  is the power law rate index. For a positive value of  $n$ , less than one, this relation characterizes the shear thinning behaviour of the fluid for a range of shear rate. This relation, however, fails to predict the apparent viscosity plateaus for very low and very high shear rates, i.e.  $\mu_0$  and  $\mu_\infty$ .

2. The Cross-power law model (Cross, 1965):

The equation

$$\mu = \mu_\infty + \left( \frac{(\mu_0 - \mu_\infty)}{1 + (c \cdot \dot{\gamma})^n} \right) , \quad (3)$$



is a more widely accepted model that overcomes the deficiencies of the simpler Ostwald de Waele equation and correctly predicts  $\mu_0$  and  $\mu_\infty$  for the two extreme shear rate cases.

## 2.2 Extensional viscosity

Extensional viscosity is a rheological property of fluids that quantifies their resistance to deformation under conditions of extension or stretching. It is more prominently studied in viscoelastic materials like polymer melts and dilute polymer solutions. This property was first studied by Trouton (1906) when he coined the term “coefficient of viscous traction ( $\lambda$ )”. Trouton experimented with pitch (a viscoelastic polymer) and studied its extensional behaviour through a series of different experimental methods, he reported similar values of  $\lambda$ , repeatably achieved through the different methods tested. In his paper, he established the relation (experimentally) between shear viscosity ( $\mu$ ) and the coefficient of viscous traction or extensional viscosity ( $\lambda$ ) as

$$\mu = \frac{1}{3}\lambda , \quad (4)$$

which was later theoretically derived by Burgers (1935). The relation,  $\lambda/\mu$  is referred to as the Trouton ratio ( $T_r$ ). While this ratio holds true for Newtonian fluids under steady and spatially uniform flows, these steady and uniform flows are almost never the case in practical applications like fiber turning, ink jet printing, blow molding etc., where extensional viscosity plays an important role. This makes modeling extensional flows and measuring extensional viscosity much more complicated than the simpler shear viscosity measurements.

For unsteady flow conditions, the concept of transient extensional viscosity  $\lambda(t)$  was introduced (Barnes et al., 1989), in which  $\lambda$  is a function of both time ( $t$ ) and strain rate ( $\dot{\epsilon}$ ). But its use should be dealt with caution, as expressed by Petrie (2006), stating the inapplicability of the Trouton ratio in correctly describing non-Newtonian (viscoelastic) extensional flows, which requires specific constitutive equations for each type.

In terms of spatial flow fields, extensional flows are of three types (Petrie, 2006):

1. Uniaxial: Refers to elongation in a single axial direction ( $x$ ) with thinning in the remaining two orthogonal directions ( $y$  and  $z$ ). This flow represents the steady and spatially uniform extension that conforms with the Trouton ratio:  $\lambda = 3\mu$  for Newtonian fluids.
2. Biaxial: Refers to extensional flow in two orthogonal directions ( $x$  and  $y$ ) simultaneously with a corresponding decrease in thickness along the third direction ( $z$ ). Like stretching a balloon. For this type of flow,  $\lambda = 6\mu$  in Newtonian fluids.
3. Planar: Refers to extensional flow in one direction ( $x$ ) with a constant width along the planar orthogonal direction ( $y$ ) and a thickness contraction in the third direction ( $z$ ). For this type of Newtonian flows,  $\lambda = 4\mu$ .

When the Trouton ration ( $T_r = \lambda/\mu$ ) is applied to non-Newtonian fluids, a conceptual ambiguity arises because shear viscosity ( $\mu$ ) is a function of shear rate ( $\gamma$ ),  $\mu(\gamma)$  and extensional viscosity ( $\lambda$ ) is a function of strain rate or the rate of elongation ( $\varepsilon$ ),  $\lambda(\varepsilon)$ , and a relation between  $\gamma$  and  $\varepsilon$  is required to be established. This relation was proposed by Jones et al. (1987) for inelastic non-Newtonian fluids, equating  $\gamma = \sqrt{3} \varepsilon$ , and defining Trouton ration as

$$T_r = \frac{\lambda(\varepsilon)}{\mu(\sqrt{3}\varepsilon)}. \quad (5)$$

It was further shown by Jones et al. (1987) that for inelastic fluids the value of  $T_r$  is 3 for all values of  $\varepsilon$ , so therefore, viscoelastic fluids will represent all values of  $T_r$  apart from 3. This only helps in establishing viscoelastic behaviour of a fluid, but with the complex nature of such fluids, getting to a mathematical equation that correctly model this behaviour and predicts the extensional viscosity, required complex mathematical analysis.

Alternatively, the elastic property of these viscoelastic non-Newtonian fluids can be characterized by a parameter called relaxation time ( $t_r$ ). It represents the time it takes for the fluid's mechanical response to return to equilibrium after being subjected to a deformation or disturbance. It is a measure of how quickly the fluid relaxes or returns to its original state once the applied force or deformation is removed.

In viscoelastic fluids, which exhibit both viscous (liquid-like) and elastic (solid-like) behavior, the relaxation time reflects the balance between these two aspects of the material's response to stress. When observed on a same time scale, a short relaxation time implies a quick return to equilibrium state after deformation indicating that the fluid behaves more like a viscous liquid and a long relaxation time implies that the fluid takes a significant amount of time to return to equilibrium after deformation. Such fluids exhibit more elastic behavior.

Here the mention of time scale is important as a fluid with short relaxation time can show elastic behavior if observed on a much shorter flow time scale and a fluid with a high relaxation time may still not show elastic dominance if observed on a longer flow time scale. This relationship between relaxation time ( $t_r$ ) and time scale of the flow ( $t_f$ ) is represented by a dimensionless parameter, Deborah number ( $De$ ), shown as

$$De = \frac{t_r}{t_f} . \quad (6)$$

So, a smaller value of  $De$  represents more viscous behaviour and a higher value indicates more elastic behaviour of the fluid. An important thing to note here is that the time scale of the flow does not merely represent the observation time, instead it reflects the time scale of the deformation

(Poole, 2012), inherit to unsteady flows, implying that as the flow approached steady state,  $t_f \rightarrow \infty$  and  $De \rightarrow 0$ .

For steady flows, another dimensionless parameter, the Weissenberg number ( $Wi$ ) named after Karl Weissenberg, is often used.  $Wi$  is the ratio of the relaxation time of the fluid and the specific process time which is represented as the reciprocal of the shear rate for steady simple shear flows, given as

$$Wi = t_r \cdot \dot{\gamma} \quad (7)$$

or

$$Wi = t_r \cdot \left( \frac{\partial V}{\partial y} \right). \quad (7.1)$$

As described by Poole (2012), the Weissenberg number assesses the extent of anisotropy or alignment produced by deformation and is suitable for characterizing flows with a consistent stretching history, like simple shear. Conversely, the Deborah number is better suited for characterizing flows with a variable stretching history and fundamentally quantifies the rate at which elastic energy is either stored or released.

## 2.3 Friction in pipe flow

Whenever a fluid is set in motion, either over an open surface or enclosed within a pipe or a duct, the liquid molecules face resistance to this motion due to friction between two fluid molecules or between the fluid molecules and the surface over which they are flowing. This surface is generally termed as the wall (the pipe's inner surface). There is an inertial resistance at play as well, but it is only experienced significantly during change in flow rates, it diminishes once a steady mass flow rate is reached.

Considering pipe flow, this resistance to the flow is what creates the pressure differential that is associated with the flow. As the energy from the pump is transferred from one fluid element to another, each fluid element experiences a cumulative resistance from all elements ahead of it in the flow direction, so the fluid element upstream experiences higher resistance compared to the fluid element downstream and thus the pressure at each cross-section drops as we go downstream of the flow.

This resistance is influenced by fluid density ( $\rho$ ), fluid viscosity ( $\mu$ ), fluid velocity ( $V$ ), pipe inner diameter ( $D$ ) and absolute roughness of the pipe ( $\epsilon$ ). It can be quantified by a dimensionless parameter called friction factor ( $f$ ) and through dimensional analysis (Benedict, 1980) can be shown to be a function of Reynold's number ( $Re$ ) and relative roughness ( $k = \epsilon/D$ ) of the pipe. The pressure-drop ( $\Delta P$ ), associated with this resistance for a given length  $L$  of a circular pipe with diameter  $D$  can be characterized by the Darcy–Weisbach equation (Darcy and Weisbach, 1857)

$$\Delta P = f \cdot L \cdot \left(\frac{\rho}{2}\right) \cdot \left(\frac{V^2}{D}\right), \quad (8)$$

this can be re-arranged to equate  $f$  as

$$f = \frac{D \cdot \left(\frac{\Delta P}{L}\right)}{\left(\frac{1}{2}\right) \cdot \rho \cdot V^2} . \quad (9)$$

The frictional resistance can also be represented by another dimensionless parameter called the mean skin friction coefficient ( $C_f$ ) defined by Von Karman (1946), which is the ratio of shear stress at the wall ( $\tau_w$ ) and the dynamic pressure, expressed as

$$C_f = \frac{\tau_w}{\left(\frac{1}{2}\right) \cdot \rho \cdot V^2} , \quad (10)$$

Or

$$C_f = \frac{\left(\frac{D}{4}\right) \cdot \left(\frac{\Delta P}{L}\right)}{\left(\frac{1}{2}\right) \cdot \rho \cdot V^2} . \quad (10.1)$$

From (9) and (10.1) it can be shown that

$$f = 4 C_f , \quad (11)$$

the representation of  $f$  and  $C_f$  requires  $\Delta P$  to be known, and this can only be achieved through direct measurements on a pipe flow setup. But as discussed earlier in this section,  $f$  being a function of  $Re$  and  $k$ , there was a lot of interest and therefore work done to derive an expression to calculate the value of  $f$  directly from the known  $Re$  and  $k$ .

For Laminar flows, the work of Hagen and Poiseuille (1839) provided the exact solution to the Navier-Stokes equation

$$\Delta P = \frac{128 \cdot \mu \cdot Q \cdot L}{\pi D^4}, \quad (12)$$

here  $Q$  is the volumetric flow rate. A corresponding equation for  $f$  can be achieved by equating (12) in (9), obtaining

$$f = \frac{64}{Re}, \quad (13)$$

this clearly shows the independence of friction factor from the pipe roughness for the laminar flow regime. For Turbulent flows, since there is no exact solution for the Navier-Stokes equation, arriving to an equation was not that straight forward. During the first half of the 20<sup>th</sup> century, research was focused on both experimental and analytical evaluation of turbulent flow in smooth and rough pipes, and it will soon be evident that pipe roughness plays an important role in predicting the frictional losses.

Towards the experimental side, the most notable work was from Nikuradse (1933), where he conducted an extensive study on artificially roughened pipes for a wide range of materials and surface roughness to systematically understand the impact of pipe roughness on frictional losses. His work provided key contributions in our understanding of fluid flow in rough pipes and provided a relative roughness scale (Nikuradse sand scale) based on the sand roughness used for artificial roughness.

At the same time, Prandtl (1933), advancing on the analytical work of Blasius (1911) for smooth pipes, developed the theoretical law of friction in smooth pipes for Newtonian fluids, showing the relation between friction factor ( $f_s$ ) and  $Re$  (Virk et al., 1970; Virk, 1971) as



$$\frac{1}{\sqrt{f_s}} = 4 \log(Re \sqrt{f_s}) - 0.4 , \quad (14)$$

here,  $f_s$  represents the Fanning friction factor which equated to the Darcy friction factor ( $f$ ) as  $f_s = (1/4)f$ , and considering equation 11,  $f_s = C_f$ . Equation 14 showed good agreement with the experimental data from Nikuradse (1932) for smooth pipes.

Utilizing the valuable experimental data from Nikuradse for rough pipes, Von Karman proposed an expression for friction factor ( $f_r$ ) for fully rough pipes (Benedict, 1980)

$$\frac{1}{\sqrt{f_r}} = 2 \log \left( \frac{Re}{\varepsilon} \right) + 1.74 . \quad (15)$$

With these developments a family of friction factor –  $Re$  curve were now available for smooth and fully rough region with different relative roughness, but there was an intermediate ‘transition region’ that was still unresolved.

Colebrook and White (1937) proposed an expression for this transition region and later combined it with the expression for the smooth pipe (14) and fully rough region (15) proposing a common solution for both smooth and rough pipes, expressed as

$$\frac{1}{\sqrt{f}} = -2 \text{Log} \left[ \frac{\varepsilon}{3.7 D} + \frac{2.51}{Re \sqrt{f}} \right] , \quad (16)$$

an implicit equation that can be solved numerically. This completed the picture for mapping the friction factor curves for all flow regimes and pipe roughness. But this data was still scattered and based on the artificially roughened pipes. It took the work of Moody (1944) to combine the laminar, the turbulent smooth pipe, the turbulent transition, and fully rough region into one single

plot that is famously known as the ‘*The Moody plot*’ (figure 3). Moody’s work also provided the effective roughness for different commercial pipes on the Nikuradse sand scale, that allowed the use of this plot for more practical applications since the empirical solutions through which this plot was derived was based on the Nikuradse scale. The moody plot is still widely used in commercial applications where a quick approximate estimation of the friction factor is desired over an accurate one.

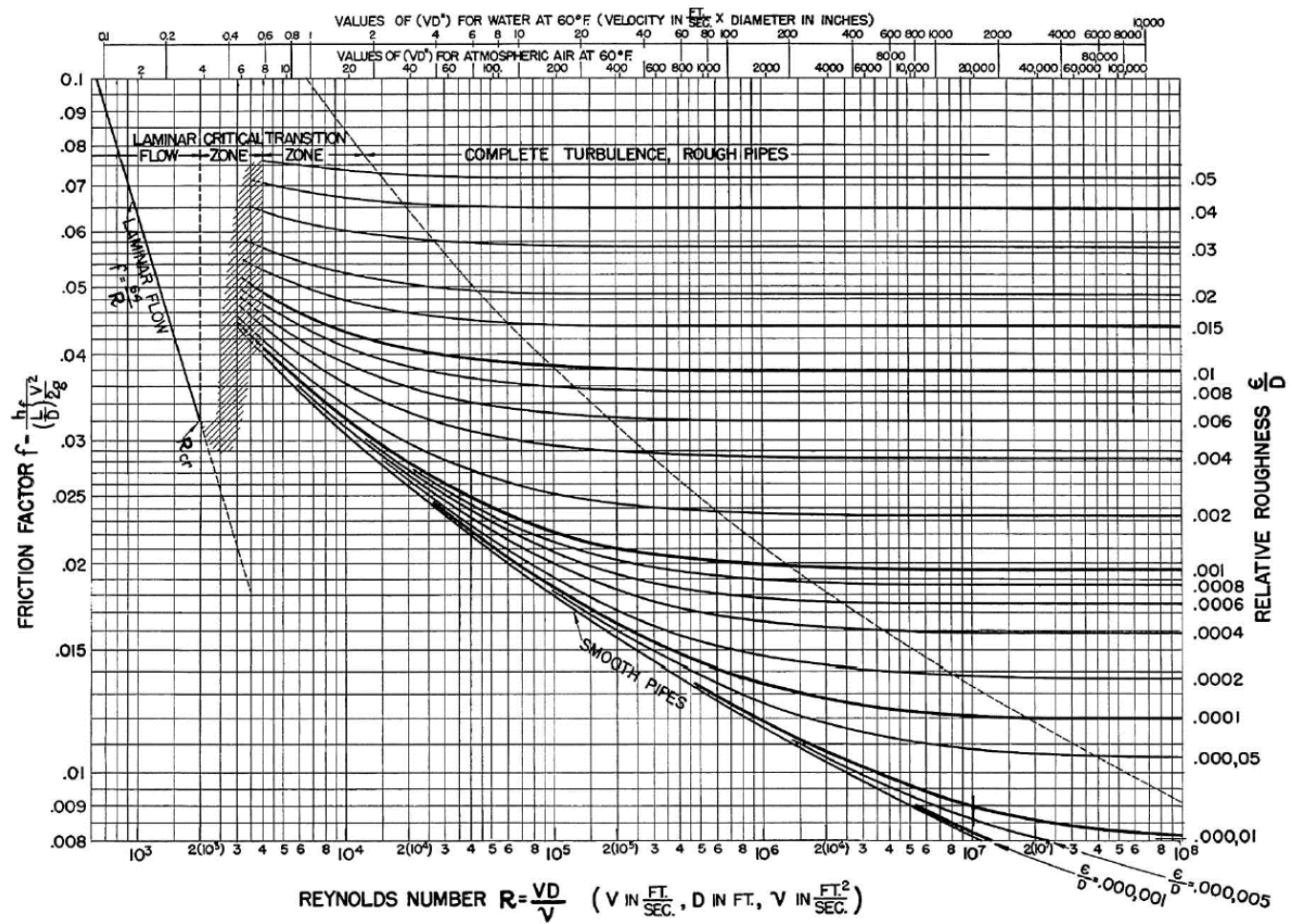


Figure 3: The ‘Moody plot’ (Moody, 1944) presenting the Darcy friction factor ( $f$ ) versus  $Re$  curves for laminar, transition and fully rough region, specific to different material roughness. With permission from the American Society of Mechanical Engineers (ASME).

## 2.4 Polymer drag reduction

Polymer drag reduction is a phenomenon of reduction in frictional losses in turbulent flows by the addition of a small quantity of high molecular weight polymers. Since the discovery in the late 1940s (Toms, 1948), polymer drag reduction in fluid flow has been studied extensively to understand the physics behind the phenomenon, as well as to optimizing the mechanism for various practical applications including fluid pipeline transport, firefighting, water distribution, marine transport, aviation, agriculture etc.

Various types of polymers have been studied for their drag-reducing properties. polyacrylamides (PAM), polyethylene oxide (PEO), and xanthan gum are among the commonly investigated polymers. PAM, with its long-chain structure, flexibility and water solubility is particularly well-known for its effectiveness in reducing drag.

The mechanism behind polymer drag reduction can be attributed to the elastic properties of the polymer molecules (Tabor and de Gennes, 1986). As the fluid moves through the pipeline, the polymer molecules align themselves along the flow direction and the turbulent flow of the fluid stretches these polymer molecules, dissipating some of the turbulent energies (small eddies) in the process and reducing the overall turbulence and vortex shedding within the fluid. This leads to a more streamlined flow profile, resulting in a reduction of losses due to viscous friction, which translates into reduced pressure drop and enhanced flow efficiency. This simplistic explanation does not account for the lack of detailed mathematical correlation available at present between the near wall turbulence and friction factor that can be used to precisely predict DR, leaving a small gap in our understanding, that requires further experimental and analytical work.

The earlier work for understanding the mechanism responsible for drag reduction involved experimental measurements of mean velocity profile, notably, using the laser-Doppler flowmeter by Goldstein et al. (1969), Rudd (1971, 1972) and Kumor et al. (1973), specifically studying the turbulent boundary layer. Many velocity profile models were proposed because of these investigations, of which the three-layer model reported by Virk et al. (1970) and Virk (1971), with a viscous sublayer, an elastic sublayer, and a turbulent core, was in most agreement with the then available experimental results.

Recent advancement in experimental techniques like particle image velocimetry (PIV) and computational capabilities have expanded and refined our understanding of this phenomenon. White and Mungal (2008) had meticulously summarized the progress in this field so far. Their work highlights the two main explanations for the onset of DR, viscous effects, and elastic effects.

Viscous effects, advocated by Lumley (1969), L'vov et al. (2004), and Ryskin (1987), propose that polymer stretching in turbulent flow increases effective viscosity. Polymers stretch just beyond the viscous sublayer, called the buffer layer, boosting elongational viscosity. This elevated viscosity reduces turbulence, enlarges the buffer layer, and lowers wall friction.

Recent work by L'vov et al. (2004) and supported by Benzi et al. (2006) suggests another view. They propose that polymer stretching leads to a linearly increasing space-dependent effective viscosity from the wall.

Tabor and de Gennes (1986) introduce the elastic theory. It argues that partially stretched polymers store elastic energy, becoming significant for DR. This theory predicts DR onset when cumulative elastic energy equals kinetic energy within the buffer layer, disrupting the energy cascade,

thickening the buffer layer, and inducing DR. Experimental data supports the merit of both theories.

There are various factors that contribute towards the degree of drag reduction achieved for a particular polymer solution. Polymer concentration, being one of the factors, has a significant effect on drag reduction. Generally, as the polymer concentration is increased, the drag reduction increases due to the reduction in Reynolds shear stress, which accounts for most of the turbulence in the fluid. However, over a certain concentration the Reynolds shear stresses becomes zero and any further increase in the polymer concentration does not translate to further drag reduction. On the contrary, this further increase in polymer concentration increases the shear viscosity of the solution, thus in fact increasing turbulent friction. This region of the flow regime was studied by Virk (Virk et al., 1970; Virk, 1971) and was termed as ‘maximum drag reduction (MDR)’, and since DR being independent of the polymeric parameters, he proposed a universal Fanning friction factor relationship for MDR, expressed as

$$\frac{1}{\sqrt{f_s}} = 19.0 \log(R_e \cdot \sqrt{f_s}) - 32.4 . \quad (17)$$

One application where the concept of polymer drag reduction has been utilized to a greater extent, is the transport of hydrocarbons fluids in pipeline over very large distances. The oil extracted from oil rigs in offshore and remote areas is required to be transported to the refining facilities which are generally near big cities and sometimes refined oil products are also transported from one location to another through these pipelines. Pumping these large volumes of fluid over such large spans at high flow rates has its incentives but it also implies overcoming the extensive hydrodynamic losses due to turbulent flow in the pipeline, and thus requires a great deal in

pumping power. The idea of reducing turbulence using polymer additives sparked great interest, which translated equally to the research and development that followed.

Lescarbourea et al. (1971) conducted a comparative polymer drag reduction test in an 8-inch and 12-inch crude oil pipeline running 28 miles and 32 miles long respectively, using a drag reducer code named CDR and few grades of polyisobutylene. He reported around 50% maximum drag reduction with CDR for the case of 1150 ppm polymer concentration. His results also aligned with his 1-inch pipe lab tests when scaled up using flow velocity instead of pipe diameter. He also highlights that the reason for initial slow progress in this field was due to the limited availability of drag reducers in aliphatic hydrocarbons, leading to insufficient research base for companies to implement it on a large scale. The first commercial large-scale use of polymer drag reduction was for the Trans Alaskan Pipeline System (TAPS) during 1979 (Burger et al., 1982). They utilized the same drag reducer CDR as reported by Lescarbourea and reported an increase in throughput of around 200,000 barrels per day (approximately 15% increase).

The lack of mathematical understanding of these complex turbulent flows has not slowed down progress on the experimental front. Nadolink and Haigh (1995) have meticulously summarized this progress with over 2500 references up to 1995, followed by Graham (2004), expanding on the progress in computational simulations of these flows, specifically through direct numerical simulations (DNS), that allowed analysis of the near-wall coherent structures, that are observed to be significantly modified by viscoelasticity.

Specific experimental work for modeling drag reduction through polymer solution rheology is presented by Owolabi et al. (2017), studying the drag reduction with polyacrylamide (PAM) solution in water at different concentrations in circular pipe and duct flows in a flow loop setup. Their work also presents shear viscosity and relaxation time measurements for samples collected

at different time periods during the flow tests and were able to relate the %DR to  $Wi$  with the data from both pipe and duct flow, converging to the relation  $\%DR = 2C_1[1/(1+e^{Wi_{cr}-Wi}) - Wi_{cr}]$ , where  $C_1$  is the limiting value of %DR as  $Wi \rightarrow \infty$ , reported to be 64 and  $Wi_{cr}$  represents the critical  $Wi$  for the onset of DR, reported as  $Wi_{cr} = 0.5$ . Additionally,  $Wi \geq 5$  was reported for MDR.

The current work in this area is focused towards understanding the effect of molecular weight, solubility, macromolecular size, and polymer elastic properties on the drag reducing ability along with improvement in techniques to optimize and synthesize these polymers (Nesyn et al. 2018).

## Chapter 3

# Measurements in water-based polymer solutions

This chapter provides a detailed description of the pipe flow facility used for the water-based polymer solution test, it discusses the main component used to run the facility and how each component contribute towards obtaining the friction factor data from the pipe flow test. The details of all the test procedures, measurement analysis and calculations used are presented here. This is followed by the discussion on the shear viscosity and extensional viscosity measurements conducted on the polymer solution collected from the pipe flow test and how these measurements are used in relation to each other. Finally discussing the uncertainty in the measurements of  $C_f$ ,  $Re$  and  $Wi$ .

### 3.1 Details of the pipe flow facility

The experimental setup for the water-based polymer solution test utilizes a 2-inch inner diameter (ID), horizontal pipe loop system, comprising of a vertical tank connected to a centrifugal pump



inlet. The pump outlet connects to the pipe loop with a total length of 22 m (including a 6.25 m long straight test section), the loop runs back into the tank and pump inlet, as shown in figure 4.

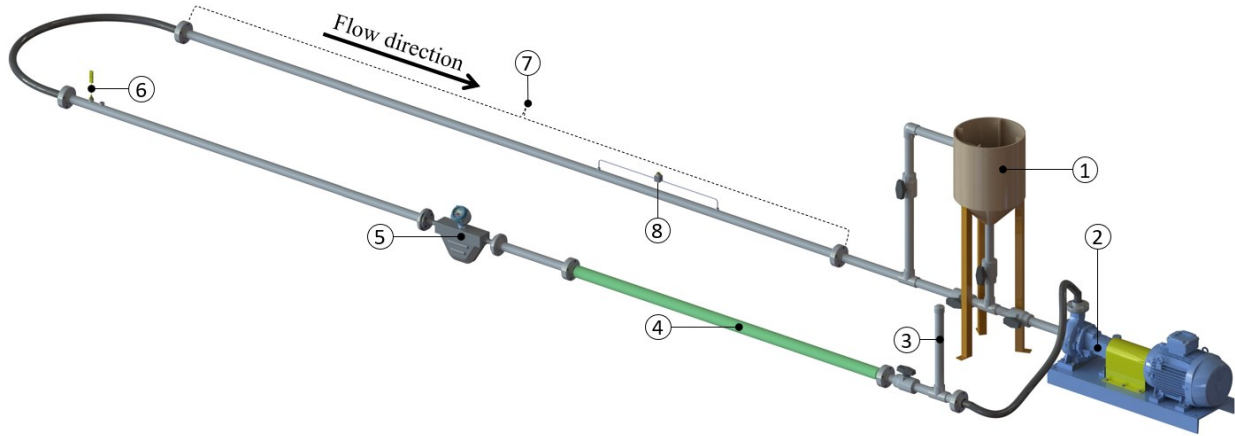


Figure 4: Overview of the pipe flow setup used for water-based tests, highlighting each component unit and flow direction.

The flow can be executed in an open loop configuration, where the flow runs through the tank with an open surface, or in a closed loop configuration, where the flow runs directly back into the pump inlet, bypassing the tank (refer to figure 5).

		Open Loop		Closed Loop	
V1	→	Open		V1	Closed
V2	→	Closed		V2	Open
V3	→	Open		V3	Open
V4	→	Open		V4	Open
V5	→	Open		V5	Open

Figure 5: Valve configuration details for pipe flow setup used for water-based test, providing configuration for open and closed loop system.

This flow loop allows controlling the flow rates and temperature of the fluid, while measuring the pressure drop for the fully developed turbulent flow in the test section. Figure 4 shows the flow loop system with the key components highlighted, which are detailed as follows:

1. Tank: 200 liters vertical plastic tank with a 2-inch outlet and inlet.
2. Pump: Georgia Iron Works 2X3LCC slurry pump powered by a TECO Westinghouse 40 HP motor.
3. Pulsation dampener: In-house fabricated air column dampener to stabilize the flow.
4. Heat exchanger: In-house fabricated, concentric tube design, with a 4-inch tube jacketing the 2-inch flow pipe, with inlet and outlet ports on the 4-inch pipe to run cold/hot water to regulate the temperature.
5. Coriolis flow meter: Micro motion 2-inch F-Series Coriolis flow meter (F200S418C2BAEZZZZ) with a 2700 series field mount transmitter (2700R12BBAEZZZ) for mass flow readings.
6. Thermocouple: K-type thermocouple from Omega for temperature readings.
7. Test section: The test section is a 6.25 m long straight stainless-steel pipe with an upstream pressure port at 3.75 m from the upstream edge and the distance between the upstream and downstream port ( $L$ ) = 1.75 m. Three different test sections are used with 1-inch, 1.5-inch, and 2-inch inner pipe diameter.

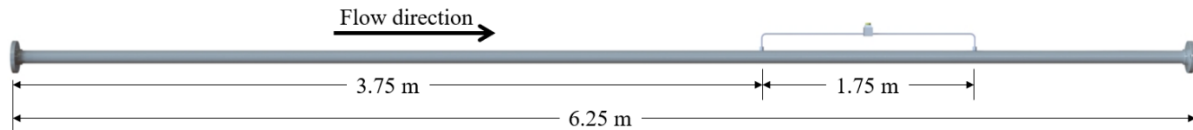


Figure 6: Details of the test section used for water-based test with measurements of the development region, distance between the pressure ports and overall test section length.

8. Pressure transducer: A valyline DP-15 pressure transducer was used, connected to the pressure port on the test section through 1/8-inch double-ferrule stainless-steel tube fittings. The diaphragm numbers used in the pressure transducer are: 3-22 ( $\pm 0.20$  psi) for 2-inch pipe size, 3-24 ( $\pm 0.32$  psi) for 1.5-inch pipe size and 3-30 ( $\pm 1.25$  psi) for 1-inch pipe size.

### 3.2 Preparation of the polymer solution

The solution studied is a 50 ppm (50 mg/l) solution of polyacrylamide (PAM) in water. PAM is a water soluble, high molecular weight polymer with a chemical structure  $\text{-(CH}_2\text{CHCONH}_2\text{)-}_n$ . For a total test volume of 115 liters, 5.75 g of PAM is used to get 50 ppm concentration. A batch of 15 liters of water (at room temperature) is mixed with 5.75 g of PAM in a small tank, using an overhead mixer with a 3-inch impeller diameter, running at a very low RPM of about 20-30 to avoid any mechanical degradation of the polymer. The solution is mixed for 2 hours, and after that the mixing is stopped, and the impeller is lifted out of the solution to allow the residual polymer on the impeller to drip down into the solution. The solution is then allowed to sit for 24 hours, to facilitate the escape of microbubbles and homogenization of the solution. This 15-liter batch will subsequently be mixed with the remaining 100 liters of water in the pipe flow loop, before the test.

### 3.3 Test preparation and procedures

This section details the preparations done before the test and all test procedures used for the water-based testing. A total of three test sections (1-inch, 1.5-inch, and 2-inch inner pipe diameter) are tested separately. Each following the same procedure as described in the following sections.

#### 3.3.1 Calculation of mass flow rates

A total of five averaged  $\Delta P$  readings were collected per test by setting five mass flow rates ( $\dot{M}$ ) corresponding to  $Re$ : 60000, 70000, 80000, 90000 and 100000 as a baseline. These calculations were based on the viscosity of water ( $\mu = 0.0010023$  kg/m-s) at  $20 \pm 0.5$  °C. These mass flow rates are calculated using the relation

$$\dot{M} = \frac{\pi \cdot D \cdot Re \cdot \mu}{4}, \quad (18)$$

and are presented in table 1 corresponding to each  $Re$  value and for each pipe size.

Pipe size = 1-inch $D = 0.0267$ m		Pipe size = 1.5-inch $D = 0.0413$ m		Pipe size = 2-inch $D = 0.0525$ m	
Re	$\dot{M}$ (kg/s)	Re	$\dot{M}$ (kg/s)	Re	$\dot{M}$ (kg/s)
60000	1.261	60000	1.932	60000	2.480
70000	1.471	70000	2.253	70000	2.893
80000	1.681	80000	2.575	80000	3.306
90000	1.891	90000	2.897	90000	3.720
100000	2.101	100000	3.219	100000	4.133

Table 1: Mass flow rate calculation listed for each pipe size with the measured inner diameter (D) per column, showing the mass flow rate required to achieve the corresponding  $Re$  for pipe flow test with water.

### 3.3.2 Pressure transducer calibration

The pressure transducer is calibrated using Omega DPI 610 pressure calibrator. Three consecutive calibrations are conducted for each diaphragm, with the transducer adjusted through the demodulator to output 0-10 volts corresponding to 0-max psi rated for that diaphragm. For each calibration, ten equally spaced pressure values are taken covering the full pressure range of the diaphragm and voltage output from transducer is recorded for each pressure point for both up and down pressure sweep. The voltage versus pressure is plotted to confirm the linearity of the curve and good overlap between up and down sweep which indicates no hysteresis loss.

### 3.3.3 De-airing and transducer bleeding procedure

When the loop is first filled with water, there are many air pockets all around the loop at locations like pipe joints, pipe bends and transducer tubing. These pockets, if not removed, can mix with the flow stream, and negatively impact the measurements. So, to ensure the removal of all air pockets and micro bubbles, a systematic process is followed to get the same level of flow quality every time. This process is explained step by step as follows:

Step 1: After water is introduced into the loop, set open loop valve configuration.

Step 2: Open transducer bypass valve and then close both the pressure transducer valves.

Step 3: Run the pump at 600 RPM for 5 minutes to allow bigger air bubbles to escape from the open surface in the tank.

Step 4: Stop the pump and switch to close loop configuration with tank outlet open.

Step 5: Slowly ramp up the RPM from 0 to 800 for 30 seconds, this will dislodge smaller air bubbles trapped in the pipe joints. These bubbles will now be visible in the flow stream.

Step 6: Gradually reduce the RPM from 800 to 400 and run for 5 minutes. This will allow the dislodged bubbles to escape through the tank inlet and outlet columns.

Step 7: Repeat step 5 and 6 two more times.

Step 8: Stop the pump and allow the fluid to rest for 10 minutes. This will allow the micro bubbles in the stream to rise and accumulate to form larger bubbles.

Step 9: Repeat step 5 and 6 two more times.

Step 10: Continue running the pump at 400 RPM for 10-15 minutes, use this run time to regulate the fluid temperature to achieve  $20 \pm 0.5$  °C.

Step 11: Stop the pump, close the tank outlet valve, and with the pressure transducer bypass valve open, open both bleed valves.

Step 12: Very slowly open both pressure port valves, allowing water into the transducer. This will start the bleeding. Let the bleeding continue for 3-4 minutes.

Step 13: Close both bleed valves and open the tank outlet valve.

Step 14: With the transducer bypass valve open, run the pump at 600 RPM for 2 minutes. This will push out any air bubbles in the transducer tubing, through the bypass line into the main pipe, which can then be escaped out.

Step 15: Stop the pump and close the transducer bypass valve.

Step 16: Verify that the fluid temperature is within  $20 \pm 0.5$  °C, if not, run the pump at 400 RPM with the heat exchanger running till the correct temperature is achieved.

The system will now be ready for the test to begin.

### 3.3.4 Test procedure for baseline water test

For each test section, three independent tests with water are conducted to confirm alignment with the Newtonian  $C_f$ - $Re$  curve (14) and repeatability of the results. Before the test, the tank is filled with 100 liters of water which is introduced into the loop, the loop de-airing and transducer bleeding process is then executed as detailed in section 3.3.3. The test is run using the LabVIEW software with a PID controller, and since a centrifugal pump is utilized here, the operator can either control the pump RPM in manual-mode or set the mass flow rates in auto-mode, which automatically adjusts the pump RPM to get the set mass flow rate. Table 1 breaks down the test procedure steps to run the baseline water test for the five mass flow values (refer to section 3.3.1) for each pipe size, aligning each step with the data log time and providing actions and set values against each step, while maintaining the flow temperature within  $20 \pm 0.5$  °C

Step	Log time stamp	Action				Temperature condition	
1	-	Once transducer is calibrated, loop is filled and de-aired and transducer bleeding is completed, set closed loop configuration, and close the tank outlet valve.				20±0.5 °C	
2	-	Turn ON VFD, flow meter and transducer demodulator, verify pump is at zero RPM.					
3		Open pressure port valves and close the transducer bypass valve.					
4	0	Start data log.					
5	120	In manual mode, gradually increase pump RPM to 600.					
			For 1-inch pipe size	For 1.5-inch pipe size	For 2-inch pipe size		
6	420	Set auto mode, then set $\dot{M}$ (kg/s) to →	1.261	1.932	2.480		
7	780	In auto mode, set $\dot{M}$ (kg/s) to →	1.471	2.253	2.893		
8	1140	In auto mode, set $\dot{M}$ (kg/s) to →	1.681	2.575	3.306		
9	1500	In auto mode, set $\dot{M}$ (kg/s) to →	1.891	2.897	3.720		
10	1860	In auto mode, set $\dot{M}$ (kg/s) to →	2.101	3.219	4.133		
11	2220	Switch to manual mode and gradually reduce pump RPM to zero.					-
12	2340	Stop data log.					-
13	-	Open the transducer bypass valve and then close both pressure port valves.					-
14	-	Turn OFF VFD, flow meter and transducer demodulator					-
15	-	Drain the loop.				-	

Table 2: Step-by-step test procedure aligning with the LabVIEW log time stamp, for baseline water pipe flow test for all three pipe sizes.



### 3.3.5 Polymer degradation test

The 50 ppm polymer solution was expected to result in 65-75% DR compared to the water data. So, to get more data points on the  $C_f-Re$  plot, lower concentrations were required to be tested. A way to simulate lower concentration is to intentionally degrade the polymer solution by means of mechanical degradation, which breaks down the long chain molecules and can lower the %DR. This was achieved by designing a polymer degradation test that runs a 50 ppm solution and progressively degrades it by running the pump at high RPMs for a close-to-exponential increments in time, for example: time intervals of 1 – 2 – 4 – 8 – 12 – 16 – 20 minutes was used, and after each degradation step, dropping the mass flow to a known value that was tested for water to obtain the %DR after each degradation. This data was then used to plot %DR versus degradation time ( $t_{dg}$ ) which was then used to derive a mathematical model to calculate  $t_{dg}$  required to get an evenly spaced %DR, to populate the  $C_f-Re$  plot evenly.

For this test, polymer solution was prepared using the process detailed in section 3.2. The tank is filled with 70 liters of tap water at room temperature. Water is then introduced in the loop and ‘de-airing and transducer bleeding process’ is followed as detailed in section 3.3.3. Next, the tank outlet valve is closed, and the 15 liters batch of polymer solution is poured into the tank. The same container is rinsed with 15 liters of water twice, and added to the tank, to extract any residual polymer stuck to the container wall. This completes the 115 liters of polymer solution in the pipe flow system. The tank outlet valve is then slowly opened, and the system is allowed to rest for 10 minutes so any new air bubble introduced due to pouring can escape. After that the below test procedure is followed for the degradation test.

Note: Since the high RPM degradation will require isolating the pressure transducer to protect it from over-pressurizing, the below two terms are used frequently, as defined, in the test procedure.

1. Isolate pressure transducer = Open the transducer bypass valve, then close both pressure port valves.
2. Reconnect pressure transducer = Open both pressure port valves, then close the transducer bypass valve

Step	Log time stamp	Action				Temperature condition
1	-	Once transducer is calibrated, loop is filled and de-aired, transducer bleeding is completed and polymer batch is added to the tank, set open loop configuration.				20±0.5 °C
2	-	Turn ON VFD, flow meter and transducer demodulator, verify pump is at zero RPM.				
3	-	Open pressure port valves and close the transducer bypass valve.				
4	0	Start data log.				
5	120	In manual mode, gradually increase pump RPM to 600. This will mix the polymer solution evenly.				
6	410	Switch to closed loop configuration and close tank outlet.				
			For 1-inch pipe size	For 1.5-inch pipe size	For 2-inch pipe size	
7	420	Set auto mode, then set $\dot{M}$ (kg/s) to →	1.681	2.575	3.306	
8	770	Isolate pressure transducer				
9	780	set manual mode, gradually increase pump RPM to →	1300	1300	1400	
10	810	set auto mode, then set $\dot{M}$ (kg/s) to →	1.681	2.575	3.306	
11	820	Reconnect pressure transducer				
12	1160	Isolate pressure transducer				
13	1170	set manual mode, gradually increase pump RPM to →	1300	1300	1400	

14	1230	set auto mode, then set $\dot{M}$ (kg/s) to $\rightarrow$	1.681	2.575	3.306	20±0.5 °C
15	1240	Reconnect pressure transducer				
16	1580	Isolate pressure transducer				
17	1590	set manual mode, gradually increase pump RPM to $\rightarrow$	1300	1300	1400	
18	1710	set auto mode, then set $\dot{M}$ (kg/s) to $\rightarrow$	1.681	2.575	3.306	
19	1720	Reconnect pressure transducer				
20	2060	Isolate pressure transducer				
21	2070	set manual mode, gradually increase pump RPM to $\rightarrow$	1300	1300	1400	
22	2310	set auto mode, then set $\dot{M}$ (kg/s) to $\rightarrow$	1.681	2.575	3.306	
23	2320	Reconnect pressure transducer				
24	2660	Isolate pressure transducer				
25	2670	set manual mode, gradually increase pump RPM to $\rightarrow$	1300	1300	1400	
26	3150	set auto mode, then set $\dot{M}$ (kg/s) to $\rightarrow$	1.681	2.575	3.306	
27	3160	Reconnect pressure transducer				
28	3500	Isolate pressure transducer				
29	3510	set manual mode, gradually increase pump RPM to $\rightarrow$	1300	1300	1400	
30	4230	set auto mode, then set $\dot{M}$ (kg/s) to $\rightarrow$	1.681	2.575	3.306	
31	4240	Reconnect pressure transducer				
32	4580	Isolate pressure transducer				
33	4590	set manual mode, gradually increase pump RPM to $\rightarrow$	1300	1300	1400	
34	5550	set auto mode, then set $\dot{M}$ (kg/s) to $\rightarrow$	1.681	2.575	3.306	
35	5560	Reconnect pressure transducer				
36	5900	Isolate pressure transducer				
37	5910	set manual mode, gradually increase pump RPM to $\rightarrow$	1300	1300	1400	
38	7110	set auto mode, then set $\dot{M}$ (kg/s) to $\rightarrow$	1.681	2.575	3.306	

39	7120	Reconnect pressure transducer				20±0.5 °C
40	7460	Isolate pressure transducer				
41	7470	set manual mode, gradually increase pump RPM to →	1300	1300	1400	
42	8910	set auto mode, then set $\dot{M}$ (kg/s) to →	1.681	2.575	3.306	
43	8920	Reconnect pressure transducer				
44	9440	Isolate pressure transducer				
45	9450	set manual mode, gradually increase pump RPM to →	1300	1300	1400	
46	11130	set auto mode, then set $\dot{M}$ (kg/s) to →	1.681	2.575	3.306	
47	11140	Reconnect pressure transducer				
48	11480	Isolate pressure transducer				
49	11490	set manual mode, gradually increase pump RPM to →	1300	1300	1400	
50	13410	set auto mode, then set $\dot{M}$ (kg/s) to →	1.681	2.575	3.306	
51	13420	Reconnect pressure transducer				
52	13770	Switch to manual mode and gradually reduce pump RPM to zero.				
53	13890	Stop data log.				-
54	-	Isolate pressure transducer				-
55	-	Turn OFF: VFD, flow meter and transducer demodulator				-
56	-	Drain the loop and rinse it with water twice.				-

Table 3: Step-by-step test procedure aligning with the LabVIEW log time stamp, for water-based polymer solution degradation test, for all three pipe sizes.

From the above test, the averaged  $\Delta P$  value for the constant mass flow rate period after each degradation step is utilized along with the  $\Delta P$  value from the baseline water test for the same mass flow rate to obtain the value of %DR after each degradation period as  $(\Delta P_{water} - \Delta P_{polymer}) / \Delta P_{water} \times 100$ . This %DR value is plotted against the degradation time duration up to each %DR point. The  $\Delta P$  versus time plot for the whole test is shown in

figure 7 and the %DR versus Degradation time duration is presented in figure 8. These plots are for the 1.5-inch pipe size degradation test. The 1-inch and 2-inch tests showed similar plots.

The curve in figure 8 fits an exponential model:  $(a \cdot e^{bx} + c \cdot e^{dx})$ , with  $a$ ,  $b$ ,  $c$ , and  $d$  representing the coefficients and  $x$  representing the time. This was used to derive the required  $t_{dg}$  to achieve an evenly spaced %DR for the polymer solution test.

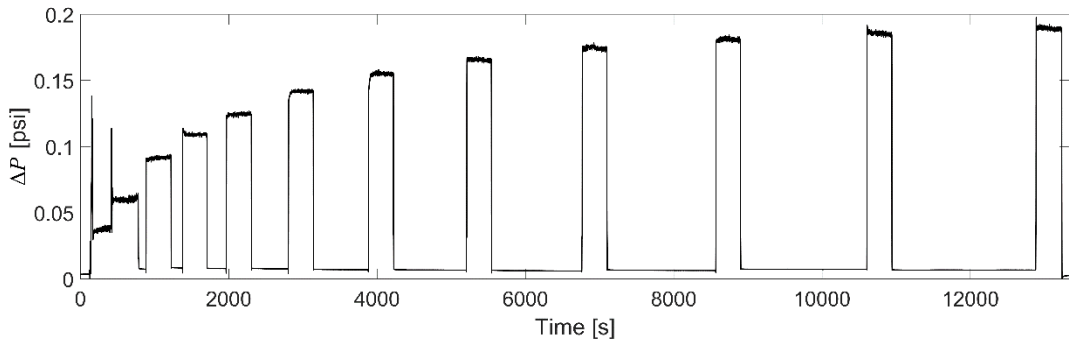


Figure 7:  $\Delta P$  versus time plot for polymer degradation test detailed in table 3, this specific plot is from the 1.5-inch pipe size test, the test with other two pipe sizes exhibit similar plots.

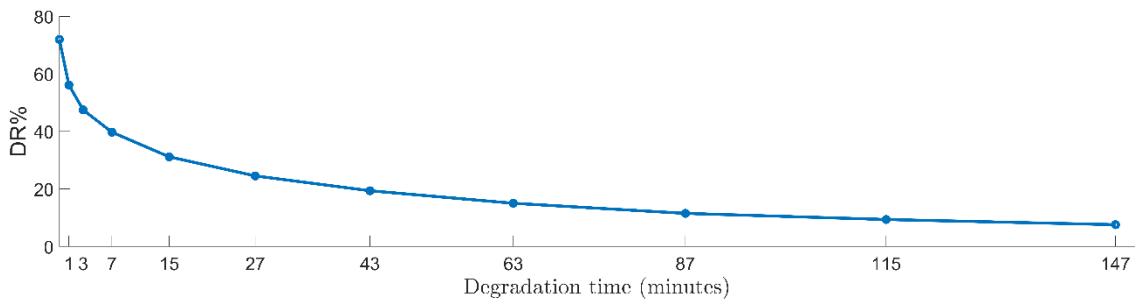


Figure 8: %DR versus degradation time plot for polymer degradation test in 1.5-inch pipe size, degradation was performed at 1300 pump PRM, the test with other two pipe sizes exhibit similar plots.

### 3.3.6 Polymer solution test

The preparation for the polymer test is the same as for the polymer degradation test. Polymer solution was prepared using the process detailed in section 3.2. The tank is filled with 70 liters of tap water at room temperature. Water is then introduced in the loop and ‘de-airing and transducer bleeding process’ is followed as detailed in section 3.3.3. At this stage, with water in the loop, the five mass flow rates mentioned in table-2 are run for 60 seconds each, to cross check the pressure drop readings with the baseline water test to ensure no deviation due to contamination or calibration shift. Next, the tank outlet valve is closed, and the 15 liters batch of polymer solution is poured into the tank. The same container is rinsed with 15 liters of water twice, and added to the tank, to extract any residual polymer stuck to the container wall. This completes the 115 liters of polymer solution in the pipe flow system. The tank outlet valve is then slowly opened, and the system is allowed to rest for 10 minutes so any new air bubble introduced due to pouring can escape. The below test procedure is followed for the polymer test.

Step	Log time stamp	Action	Temperature condition
1	-	Once transducer is calibrated, loop is filled and de-aired, transducer bleeding is completed and polymer batch is added to the tank, set open loop configuration.	20±0.5 °C
2	-	Turn ON VFD, flow meter and transducer demodulator, verify pump is at zero RPM.	
3	-	Open pressure port valves and close the transducer bypass valve.	
4	0	Start data log.	
5	120	In manual mode, gradually increase RPM to 600. This will mix the polymer solution evenly.	
6	400	Isolate Pressure Transducer	
7	410	Switch to closed loop configuration and close tank outlet.	

			For 1- inch pipe size	For 1.5- inch pipe size	For 2- inch pipe size		
8	420	Set manual mode, gradually increase pump RPM to →	1300	1300	1400	20±0.5 °C	
9	↑ + $t_{dg}$	Set auto mode, then set $\dot{M}$ (kg/s) to →	1.261	1.932	2.480		
10	↑ + 10	Reconnect Pressure Transducer					
11	↑ + 10	Collect baseline sample – 100 ml					
12	↑ + 160	Collect Re: 60000 sample – 100 ml					
13	↑ + 180	In auto mode, set $\dot{M}$ (kg/s) to →	1.471	2.253	2.893		
14	↑ + 180	Collect Re: 70000 sample – 100 ml					
15	↑ + 180	In auto mode, set $\dot{M}$ (kg/s) to →	1.681	2.575	3.306		
16	↑ + 180	Collect Re: 80000 sample – 100 ml					
17	↑ + 180	In auto mode, set $\dot{M}$ (kg/s) to →	1.891	2.897	3.720		
18	↑ + 180	Collect Re: 90000 sample – 100 ml					
19	↑ + 180	In auto mode, set $\dot{M}$ (kg/s) to →	2.101	3.219	4.133		
20	↑ + 180	Collect Re: 100000 sample – 100 ml					
21	↑ + 180	Switch to manual mode and gradually reduce RPM to zero.					-
22	↑ + 120	Stop data log.					-
23	-	Isolate Pressure Transducer					-
24	-	Turn OFF: - VFD, flow meter and transducer demodulator					-
25	-	Drain the loop and rinse it with water twice.					-

Table 4: Step-by-step test procedure aligning with the LabVIEW log time stamp, for water-based polymer solution test, for all three pipe sizes.

In the above test procedure, log stamp 420 is the start of degradation period and  $\uparrow + t_{dg}$  (indicating  $420 + t_{dg}$ ) gives the end time stamp for the degradation.  $t_{dg}$  value was adjusted based on the degradation test results to achieve different DR% which are evenly spaced out between MDR and the Newtonian values.

### 3.4 Calculation of skin-friction coefficient

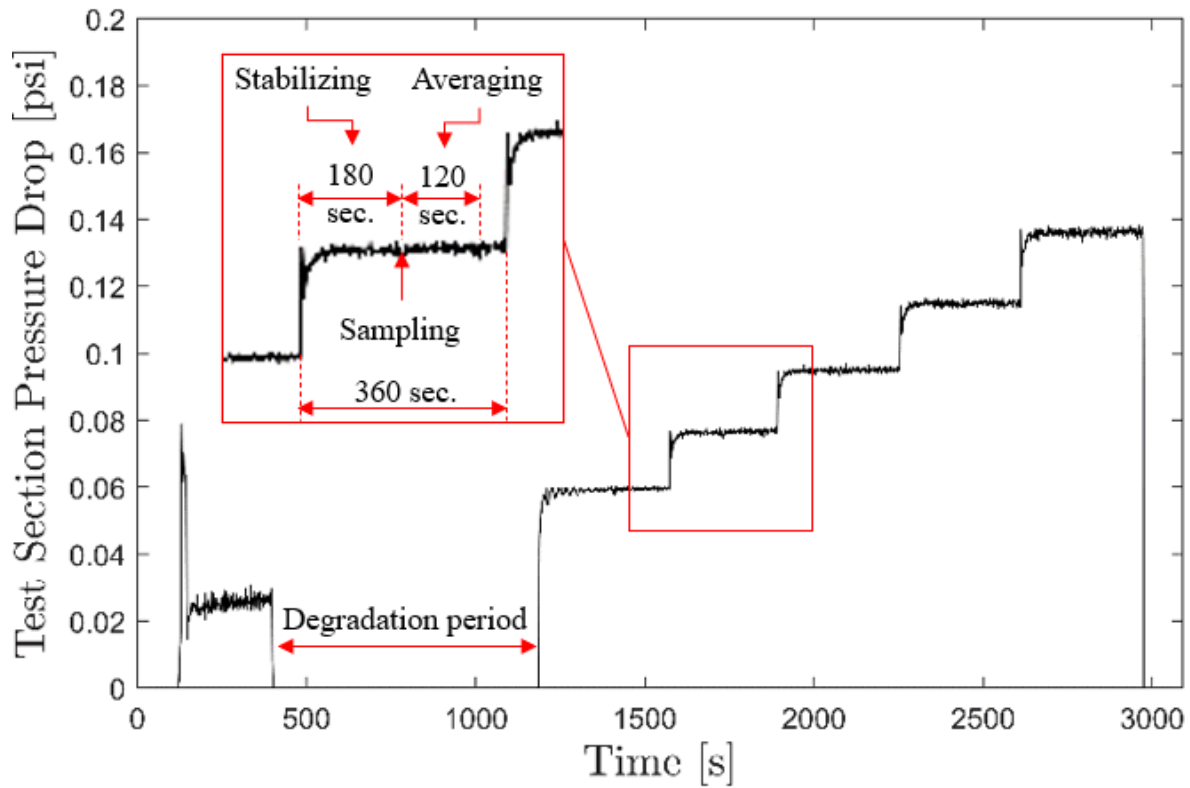


Figure 9:  $\Delta P$  versus time plot example from the polymer solution pipe flow test, explaining the sampling and data averaging method used to obtain the five averaged  $\Delta P$  values for each test.

As detailed in figure 9, each mass flow was run for 360 seconds, the first 180 seconds were kept for stabilizing the pressure value and the data for the next 120 seconds was used to average the  $\Delta P$



readings. At the start of each averaging, a sample was collected from the pipe flow loop which was tested for shear viscosity and extensional viscosity measurements (detailed in section 3.5 and 3.6 respectively) on the same day as the polymer solution test (refer to appendix B for  $\Delta P$  versus  $t$  plots for each test).

The pipe flow setup provided the data log of  $\Delta P$ ,  $\dot{M}$  and temperature ( $T$ ), these values are averaged as shown in figure 9, to get five values of  $\Delta P$  corresponding to the five mass-flow rates ( $\dot{M}$ ) and five temperature ( $T$ ) readings. A temperature model (Cheng, 2008) was used to calculate the density of water ( $\rho_w$ ), given as

$$\rho_s = 1000 \left( 1 - \left| \frac{(T - 4)}{622} \right|^{1.7} \right), \quad (19)$$

which was substituted for the polymer solution density ( $\rho_s$ ) since the polymer concentration is very low (50 ppm). The bulk flow velocity ( $V_b$ ) is calculated from the measured  $\dot{M}$  and the calculated  $\rho_s$  values, as

$$V_b = \frac{\dot{M}}{A \cdot \rho_s} ; \quad A = \frac{\pi \cdot D^2}{4} . \quad (20)$$

With the value of  $\rho_s$ ,  $V_b$  and  $\Delta P$  known,  $C_f$  is calculated corresponding to all five  $\Delta P$ , by the equation

$$C_f = \frac{\tau_w}{\left(\frac{1}{2}\right) \cdot \rho_s \cdot V_b^2} = \frac{\left(\frac{D}{4}\right) \cdot \left(\frac{\Delta P}{L}\right) \cdot (6894.76)}{\left(\frac{1}{2}\right) \cdot \rho_s \cdot V_b^2}, \quad (21)$$

here 6894.76 is the conversion factor from PSI to Pascal.

### 3.5 Shear viscosity measurements

Discovery hybrid rheometer with a double gap concentric cylinder cups and rotor attachment (figure 10) was used to measure the shear viscosity ( $\mu_s$ ) for the five polymer solution samples from the pipe flow setup. This setup was also equipped with a Peltier cup attachment that was connected to a heat exchanger unit to regulate the test fluid temperature. Trios software was used to connect to the rheometer, setup measurement parameters and analyze the results.

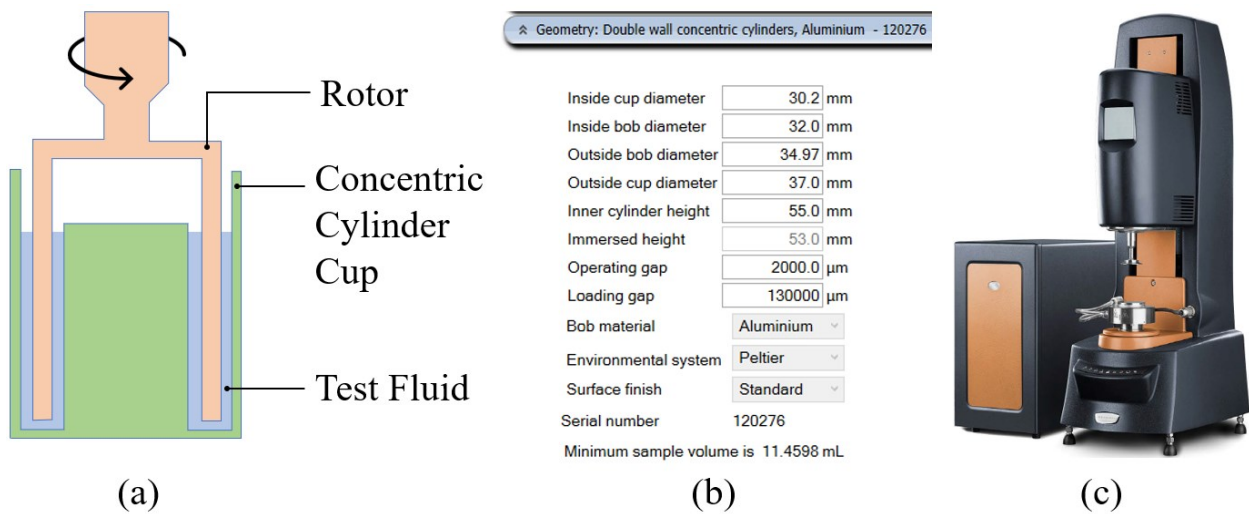


Figure 10: (a) Cross-section view of the double wall concentric cylinder cup and rotor attachment. (b) Geometry parameters for double wall concentric cylinder cup. (c) Image reference for the TA Discovery Hybrid Rheometer used for shear viscosity measurements.

For this measurement, a flow sweep test was conducted by setting a logarithmic shear rate sweep from 0.1 1/s to 1000 1/s, with ten points per decade, giving a total of 41 shear rates ( $\gamma_s$ ) values, maintaining the Peltier cup at 20 °C. Each shear rate is maintained for 30 seconds, of which the initial 10 seconds is the equilibration time and the next 20 seconds is the averaging time. The sensor on the rotor registers the torque value corresponding to each shear rate, this torque value represents the shear stress ( $\tau_w$ ), which is divided by the shear rate ( $\gamma_s$ ) to get the viscosity value. On

the viscosity versus shear rate plot (figure 11), the data for shear rate lower than 4 1/s was excluded, as that is closer to the lower limit of measurement for the rheometer and the viscosity readings shows high inconsistency in that region. Additionally, the data for shear rates above 200 1/s was also excluded as viscosity readings show a sharp increase due to the formation of Taylor vortices at these high shear rates.

The plot region between shear rate 4 1/s to 200 1/s was used, applying a cross fit model to generate the below four parameters (refer to appendix C for shear viscosity data for each test):

1. Zero-rate viscosity ( $\mu_0$ ): viscosity (Pa.s) at zero shear rate.
2. Infinite-rate viscosity ( $\mu_\infty$ ): viscosity (Pa.s) at infinite shear rate.
3. Consistency ( $c$ ): neutral time (s) at which the linear behavior changes to power law.
4. Rate index ( $n$ ): flow index.

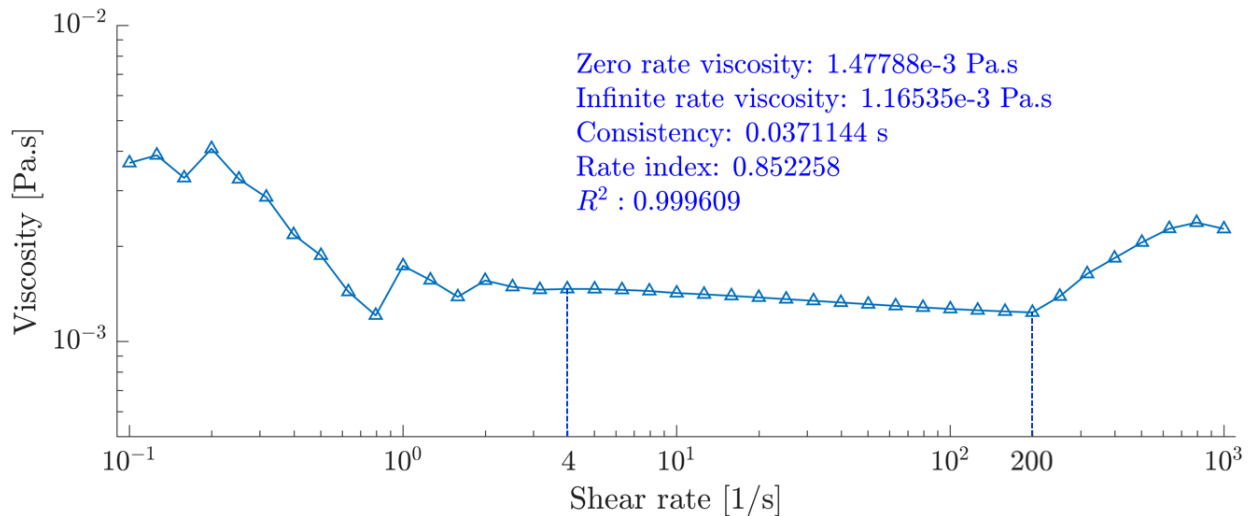


Figure 11: Viscosity versus shear rate plot example for water-based polymer solution, showing the portion of the reading used between the shear rate value 4 1/s and 200 1/s to obtain zero-rate viscosity ( $\mu_0$ ), infinite-rate viscosity ( $\mu_\infty$ ), consistency ( $c$ ), and rate index ( $n$ ).

These four parameters were used to calculate the shear viscosity ( $\mu_s$ ) of the polymer solution samples using the cross-power law model (Cross, 1965), expressed as

$$\mu_s = \mu_\infty + \frac{(\mu_0 - \mu_\infty)}{1 + (c \cdot \gamma_s)^n} , \quad (22)$$

this can be re-arranged as

$$\mu_s = \frac{\tau_w}{\gamma_s} = \mu_\infty + \frac{(\mu_0 - \mu_\infty)}{1 + (c \cdot \gamma_s)^n} , \quad (22.1)$$

And

$$(\mu_\infty \cdot \gamma_s) + \frac{(\mu_0 - \mu_\infty) \cdot \gamma_s}{1 + (c \cdot \gamma_s)^n} - \tau_w = 0 . \quad (22.2)$$

Equation 22.2 was solved numerically in MATLAB, to obtain the value of  $\gamma_s$ , which is then substituted back in equation 22 to obtain  $\mu_s$ . Now, with the value of  $\mu_s$  known,  $Re$  can be calculated from the equation

$$Re = \frac{\rho_s \cdot V_b \cdot D}{\mu_s} . \quad (23)$$

With the value of  $C_f$  calculated from (21) and corresponding value of  $Re$  from (23) for each of the five sample points per test. All test data can be combined into a single  $C_f$  versus  $Re$  plot for each pipe size (detailed in section 4.1).

### 3.6 Extensional viscosity measurements

For the extensional viscosity measurements, a dripping setup (figure 12a) was devised, that consists of a syringe pump connected to a nozzle, set at a flow rate of 0.2 ml/min. At this rate each polymer solution drop takes about 5 seconds to extend down and detach from the nozzle, allowing enough time for the camera to detect and activate recording. As the drop starts to detach from the nozzle, it forms an extensional filament (figure 12b) that becomes thinner with time and eventually breaks off. A light source was placed behind the nozzle for illumination, and a Photron FASTCAM Nova S9 high speed camera was used to capture this filament evolution.

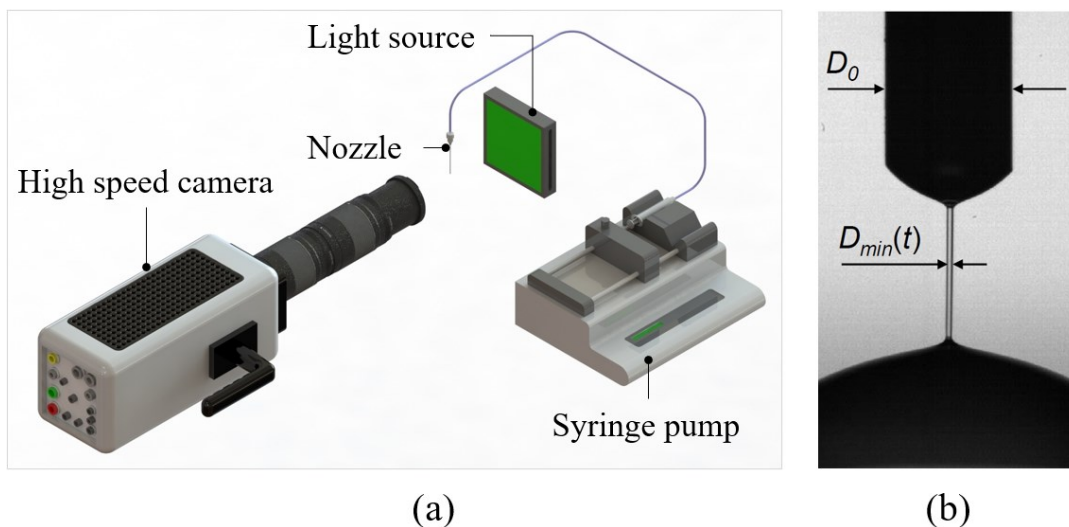


Figure 12: (a) CAD representation of the dripping setup used for extensional viscosity measurements. (b) An image frame from the high-speed camera showing the extensional filament as the fluid drop detaches from the nozzle, with  $D_{min}(t)$  and  $D_0$  measurements.

Here,  $D_0$  represents the nozzle diameter and  $D_{min}(t)$  is the time varying minimum diameter of the filament. This filament evolution was plotted on a semi log scale as the log of the normalized minimum diameter ( $D_{min} / D_0$ ) versus time ( $t$ ) (refer to appendix D for plots from each test). The filament evolution, as captured with the high-speed camera is demonstrates in figure 13, in this

figure the uneven time stamp gap should be noted, this is because the initial necking takes a longer time compared to the thinning towards the end.

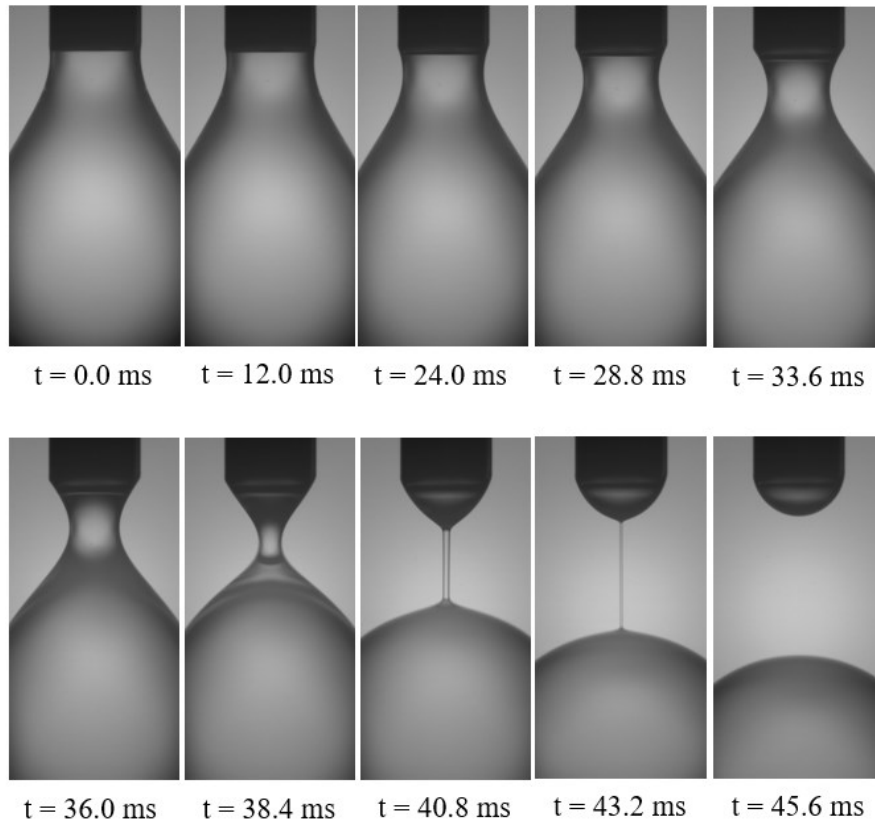


Figure 13: Evolution of a 50 ppm polymer solution filament is shown with respect to time ( $t$ ), the first frame (0 ms) represents the start time when  $D_{min} \approx D_0$ .

Figure 14 shows the semi log plot for this evolution. Here, initial regime (A), which involves the major portion of the filament thinning, involves viscous effects that cannot be neglected. For the following portion of the thinning process (B) that demonstrates an exponential decrease of the minimum diameter, the viscous stresses become low enough to be neglected and only the elastic and capillary stresses dominate the balance of forces.

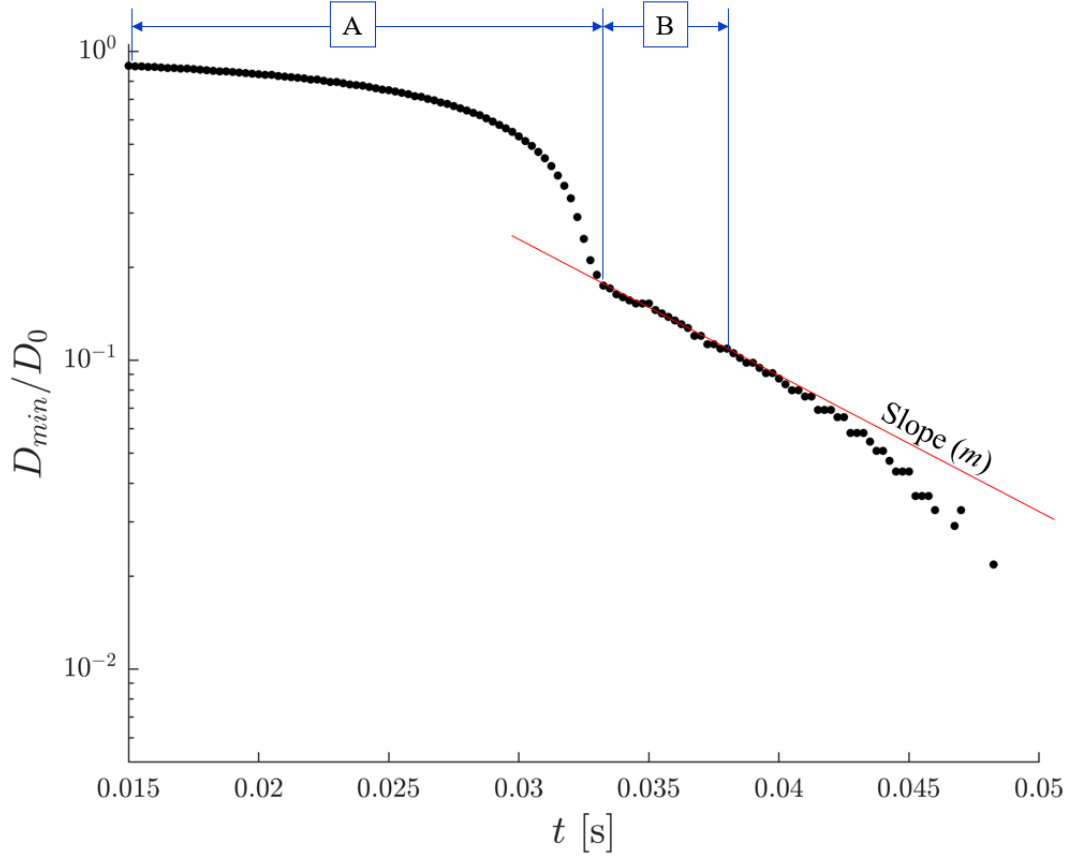


Figure 14: Log of the normalized minimum diameter ( $D_{min}/D_0$ ) of the filament versus time ( $t$ ) plot for a 50 ppm water-based polymer solution, highlighting the slope  $m$ , used for the calculation of the relaxation time  $t_r$ .

This region, showing an exponential decrease in filament minimum diameter, is expressed by Anna et al. (2001) as

$$D_{min}(t) = \left( \frac{\eta_p \cdot D_1^4}{2 \cdot t_r \cdot \sigma} \right)^{1/3} \cdot \exp\left(-\frac{t}{3 \cdot t_r}\right), \quad (24)$$

where,  $\eta_p$  is the polymeric contribution to the viscosity,  $\sigma$  is the surface tension and  $D_1$  is the minimum diameter at the start of the elastic regime in analysis, as considered by Anna et al., (2001). On dividing both side by  $D_0$  and taking natural log of both side of equation 24, we obtain

$$\frac{D_{min}(t)}{D_0} = \frac{1}{D_0} \left( \frac{\eta_p \cdot D_1^4}{2 \cdot t_r \cdot \sigma} \right)^{1/3} \cdot \exp\left(-\frac{t}{3 \cdot t_r}\right), \quad (24.1)$$

and

$$\ln\left(\frac{D_{min}(t)}{D_0}\right) = \ln\left[\frac{1}{D_0} \left( \frac{\eta_p \cdot D_1^4}{2 \cdot t_r \cdot \sigma} \right)^{1/3}\right] + \left(-\frac{t}{3 \cdot t_r}\right). \quad (24.2)$$

This expression represents the slope – intercept form for semi log plot:  $\ln(y) = mx + \ln(b)$ , with  $m$  and  $b$  representing slope and vertical intercept respectively. This, when represented in terms of the log of the normalized minimum diameter ( $D_{min}/D_0$ ) versus time ( $t$ ) gives

$$\ln\left(\frac{D_{min}(t)}{D_0}\right) = \ln(b) + (m \cdot t). \quad (25)$$

By comparing 24.2 and 25, we get the relationship between the relaxation time ( $t_r$ ) and slope ( $m$ ) as

$$m = -\frac{1}{3 \cdot t_r}; \quad \text{or} \quad t_r = -\frac{1}{3 \cdot m}. \quad (26)$$

From the  $\ln(D_{min}/D_0)$  versus time ( $t$ ) data, the portion of the exponential decrease of the minimum diameter was extracted and a linear fit is applied using MATLAB ‘*lmdivide*’ function to solve for slope ( $m$ ) and y-intercept ( $b$ ). With this value of slope, the relaxation time ( $t_r$ ) was calculated using equation 26 (refer to appendix D for relaxation time value of each sample point).

With the relaxation time ( $t_r$ ) value from (26) and shear rate ( $\gamma_s$ ) calculated from (22.2), The Weissenberg number ( $Wi$ ) for each sample point is calculated using equation 7.



### 3.7 Uncertainty analysis for $C_f$ , $Re$ and $Wi$ .

Here we estimate the uncertainty associated with the measurements of  $C_f$ ,  $Re$  and  $Wi$  by identifying the measurements uncertainties for all the independent readings and measurements obtained from the flow loop, shear viscosity measurements and extensional viscosity measurements, and applying the propagation of uncertainties progressively to the indirect measurements and calculations, up to the equations for  $C_f$ ,  $Re$  and  $Wi$ , to obtain their relative uncertainties.

The process used to calculate the relative uncertainty is briefly explained as follows. For a variable  $z$ , which is a function of variables  $p$ ,  $q$ , and  $r$  ( $z = F(p, q, r)$ ), the relative uncertainty of  $z$  ( $\delta_z/z$ ), for the absolute uncertainties of the independent variables  $p$  ( $\delta_p$ ),  $q$  ( $\delta_q$ ), and  $r$  ( $\delta_r$ ) is given by

$$\frac{\delta_z}{z} = \sqrt{\left[\left(\frac{\delta_p}{p}\right)^2 + \left(\frac{\delta_q}{q}\right)^2 + \left(\frac{\delta_r}{r}\right)^2\right]}, \quad (27)$$

To calculate the percentage uncertainty (relative uncertainty  $\times 100$ ) of  $C_f$ ,  $Re$  and  $Wi$ , we need to first establish the absolute uncertainty of all the independent parameters that  $C_f$ ,  $Re$  and  $Wi$  are a function of. These parameters are listed below with their absolute uncertainty calculations.

1. Temperature ( $T$ ) in °C: The resolution of the readings from the thermocouple is 0.1 °C. So, the absolute uncertainty for this reading will be  $\pm 0.05$  °C.
2. Mass flow rate ( $\dot{M}$ ) in kg/s: The resolution of the reading from the flow meter is 0.0001 kg/s. So, the absolute uncertainty for this reading will be  $\pm 0.00005$  kg/s or  $\pm 5e-5$  kg/s.
3. Pressure drop ( $\Delta P$ ) in psi: The resolution of the reading from the pressure transducer calibration is 0.001 psi. So, the absolute uncertainty for this reading will be  $\pm 0.0005$  psi or  $\pm 5e-4$  psi.

4. Pipe inner diameter ( $D$ ) in m: The least count of the diameter gauge to measure the inner diameter is 0.1 mm or 0.0001 m. So, the absolute uncertainty for this measurement will be  $\pm 0.0001$  m or  $\pm 1e-4$  m.
5. Length between pressure port ( $L$ ) in m: This is measured using a standard measuring tape with the least count of 1 mm or 0.001 m. So, the absolute uncertainty for this measurement will be  $\pm 0.001$  m or  $\pm 1e-3$  m.
6. Zero rate viscosity ( $\mu_0$ ) in Pa.s: The resolution of the readings from the torsional rheometer is  $1e-8$  Pa.s. So, the absolute uncertainty for this reading will be  $\pm 5e-8$  Pa.s.
7. Infinite rate viscosity ( $\mu_\infty$ ) in Pa.s: The resolution of the readings from the torsional rheometer is  $1e-8$  Pa.s. So, the absolute uncertainty for this reading will be  $\pm 5e-8$  Pa.s.
8. Consistency ( $c$ ) in s: The resolution of the readings from the torsional rheometer is  $1e-7$  s. So, the absolute uncertainty for this reading will be  $\pm 5e-7$  s.
9. Minimum diameter of the filament ( $D_{min}$ ) in m: This measurement is generated from the pixel resolution and magnification of the high-speed camera, giving the measurement resolution of 0.0046 mm or  $4.6e-6$  m per pixel. So, the absolute uncertainty for this measurement will be  $\pm 4.6e-6$  m.
10. Nozzle diameter ( $D_0$ ) in m: This measurement is generated from the pixel resolution and magnification of the high-speed camera, giving the measurement resolution of 0.0046 mm or  $4.6e-6$  m per pixel. So, the absolute uncertainty for this measurement will be  $\pm 4.6e-6$  m.
11. Time ( $t$ ) in s: The time reading is generated from the frame rate of the high-speed camera, for our measurements the minimum frame rate used was 4000, giving the least count of  $2.5e-4$  s. So, the absolute uncertainty for this reading will be  $\pm 1.2e-4$  s.

Table 5 lists the absolute uncertainty for the independent variables and the corresponding percentage uncertainty of  $C_f$ ,  $Re$  and  $Wi$  along with the equation reference.

(a)	Percentage uncertainty, $C_f$	Absolute uncertainty for independent parameters					Equation reference
	$\pm 0.8\%$	$T$ (°C)	$\dot{M}$ (kg/s)	$\Delta P$ (psi)	$D$ (m)	$L$ (m)	(19 – 21)
(b)	Percentage uncertainty, $Re$	Absolute uncertainty for independent parameters					Equation reference
	$\pm 0.8\%$	$T$ (°C)	$\dot{M}$ (kg/s)	$D$ (m)	$\mu_0$ (Pa.s)	$\mu_\infty$ (Pa.s)	$c$ (s)
(c)	Percentage uncertainty, $Wi$	Absolute uncertainty for independent parameters			Equation reference		
	$\pm 6.0\%$	$D_{min}$ (m)	$D_0$ (m)	$t$ (s)	(7) (26)		

Table 5: Percentage uncertainty calculations for (a)  $C_f$ , (b)  $Re$  and (c)  $Wi$ , with absolute uncertainty for independently measured variables for each of them, along with reference to the equation used.

## Chapter 4

# Results

This section brings together the measurements of  $C_f$ ,  $Re$  and  $Wi$  obtained from section 3.4, 3.5 and 3.6 respectively and presents graphically as  $C_f$  versus  $Re$  plots and combines that with the value of  $Wi$  for each data point by color mapping. This allows for observation of any relation between  $C_f$ ,  $Re$ , and  $Wi$ , and understand the dependency of  $C_f$  on  $Wi$  and  $Re$ . Furthermore, this section also discusses the transition from the value of  $Wi$  calculated from wall shear rate to a calculated value of  $Wi$  using bulk shear rate, to eliminate the dependency of  $Wi$  on  $\Delta P$ , so a correlation between  $Wi$  and  $C_f$  can be establish without the need of conducting pipe flow tests (refer to section 4.2 for details).

### 4.1 Friction Factor

As discussed in section 3.3.4, for the water-based polymer solution test, we first obtained a set of data for  $C_f$  and  $Re$  for the baseline water test to confirm the alignment with the Newtonian values. Three tests per pipe size were conducted to check repeatability, the average of the three tests are presented for each pipe size in figure 15.

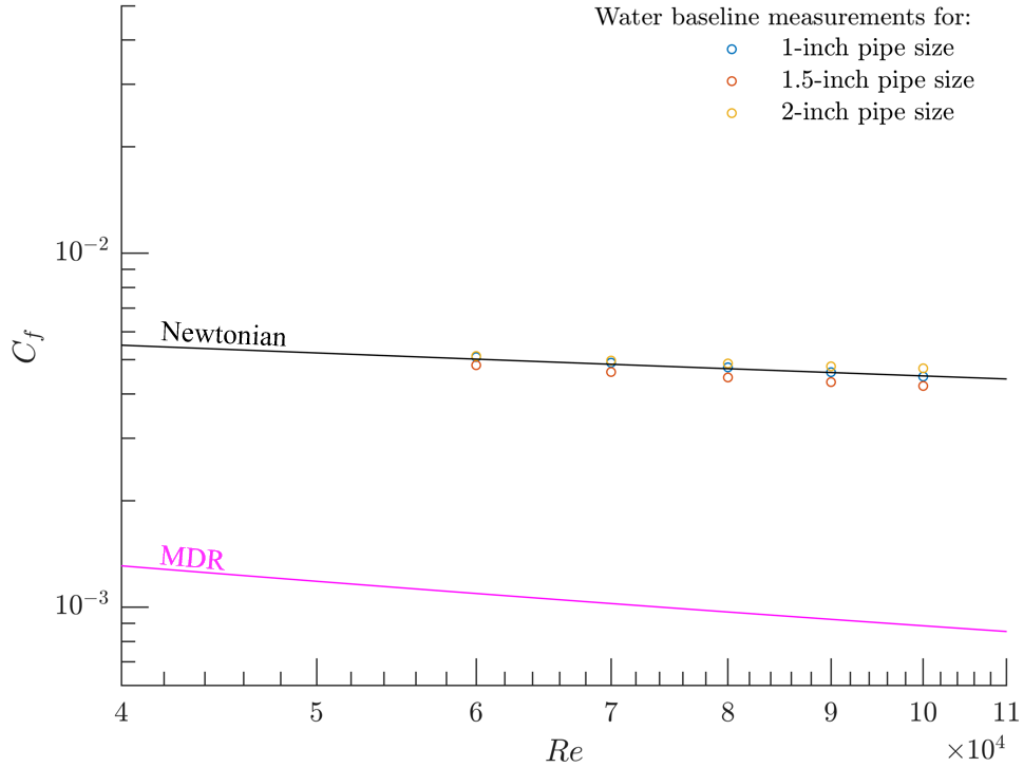


Figure 15:  $C_f$  versus  $Re$  plot for baseline water test showing the average of three test measurements for each pipe sizes.

In the above plot, the black curve represents the relation between  $C_f$  and  $Re$  for Newtonian fluids in smooth pipes, given by the equation 14, and the magenta color curve is representing the MDR asymptote curve as reported by Virk et al. (1970) and Virk (1971) in equation 17. The water baseline test measurements, being Newtonian, showed good alignment with the Newtonian curve. The 1-inch pipe size test shows a very close alignment, and the 1.5-inch and 2-inch pipe size test showed a small but consistent off-set from the Newtonian values but still within the uncertainty for the  $C_f$  as discussed in section 3.7. The close alignment and repeatability of these measurements provided enough confidence to proceed with the polymer solution tests.

The polymer solution test provided a set of data for  $C_f$ ,  $Re$  and  $Wi$  for five different  $Re$  flow and 6-8 different %DR, amounting to 30-40 data points per pipe size. The outcome of each test in terms of the %DR achieved and the  $C_f-Re$  relation for each test is discussed next.

For the 1-inch pipe size, a total of 8 polymer tests were conducted with different degradation time for each test aiming to achieve an evenly spaced %DR. Table 6 provide the details of the %DR achieved corresponding to the degradation time identified for that test. Here, %DR is calculated as  $(\Delta P_{water} - \Delta P_{polymer}) / \Delta P_{water} \times 100$ , where  $\Delta P_{water}$  and  $\Delta P_{polymer}$  are the average  $\Delta P$  value at mass flow of 1.681 kg/s, for water and polymer solution respectively.

Test	Degradation duration at 1300 RPM (s)	Average $\Delta P$ at mass flow of 1.681 kg/s (PSI)	%DR (%)
Water (Baseline)	-	0.816	0.0
Polymer test 1	0	0.194	76.2
Polymer test 2	30	0.223	72.7
Polymer test 3	50	0.302	63.0
Polymer test 4	90	0.346	57.5
Polymer test 5	220	0.412	49.6
Polymer test 6	600	0.486	40.4
Polymer test 7	1500	0.569	30.2
Polymer test 8	2880	0.596	27.0

Table 6: %DR achieved corresponding to the degradation time for the water-based polymer solution in 1-inch pipe size.

A total of 40  $C_f$  values were obtained from these eight polymer solution tests, each corresponding to a  $Re$  value, as presented in figure 16.

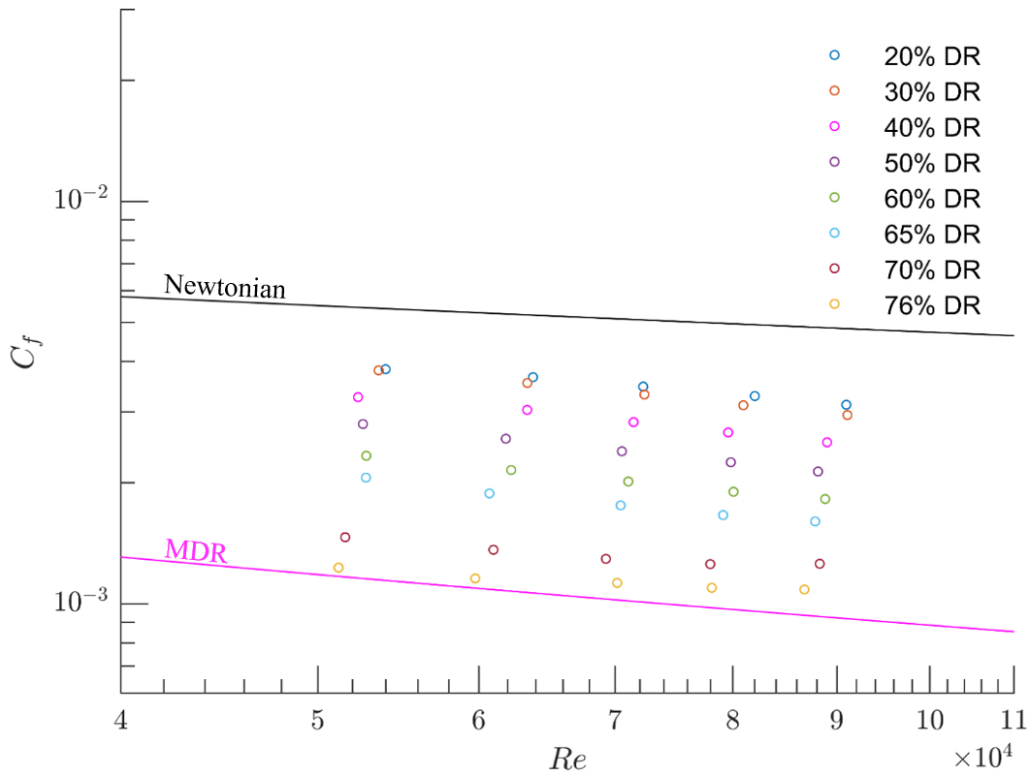


Figure 16:  $C_f$  versus  $Re$  plot for water-based polymer solution test in 1-inch pipe size, showing the five measurements for each %DR.

Here, each row of the same color data points represents the five mass flow rates measured for a specific %DR, and as the %DR decreases for each consecutive test, due to higher degradation, each row shifts up almost parallel to each other, implying no major polymer degradation within the range of  $Re$  measured. This applies more to 65% and lower DR cases. A small detachment of the 76% and 70% DR data points from the MDR line is seen for higher  $Re$  values because, for both these cases the initial polymer degradation was very less, and for higher  $Re$  values, the higher pump RPM caused some degradation in the polymer solution resulting in a lower %DR. Additionally, It can be observed that the 76% DR row, which is the undegraded 50 ppm polymer solution, almost approaches the MDR, the maximum drag reduction asymptote presented in equation 20. This implies that a concentration increase above 50 ppm would not result in any

significant increase in the DR, on the contrary, DR may decrease due to the increase in viscosity of the solution.

One more thing to note here is the shift in the  $Re$  values for each data point from the baseline  $Re$  values of 60000, 70000, 80000, 90000, and 100000 mentioned in section 3.3.1. This reduction in  $Re$  of about 10000 for each data point can be attributed to the increase in viscosity of the polymer solution compared to water.

For 1.5-inch pipe size, a total of 7 polymer tests were conducted with different degradation time for each test aiming to achieve an evenly spaced %DR. Table 7 provide the details of the %DR achieved corresponding to the degradation time identified for that test. If we compare the %DR value for the undegraded polymer solution (test 1) between 1-inch and 1.5-inch pipe size, it aligns with the observation by Lescarboursa et al. (1971), that for a particular polymer concentration, the DR reduced as the pipe size increases.

Test	Degradation duration at 1300 RPM (s)	Average $\Delta P$ at mass flow of 2.575 kg/s (PSI)	%DR (%)
Water (Baseline)	-	0.204	0.0
Polymer test 1	0	0.059	71.2
Polymer test 2	20	0.072	64.8
Polymer test 3	60	0.085	58.4
Polymer test 4	160	0.102	50.1
Polymer test 5	340	0.119	41.8
Polymer test 6	1000	0.137	32.8
Polymer test 7	3200	0.158	22.9

Table 7: %DR achieved corresponding to the degradation time for the water-based polymer solution in 1.5-inch pipe size.

A total of 35  $C_f$  values were obtained from these seven polymer solution tests, each corresponding to a  $Re$  value, as presented in figure 17.



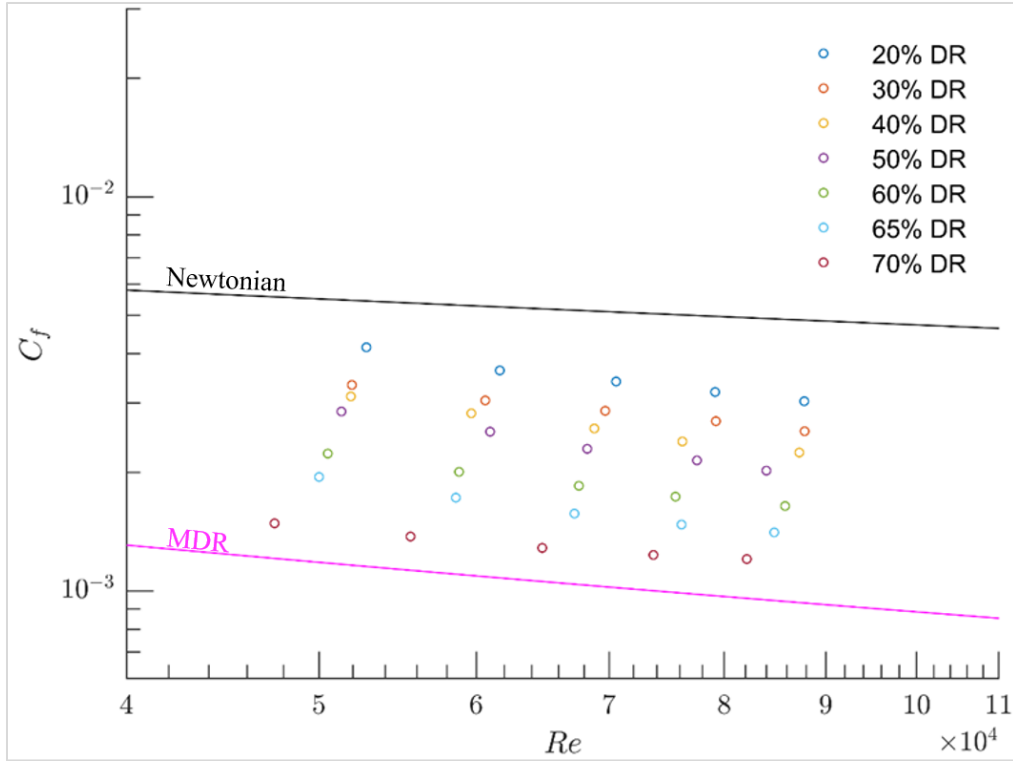


Figure 17:  $C_f$  versus  $Re$  plot for water-based polymer solution test in 1.5-inch pipe size, showing the five measurements for each %DR.

A similar shift in the  $Re$  values is observed due to the viscosity change as seen for the 1-inch case and the parallel trend of each %DR case also aligns with the previous observation from figure 16. For 1-inch and 1.5-inch pipe size test, the degradation was limited to 1300 pump PRM to manage the line pressure impact on the pump bearing seal, and for this reason the lowest %DR achieved was in the range of 20-30%.

For 2-inch pipe size, a total of 6 polymer tests were conducted with different degradation time for each test aiming to achieve an evenly spaced %DR. Table 8 provide the details of the %DR achieved corresponding to the degradation time identified for that test. The %DR value for the undegraded polymer solution (test 1) for 2-inch pipe size further supports the observation made previously that, for a particular polymer concentration, the DR reduced as the pipe size increases.

Test	Degradation duration at 1400 RPM (s)	Average $\Delta P$ at mass flow of 3.306 kg/s (PSI)	%DR (%)
Water (Baseline)	-	0.111	0.0
Polymer test 1	0	0.046	58.6
Polymer test 2	20	0.052	52.9
Polymer test 3	90	0.060	45.9
Polymer test 4	240	0.079	28.4
Polymer test 5	750	0.096	13.8
Polymer test 6	1960	0.104	6.7

Table 8: %DR achieved corresponding to the degradation time for the water-based polymer solution in 2-inch pipe size.

A total of 30  $C_f$  values were obtained from these seven polymer solution tests, each corresponding to a  $Re$  value, as presented in figure 18.

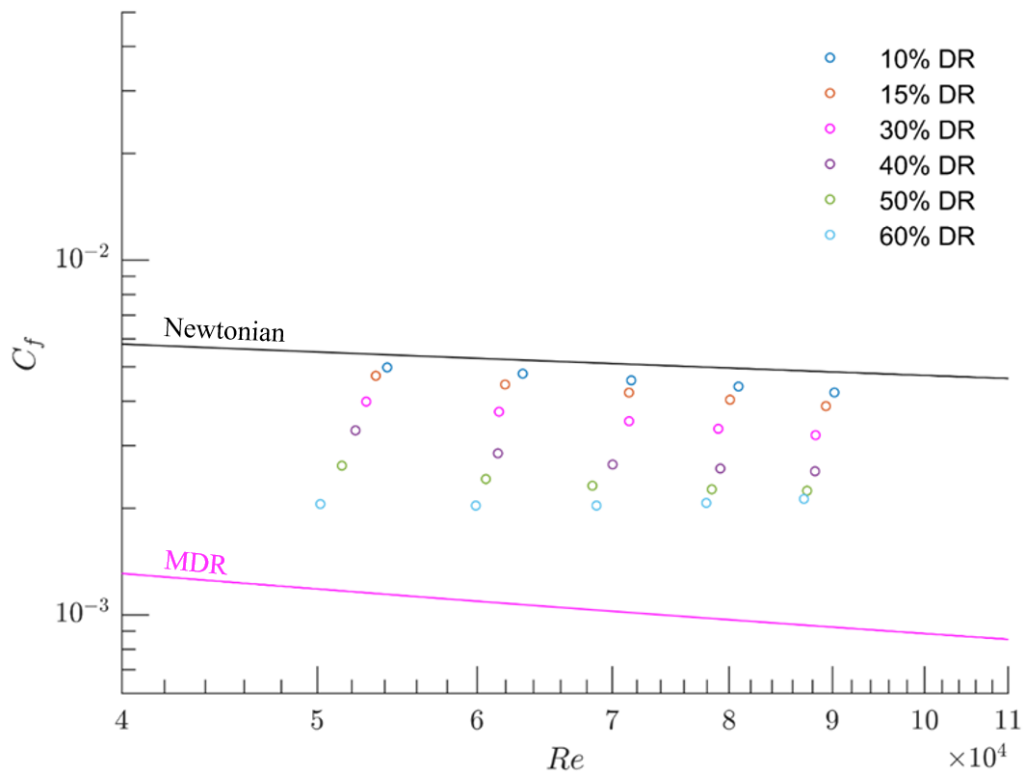


Figure 18:  $C_f$  versus  $Re$  plot for water-based polymer solution test in 2-inch pipe size, showing the five measurements for each %DR.

For the 2-inch pipe size as the line pressure for the same RPM reduces compared to 1-inch and 1.5-inch pipe sizes, the degradation was conducted at 1400 pump RPM, allowing to reach the lowest %DR of 6.7%, and populating the region of the plot that was not possible with smaller pipe diameters. Other observations like the shift in  $Re$  values and parallel shift between each %DR are similar to the previous cases.

## 4.2 Relation between $C_f$ , $Re$ and $Wi$

Each point on the  $C_f$ - $Re$  plot represents a sample collected from the pipe flow setup. This sample was tested for extensional viscosity measurements (refer to section 3.6) and a corresponding Weissenberg number ( $Wi$ ) value was associated for each sample point. These values were projected onto the  $C_f$ - $Re$  plot using a color map and an alternate representation as a contour map, shown in figure 19 and 20 respectively for the 1-inch pipe size test. Subsequently, figure 21-22 and figure 23-24 represent the plots for 1.5-inch and 2-inch pipe size test respectively. The aim of these projections is to observe how the value of  $C_f$  changes in relation to  $Wi$  and  $Re$  along the entire data point range, and can a relation be established between these parameters based on the pattern observed.

It is to be noted, however, that even though the tests were designed so that the data point range fills most of the region between the Newtonian and MDR curve, there are a few localized regions where the point density is lower than other regions and this variance in point density can impact the contour projections in those areas. So, an objective approach and cross-referencing between color and contour plots are required for analyzing the plots.

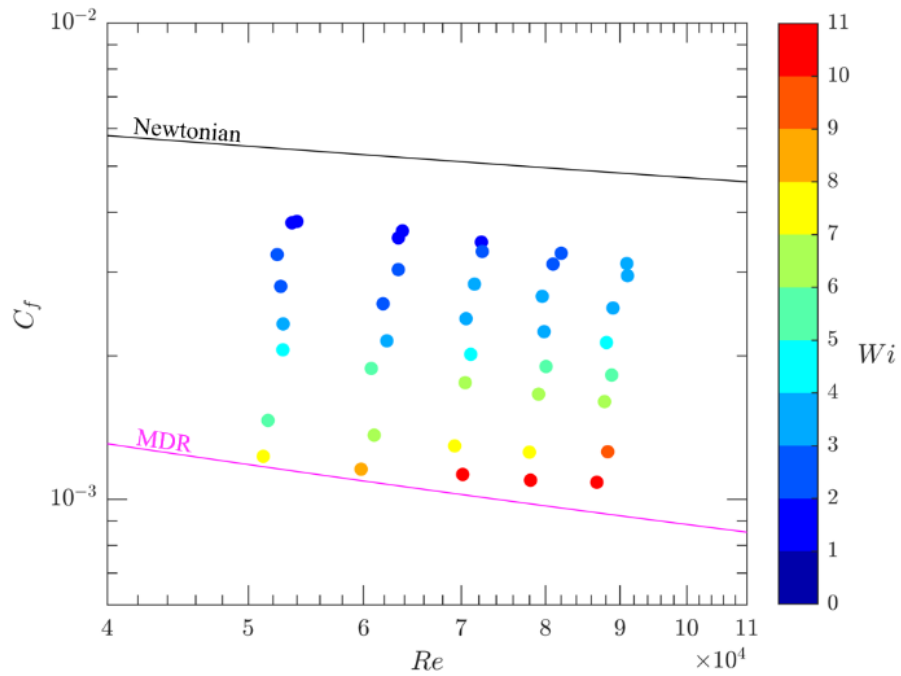


Figure 19: Data points on the  $C_f - Re$  plot are color mapped with the measured value of  $Wi$  for 1-inch pipe size.

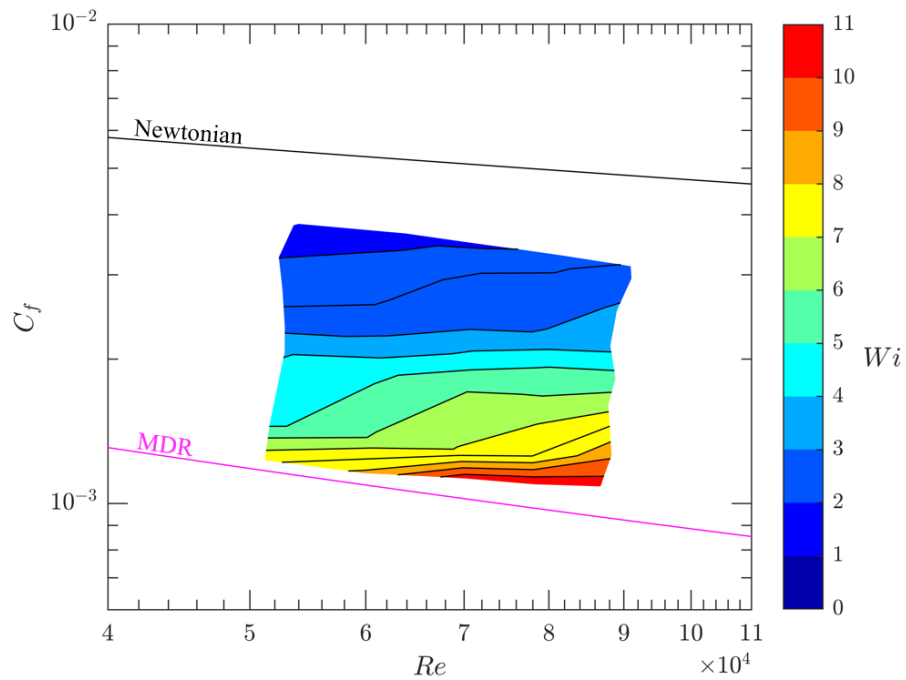


Figure 20: Data points on the  $C_f - Re$  plot are contour mapped with the measured value of  $Wi$  for 1-inch pipe size.

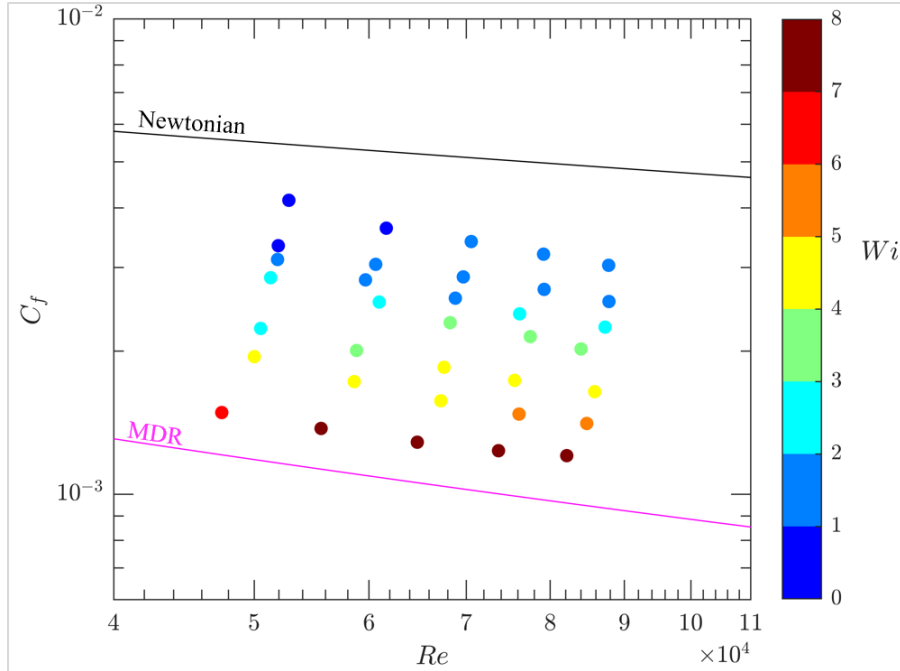


Figure 21: Data points on the  $C_f - Re$  plot are color mapped with the measured value of  $Wi$  for 1.5-inch pipe size.

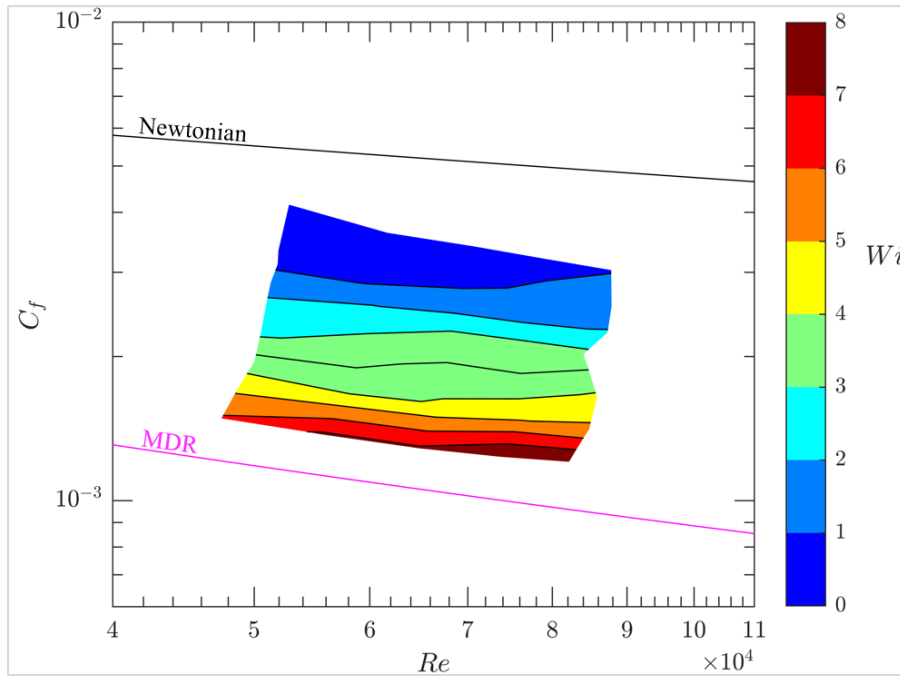


Figure 22: Data points on the  $C_f - Re$  plot are contour mapped with the measured value of  $Wi$  for 1.5-inch pipe size.

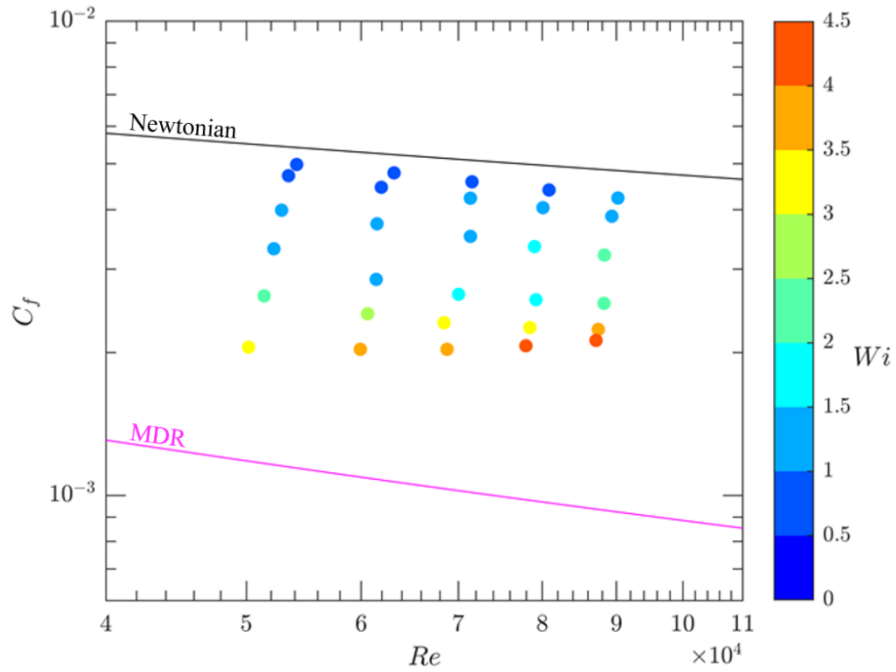


Figure 23: Data points on the  $C_f$ – $Re$  plot are color mapped with the measured value of  $Wi$  for 2-inch pipe size.

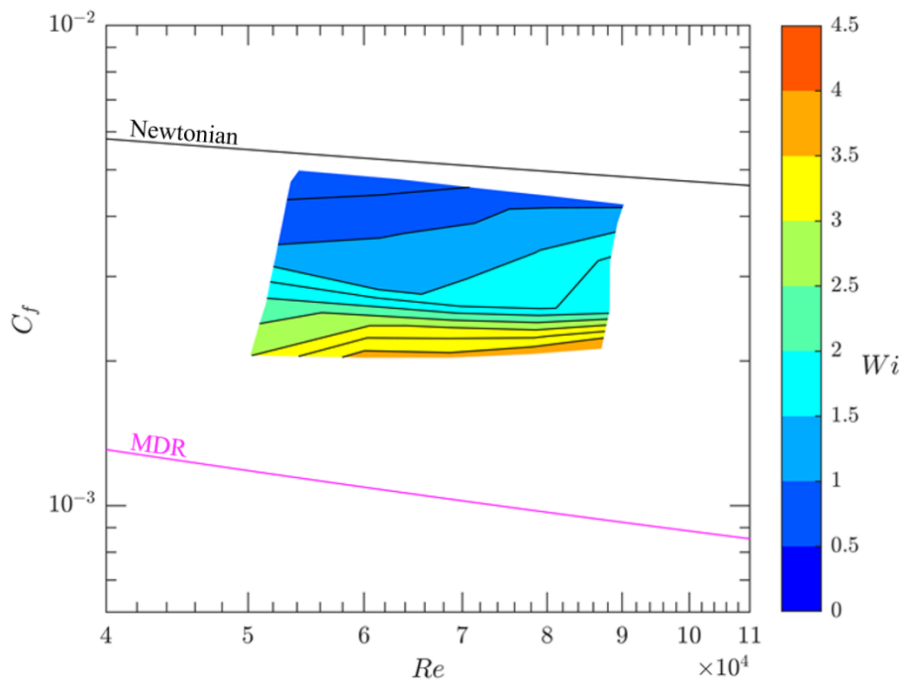


Figure 24: Data points on the  $C_f$ – $Re$  plot are contour mapped with the measured value of  $Wi$  for 2-inch pipe size.

The contour plots (20, 22 and 24), show a general horizontal alignment of the  $Wi$  value bands. From figures 19 and 20, it can be observed that a band for a particular value of  $Wi$  is aligned more horizontally towards the upper portion of the region where the data point density is more even compared to the lower portion. Same can be seen in figures 23 and 24 showing horizontal band towards the lower and higher up region, the middle portion when cross-referenced with the point data, show lower point density in that zone. This trend is more clearly observed in figures 21 and 22 with a more even and close-to-horizontal alignment of individual  $Wi$  bands, throughout the region. This demonstrates that the value of  $C_f$  changes significantly in relation to  $Wi$  and not so significantly compared to the change in  $Re$ , pointing towards a strong dependency of  $C_f$  on  $Wi$ , it can also be observed that the  $Wi$  band thickness increases as the  $Wi$  value decreases, suggesting that the rate of decrease in the value of  $Wi$  slows down as  $C_f$  increases. This change in  $Wi$  when compared to change in  $C_f$  suggests a roughly exponential relation between  $Wi$  and  $C_f$ . This provides evidence for the relation between the extensional properties of the polymer solution and drag reduction.

These relations lay a strong foundation towards developing a model describing the relationship between  $C_f$ ,  $Re$  and  $Wi$ , with the ability to predict one from the other. However, in order to achieve that and truly develop a predictive model by eliminating the need for extensive pipe flow tests, we require an alternative approach in calculating  $Wi$ , since the current method (refer to section 3.6) utilizes wall shear rate ( $\gamma_s$ ) which is calculated using equation 25.2, that requires the knowledge of shear stress at the wall ( $\tau_w$ ), which in turn is calculated using the pressure drop ( $\Delta P$ ) from the pipe flow test (refer to equation 24).

### 4.3 $Wi$ calculated from bulk shear rate ( $\gamma_b$ )

The irony of predicting  $C_f$  from  $Wi$  without pipe flow tests, while  $Wi$  being a function of  $\Delta P$  warrants for an alternate approach.  $Wi$  can also be calculated from the bulk shear rate ( $\gamma_b$ ) in pipe flow, which is a function of the bulk velocity ( $V_b$ ) and pipe diameter ( $D$ ) and is expressed as

$$\gamma_b = \frac{8 \cdot V_b}{D} . \quad (28)$$

With this representation of shear rate, the Weissenberg number calculated from bulk shear rate ( $Wi_c$ ) can be expressed as

$$Wi_c = \frac{8 \cdot V_b \cdot t_r}{D} . \quad (29)$$

With the above equation, a set of  $Wi_c$  values can be obtained corresponding to all data points presented in the previous section for all three pipe sizes. The following three figures (25, 26 and 27) represent the  $C_f-Re$  plot with the data points projected with the value of  $Wi_c$  and presented as a contour plot. These are similar to figures 20, 22 and 24 respectively with just  $Wi$  replaced by  $Wi_c$ . This gives an opportunity to compare the observations between  $Wi_c$  and  $Wi$  projections (from the previous section).



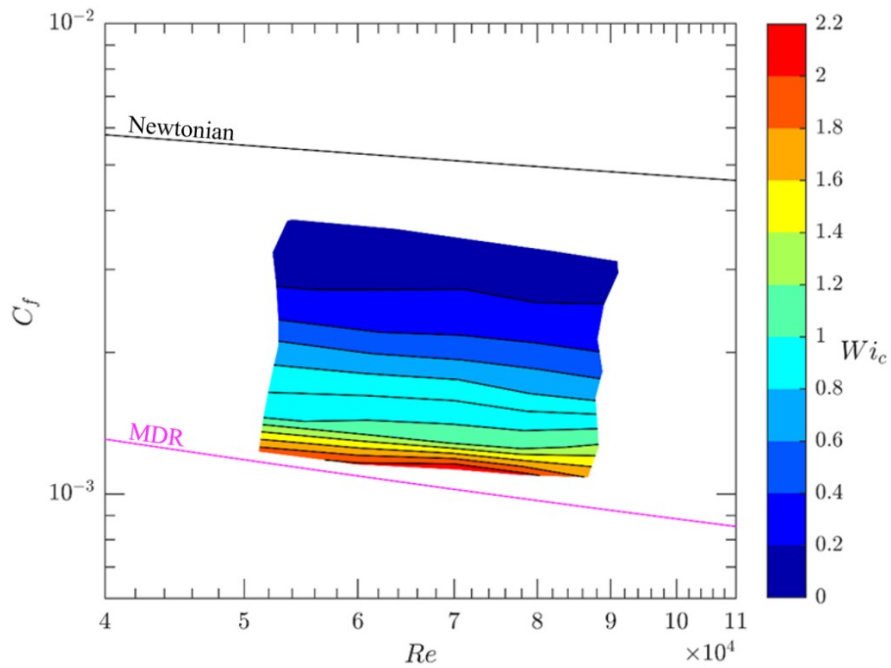


Figure 25: Data points on the  $C_f - Re$  plot are contour mapped with the calculated value of  $Wi_c$  for 1-inch pipe size.

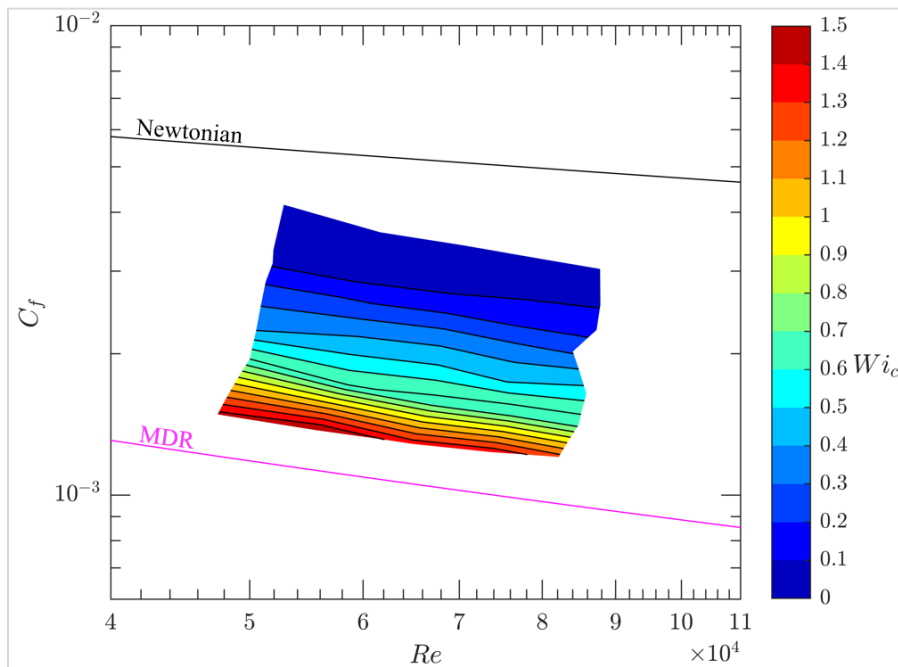


Figure 26: Data points on the  $C_f - Re$  plot are contour mapped with the calculated value of  $Wi_c$  for 1.5-inch pipe size.

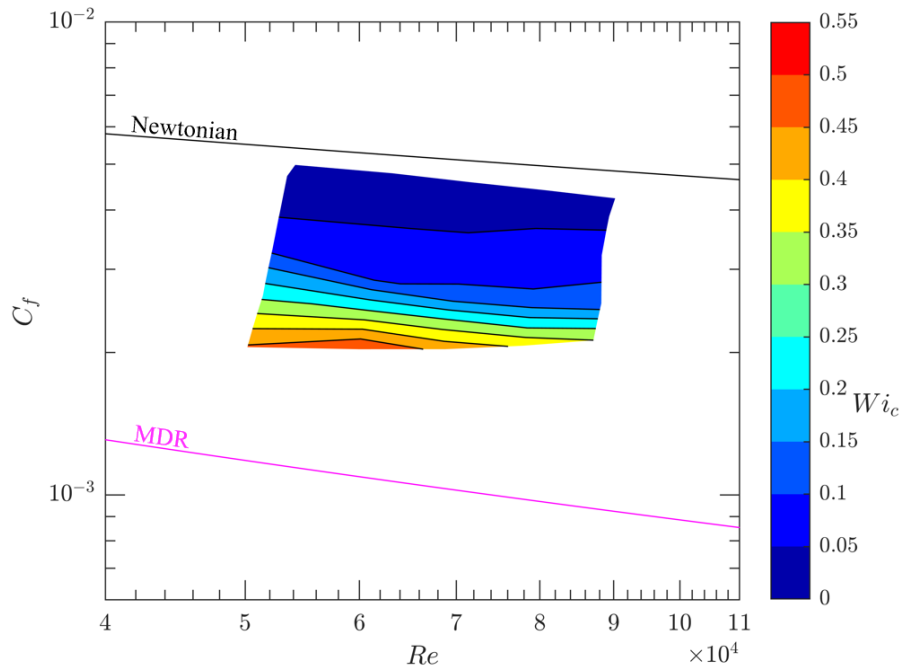


Figure 27: Data points on the  $C_f$ – $Re$  plot are contour mapped with the calculated value of  $Wi_c$  for 2-inch pipe size.

These updated plots with  $Wi_c$  show similar trends and observations as compared to the plots with  $Wi$ , providing confidence in utilizing  $Wi_c$  in place of  $Wi$ . Similar to previous observations, these plots exhibit the same horizontal alignment of the  $Wi_c$  bands, where the change in the value of  $Wi_c$  is less significant as one moves along the horizontal axis ( $Re$ ), suggesting a low dependence of  $Wi_c$  on  $Re$ , and showing significant change in the value of  $Wi_c$  along the vertical axis ( $C_f$ ), suggestive of high dependency of  $C_f$  on  $Wi_c$ . The increase in the  $Wi_c$  band thickness as the value of  $Wi_c$  decreases is also observed, which means that the rate of decrease in the value of  $Wi_c$  slows down as  $C_f$  increases, aligning with the previous observation.

Figure 28 shows this relation between  $C_f$  and  $Wi_c$ , when expressed on a linear scale.

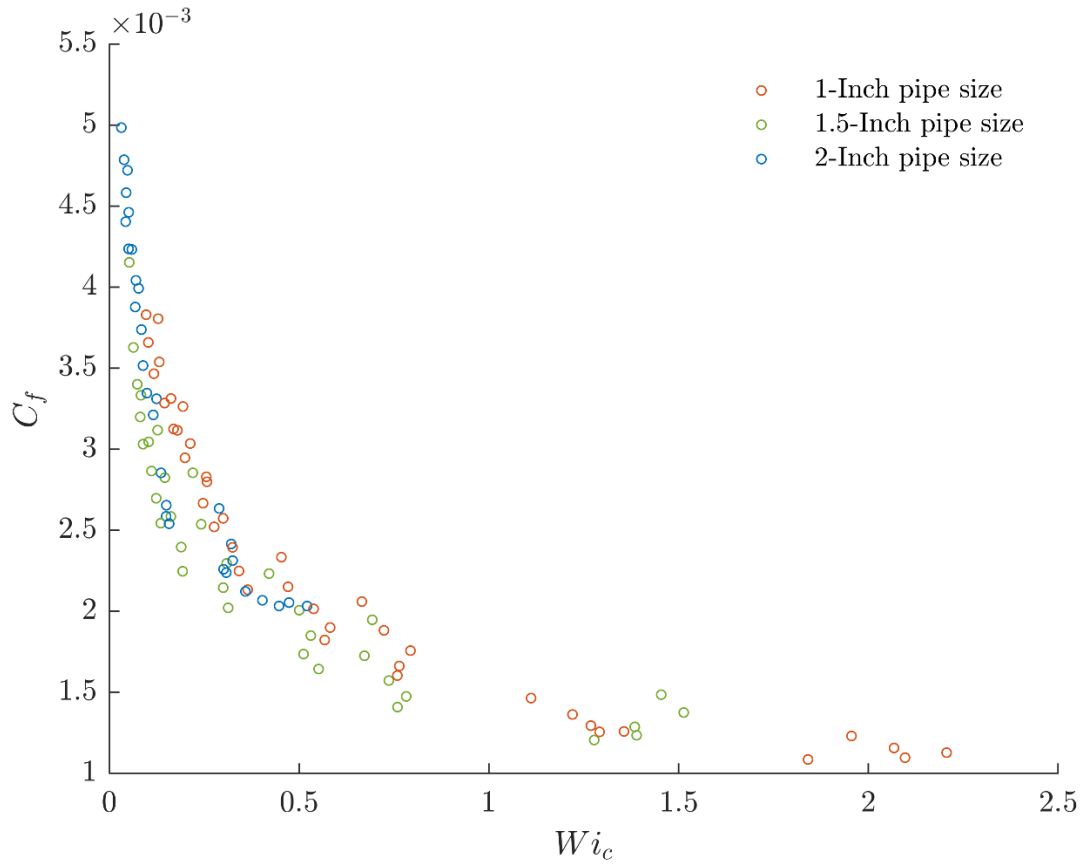


Figure 28:  $C_f$  versus  $Wi_c$  plotted for all three pipe sizes are expressed on a linear scale to show the relation between these two parameters.

This presents a good foundation for establishing a relationship between  $C_f$ ,  $Wi_c$ , and  $Re$ , and towards the development of a robust predictive model for DR through polymer rheology. The extensive water-based pipe flow and rheological tests provided a strong base of repeatable test data and the alignment of the observations between  $Wi$  and  $Wi_c$  will serve as a proof of concept and will highly influence the way the diesel-based polymer solution tests will be designed and conducted.

## Chapter 5

# Design and commissioning of a hydrocarbon flow loop

The test with water-based polymer solution gave a good insight into the relationship between  $C_f$ ,  $Re$  and  $Wi$ , but as discussed earlier, with the differences between the drag reducing polymers for water and hydrocarbons in terms of molecular weight, solubility and drag reducing capabilities, to achieve our objective of developing a predictive model for polymer drag reduction in hydrocarbons, a similar test approach is required with hydrocarbons. This presented a need for a flow facility that can safely run hydrocarbon-based polymer solutions and can produce repeatable measurements. As discussed earlier, the choice of using diesel as the base fluid was based on the facts that, firstly, diesel has a higher flash point ( $> 52$  °C) and low volatility, making it safer to handle at room temperature, and in a closed lab environment compared to other easily available hydrocarbons like gasoline and kerosine, and secondly, it has a much lower viscosity than crude oil, making the flow loop design simpler, manageable pump requirements and easier drainage of the loop for repeating tests. The flow loop facility developed for tests with diesel is similar in concept as the water test facility (detailed in section 3) with the key difference being the loop pipe size is 1-inch, a positive displacement pump is used instead of a centrifugal pump that was used in

the water-based flow loop, all components are rated for use with diesel, and the loop is designed to achieve flow  $Re$  up to 30000.

For designing the diesel flow loop, space was an important factor. With limited space in the lab, a vertical loop structure was adopted, that allowed the setup to have a small footprint area. This, in hindsight, provided easier access to equipment and sensors. The other major factor that influenced the design of the loop was the size and layout of the pump-motor assembly, as the loop's plumbing would have to be designed around that. The criteria that governed the selection of the pump and motor were compatibility with diesel fuel, capability to achieve flow rates up to 9.0 m<sup>3</sup>/hr (~40 gpm) based on our calculation to achieve  $Re$  up to 30000, achieve this flow rate at low RPMs to avoid excessive polymer degradation, electrical compatibility with the available outlets in the lab, and cost. Once the space and pump-motor assembly design were established, the diesel loop, following the same concept from the water-based loop, was designed with a storage tank that can be used for mixing the polymer, the tank inlets into the positive displacement pump, that feeds into a 1-inch pipe loop. The loop consists of a pressure relief valve for safety, a pulsation dampener to stabilize the flow, a heat exchanger to regulate the temperature, a flow meter to measure flow rates, a thermocouple to measure fluid temperature, two pressure ports with tubing to a differential pressure transducer for  $\Delta P$  measurements, diversion valves setup to be able to run the loop in either open or closed loop configurations and drainage ports at the lowest level before and after the pump stator, as the stator-rotor assembly is liquid tight seal in a positive displacement pump.

Additional safety features that were incorporated in the loop's design includes stainless steel spill trays placed under the entire loop for spill containment, proper ventilation ducts above the tank to extract any escaping vapors, and containment of diesel from the pressure transducer during the

bleeding process. Figure 29 shows an overview of the diesel flow loop with the key components highlighted. These components are detailed as follows:

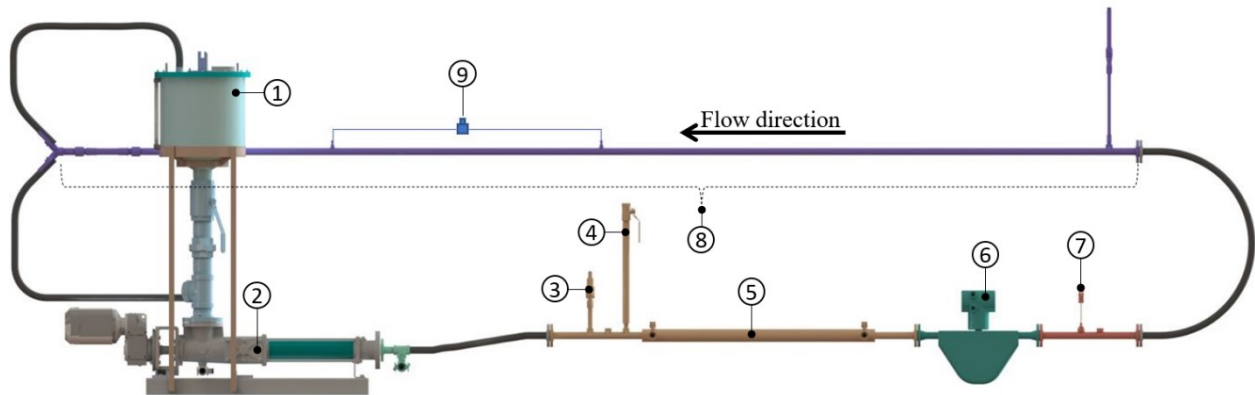


Figure 29: Overview of the pipe flow setup used for diesel-based tests, highlighting each component unit and flow direction.

1. Tank: 50 liters vertical stainless-steel tank with a 3-inch outlet.
2. Pump: NETZSCH progressive cavity pump, model-NM038BY01L06B, powered by a 3HP NORD gear motor (refer to appendix F for pump curve).
3. Pressure relief valve: Adjustable pressure relief valve set at 60 psi.
4. Pulsation dampener: In-house fabricated air column dampener to stabilize the flow.
5. Heat exchanger: In-house fabricated, concentric tube design, with a 2-inch tube jacketing the 1-inch flow pipe, with inlet and outlet ports on the 2-inch pipe to run cold/hot water to regulate the temperature.
6. Coriolis flow meter: Micro motion 1-inch F-Series Coriolis flow meter (F100S128CCAAEZZZZ) with an integral mount 1700 series transmitter (1700I12ABASZZZ) for mass flow readings.
7. Thermocouple: K-type thermocouple from Omega for temperature readings.

8. Test section: The test section is a 1-inch inner diameter, 5.08 m (200-inch) long, straight stainless-steel pipe with an upstream pressure port at 2.54 m (100-inch) from the upstream edge and the distance between the upstream and downstream port ( $L$ ) = 1.27 m (50-inch).
9. Pressure transducer: A Validyne DP-15 pressure transducer is used and is connected to the pressure port on the test section through 1/8-inch double-ferrule brass tube fittings. The Diaphragm used in the pressure transducer is: 3-32 ( $\pm 2.0$  psi).

Refer to appendix A for detailed drawing of the components and assembly of the diesel flow loop. The scope of the current work includes the design, development, and commissioning of the diesel loop. The following section details the baseline test procedure and results, that verify the loop stability and repeatability, making the loop ready for future polymer testing.

Once the loop component assembly was completed and the pump was commissioned, the entire loop was dry tested for leaks using compressed air. Upon the confirmation of no active leaks, the loop was filled with diesel fuel and the first trial run was conducted following the safe operating procedure (appendix E). During this run, the pump-VFD calibration was completed, and all equipment readings were verified. This trial also helped clean the loop from inside. The diesel was filtered at a high flow rate and then drained completely. Fresh Diesel was then introduced in the loop and was made to run through a finer filter to extract any remaining contaminant. A chiller unit was connected to the heat exchanger for temperature stabilization and the loop was run progressively to its limits to verify the  $Re$  range. The loop was able to achieve  $Re$  of 30000 at 372 RPM of the pump (maximum rated pump RPM is 400).

## 5.1 Calculation of mass flow rate

The test  $Re$  for diesel test was set to 5000, 10000, 15000, 20000, 25000 and 30000 as a baseline, a diesel sample was tested for shear viscosity following the same procedure as mentioned in section 3.5. Measured viscosity of diesel ( $\mu_d$ ) = 0.00344 kg/m-s, at  $20\pm 0.5$  °C. and measured density of diesel ( $\rho_d$ ) = 843.0 kg/m<sup>3</sup>, at  $20\pm 0.5$  °C. Table 9 mentions the mass flow rate values corresponding to the  $Re$  range using equation (21) and its corresponding VFD set value to achieve that mass flow.

Pipe size = 1-inch $D = 0.0267$ m		
Re	$\dot{M}_d$ (kg/s)	VFD (Hz)
5000	0.360	8.9
10000	0.720	17.4
15000	1.080	26.0
20000	1.440	34.8
25000	1.800	43.7
30000	2.160	52.9

Table 9: Mass flow rates with their corresponding VFD set point values are listed to achieve the required  $Re$  for pipe flow test with diesel for 1-inch pipe size with a measured inner diameter ( $D$ ).

## 5.2 De-airing and transducer bleeding procedure:

When the loop is first filled with diesel, there are many air pockets all around the loop at locations like pipe joints, pipe bends and transducer tubing. These pockets, if not removed, can mix with the flow stream, and negatively impact the measurements. So, to ensure the removal of all air pockets and micro bubbles, a systematic process is followed to get the same level of flow quality every time. This process is explained step by step as follows:

Step 1: Ensure open loop valve configuration (refer to appendix E for valve configuration).



Step 2: Ensure both the pressure transducer valves are closed.

Step 3: Set the VFD at 10 Hz for 5 minutes to allow bigger air bubbles to escape from the open surface in the tank.

Step 4: During this 5 minute, in open loop configuration, open Valve-V3 for 5 seconds then close it. This is to let any trapped bubbles escape from the closed loop section.

Step 5: Stop VFD and let the system rest for 5 minutes. This will allow micro bubbles to coagulate into bigger bubbles.

Step 6: Set the VFD to 20 Hz for 15 seconds, this will dislodge air bubbles trapped in the pipe joints. These bubbles will now be visible in the flow stream.

Step 7: Bring the VFD down from 20 Hz to 8 Hz and run for 5 minutes. Follow step 4 intermittently. This will allow the dislodged bubbles to escape through the tank open surface.

Step 8: Repeat steps 5 to 7 two more times.

Step 8: Stop VFD and allow the fluid to rest for 10 minutes. This will allow any remaining micro bubbles in the stream to rise and accumulate, forming bigger bubbles.

Step 9: Repeat steps 5 to 7 two more times.

Step 10: Continue running the VFD at 10 Hz for 10-15 minutes, use this run time to regulate the fluid temperature to achieve  $20 \pm 0.5^\circ\text{C}$ .

Step 11: Set VFD to 15 Hz (still in open loop configuration). With the pressure transducer bypass valve open, open both bleed valves.

Step 12: Very slowly open both pressure port valves, allowing diesel into the transducer. This will start the bleeding. Let the bleeding continue for 3-4 minutes.

Step 13: Close both bleed valves.

Step 14: With the transducer bypass valve open, keep running at 15 Hz for 2 minutes. This will push out any air bubbles in the transducer tubing, through the bypass line into the main pipe, which can then be escaped out in the tank.

Step 15: Stop VFD and close the transducer bypass valve.

Step 16: Ensure fluid temperature within  $20 \pm 0.5$  °C, if not, set the VFD at 10 Hz with the heat exchanger running till the correct temperature is achieved.

The system will now be ready for the test to begin.

### 5.3 Test procedure for baseline diesel test.

Three independent tests with diesel are conducted to confirm alignment with the Newtonian  $C_f-Re$  curve (14) and repeatability of the results. Before the test, the tank is filled with 35 liters of diesel, which is introduced into the loop, the loop de-airing and transducer bleeding process is then executed as detailed in section 5.2. The test is run using the LabVIEW software, the operator can control the VFD frequency (Hz) that translates to the pump RPM to achieve the required mass flow rates (refer to table 9). Table 10 breaks down the test procedure steps to run the baseline diesel test for the six mass-flow values and aligns each step with the data log time and providing actions or a frequency set values against each step, while maintaining the flow temperature within  $20 \pm 0.5$  °C.

Step	Log time stamp	Action (Diesel test)			Temperature condition	
1	-	Set closed loop configuration and tank outlet open.			20±0.5 °C	
2	-	Turn ON: VFD (set at zero Hz), flow meter and transducer demodulator.				
3		Open both pressure port valves and close the transducer bypass valve.				
4	0	Start data log.				
5	120	Set VFD to 10 Hz.				
			Hz	Verify $\dot{M}_d$ values		
6	420	Set VFD →	8.9	0.360		
7	780	Set VFD →	17.4	0.720		
8	1140	Set VFD →	26.0	1.080		
9	1500	Set VFD →	34.8	1.440		
10	1860	Set VFD →	43.7	1.800		
11	2220	Set VFD →	52.9	2.160		
12	2580	Set VFD →	0.0	0.0		
13	2700	Stop data log.				-
14	-	Open the transducer bypass valve and then close both pressure port valves.				-
15	-	Turn OFF: - VFD, flow meter and transducer demodulator				-
16	-	Drain the loop. (refer to appendix E for procedure)			-	

Table 10: Step-by-step test procedure aligning with the LabVIEW log time stamp, for baseline diesel pipe flow test for 1-inch pipe sizes.

## 5.4 Measurements

Three tests were conducted as per the procedure mentioned in section 5.3 to get the baseline data and confirm repeatability. The pressure drop ( $\Delta P$ ) versus time ( $t$ ) plots are presented for all three tests.

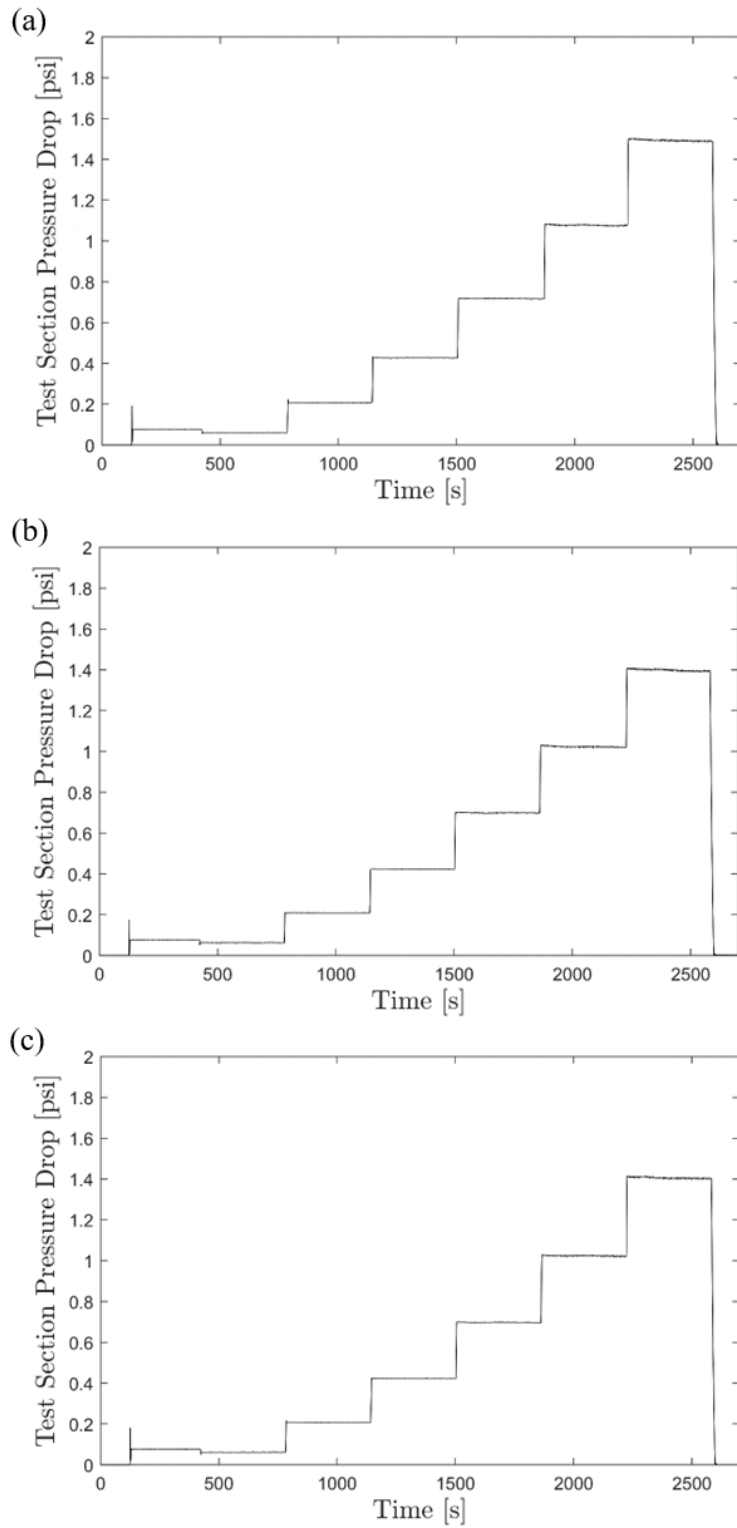


Figure 30:  $\Delta P$  versus time ( $t$ ) plots for diesel baseline test in 1-inch pipe sizes for (a) Test 1, (b) Test 2, and (c) Test 3, showing the measurements for six  $Re$  values for each test.

It can be observed from figure 30 that the change in the value of  $\Delta P$  is immediate as the mass flow rate changes and stays stable for the entire duration of 6 minutes. This is due to the positive displacement pump that gives an immediate change in mass flow as the RPM increases and a steady flow rate for a fixed RPM of the pump, unlike the centrifugal pump that required a PID controller to achieve this (refer to the water-based plots in appendix B to observe the contrast). All three plots demonstrate a stable  $\Delta P$  measurement and repeatable results.

The  $\Delta P$  values were utilized from these tests along with the density and viscosity values (section 5.1) to calculate  $C_f$  (reference to equations 20 and 21) and  $Re$  (reference to equation 23). The  $C_f$ – $Re$  data for the three tests are presented in figure 31.

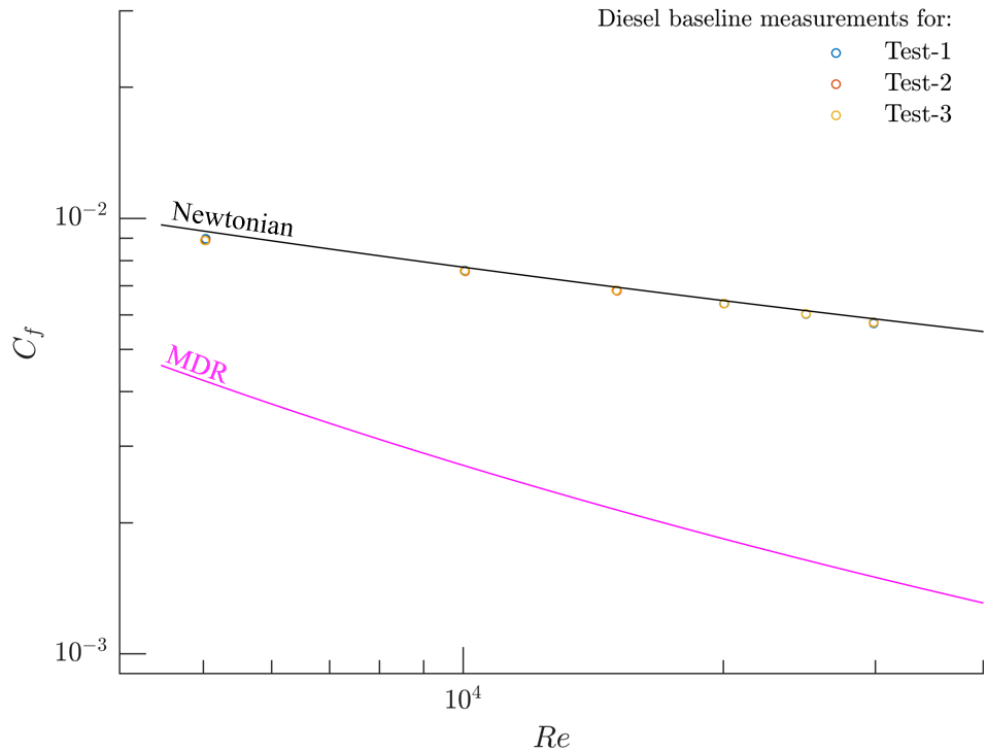


Figure 31:  $C_f$  versus  $Re$  plot for diesel baseline test in 1-inch pipe sizes, showing the overlapped measurements of three tests each for six  $Re$  values.

The tests results show good alignment with the Newtonian  $C_f - Re$  curve (14), there is a small noticeable off-set between the data points and the Newtonian curve, but this variance is within the measurement uncertainty discussed in section 3.7. The different colors for each test are not clear because of a good overlap between the three tests, suggesting good repeatability.

These results demonstrate that the diesel loop is working as it was designed to and can achieve the maximum required  $Re$  of 30000. The results also indicate the effectiveness of the de-airing and transducer bleeding process, and the stability of the heat exchanger in maintaining the temperature within  $20 \pm 0.5$  °C. Additionally, these tests have also provided the opportunity to test the loop filling and draining process and fine tune any step to ensure personnel and equipment safety. All of this provides the required confidence in the diesel flow loop and confirms its readiness for the future polymer solution tests.

## Chapter 6

# Conclusions and future work

The following sections discuss the conclusion of the water-based polymer tests, its impact on the design of diesel tests, and lay down the framework for the future experimental work to be conducted on the diesel flow loop.

### 6.1 Conclusion

Drag reduction in turbulent pipe flow has a major impact in hydrocarbon transport through pipelines over long distances, but the lack of mathematical understanding of this phenomenon has limited it to a trial-based use in industries. The present work on the water-based polymer solution tests have played an important role in expanding our understanding of how the rheological properties of polymer solutions influence drag reduction in turbulent pipe flows and is an important first step towards the progressive development of the model to predict DR from rheology.

Through the baseline tests measurement, and its alignment to the Newtonian values, the measurement capability and repeatability of the water flow loop was established, which was

crucial for the validation of all later tests and measurements. The polymer solution tests, thereafter, provided a significant data set over a wide range of  $C_f$  and  $Re$ . The span of this data set, along with the extensional rheological measurements for  $Wi$  for each data point has helped in drawing a correlation for the values of  $Wi$  based on  $C_f-Re$  point grid. These contour map projections have provided the following key observations:

1. The horizontal alignment of the  $Wi$  value bands on the  $C_f-Re$  data set in the contour map demonstrates that  $C_f$  has a high dependency on  $Wi$ , and a low dependency on  $Re$ .
2. The change in the value of  $C_f$  compared to the value of  $Wi$  is not a linear relation and can be observed from the varying thickness of the  $Wi$  bands. This suggests that the decay of  $Wi$  slows down for a constant increase in  $C_f$ .
3.  $Wi$  and  $C_f$  are inversely related. So, as the value of  $Wi$  increases, the  $C_f$  value decreases. In other words, the higher the relaxation time of a solution, the lower will be its  $C_f$ , leading to a higher drag reduction.

These observations will serve as a foundation for the development of an initial model to predict drag reduction from the extensional properties of the solution and have been instrumental in establishing confidence that will drive the future work on diesel, which will provide scalable models that can be utilized at a larger scale.

The water test facility has also provided a good reference for the design and fabrication of the diesel flow loop, which extends further in terms of safety and ease of use. The successful assembly and commissioning of the diesel flow loop was achieved, and the three baseline test results for the relation between  $C_f$  and  $Re$  exhibits a close and consistent alignment to the expected Newtonian values, deeming the diesel flow loop measurement both accurate and repeatable.



## 6.2 Future work

The future work entails test on the diesel flow loop similar to the water-based polymer solution tests, a detailed account is summarized as follows:

1. Six  $Re$  values and their corresponding mass flow rates have been identified for the diesel-polymer test (refer to section 5.1)
2. A polymer concentration test will be run to identify the relation between concentration (ppm) and %DR. This will be an exclusive test for diesel loop as intentional degradation method that was applied for the water-polymer test using the centrifugal pump will not work for the diesel loop due to the use of positive displacement (low shear) pump.
3. Once the ppm - %DR relation is established, the diesel-polymer test can be designed and executed.
4. Based on the results from the diesel test a correlative model will be developed and it will be tested experimentally.
5. The success of the diesel tests will pave the path for future tests with progressively larger diameter pipes, aiming at refining the predictive model as more and more data is gathered.

# References

- Anna, S. L., and G. H. McKinley. "Elasto-capillary thinning and breakup of model elastic liquids." *Journal of Rheology* 45, no. 1 (2001): 115-138.
- Barnes, H. A., J. F. Hutton, and K. Walters. *An introduction to rheology*. Vol. 3. Elsevier (1989): 75-96
- Benedict, R. P. "Fundamentals of pipe flow." (No Title) (1980): 6.2, 229-230.
- Benedict, R. P. "Fundamentals of pipe flow." (No Title) (1980): 6.5, 235.
- Benedict, R. P. "Fundamentals of pipe flow." (No Title) (1980): 6.6, 237.
- Benzi, R., E. DE ANGELIS, V. S. L'vov, I. Procaccia, and V. Tiberkevich. "Maximum drag reduction asymptotes and the cross-over to the Newtonian plug." *Journal of Fluid Mechanics* 551 (2006): 185-195.
- Blasius P.R.H., "The Similarity Law for Friction Processes in Liquids," *Phys. Z.*, Vol. 12 (1911): 1175.
- Burger, E. D., W. R. Munk, and H. A. Wahl. "Flow increase in the Trans Alaska Pipeline through use of a polymeric drag-reducing additive." *Journal of petroleum Technology* 34, no. 02 (1982): 377-386.

- Burgers, J. M. "Mechanical considerations-model systems-phenomenological theories of relaxation and of viscosity." First report on viscosity and plasticity 1 (1935).
- Cheng, N. S. "Formula for the viscosity of a glycerol– water mixture." *Industrial & engineering chemistry research* 47, no. 9 (2008): 3285-3288.
- Chhabra, R. P. "Non-Newtonian fluids: an introduction." *Rheology of complex fluids* (2010): 3-34.
- Colebrook, C. F., and C. M. White. "Experiments with fluid friction in roughened pipes." *Proceedings of the Royal Society of London. Series A-Mathematical and Physical Sciences* 161, no. 906 (1937): 367-381.
- Cross, M. M. "Rheology of non-Newtonian fluids: a new flow equation for pseudoplastic systems." *Journal of colloid science* 20, no. 5 (1965): 417-437.
- Darcy, H., and J. Weisbach. "Investigations on the motion of water in pipes and the laws derived from it." *Journal for Pure and Applied Mathematics*, 56 (1857): 237-318.
- Goldstein, R. J., R. J. Adrian, and D. K. Kreid. "Turbulent and transition pipe flow of dilute aqueous polymer solutions." *Industrial & Engineering Chemistry Fundamentals* 8, no. 3 (1969): 498-502.
- Goudar, C. T., and J. R. Sonnad. "Comparison of the iterative approximations of the Colebrook-White equation: Here's a review of other formulas and a mathematically exact formulation that is valid over the entire range of Re values: *Fluid Flow and Rotating Equipment*." *Hydrocarbon processing (International ed.)* 87, no. 8 (2008).

- Graham, M. D. "Drag reduction in turbulent flow of polymer solutions." *Rheology reviews* 2, no. 2 (2004): 143-170.
- Hagen, G., and J. L. Poiseuille. "Memoir on the Viscosity of Liquids." *Ann. Chim. Phys.*, 73 (1839): 337-381.
- Jones, D. M., K. Walters, and P. R. Williams. "On the extensional viscosity of mobile polymer solutions." *Rheologica Acta* 26 (1987): 20-30.
- Von Karman, Th. "On laminar and turbulent friction." (1946).
- Kumor, S. M., and N. D. Sylvester. "Effects of a drag-reducing polymer on the turbulent boundary layer." In *AICHE Symposium Series*, vol. 69, no. 130. 1973.
- L'vov, V. S., A. Pomyalov, I. Procaccia, and V. Tiberkevich. "Drag reduction by polymers in wall bounded turbulence." *Physical review letters* 92, no. 24 (2004): 244503.
- Lescarbourea, J. A., J. D. Culter, and H. A. Wahl. "Drag reduction with a polymeric additive in crude oil pipelines." *Society of Petroleum Engineers Journal* 11, no. 03 (1971): 229-235.
- Lumley, J. L. "Drag reduction by additives." *Annual review of fluid mechanics* 1, no. 1 (1969): 367-384.
- Moody, L. F. "Friction factors for pipe flow." *Transactions of the American Society of Mechanical Engineers* 66, no. 8 (1944): 671-678.
- Nadolink, R. H., and W. W. Haigh. "Bibliography on skin friction reduction with polymers and other boundary-layer additives." (1995): 351-460.

- Nesyn, G. V., R. Z. Sunagatullin, V. P. Shibaev, and A. Y. Malkin. "Drag reduction in transportation of hydrocarbon liquids: From fundamentals to engineering applications." *Journal of Petroleum Science and Engineering* 161 (2018): 715-725.
- Nikuradse J. "law of turbulent flow in smooth pipe." *Forsch.-Arb. Ing.-Wesen*, No. 356 (1932)
- Nikuradse, J. "Flow laws in rough pipes." *VDI Research Paper*, 361 (1933): 1-30.
- Owolabi, B. E., D. J. C. Dennis, and R. J. Poole. "Turbulent drag reduction by polymer additives in parallel-shear flows." *Journal of Fluid Mechanics* 827 (2017): R4.
- Petrie, C. J. S. "Extensional viscosity: A critical discussion." *Journal of Non-Newtonian Fluid Mechanics* 137, no. 1-3 (2006): 15-23.
- Poole, R. J. "The Deborah and Weissenberg numbers." *Rheol. Bull* 53, no. 2 (2012): 32-39.
- Prandtl, L. *Recent results of turbulence research*. No. NACA-TM-720. 1933.
- Rudd, M. J. "Drag Reduction." *Chem. Eng. Symp. Ser. III*, 67, 21 (1971).
- Rudd, M. J. "Velocity measurements made with a laser dopplermeter on the turbulent pipe flow of a dilute polymer solution." *Journal of Fluid Mechanics* 51, no. 4 (1972): 673-685.
- Ryskin, G. "Turbulent drag reduction by polymers: a quantitative theory." *Physical review letters* 59, no. 18 (1987): 2059.
- Serghides, T. K. "Estimate friction factor accurately." *Chemical engineering (New York, NY)* 91, no. 5 (1984): 63-64.
- Swamee, P. K., and A. K. Jain. "Explicit equations for pipe-flow problems." *Journal of the hydraulics division* 102, no. 5 (1976): 657-664.

- Tabor, M., and P. G. De Gennes. "A cascade theory of drag reduction." *Europhysics Letters* 2, no. 7 (1986): 519.
- Toms, B. A. "Proc (1st) Intern Congr Rheology, vol II." (1948): 135.
- Trouton, F. T. "On the coefficient of viscous traction and its relation to that of viscosity." *Proceedings of the Royal Society of London. Series A, Containing Papers of a Mathematical and Physical Character* 77, no. 519 (1906): 426-440.
- Virk, P. S., H. S. Mickley, and K. A. Smith. "The ultimate asymptote and mean flow structure in Toms' phenomenon." (1970): 488-493.
- Virk, P. S. "An elastic sublayer model for drag reduction by dilute solutions of linear macromolecules." *Journal of Fluid Mechanics* 45, no. 3 (1971): 417-440.
- White, C. M., and M. G. Mungal. "Mechanics and prediction of turbulent drag reduction with polymer additives." *Annu. Rev. Fluid Mech.* 40 (2008): 235-256.

## Appendix A

# Engineering drawings for diesel flow loop

This section provides an overview of the diesel flow facility (refer to figure A1), followed by highlighting the key component units (refer to figure A2) and presenting the detailed engineering drawings for each component up to the main assembly level. The drawings include GD&T, material information and welding details that were used in fabrication and assembly of the flow facility components.

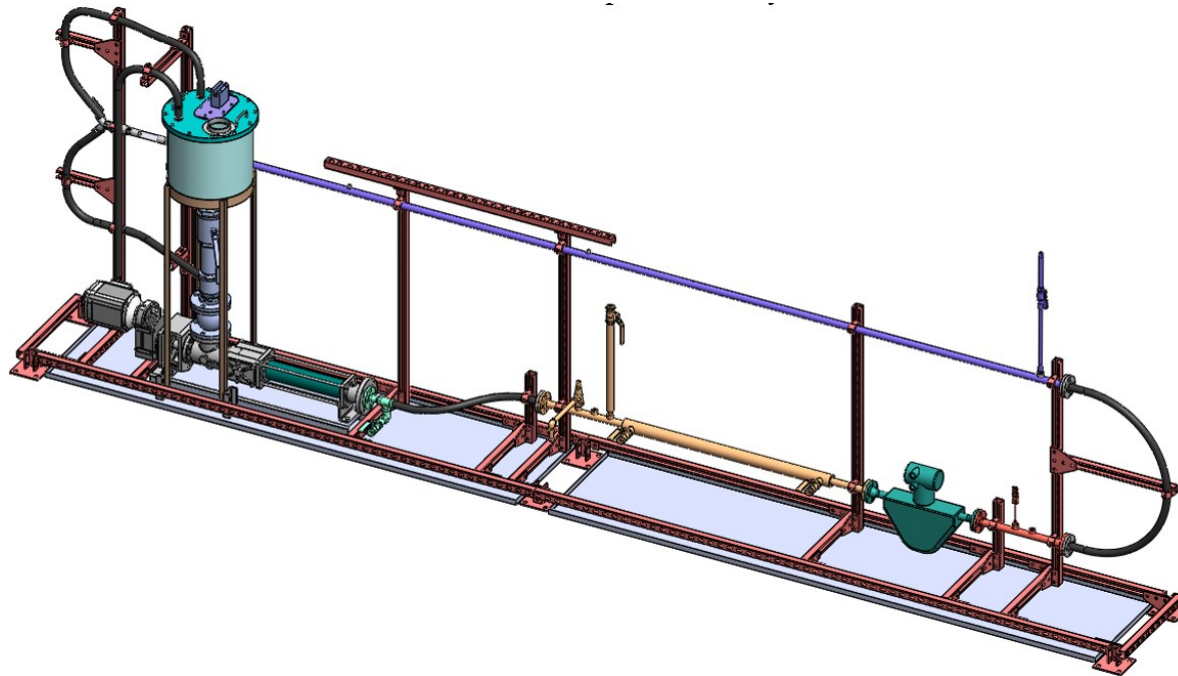


Figure A1: An overview of the diesel flow loop.

## Diesel flow loop – Drawing reference

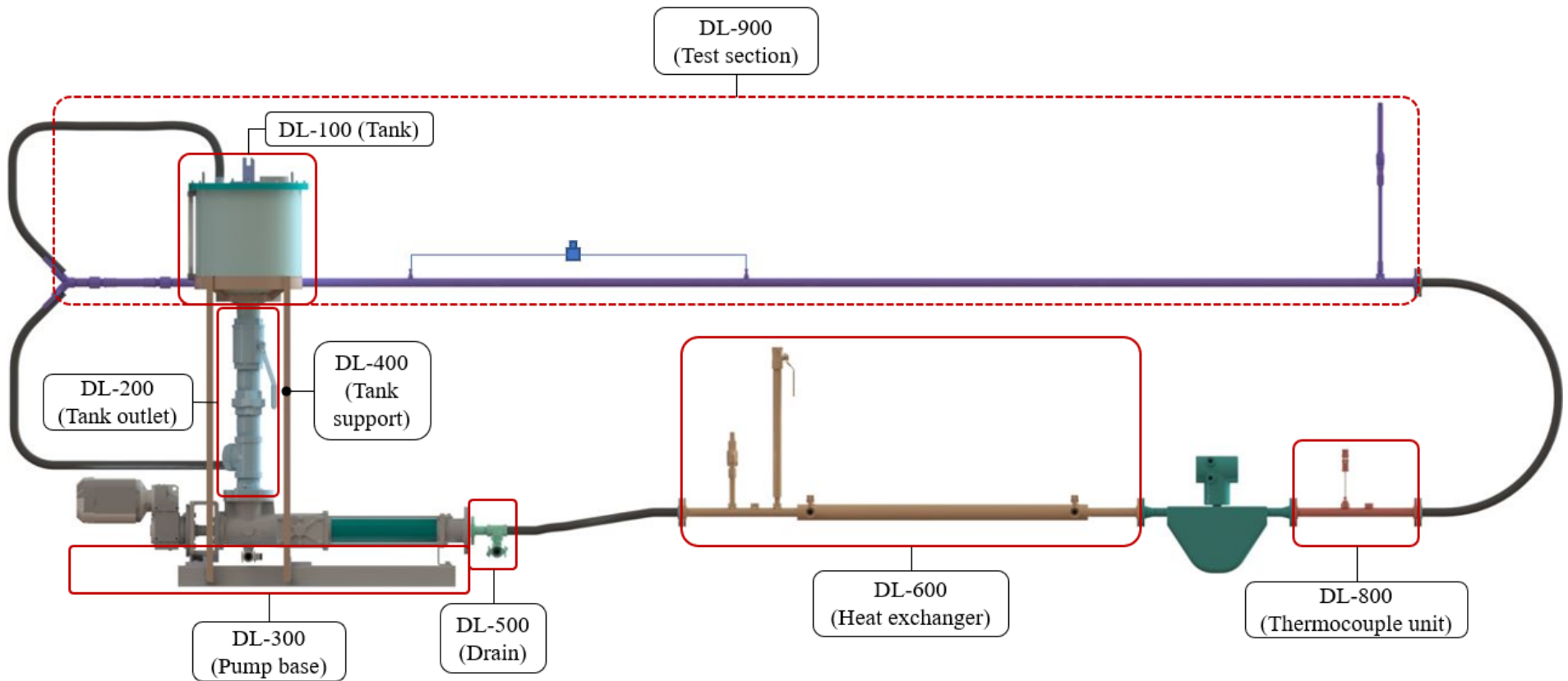
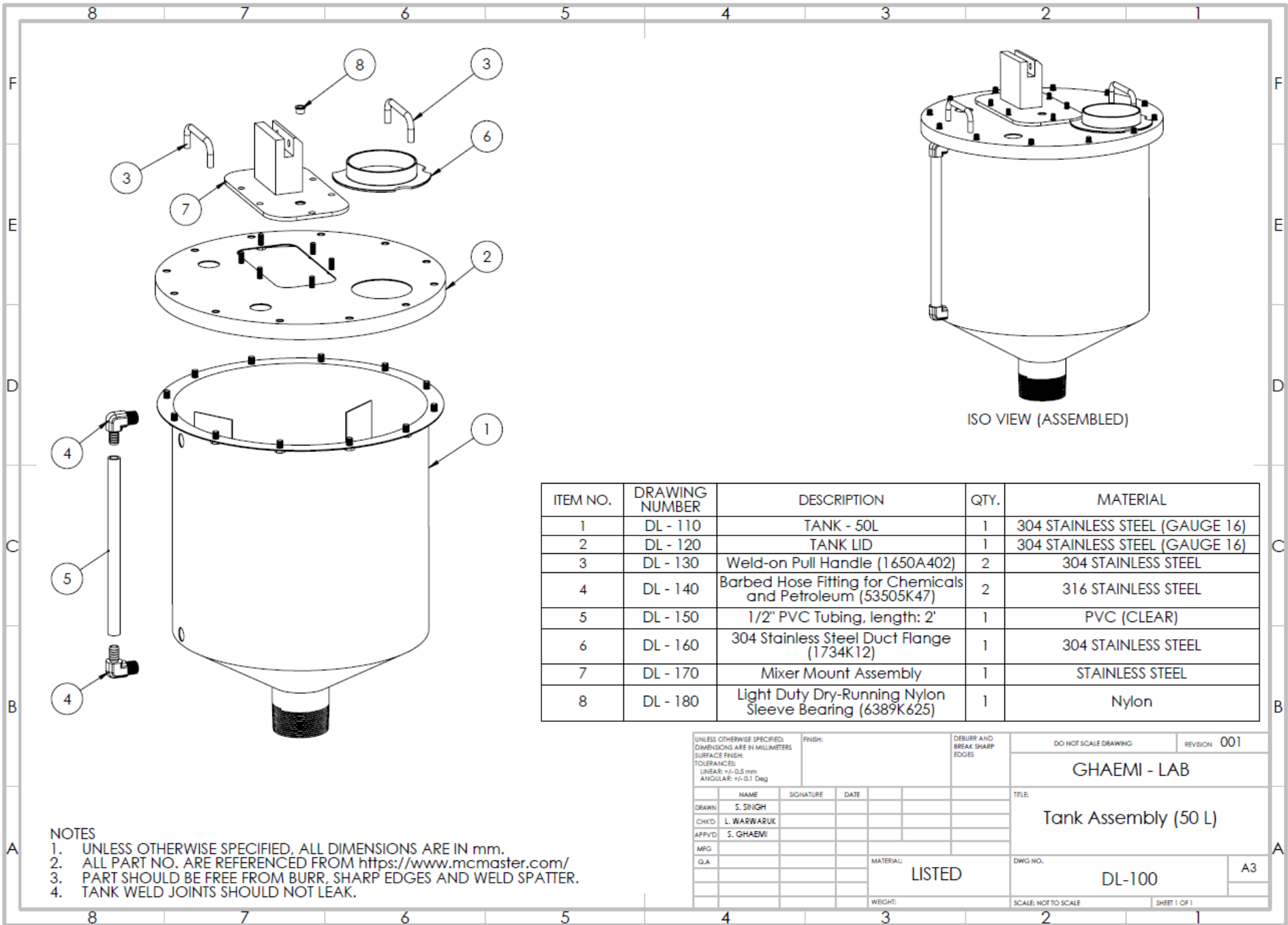


Figure A2: Diesel flow loop drawing reference that highlights key component units with reference to the drawing number.





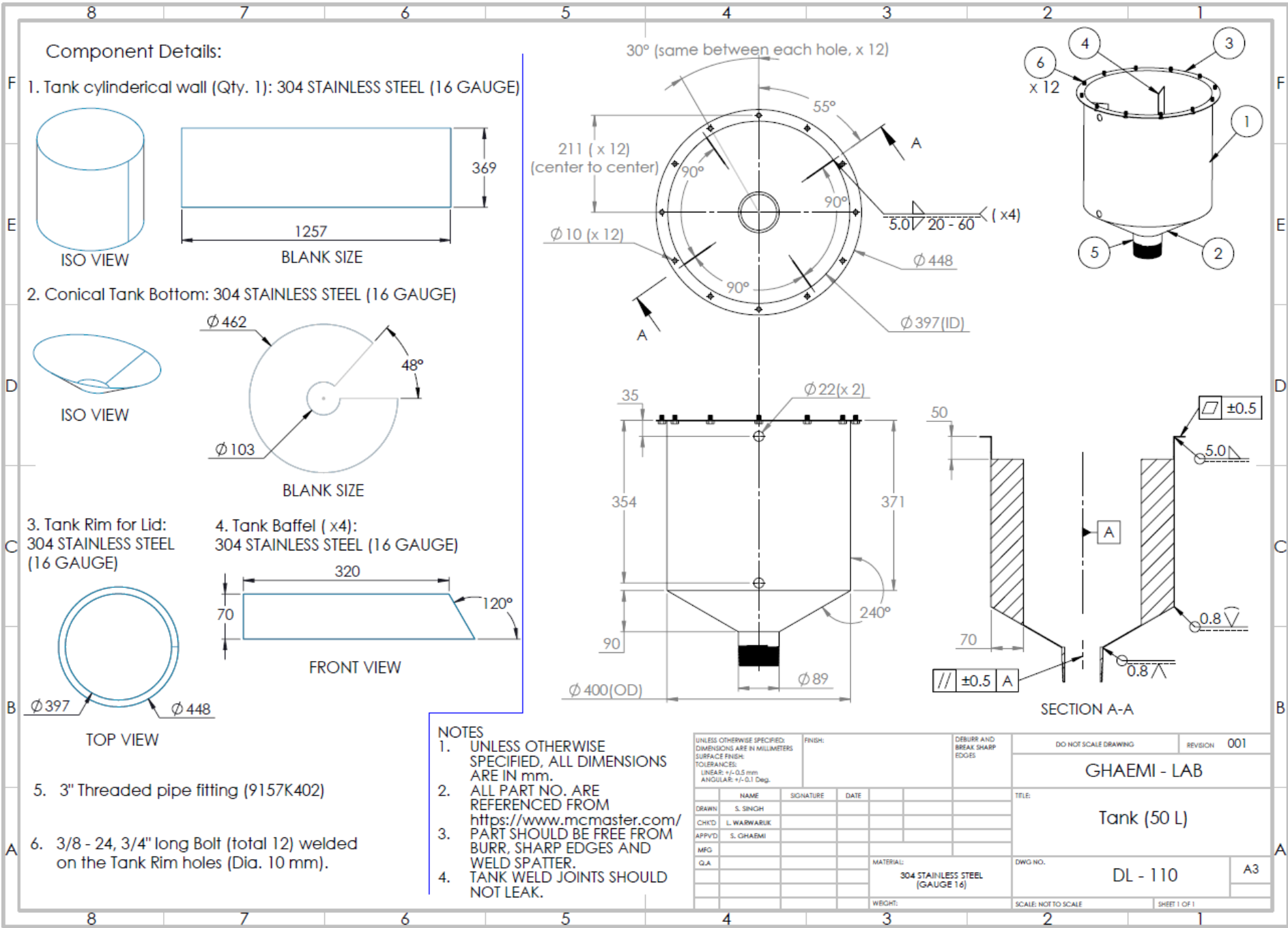
ISO VIEW (ASSEMBLED)

ITEM NO.	DRAWING NUMBER	DESCRIPTION	QTY.	MATERIAL
1	DL - 110	TANK - 50L	1	304 STAINLESS STEEL (GAUGE 16)
2	DL - 120	TANK LID	1	304 STAINLESS STEEL (GAUGE 16)
3	DL - 130	Weld-on Pull Handle (1650A402)	2	304 STAINLESS STEEL
4	DL - 140	Barbed Hose Fitting for Chemicals and Petroleum (53505K47)	2	316 STAINLESS STEEL
5	DL - 150	1/2" PVC Tubing, length: 2'	1	PVC (CLEAR)
6	DL - 160	304 Stainless Steel Duct Flange (1734K12)	1	304 STAINLESS STEEL
7	DL - 170	Mixer Mount Assembly	1	STAINLESS STEEL
8	DL - 180	Light Duty Dry-Running Nylon Sleeve Bearing (6389K625)	1	Nylon

**NOTES**

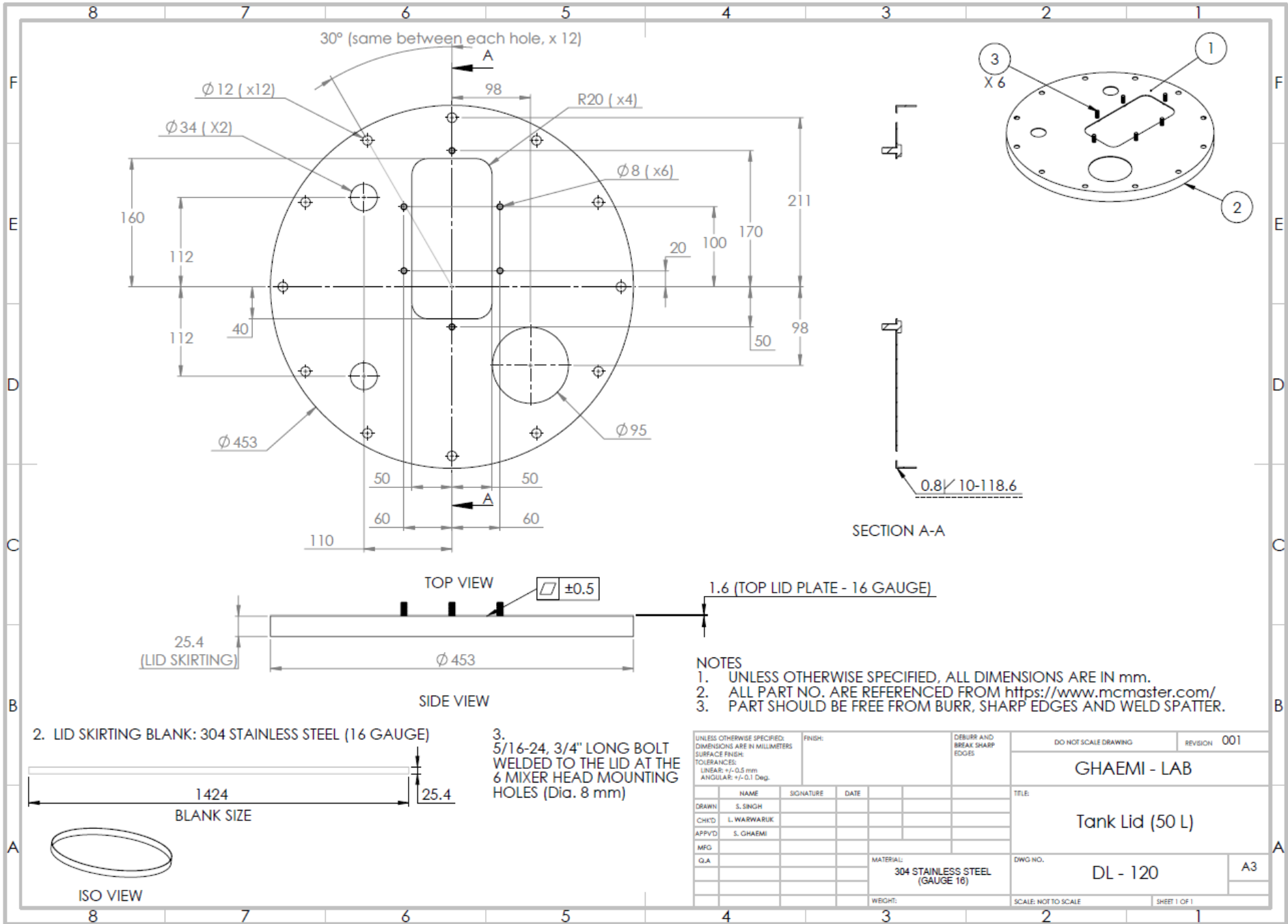
1. UNLESS OTHERWISE SPECIFIED, ALL DIMENSIONS ARE IN mm.
2. ALL PART NO. ARE REFERENCED FROM <https://www.mcmaster.com/>
3. PART SHOULD BE FREE FROM BURR, SHARP EDGES AND WELD SPATTER.
4. TANK WELD JOINTS SHOULD NOT LEAK.

UNLESS OTHERWISE SPECIFIED: DIMENSIONS ARE IN MILLIMETERS SURFACE FINISH: TOLERANCES: LINEAR: +/-.0.5 mm ANGULAR: +/-0.1 Deg		FINISH:	DEBURR AND BREAK SHARP EDGES		DO NOT SCALE DRAWING	REVISION 001
NAME	SIGNATURE	DATE	TITLE: Tank Assembly (50 L)			
DRAWN S. SINGH						
CHK'D L. WARWARUK						
APP'VD S. GHAEMI						
MFG.						
G.A.			MATERIAL: LISTED	DWG NO. DL-100		
			WEIGHT:	SCALE: NOT TO SCALE		SHEET 1 OF 1



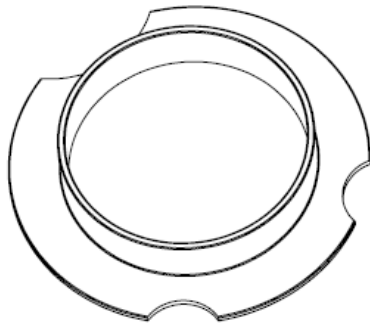
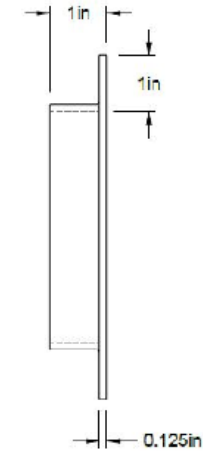
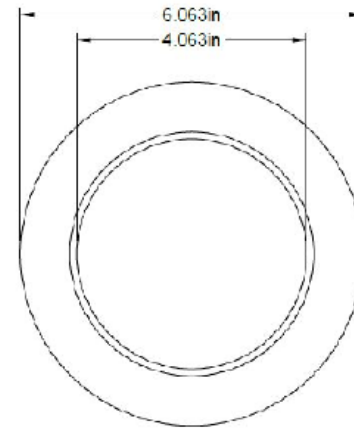
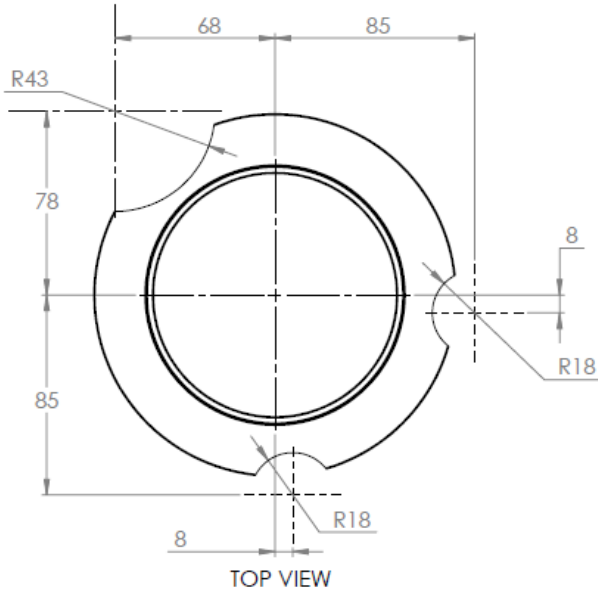
- NOTES**
- UNLESS OTHERWISE SPECIFIED, ALL DIMENSIONS ARE IN mm.
  - ALL PART NO. ARE REFERENCED FROM <https://www.mcmaster.com/>
  - PART SHOULD BE FREE FROM BURR, SHARP EDGES AND WELD SPATTER.
  - TANK WELD JOINTS SHOULD NOT LEAK.

UNLESS OTHERWISE SPECIFIED, DIMENSIONS ARE IN MILLIMETERS		FINISH:	DEBURR AND BREAK SHARP EDGES	DO NOT SCALE DRAWING	REVISION	001
SURFACE FINISH:				GHAEMI - LAB		
TOLERANCES:						
LINEAR: $\pm 0.5$ mm				Tank (50 L)		
ANGULAR: $\pm 0.1$ Deg.						
DRAWN	S. SINGH	SIGNATURE	DATE	TITLE		
CHK'D	L. WARWARUK					
APP'VD	S. CHAEMI			DWG NO.		
MFG						
G.A.				DL - 110		
		MATERIAL:		SCALE: NOT TO SCALE		
		304 STAINLESS STEEL (GAUGE 16)				
		WEIGHT:		SHEET 1 OF 1		



**MODIFICATIONS:**

Circular cutouts required on the flange for clearances



EXTERNAL PART - MODIFIED

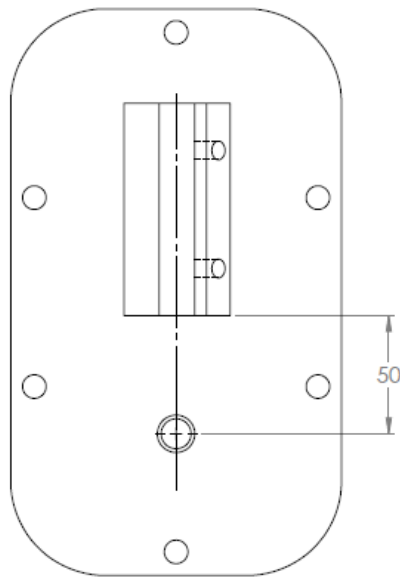
Trade Size: 4in

<b>McMASTER-CARR</b> <small>INC.</small> <b>CAD</b> <a href="http://www.mcmaster.com">http://www.mcmaster.com</a> © 2022 McMaster-Carr Supply Company <small>Information in this drawing is provided for reference only.</small>	PART NUMBER	<b>1734K12</b>
	304 Stainless Steel Duct Flange	

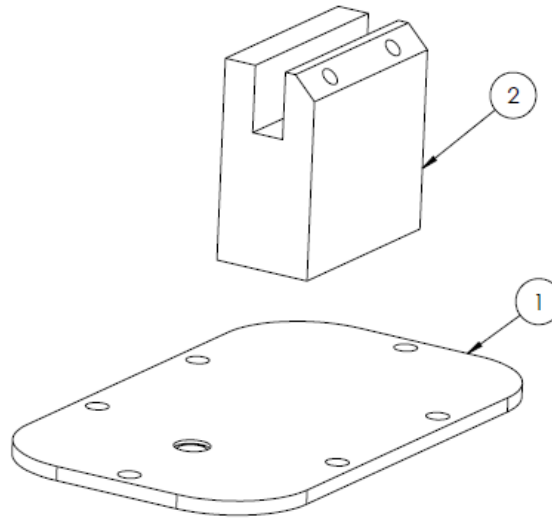
**NOTES**

- UNLESS OTHERWISE SPECIFIED, ALL DIMENSIONS ARE IN mm.
- ALL PART NO. ARE REFERENCED FROM <https://www.mcmaster.com/>
- PART SHOULD BE FREE FROM BURR AND SHARP EDGES

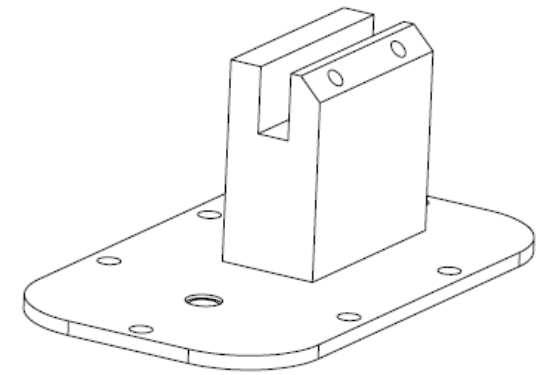
UNLESS OTHERWISE SPECIFIED: DIMENSIONS ARE IN MILLIMETERS SURFACE FINISH: TOLERANCES: LINEAR: ANGULAR:		FINISH:	DEBURR AND BREAK SHARP EDGES	DO NOT SCALE DRAWING	REVISION <b>001</b>
DRAWN S. SINGH		SIGNATURE	DATE	<b>GHAEMI - LAB</b>  <b>304 Stainless Steel Duct Flange</b> <b>McMaster Carr Part No. : 1734K12</b>	
CHKD L. WARWICK					
APPVD S. GHAEMI					
MFG					
Q.A.					
MATERIAL: <b>LISTED</b>			DWG NO. <b>DL - 160</b>	A3	
WEIGHT:			SCALE: NOT TO SCALE	SHEET 1 OF 1	



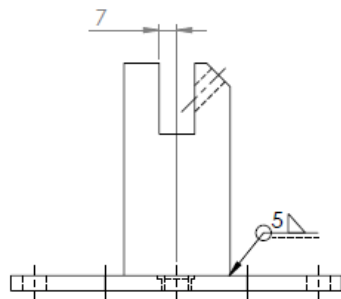
TOP VIEW



EXPLODED VIEW



ISO VIEW



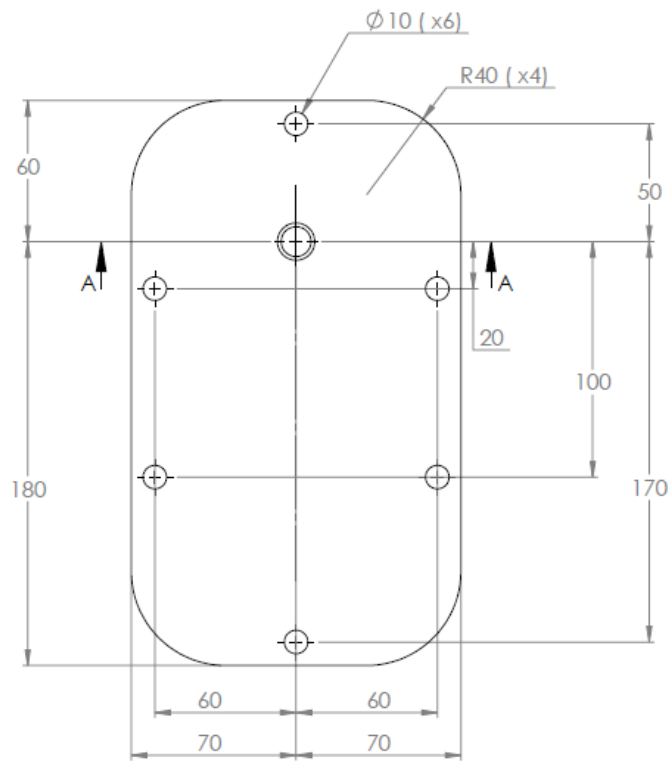
FRONT VIEW

ITEM NO.	DRAWING NUMBER	DESCRIPTION	QTY.	MATERIAL
1	DL - 171	Mixer Base Plate	1	304 STAINLESS STEEL
2	DL - 172	Mixer Mount Block	1	304 STAINLESS STEEL

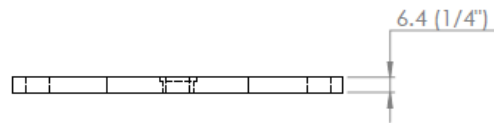
NOTES

1. UNLESS OTHERWISE SPECIFIED, ALL DIMENSIONS ARE IN mm.
2. ALL PART NO. ARE REFERENCED FROM <https://www.mcmaster.com/>
3. PART SHOULD BE FREE FROM BURR, SHARP EDGES AND WELD SPATTER.

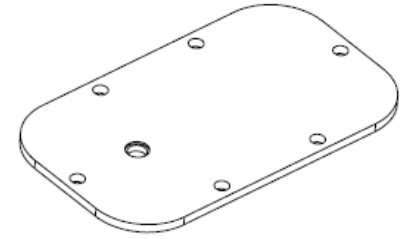
UNLESS OTHERWISE SPECIFIED: DIMENSIONS ARE IN MILLIMETERS SURFACE FINISH: TOLERANCES: LINEAR: +/- 0.5 mm ANGULAR: +/- 0.1 Deg			FINISH:	DEBURR AND BREAK SHARP EDGES	DO NOT SCALE DRAWING	REVISION 001
					GHAEMI - LAB	
					TITLE: Mixer Mount Assembly	
NAME	SIGNATURE	DATE				
DRAWN S. SINGH						
CHKD L. WARWARUK						
APPVD S. GHAEMI						
MFG						
G.A.						
			MATERIAL: LISTED	DWG NO. DL-170		
			WEIGHT:	SCALE: NOT TO SCALE		A3 SHEET 1 OF 1



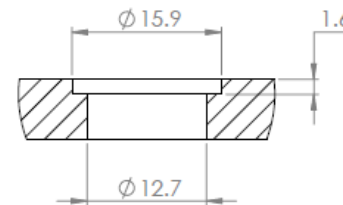
TOP VIEW



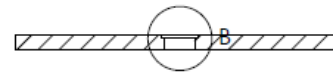
FRONT VIEW



ISO VIEW



DETAIL B

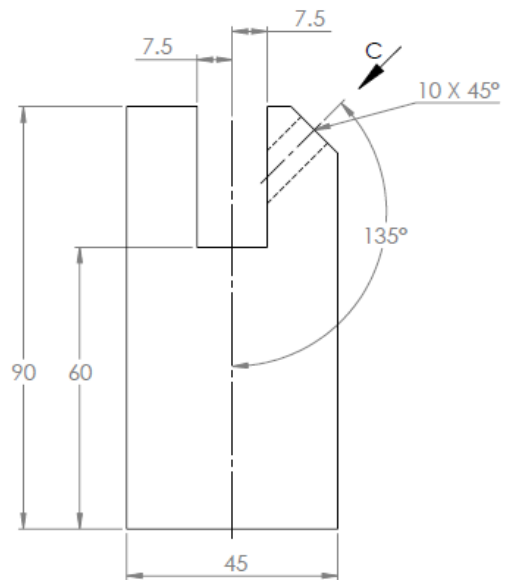


SECTION A-A

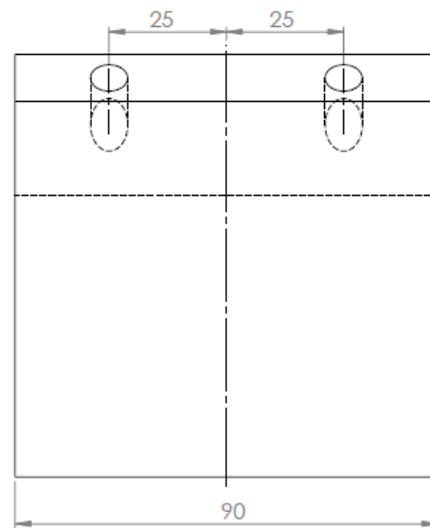
NOTES

1. UNLESS OTHERWISE SPECIFIED, ALL DIMENSIONS ARE IN mm.
2. ALL PART NO. ARE REFERENCED FROM <https://www.mcmaster.com/>
3. PART SHOULD BE FREE FROM BURR, SHARP EDGES AND WELD SPATTER.

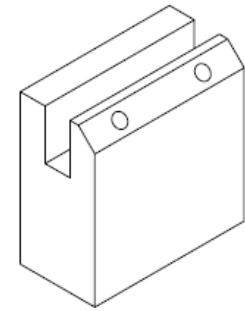
UNLESS OTHERWISE SPECIFIED: DIMENSIONS ARE IN MILLIMETERS SURFACE FINISH: TOLERANCES: LINEAR: +/- 0.5 mm ANGULAR: +/- 0.1 Deg		FINISH:	DEBURR AND BREAK SHARP EDGES	DO NOT SCALE DRAWING	REVISION 001
DRAWN: S. SINGH			TITLE: GHAEMI - LAB		
CHKD: L. WARWARUK			Mixer Base Plate		
APPRVD: S. GHAEMI			DWG NO. DL-171		
MFG:			MATERIAL: LISTED		
Q.A.			WEIGHT:		
			SCALE: NOT TO SCALE		
			SHEET 1 OF 1		



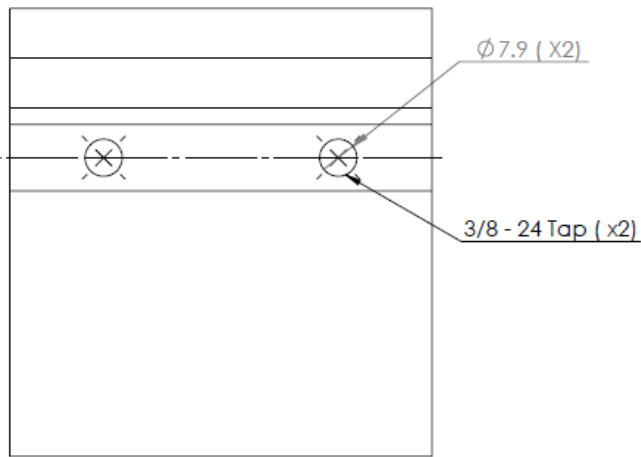
FRONT VIEW



SIDE VIEW



ISO VIEW



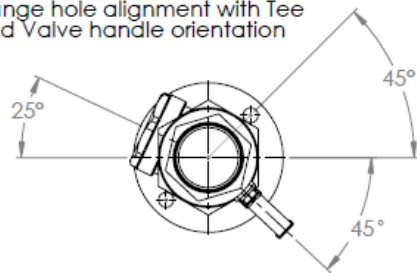
VIEW C  
45.00°

NOTES

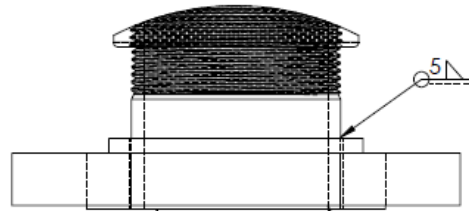
1. UNLESS OTHERWISE SPECIFIED, ALL DIMENSIONS ARE IN mm.
2. ALL PART NO. ARE REFERENCED FROM <https://www.mcmaster.com/>
3. PART SHOULD BE FREE FROM BURR, SHARP EDGES AND WELD SPATTER.

UNLESS OTHERWISE SPECIFIED: DIMENSIONS ARE IN MILLIMETERS SURFACE FINISH: TOLERANCES: LINEAR: $\pm 0.5$ mm ANGULAR: $\pm 0.1$ Deg		FINISH:	DEBURR AND BREAK SHARP EDGES	DO NOT SCALE DRAWING	REVISION 001
DRAWN S. SINGH		SIGNATURE	DATE	TITLE: GHAEMI - LAB	
CHKD L. WAWARUK				Mixer Mount Block	
APPVD S. GHAEMI				DWG NO. DL-172	A3
MFG				SCALE: NOT TO SCALE	SHEET 1 OF 1
G.A.				MATERIAL: LISTED	
				WEIGHT:	

Flange hole alignment with Tee and Valve handle orientation



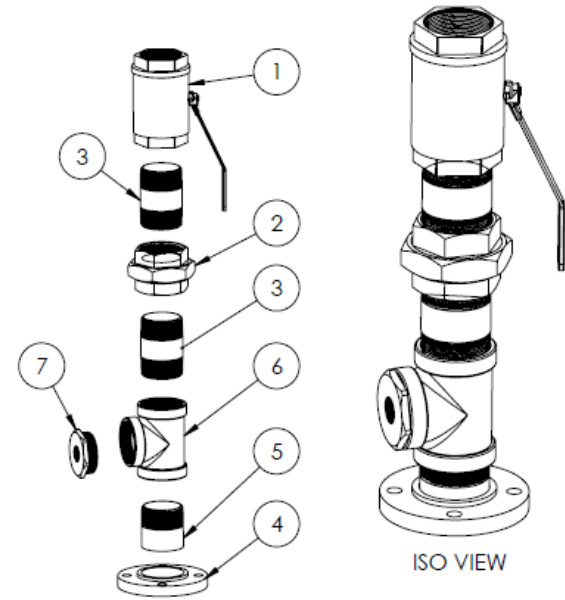
TOP VIEW



DETAIL A

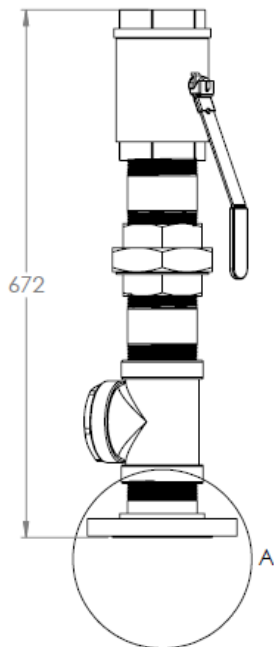
Overall Dimension is from this face

3" Nipple (#5) unthreaded face should be coplanar with the flange face



EXPLODED VIEW

ISO VIEW



FRONT VIEW

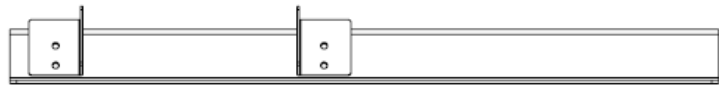
ITEM NO.	DRAWING NUMBER	DESCRIPTION	QTY.	MATERIAL
1	-	3" Full-Port ball valve (46495K28)	1	304 Stainless Steel
2	-	3" pipe union (4464K494)	1	304 Stainless Steel
3	-	3" x 5" Pipe Nipple (4830K357)	2	304 Stainless Steel
4	-	3" Slip-on Forged Pipe Flange (44685K186)	1	304 Stainless Steel
5	-	3" x 3-1/2" Pipe Nipple, one side threaded (9157K8)	1	304 Stainless Steel
6	-	3" Tee (4464K142)	1	304 Stainless Steel
7	-	3" to 1" Bushing Adapter (4464K177)	1	304 Stainless Steel

NOTES

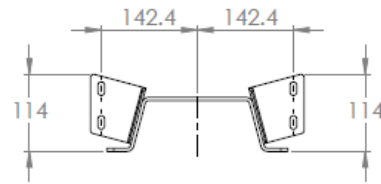
1. UNLESS OTHERWISE SPECIFIED, ALL DIMENSIONS ARE IN mm.
2. ALL PART NO. ARE REFERENCED FROM <https://www.mcmaster.com/>
3. PART SHOULD BE FREE FROM BURR, SHARP EDGES AND WELD SPATTER.
4. ALL PHERIPARAL WELD JOINTS SHOULD NOT LEAK.

UNLESS OTHERWISE SPECIFIED: DIMENSIONS ARE IN MILLIMETERS SURFACE FINISH: TOLERANCES: LINEAR: +/- 0.5 mm ANGULAR: +/- 0.1 Deg.		FINISH:	DEBURR AND BREAK SHARP EDGES	DO NOT SCALE DRAWING	REVISION 001
NAME	SIGNATURE	DATE		GHAEMI - LAB	
DRAWN: S. SINGH				TITLE: Tank Outlet Fittings	
CHKD: L. WARWARIK				DWG NO. DL - 200	
APPVD: S. GHAEMI				A3	
MFG:			MATERIAL: LISTED	SCALE: 1:10	
G.A.			WEIGHT:	SHEET 1 OF 1	

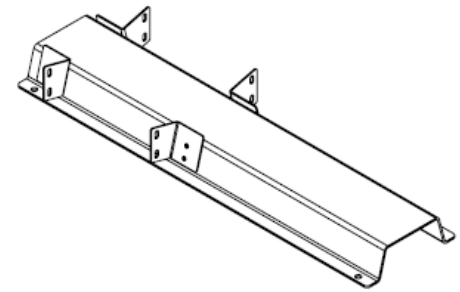




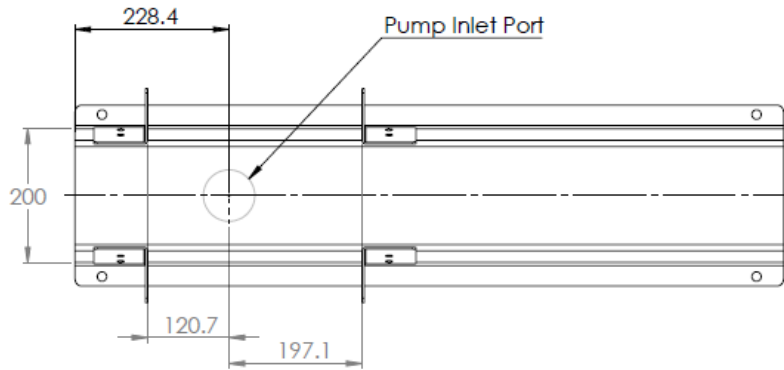
FRONT VIEW



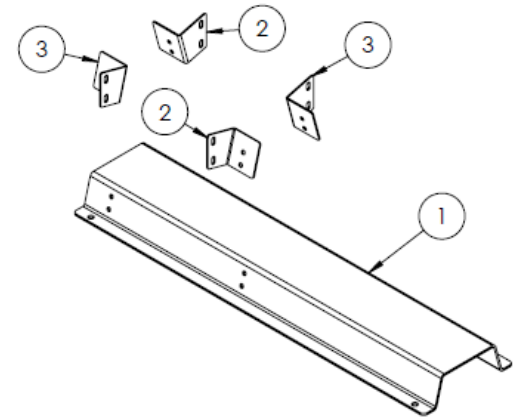
SIDE VIEW



ISO VIEW



TOP VIEW



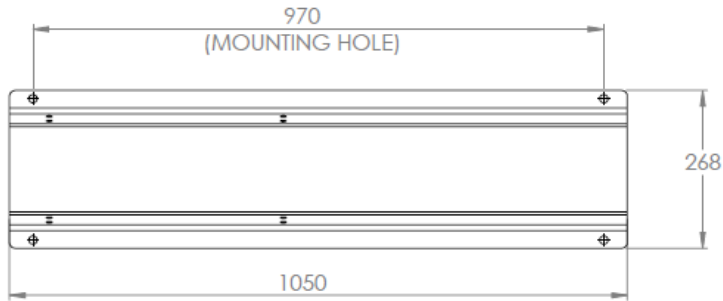
EXPLODED VIEW

ITEM NO.	PART NUMBER	DESCRIPTION	QTY.
1	DL - 310	NETZSCH Pump Base	1
2	DL - 320	Tank Frame Mounting Bracket - A	2
3	DL - 330	Tank Frame Mounting Bracket - B	2

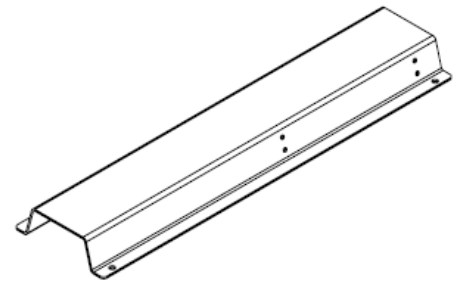
NOTES

- UNLESS OTHERWISE SPECIFIED, ALL DIMENSIONS ARE IN mm.
- PART SHOULD BE FREE FROM BURR, SHARP EDGES AND WELD SPATTER.

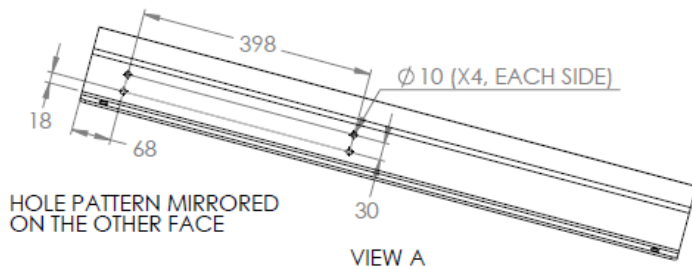
UNLESS OTHERWISE SPECIFIED: DIMENSIONS ARE IN MILLIMETERS SURFACE FINISH: TOLERANCES: LINEAR: +/- 0.5 mm ANGULAR: +/- 0.1 Deg		FINISH:	DEBURR AND BREAK SHARP EDGES	DO NOT SCALE DRAWING	REVISION 002
DRAWN: S. SINGH		SIGNATURE:	DATE:	GHAEMI - LAB	
CHKD: L. WARWARUK		TITLE:			Pump Base (Modifications)
APPRVD: S. GHAEMI		MATERIAL:			DL-300
MFG:		LISTED			A3
G.A.		WEIGHT:			SCALE: NOT TO SCALE
				SHEET 1 OF 1	



TOP VIEW



ISO VIEW

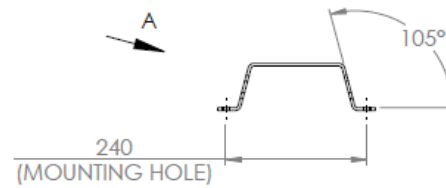


VIEW A

HOLE PATTERN MIRRORED ON THE OTHER FACE



SIDE VIEW

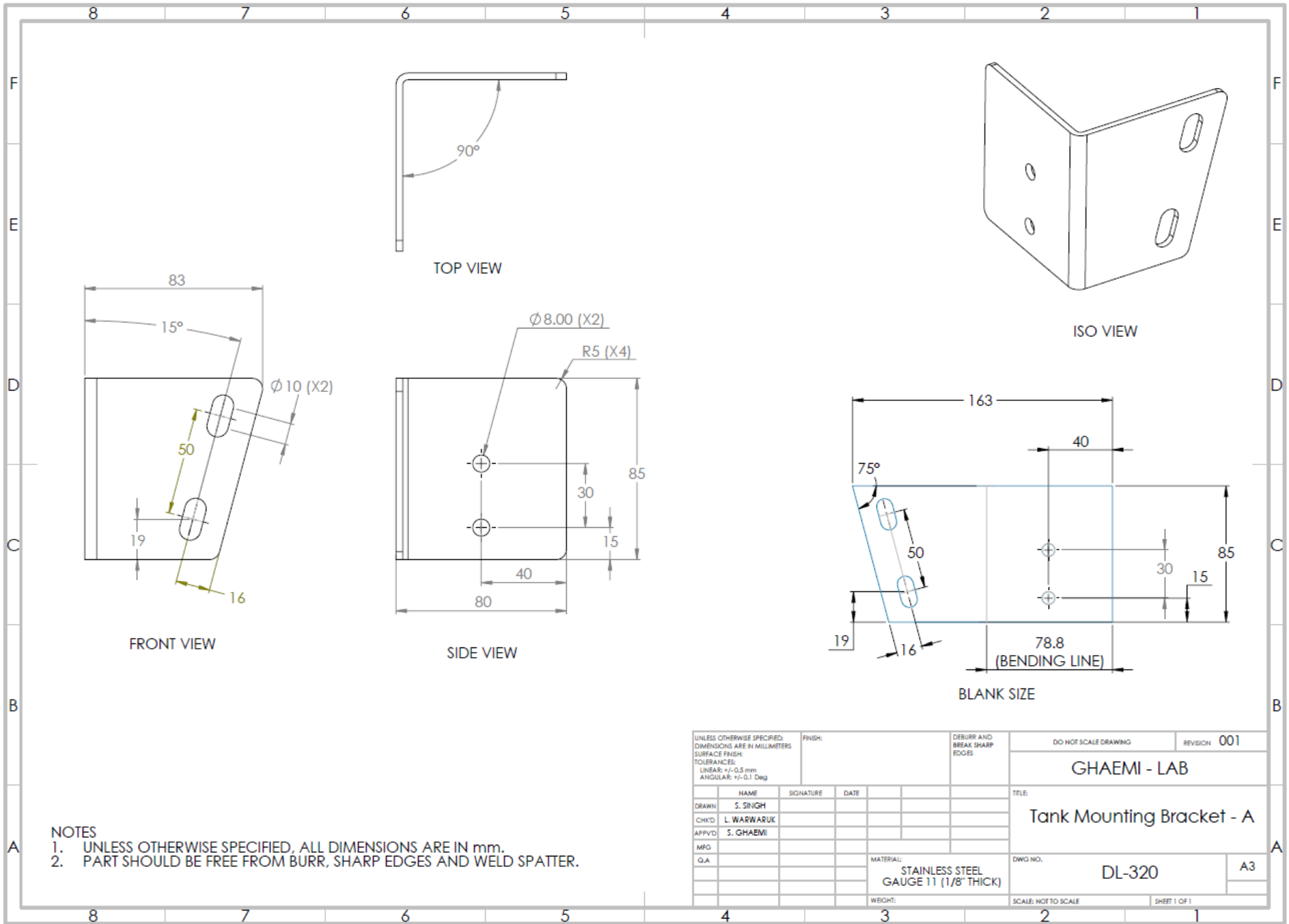


FRONT VIEW

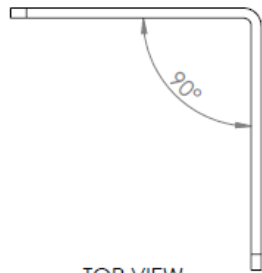
NOTES

1. UNLESS OTHERWISE SPECIFIED, ALL DIMENSIONS ARE IN mm.
2. PART SHOULD BE FREE FROM BURR, SHARP EDGES AND WELD SPATTER.

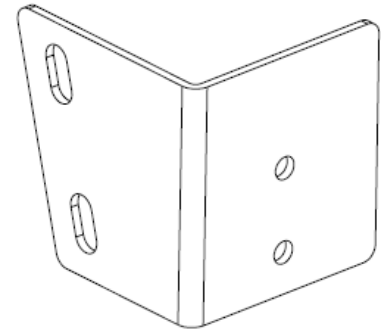
UNLESS OTHERWISE SPECIFIED: DIMENSIONS ARE IN MILLIMETERS SURFACE FINISH: TOLERANCES: LINEAR: +/- 0.5 mm ANGULAR: +/- 0.1 Deg		FINISH:	DEBURR AND BREAK SHARP EDGES	DO NOT SCALE DRAWING	REVISION 001
DRAWN: S. SINGH		SIGNATURE	DATE	TITLE: NETZSCH Pump Base	
CHKD: L. WARWARUK				DWG NO. DL-310	
APPRVD: S. GHAEMI				SCALE: NOT TO SCALE	
MFG:				SHEET 1 OF 1	
G.A.				MATERIAL: STRUCTURAL STEEL	
				WEIGHT:	



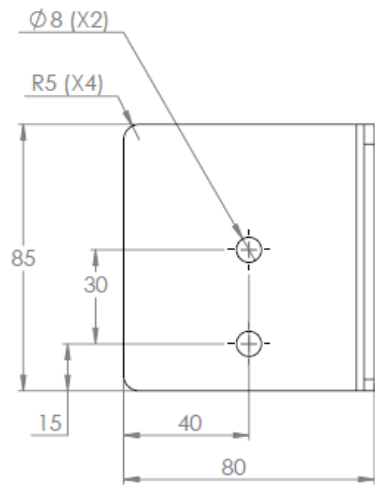
UNLESS OTHERWISE SPECIFIED: DIMENSIONS ARE IN MILLIMETERS SURFACE FINISH: TOLERANCES: LINEAR: +j-0.5 mm ANGULAR: +/- 0.1 Deg				FINISH:		DEBURR AND BREAK SHARP EDGES		DO NOT SCALE DRAWING		REVISION 001	
						<b>GHAEMI - LAB</b>					
						TITLE: <b>Tank Mounting Bracket - A</b>					
DRAWN S. SINGH		SIGNATURE		DATE		MATERIAL: STAINLESS STEEL GAUGE 11 (1/8" THICK)		DWG NO. DL-320		A3	
CHK'D L. WARWARUK						WEIGHT:		SCALE: NOT TO SCALE		SHEET 1 OF 1	
APP'VD S. GHAEMI											
MFG											
Q.A											



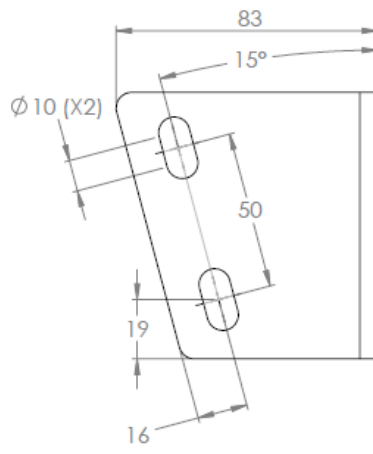
TOP VIEW



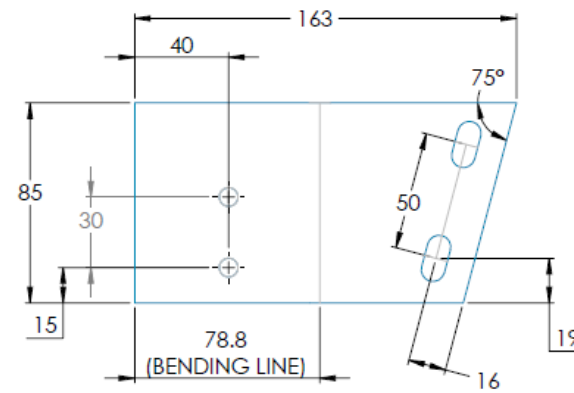
ISO VIEW



SIDE VIEW



FRONT VIEW

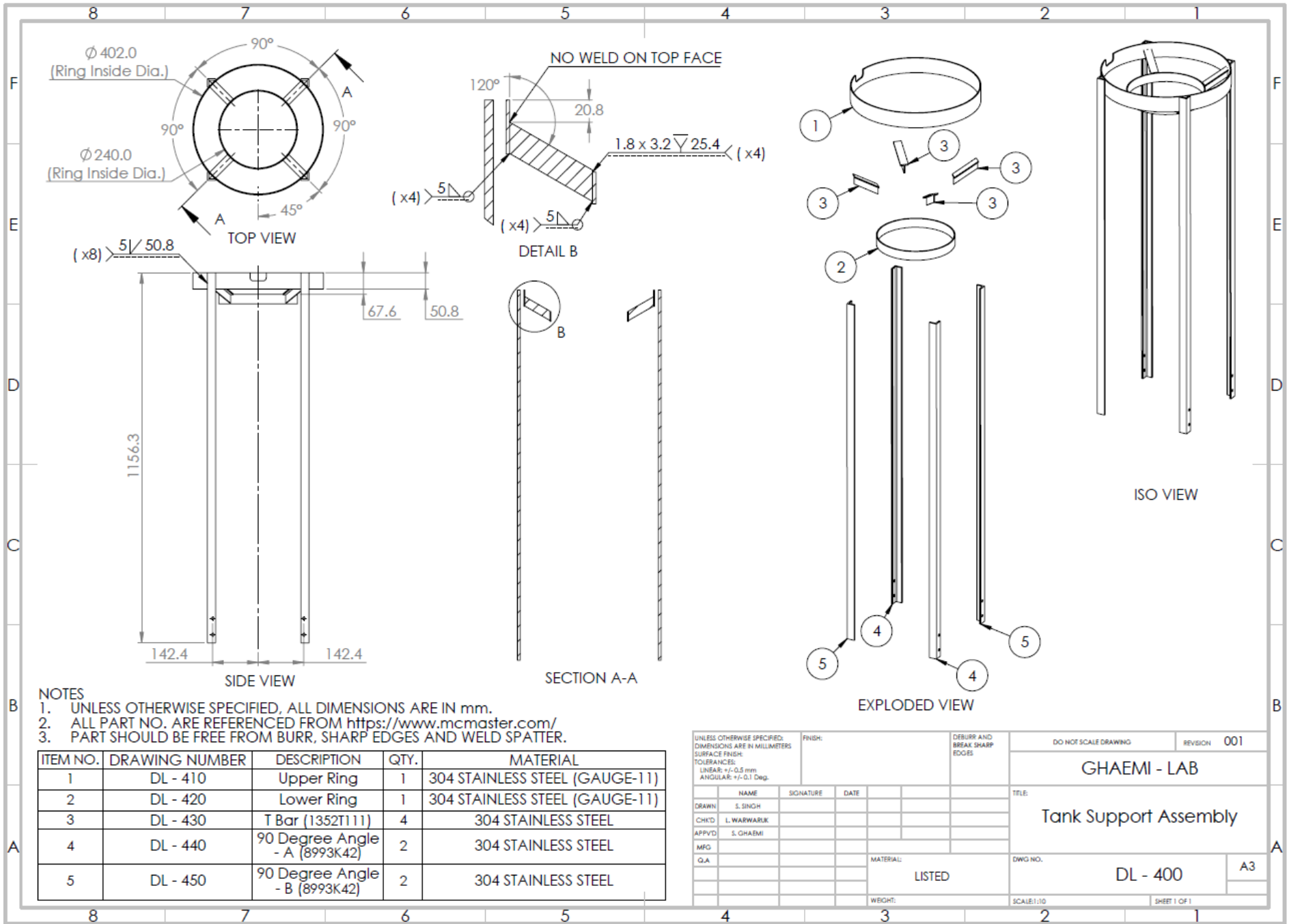


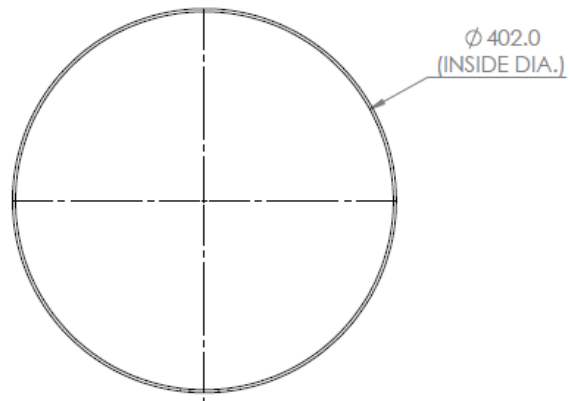
BLANK SIZE

NOTES

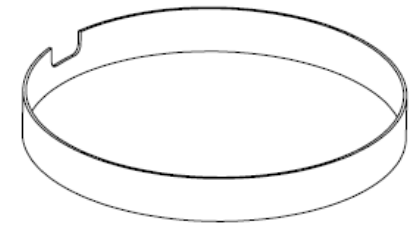
1. UNLESS OTHERWISE SPECIFIED, ALL DIMENSIONS ARE IN mm.
2. PART SHOULD BE FREE FROM BURR, SHARP EDGES AND WELD SPATTER.

UNLESS OTHERWISE SPECIFIED: DIMENSIONS ARE IN MILLIMETERS SURFACE FINISH: TOLERANCES: LINEAR: +/- 0.5 mm ANGULAR: +/- 0.1 Deg		FINISH:	DEBURR AND BREAK SHARP EDGES		DO NOT SCALE DRAWING	REVISION 001
DRAWN S. SINCH				TITLE: GHAEMI - LAB		
CHK'D L. WARWARUK				Tank Mounting Bracket - B		
APP'VD S. GHAEMI				DWG NO. DL-330		
MFG				SCALE: NOT TO SCALE		
G.A.				MATERIAL: STAINLESS STEEL GAUGE 11 (1/8" THICK)		A3
				WEIGHT:		SHEET 1 OF 1

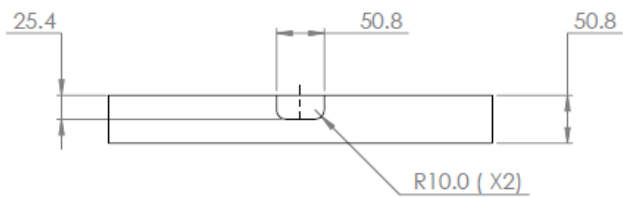




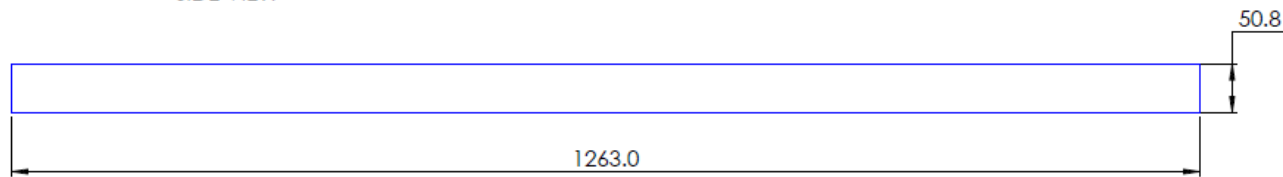
TOP VIEW



ISO VIEW



SIDE VIEW

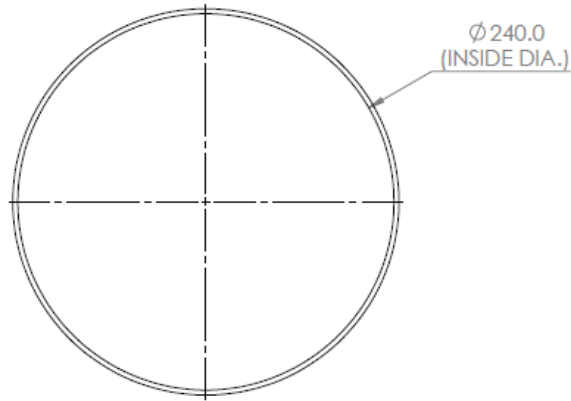


BLANK SIZE

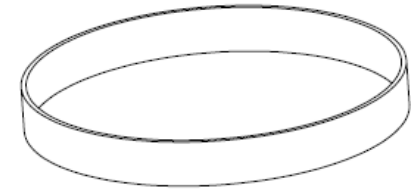
NOTES

1. UNLESS OTHERWISE SPECIFIED, ALL DIMENSIONS ARE IN mm.
2. ALL PART NO. ARE REFERENCED FROM <https://www.mcmaster.com/>
3. PART SHOULD BE FREE FROM BURR AND SHARP EDGES

UNLESS OTHERWISE SPECIFIED: DIMENSIONS ARE IN MILLIMETERS SURFACE FINISH: TOLERANCES: LINEAR: ANGULAR:		FINISH:	DEBURR AND BREAK SHARP EDGES	DO NOT SCALE DRAWING	REVISION 001
				GHAEMI - LAB	
				TITLE: TANK SUPPORT - UPPER RING	
NAME	SIGNATURE	DATE		DWG NO.	A3
DRAWN S. SINGH				DL - 410	
CHK'D L. WARWARIK				SCALE: NOT TO SCALE	SHEET 1 OF 1
APP'VD S. GHAEMI					
MFG					
G.A.					
			MATERIAL: 304 STAINLESS STEEL (GAUGE - 11)		
			WEIGHT:		



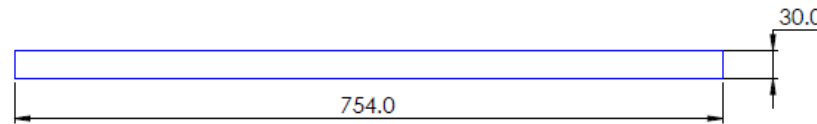
TOP VIEW



ISO VIEW



SIDE VIEW



BLANK SIZE

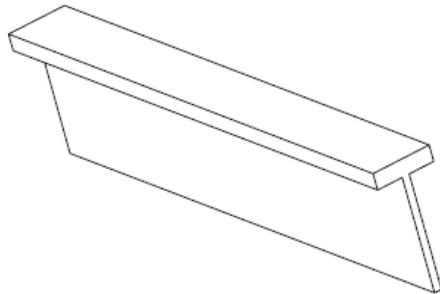
NOTES

1. UNLESS OTHERWISE SPECIFIED, ALL DIMENSIONS ARE IN mm.
2. ALL PART NO. ARE REFERENCED FROM <https://www.mcmaster.com/>
3. PART SHOULD BE FREE FROM BURR AND SHARP EDGES

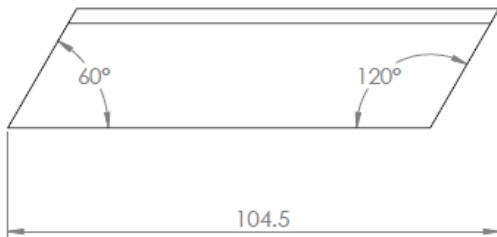
UNLESS OTHERWISE SPECIFIED: DIMENSIONS ARE IN MILLIMETERS SURFACE FINISH: TOLERANCES: LINEAR: ANGULAR:		FINISH:	DEBURR AND BREAK SHARP EDGES		DO NOT SCALE DRAWING	REVISION 001
					GHAEMI - LAB	
					TITLE:	
					TANK SUPPORT - LOWER RING	
NAME	SIGNATURE	DATE			DWG NO.	A3
DRAWN: S. SINGH					DL - 420	
CHKD: L. WARWARIK					SCALE: NOT TO SCALE	SHEET 1 OF 1
APPVD: S. GHAEMI						
MFG:						
G.A.						
			MATERIAL:			
			304 STAINLESS STEEL (GAUGE - 11)			
			WEIGHT:			

**MODIFICATIONS:**

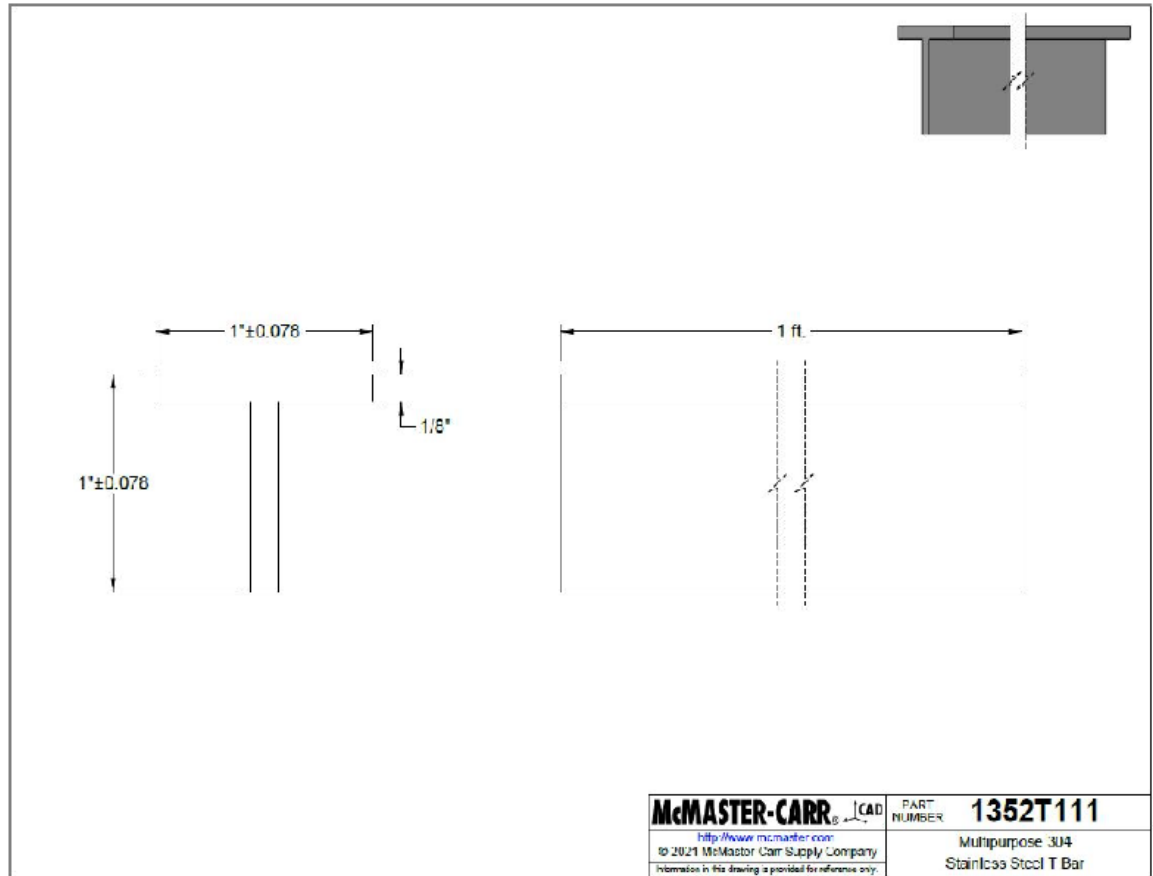
T-Bar to be cut at an angle from both sides



ISO VIEW



SIDE VIEW



<b>McMASTER-CARR</b> <small>http://www.mcmaster.com/</small>	CAD	PART NUMBER	<b>1352T111</b>
<small>© 2021 McMaster Carr Supply Company</small>		Multipurpose 304 Stainless Steel T Bar	

**NOTES**

- UNLESS OTHERWISE SPECIFIED, ALL DIMENSIONS ARE IN mm.
- ALL PART NO. ARE REFERENCED FROM <https://www.mcmaster.com/>
- PART SHOULD BE FREE FROM BURR AND SHARP EDGES

UNLESS OTHERWISE SPECIFIED: DIMENSIONS ARE IN MILLIMETERS SURFACE FINISH: TOLERANCES: LINEAR: ANGULAR:		FINISH:	DEBURR AND BREAK SHARP EDGES	DO NOT SCALE DRAWING	REVISION	001
DRAWN S. SINGH			SIGNATURE	DATE	TITLE: <b>GHAEMI - LAB</b>	
CHK'D L. WARWARIK					TANK SUPPORT - T BAR	
APP'VD S. GHAEMI					DWG NO. DL - 430	
MFG					A3	
Q.A.			MATERIAL: 304 STAINLESS STEEL		SCALE: NOT TO SCALE	
			WEIGHT:		SHEET 1 OF 1	

EXTERNAL PART - MODIFIED

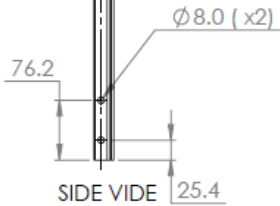
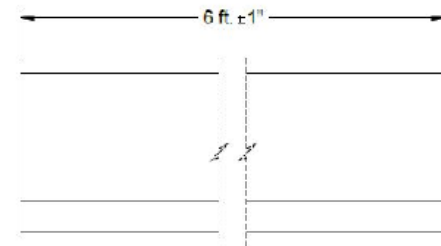
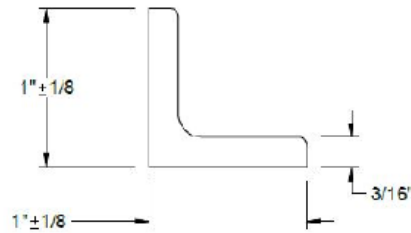
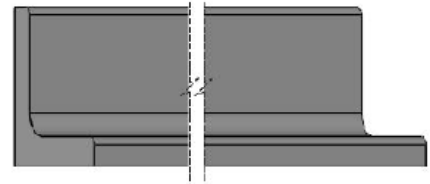


**MODIFICATIONS:**

Two holes to be made on the angle bar



ISO VIEW



SIDE VIEW



TOP VIEW

EXTERNAL PART - MODIFIED

**McMASTER-CARR** INC. **CAD** PART NUMBER **8993K42**  
<https://www.mcmaster.com>  
 © 2022 McMaster-Carr Supply Company Multipurpose 304 Stainless Steel 90 Degree Angle  
Information in this drawing is provided for reference only.

**NOTES**

1. UNLESS OTHERWISE SPECIFIED, ALL DIMENSIONS ARE IN mm.
2. ALL PART NO. ARE REFERENCED FROM <https://www.mcmaster.com/>
3. PART SHOULD BE FREE FROM BURR AND SHARP EDGES

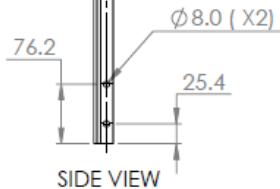
UNLESS OTHERWISE SPECIFIED: DIMENSIONS ARE IN MILLIMETERS SURFACE FINISH: TOLERANCES: LINEAR: ANGULAR:				FINISH:	DEBURR AND BREAK SHARP EDGES	DO NOT SCALE DRAWING	REVISION <b>001</b>
						<b>GHAEMI - LAB</b>	
						TITLE <b>TANK SUPPORT - T BAR (A)</b>	
DRAWN	S. SINGH	SIGNATURE	DATE			DWG NO.	<b>DL - 440</b>
CHKD	L. WADWARIK						<b>A3</b>
APPVD	S. GHAEMI						
MFG							
Q.A.							
MATERIAL: <b>304 STAINLESS STEEL</b>						SCALE: NOT TO SCALE	SHEET 1 OF 1
WEIGHT:							

**MODIFICATIONS:**

Two holes to be made on the angle bar



ISO VIEW

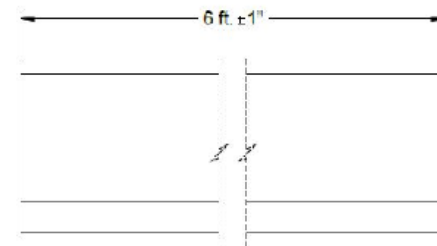
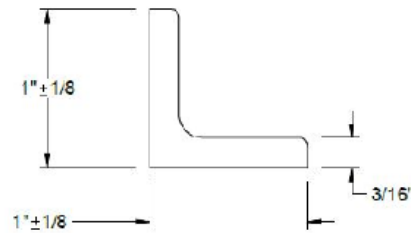


SIDE VIEW



TOP VIEW

EXTERNAL PART - MODIFIED

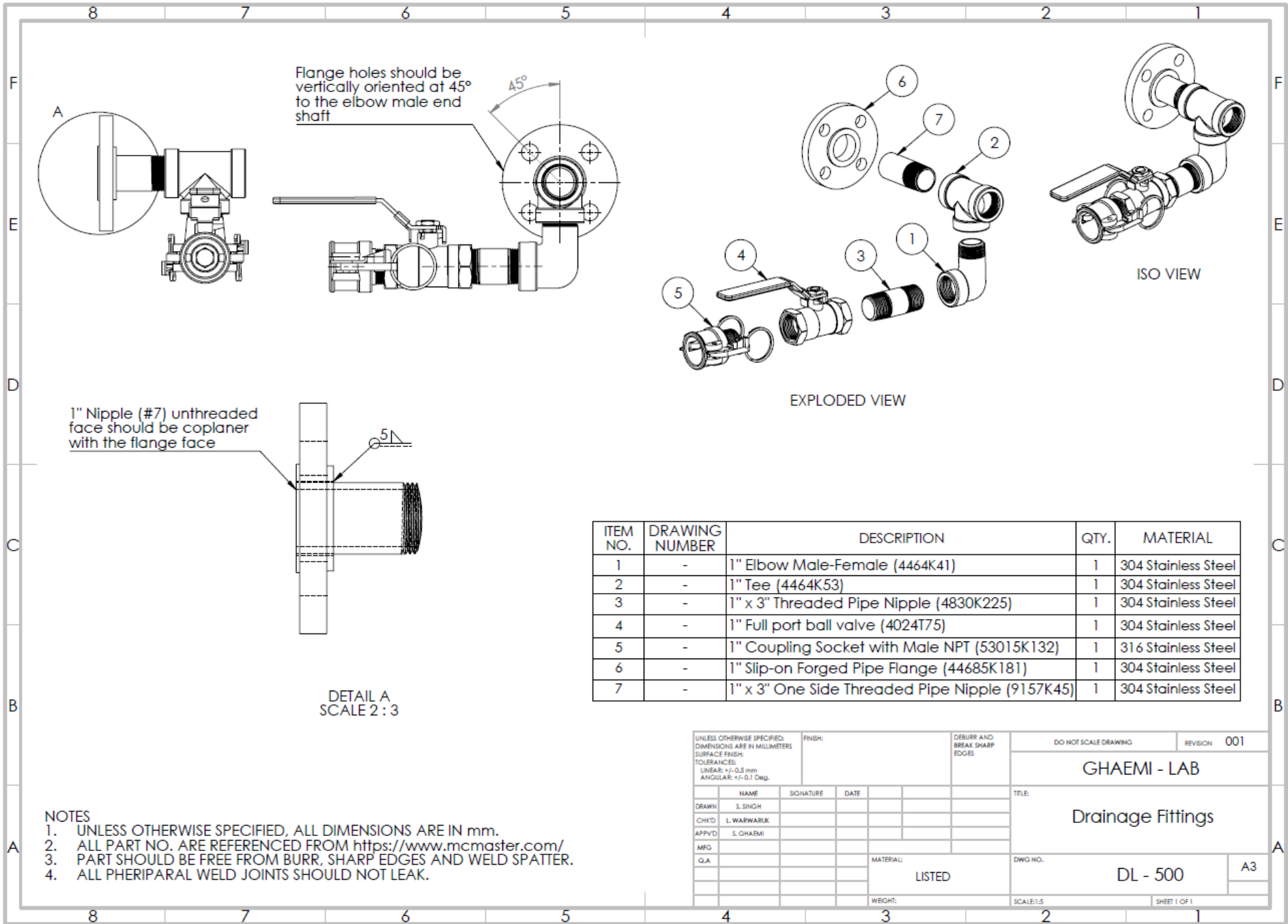


**McMASTER-CARR** INC. **CAD** PART NUMBER **8993K42**  
<http://www.mcmaster.com> Multipurpose 304 Stainless  
 © 2012 McMaster-Carr Supply Company Steel 90 Degree Angle  
Information in this drawing is provided for reference only.

**NOTES**

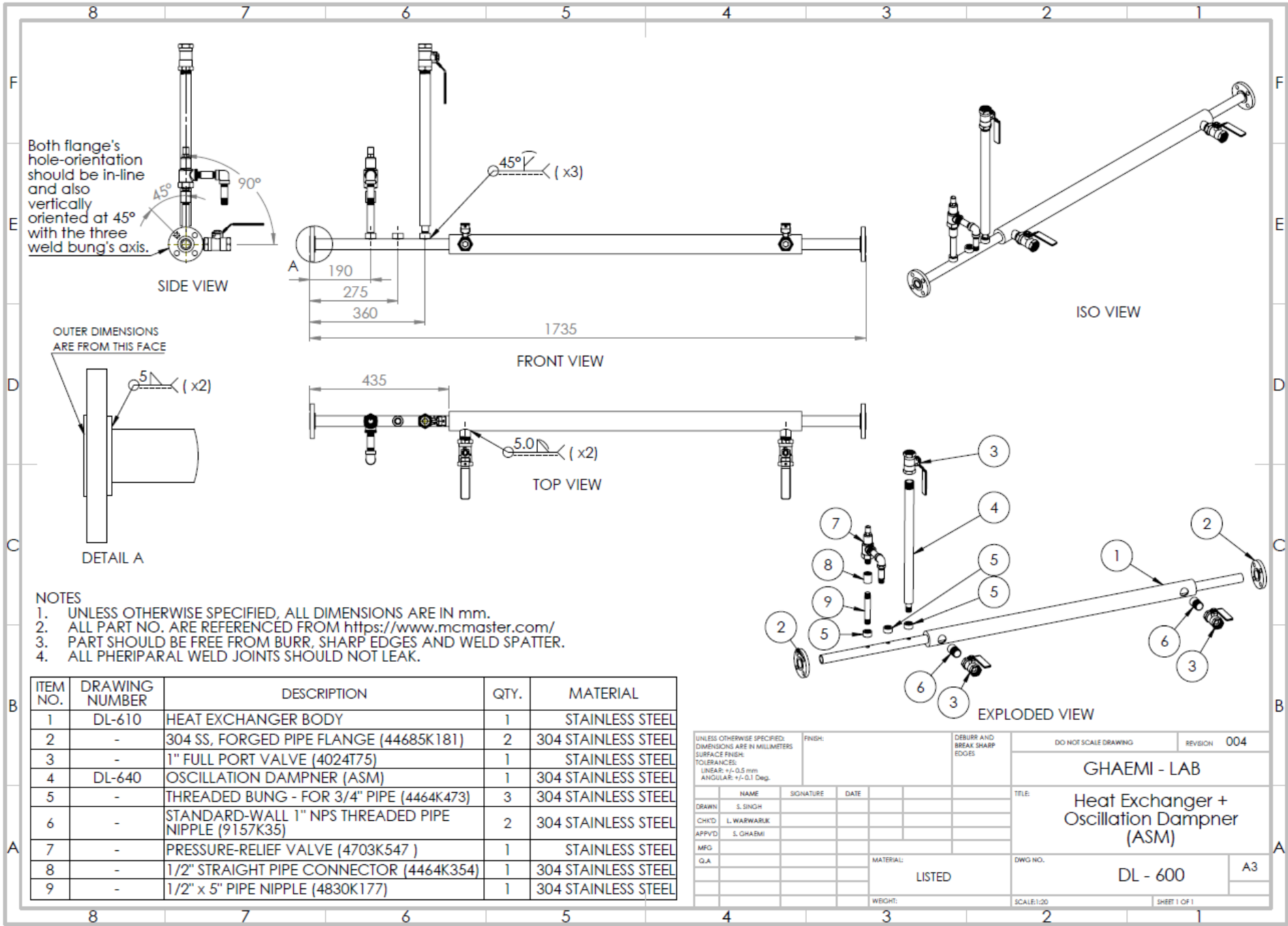
1. UNLESS OTHERWISE SPECIFIED, ALL DIMENSIONS ARE IN mm.
2. ALL PART NO. ARE REFERENCED FROM <https://www.mcmaster.com/>
3. PART SHOULD BE FREE FROM BURR AND SHARP EDGES

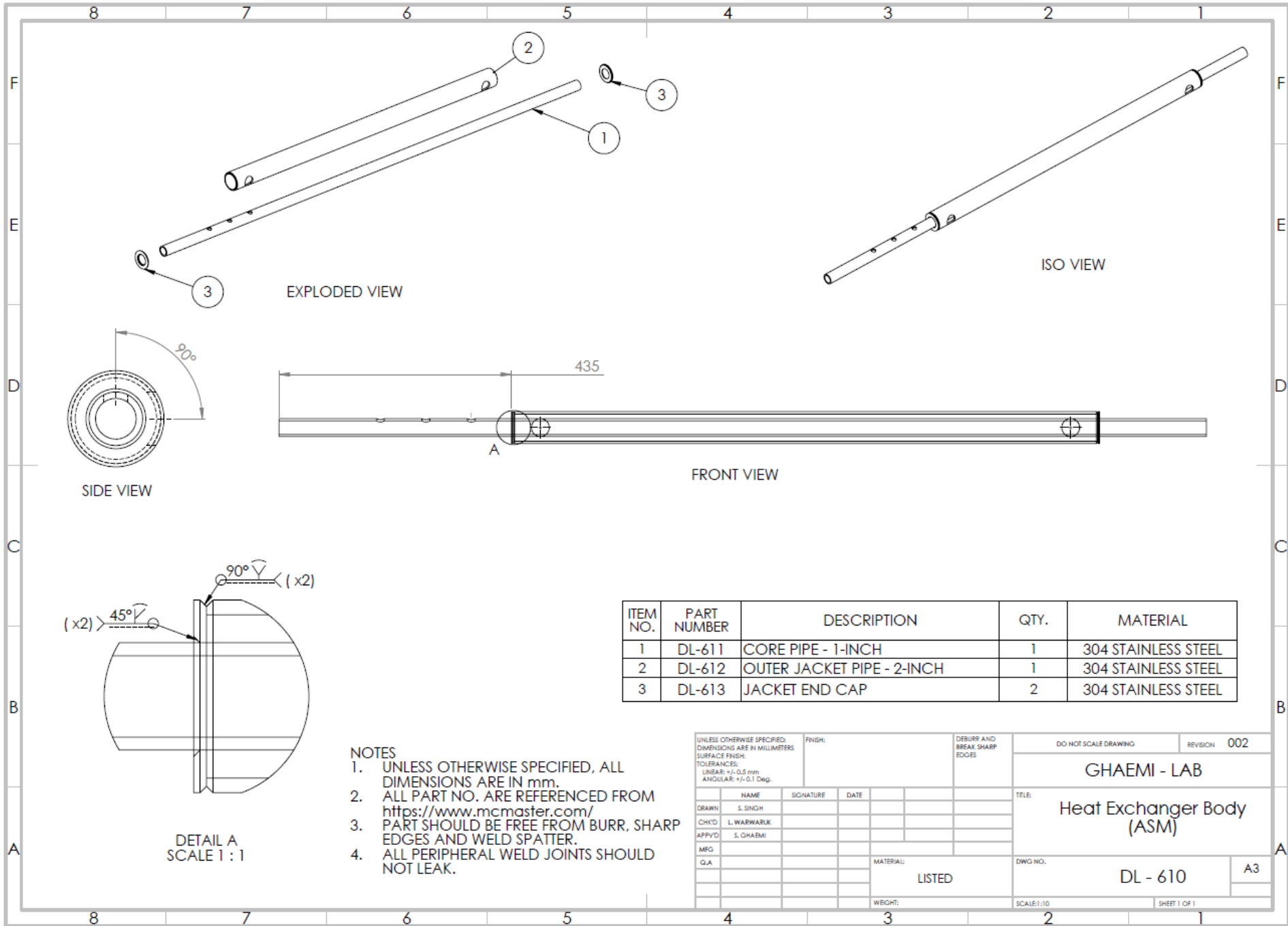
UNLESS OTHERWISE SPECIFIED: DIMENSIONS ARE IN MILLIMETERS				FINISH:	DEBURR AND BREAK SHARP EDGES	DO NOT SCALE DRAWING	REVISION <b>001</b>
SURFACE FINISH:						<b>GHAEMI - LAB</b>	
TOLERANCES:						TITLE	
LINEAR:						<b>TANK SUPPORT - T BAR (B)</b>	
ANGULAR:						DWG NO. <b>DL - 450</b>	
DRAWN	NAME	SIGNATURE	DATE			A3	
	S. SINGH					SCALE: NOT TO SCALE	
CHYO	L. WARWARIK					SHEET 1 OF 1	
APPVD	S. GHAEMI						
MFG							
Q.A					MATERIAL: <b>304 STAINLESS STEEL</b>		
					WEIGHT:		



NOTES

1. UNLESS OTHERWISE SPECIFIED, ALL DIMENSIONS ARE IN mm.
2. ALL PART NO. ARE REFERENCED FROM <https://www.mcmaster.com/>
3. PART SHOULD BE FREE FROM BURR, SHARP EDGES AND WELD SPATTER.
4. ALL PHERIPARAL WELD JOINTS SHOULD NOT LEAK.





EXPLODED VIEW

ISO VIEW

SIDE VIEW

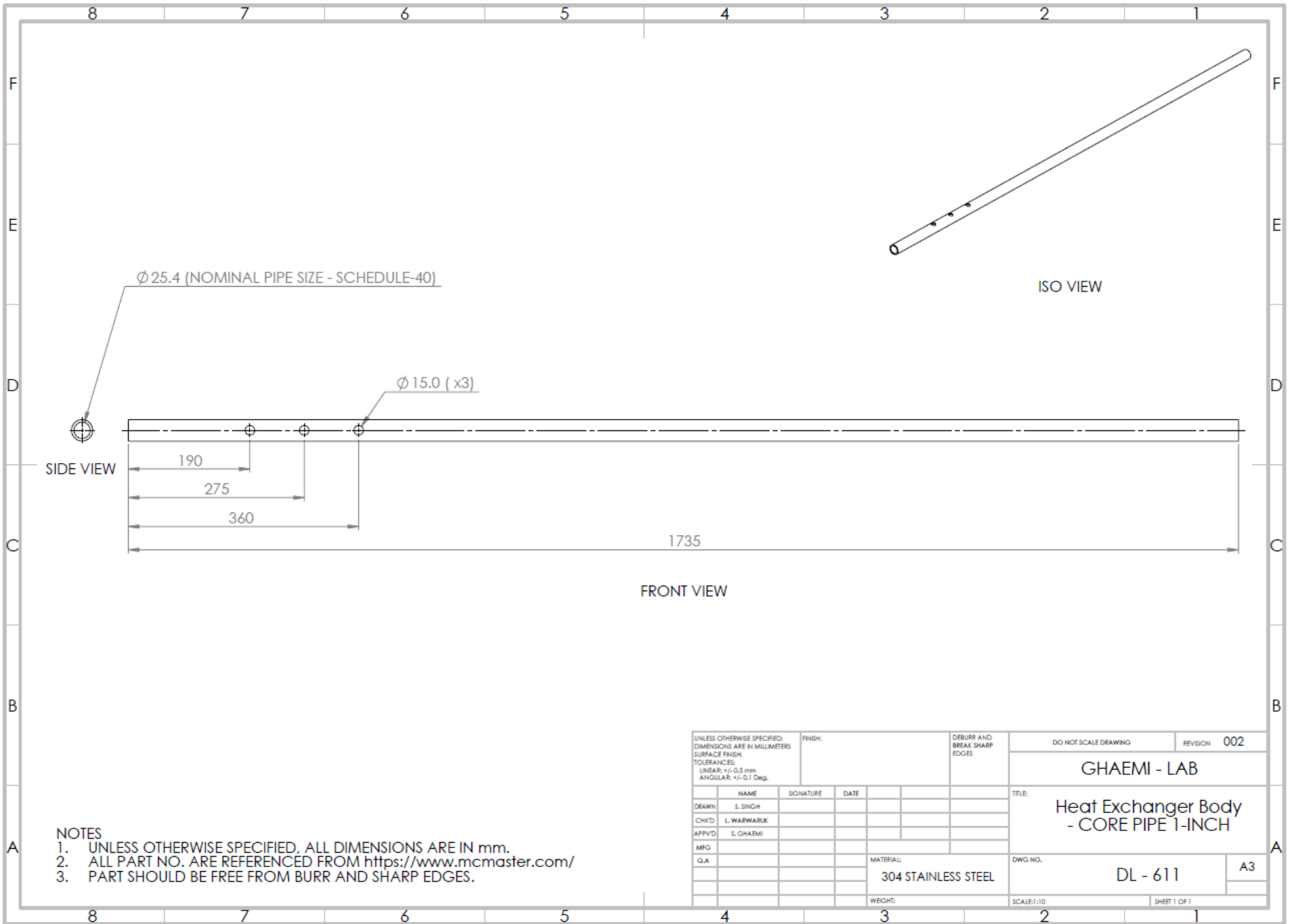
FRONT VIEW

DETAIL A  
SCALE 1 : 1

ITEM NO.	PART NUMBER	DESCRIPTION	QTY.	MATERIAL
1	DL-611	CORE PIPE - 1-INCH	1	304 STAINLESS STEEL
2	DL-612	OUTER JACKET PIPE - 2-INCH	1	304 STAINLESS STEEL
3	DL-613	JACKET END CAP	2	304 STAINLESS STEEL

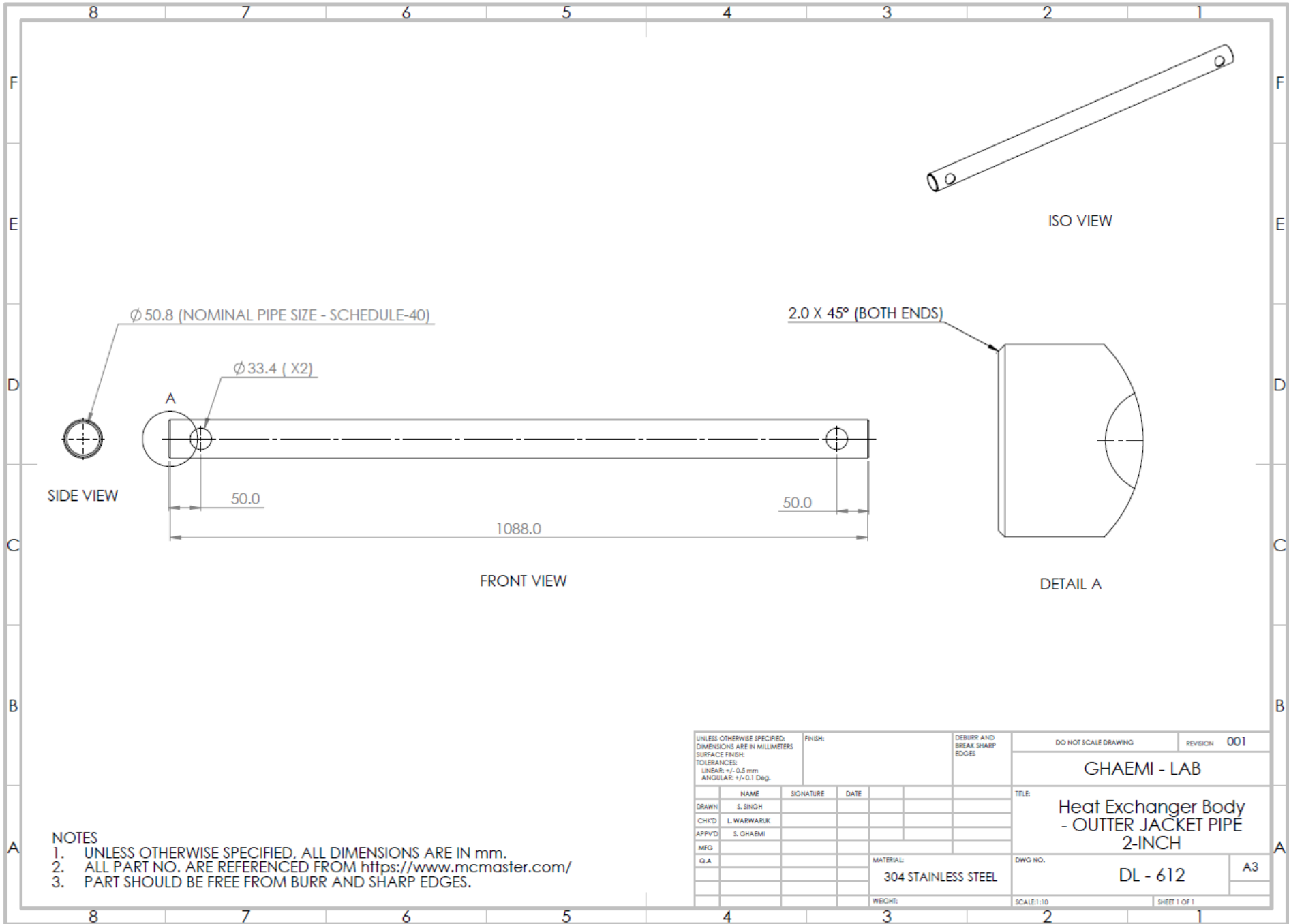
- NOTES**
- UNLESS OTHERWISE SPECIFIED, ALL DIMENSIONS ARE IN mm.
  - ALL PART NO. ARE REFERENCED FROM <https://www.mcmaster.com/>
  - PART SHOULD BE FREE FROM BURR, SHARP EDGES AND WELD SPATTER.
  - ALL PERIPHERAL WELD JOINTS SHOULD NOT LEAK.

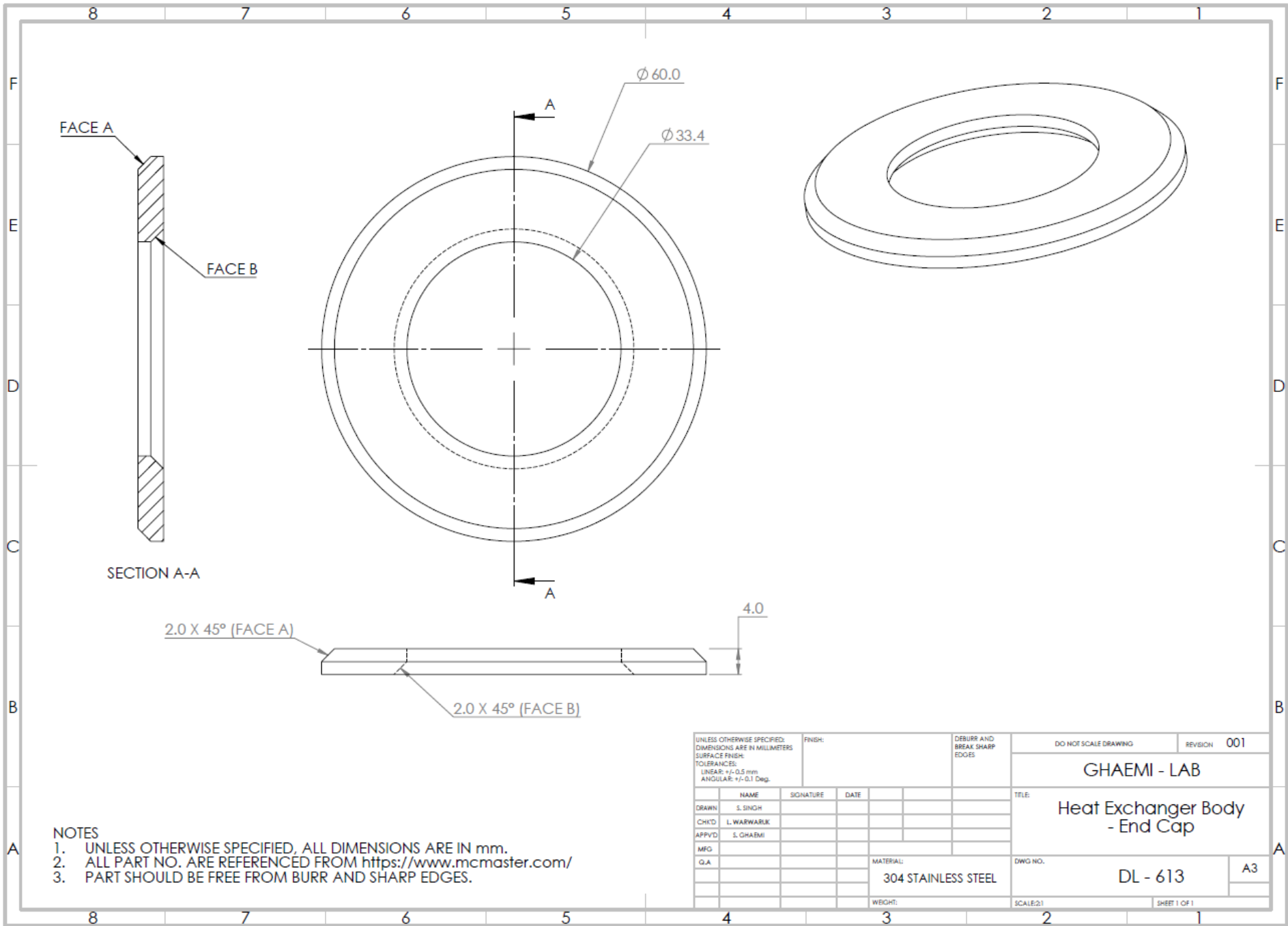
UNLESS OTHERWISE SPECIFIED: DIMENSIONS ARE IN MILLIMETERS SURFACE FINISH: TOLERANCES: LINEAR: +/- 0.5 mm ANGULAR: +/- 0.1 Deg.		FINISH:	DEBURR AND BREAK SHARP EDGES	DO NOT SCALE DRAWING	REVISION	002
NAME	SIGNATURE	DATE		GHAEMI - LAB		
DRAWN	S. SINGH			TITLE		
CHK'D	L. WARWARIK			Heat Exchanger Body (ASM)		
APP'VD	S. GHAEMI			DWG NO.		
MFG				DL - 610		
G.A.			MATERIAL: LISTED	A3		
			WEIGHT:	SCALE: 1:10		
				SHEET 1 OF 1		



- NOTES
1. UNLESS OTHERWISE SPECIFIED, ALL DIMENSIONS ARE IN mm.
  2. ALL PART NO. ARE REFERENCED FROM <https://www.mcmaster.com/>
  3. PART SHOULD BE FREE FROM BURR AND SHARP EDGES.

UNLESS OTHERWISE SPECIFIED: DIMENSIONS ARE IN MILLIMETERS SURFACE FINISH: TOLERANCES: LINEAR: +/- 0.5 mm ANGULAR: +/- 0.1 Deg.		FINISH:	DEBURR AND BREAK SHARP EDGES	DO NOT SCALE DRAWING	REVISION 002
NAME			SIGNATURE	DATE	TITLE
DRAWN S. SINGH					GHAEMI - LAB  Heat Exchanger Body - CORE PIPE 1-INCH
CHKD L. WARWARIK					
APPVD S. GHAEMI					
MFG					
G.A.					DWG NO.
			MATERIAL:		DL - 611
			304 STAINLESS STEEL		A3
			WEIGHT:		SCALE: 1:10
					SHEET 1 OF 1

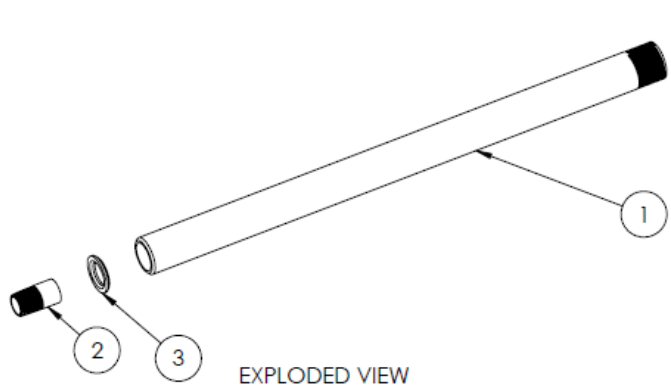




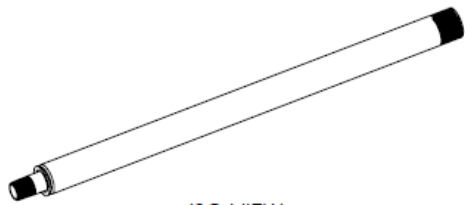
- NOTES**
1. UNLESS OTHERWISE SPECIFIED, ALL DIMENSIONS ARE IN mm.
  2. ALL PART NO. ARE REFERENCED FROM <https://www.mcmaster.com/>
  3. PART SHOULD BE FREE FROM BURR AND SHARP EDGES.

UNLESS OTHERWISE SPECIFIED: DIMENSIONS ARE IN MILLIMETERS		FINISH:		DEBURR AND BREAK SHARP EDGES		DO NOT SCALE DRAWING		REVISION 001	
SURFACE FINISH:						GHAEMI - LAB			
TOLERANCES:									
LINEAR: +/- 0.5 mm						Heat Exchanger Body - End Cap			
ANGULAR: +/- 0.1 Deg.									
NAME	SIGNATURE	DATE				TITLE:			
DRAWN S. SINGH						DL - 613			
CHK'D L. WARWARIK									
APP'VD S. GHAEMI						DWG NO.		A3	
MFG						MATERIAL:		304 STAINLESS STEEL	
Q.A.						WEIGHT:		SCALE:2:1	
								SHEET 1 OF 1	

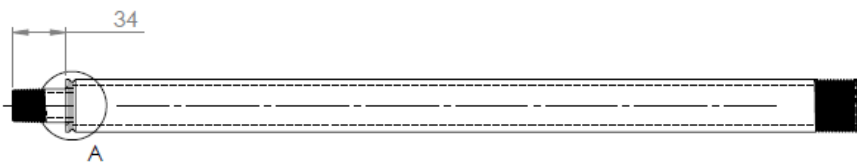




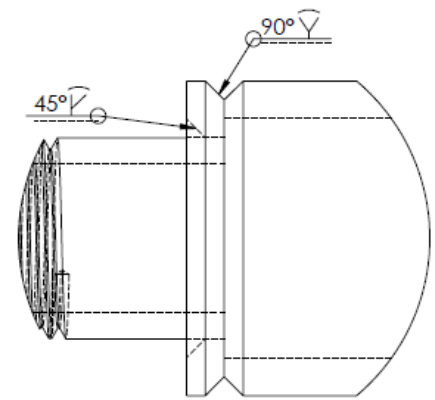
EXPLODED VIEW



ISO VIEW



FRONT VIEW

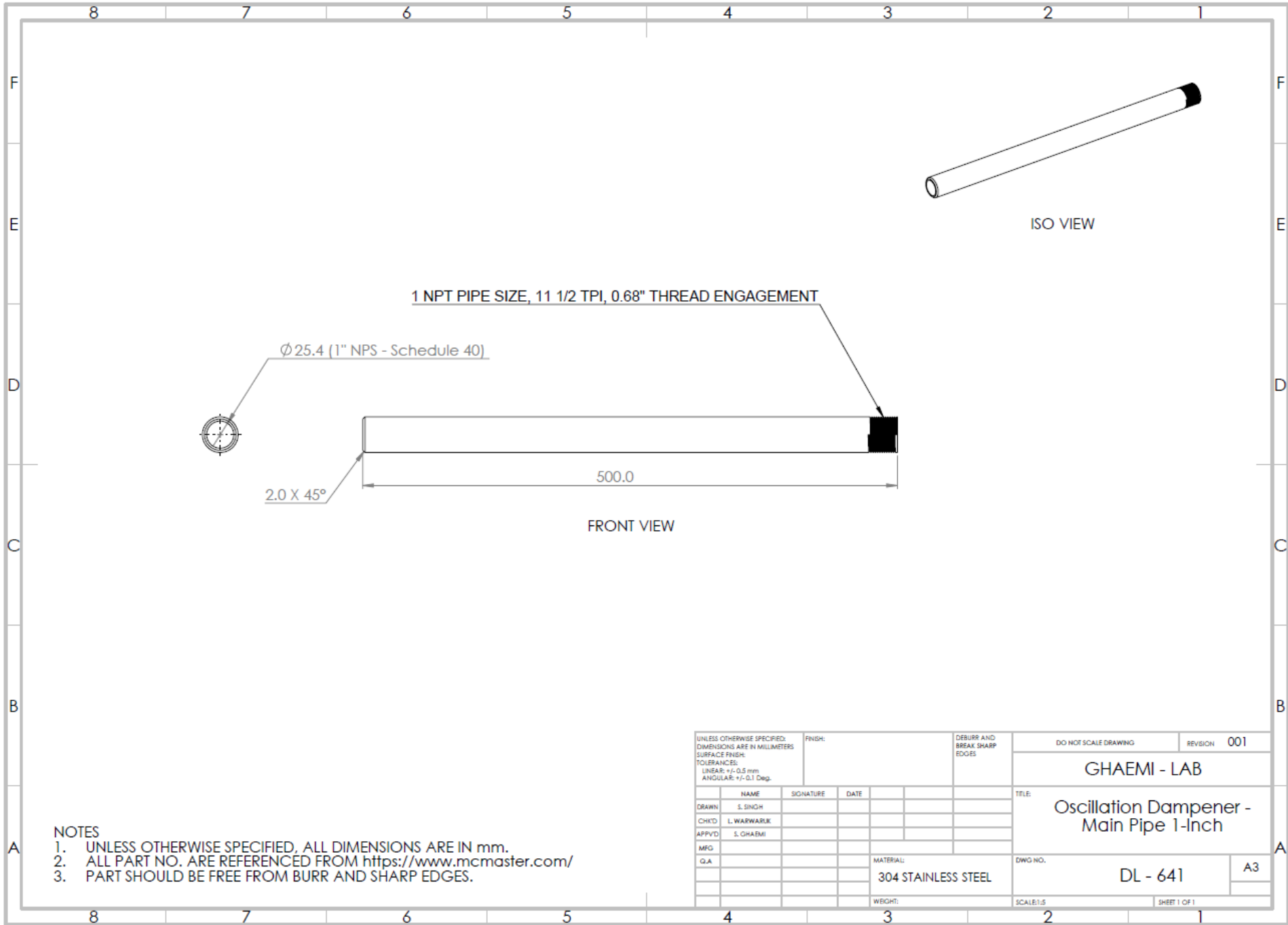


DETAIL A

ITEM NO.	PART NUMBER	DESCRIPTION	QTY.	MATERIAL
1	DL-641	OSCILLATION DAMPNER - MAIN PIPE 1-INCH	1	304 STAINLESS STEEL
2	-	STANDARD-WALL THREADED PIPE NIPPLE, THREADED ON ONE END, 1/2 NPT, 1-1/2" LONG (9157K23)	1	304 STAINLESS STEEL
3	DL-643	MAIN PIPE END CAP	1	304 STAINLESS STEEL

- NOTES
1. UNLESS OTHERWISE SPECIFIED, ALL DIMENSIONS ARE IN mm.
  2. ALL PART NO. ARE REFERENCED FROM <https://www.mcmaster.com/>
  3. PART SHOULD BE FREE FROM BURR, SHARP EDGES AND WELD SPATTER.
  4. ALL PERIPHERAL WELD JOINTS SHOULD NOT LEAK.

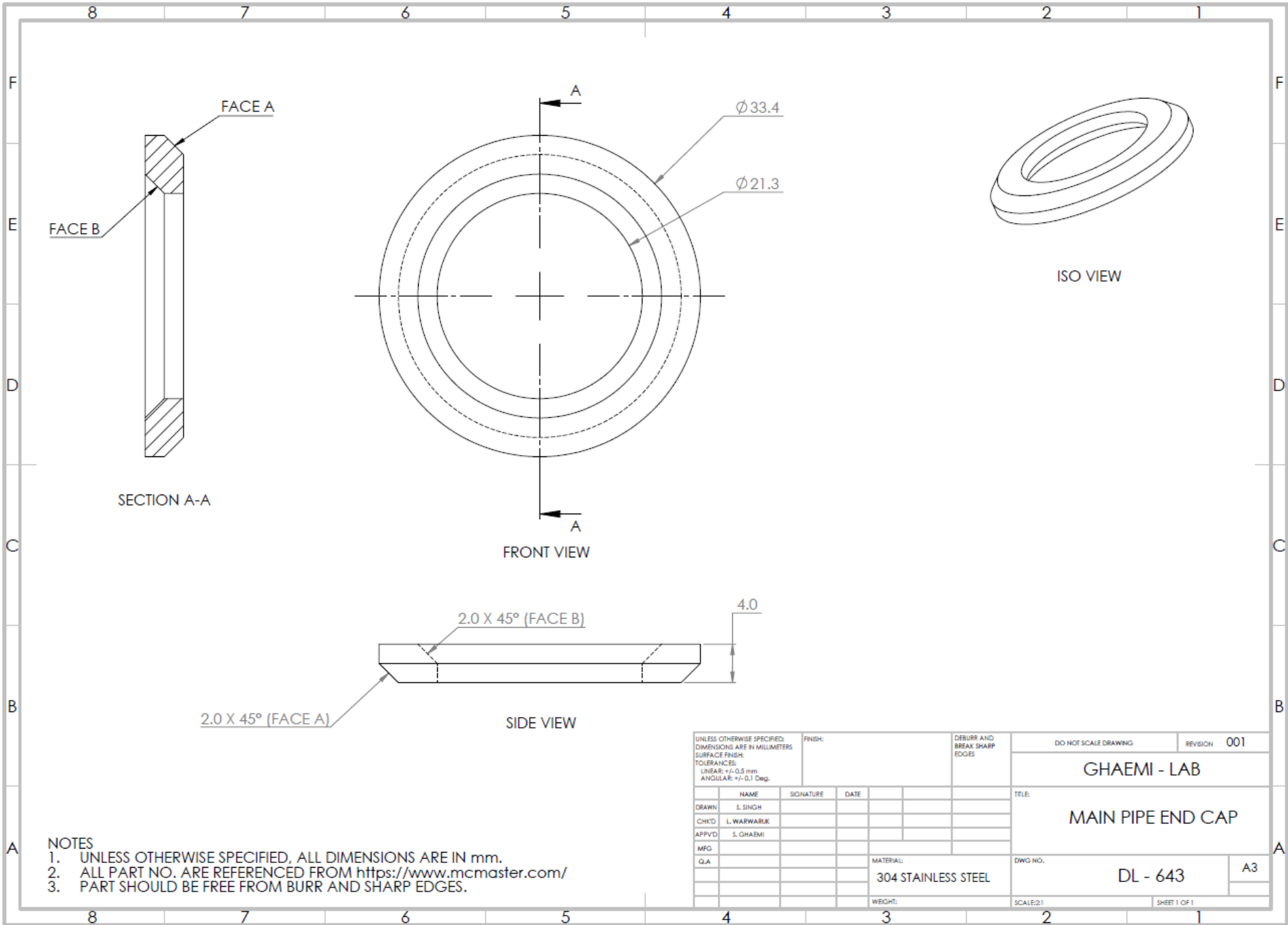
UNLESS OTHERWISE SPECIFIED: DIMENSIONS ARE IN MILLIMETERS SURFACE FINISH: TOLERANCES: LINEAR: +/-0.5 mm ANGULAR: +/-0.1 Deg.		FINISH:	DEBURR AND BREAK SHARP EDGES	DO NOT SCALE DRAWING	REVISION 001
DRAWN: S. SINGH			TITLE: GHAEMI - LAB		
CHK'D: L. WARWARK			Oscillation Dampener (ASM)		
APP'VD: S. GHAEMI			DWG NO. DL - 640		
MFG:			SCALE: 1:5		
G.A.			SHEET 1 OF 1		
MATERIAL: LISTED			A3		
WEIGHT:					



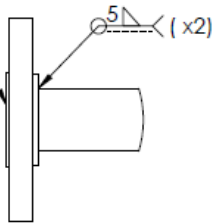
**NOTES**

1. UNLESS OTHERWISE SPECIFIED, ALL DIMENSIONS ARE IN mm.
2. ALL PART NO. ARE REFERENCED FROM <https://www.mcmaster.com/>
3. PART SHOULD BE FREE FROM BURR AND SHARP EDGES.

UNLESS OTHERWISE SPECIFIED: DIMENSIONS ARE IN MILLIMETERS SURFACE FINISH: TOLERANCES: LINEAR: +/- 0.5 mm ANGULAR: +/- 0.1 Deg.		FINISH:	DEBURR AND BREAK SHARP EDGES	DO NOT SCALE DRAWING	REVISION 001
				GHAEMI - LAB	
DRAWN: S. SINGH	SIGNATURE	DATE	TITLE: Oscillation Dampener - Main Pipe 1-Inch		
CHKD: L. WARWARIK					
APPVD: S. GHAEMI					
MFG					
G.A.			MATERIAL: 304 STAINLESS STEEL	DWG NO. DL - 641	A3
			WEIGHT:	SCALE: 1:5	SHEET 1 OF 1

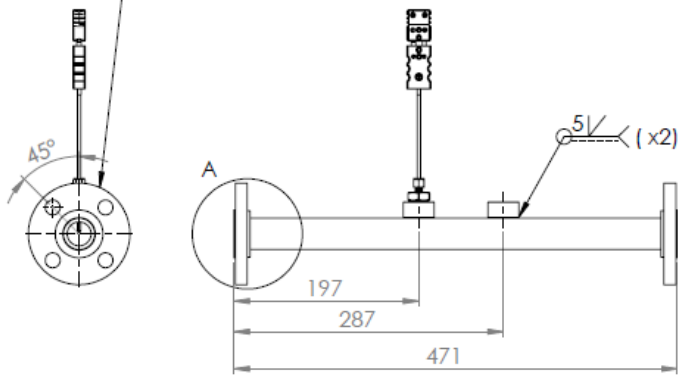


OUTER DIMENSIONS  
ARE FROM THIS FACE

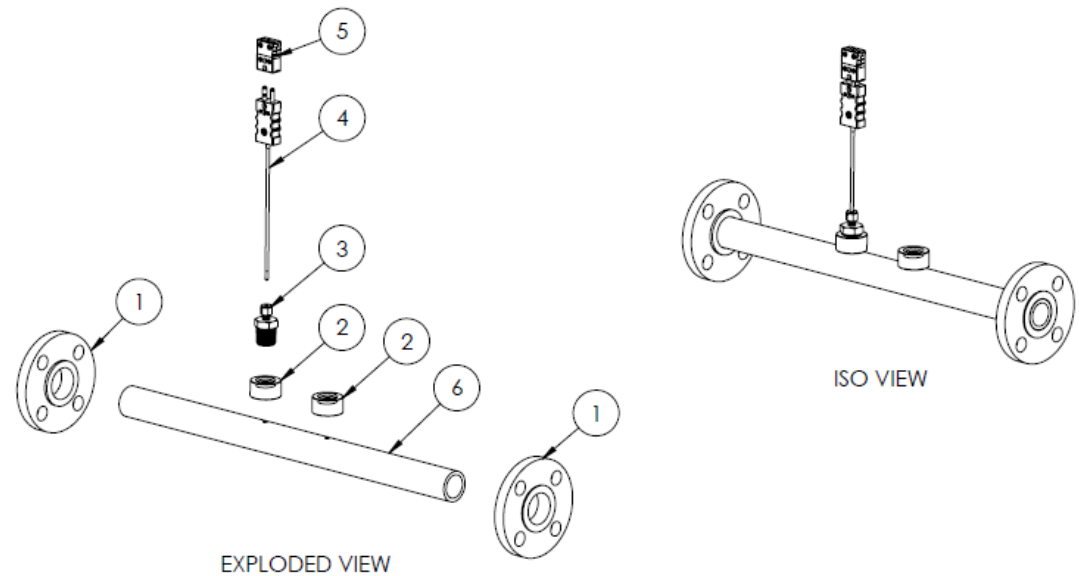


DETAIL A

Both flange's hole-orientation  
should be in-line and also  
vertically oriented at 45° with  
the two weld bung's axis.



FRONT VIEW



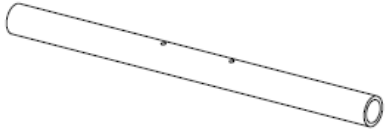
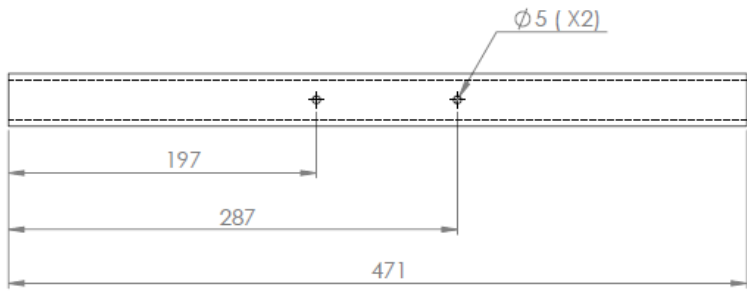
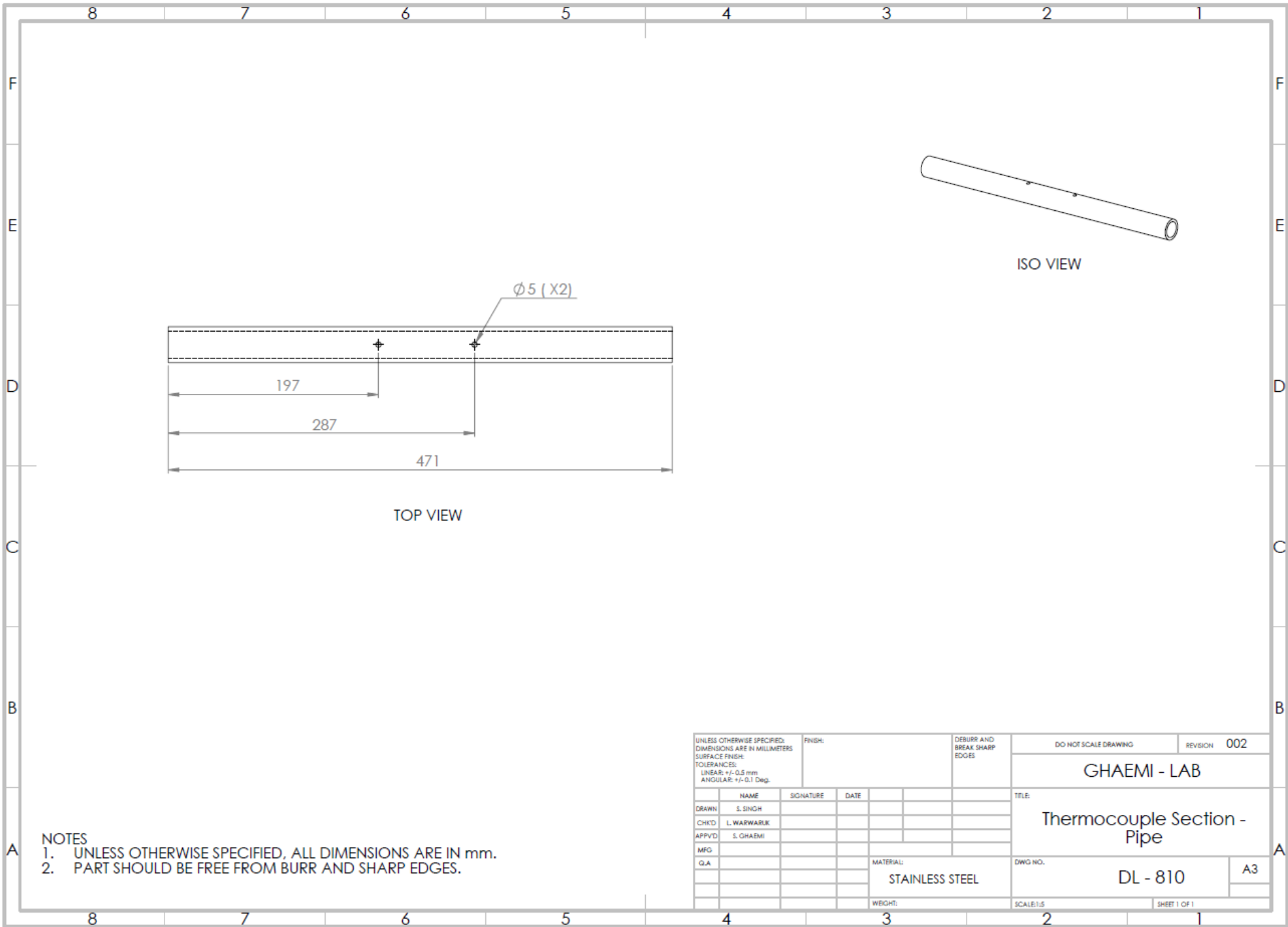
EXPLODED VIEW

ITEM NO.	DRAWING NUMBER	DESCRIPTION	QTY.	MATERIAL
1	-	Low-Pressure Forged Pipe Flange (44685K181)	2	304 Stainless Steel
2	-	Threaded Pipe Fitting (4464K473)	2	304 Stainless Steel
3	-	Yor-Lok Fitting for Stainless Steel Tubing (5182K21)	1	304 Stainless Steel
4	-	Bendable Thermocouple Probe for Liquid and Gas (K-Type)	1	
5	-	Thermocouple Connector	1	
6	DL - 810	1" Pipe (Schedule 40)	1	Stainless Steel

NOTES

1. UNLESS OTHERWISE SPECIFIED, ALL DIMENSIONS ARE IN mm.
2. ALL PART NO. ARE REFERENCED FROM <https://www.mcmaster.com/>
3. PART SHOULD BE FREE FROM BURR, SHARP EDGES AND WELD SPATTER.
4. ALL PHERIPARAL WELD JOINTS SHOULD NOT LEAK.

UNLESS OTHERWISE SPECIFIED: DIMENSIONS ARE IN MILLIMETERS SURFACE FINISH: TOLERANCES: LINEAR: +/-0.5 mm ANGULAR: +/-0.1 Deg.		FINISH:	DEBURR AND BREAK SHARP EDGES	DO NOT SCALE DRAWING	REVISION 004
NAME			SIGNATURE	DATE	TITLE
DRAWN S. SINGH					GHAEMI - LAB  Thermocouple Section
CHK'D L. WARWARIK					
APP'VD S. GHAEMI					
MFG					
G.A.			MATERIAL:		DWG NO.
			LISTED		DL - 800
			WEIGHT:		A3
			SCALE:1:15		SHEET 1 OF 1

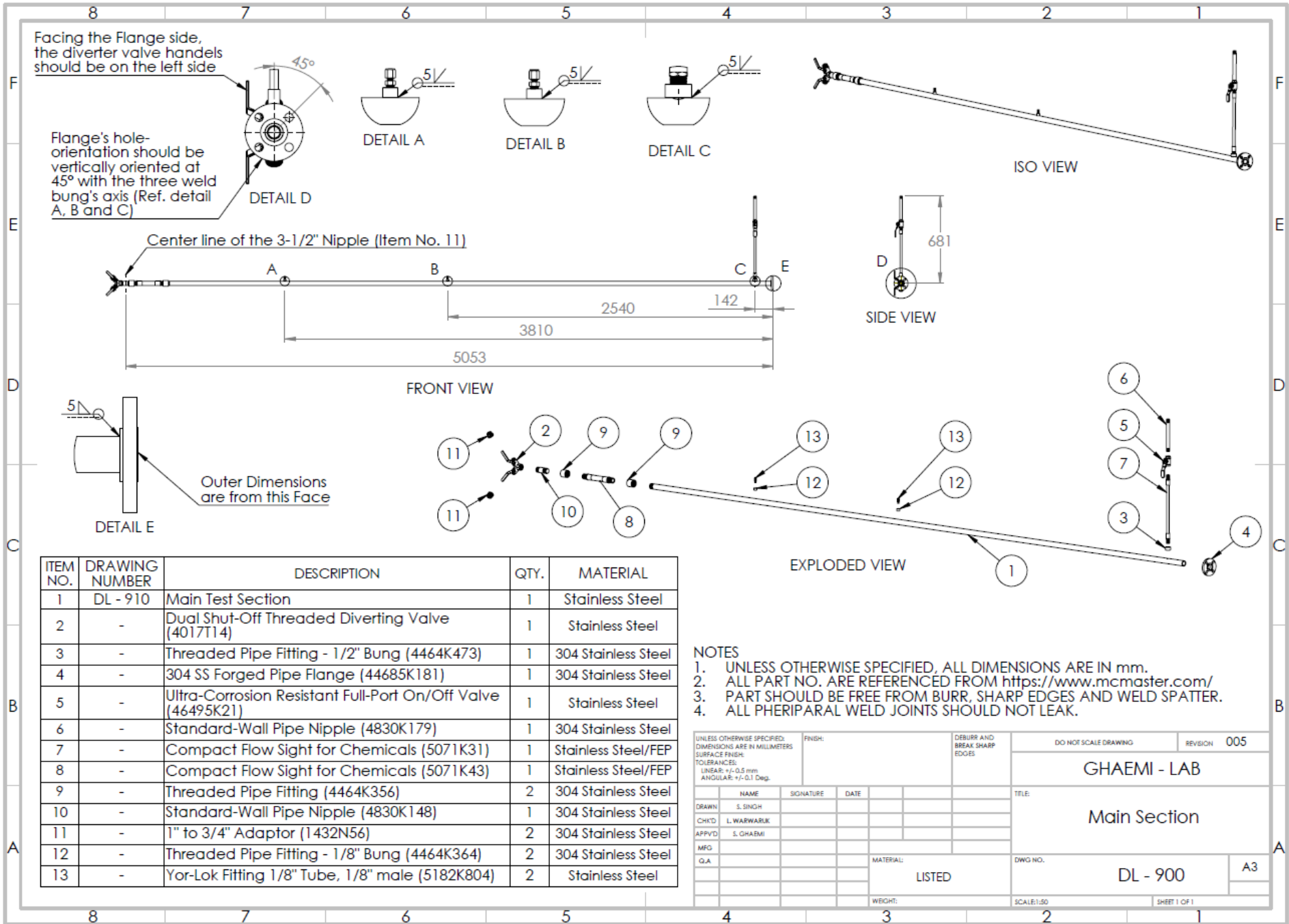


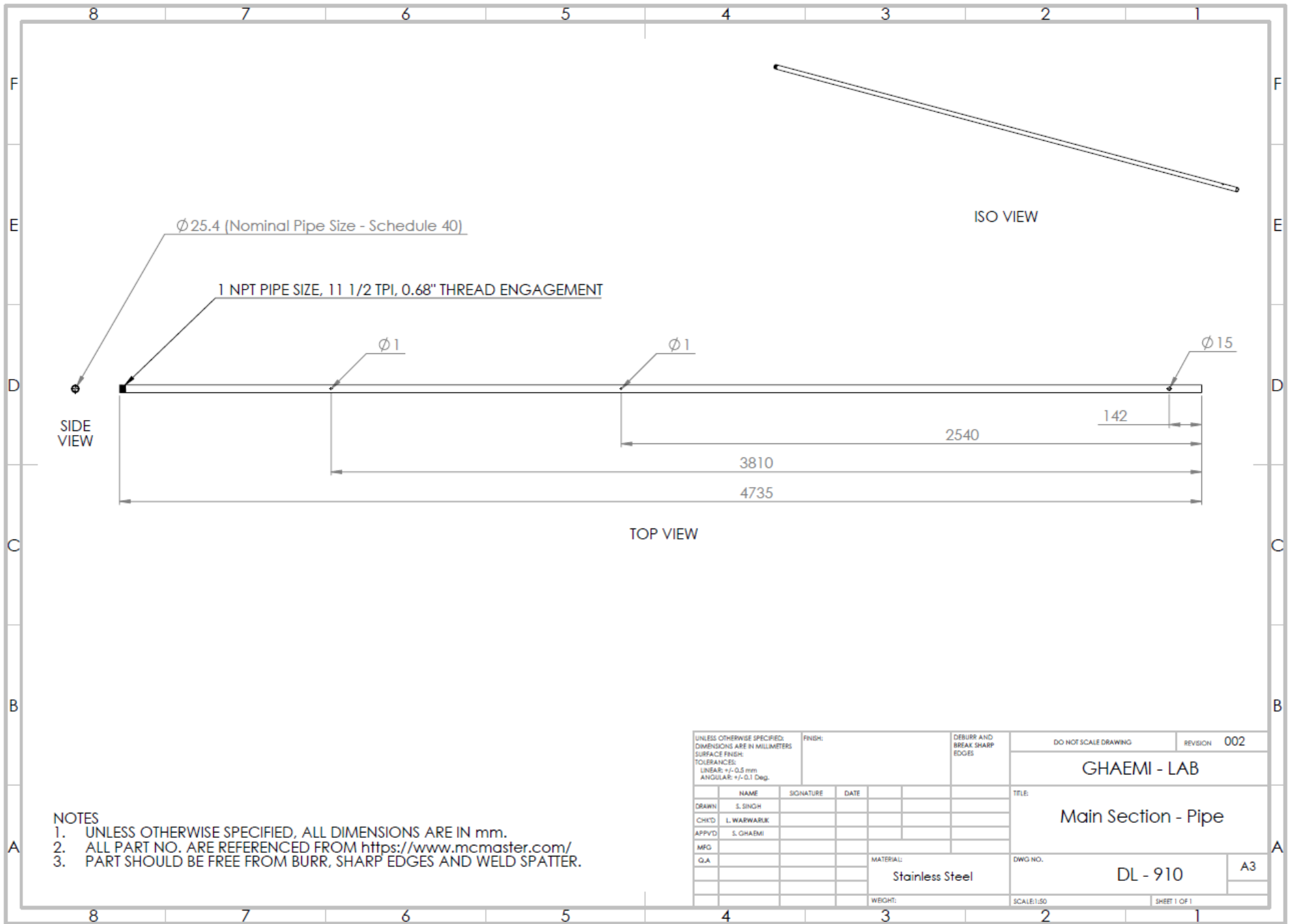
ISO VIEW

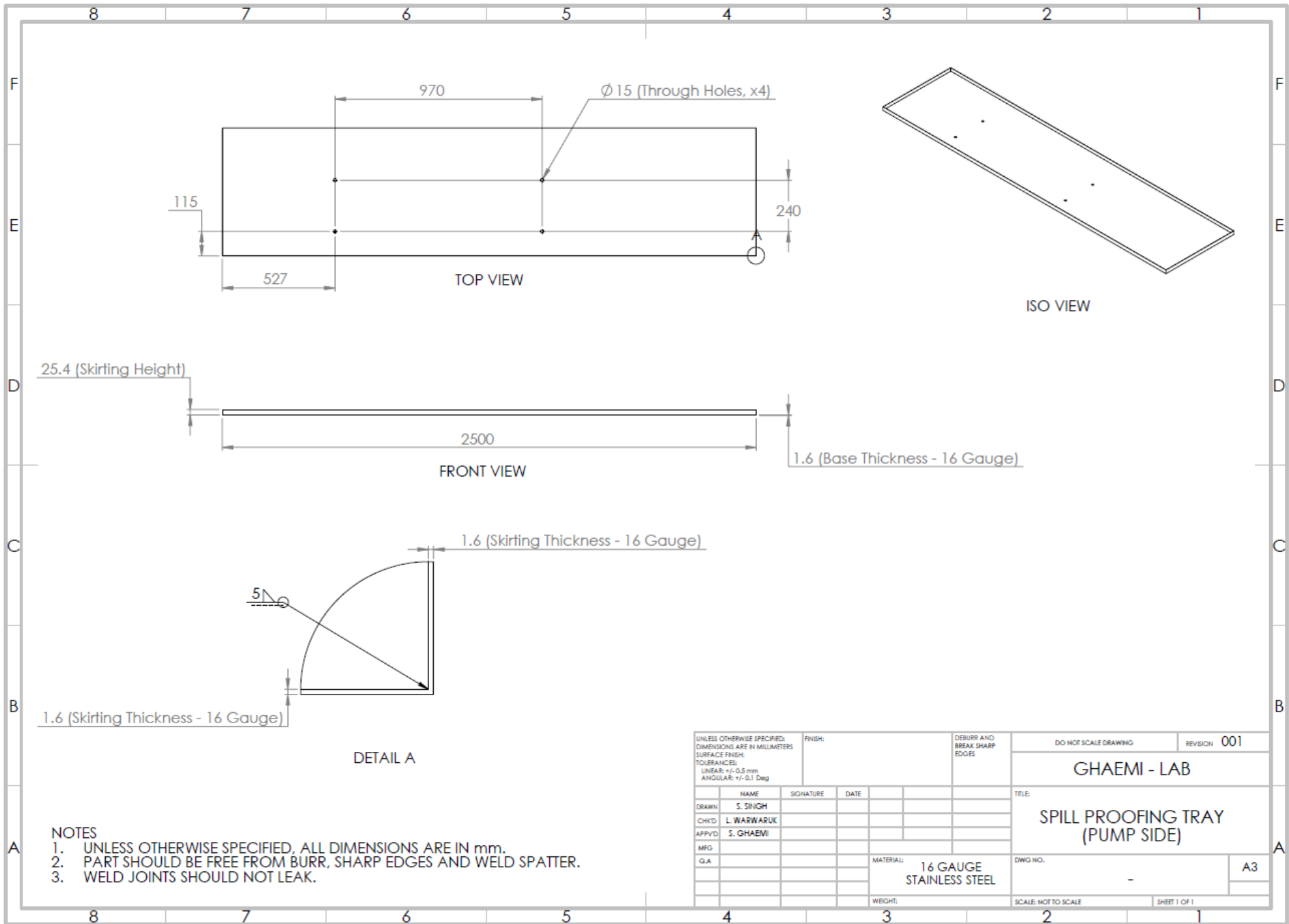
TOP VIEW

- NOTES
1. UNLESS OTHERWISE SPECIFIED, ALL DIMENSIONS ARE IN mm.
  2. PART SHOULD BE FREE FROM BURR AND SHARP EDGES.

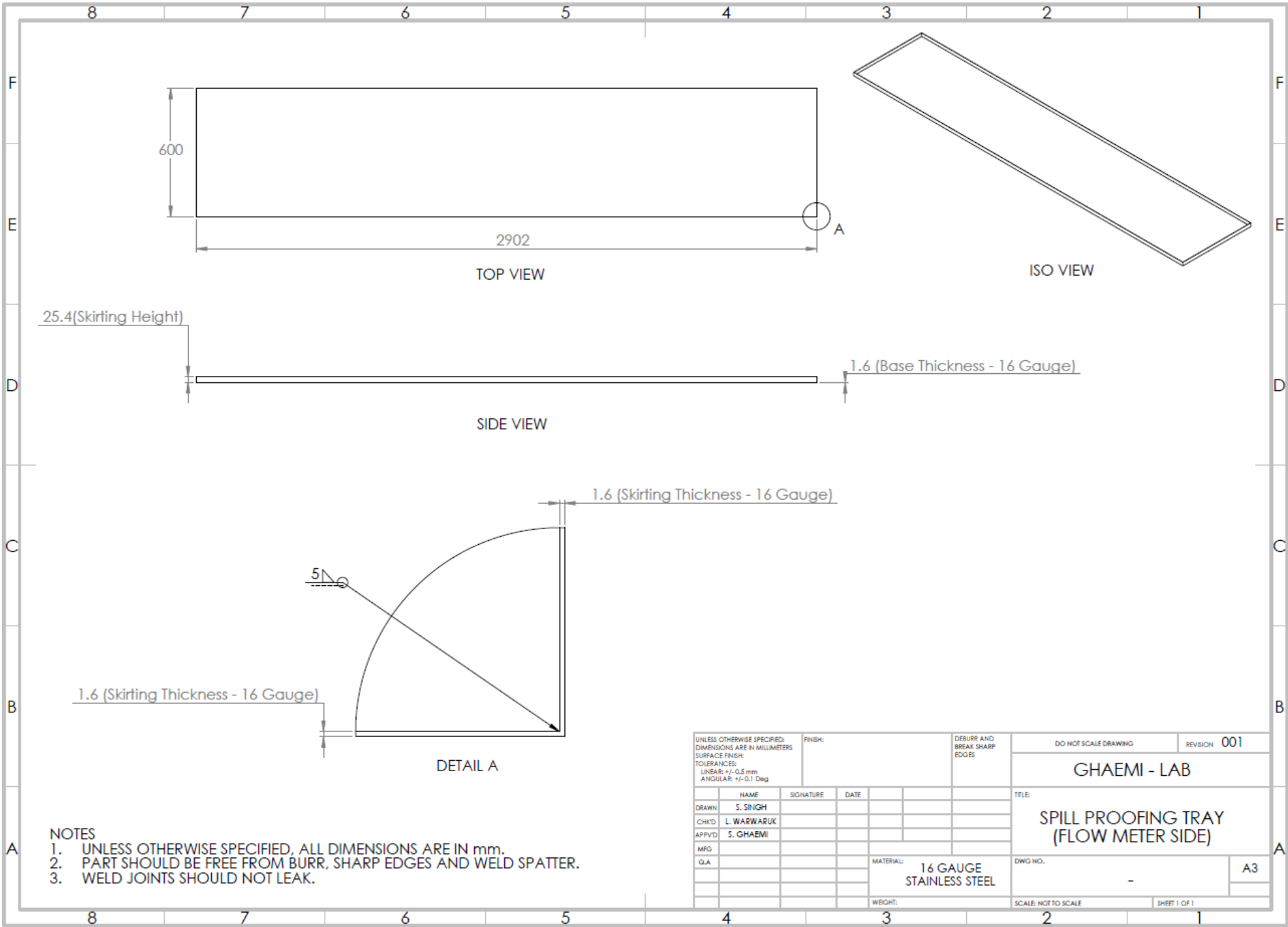
UNLESS OTHERWISE SPECIFIED: DIMENSIONS ARE IN MILLIMETERS				FINISH:		DEBURR AND BREAK SHARP EDGES		DO NOT SCALE DRAWING		REVISION 002	
SURFACE FINISH:								GHAEMI - LAB			
TOLERANCES: LINEAR: +/- 0.5 mm ANGULAR: +/- 0.1 Deg.								TITLE: Thermocouple Section - Pipe			
DRAWN	S. SINGH	SIGNATURE	DATE					DWG NO.		DL - 810	
CHK'D	L. WARWARIK									A3	
APP'VD	S. GHAEMI										
MFG											
G.A.							MATERIAL:				
							STAINLESS STEEL				
							WEIGHT:	SCALE: 1:15		SHEET 1 OF 1	











## Appendix B

### Pressure-drop ( $\Delta P$ ) versus time ( $t$ ) plots

This section provides the pressure-drop ( $\Delta P$ ) versus time ( $t$ ) data from the pipe flow tests for water-based polymer solution. The data for each %DR and all three test sections are presented. As detailed in table 4, after the initial 2 minutes at zero flow rate, the pump was set at 600 RPM for the next 5 minutes to mix the polymer solution batch with the de-aired water in the loop. As the pump ramps up, it takes a while for the polymer solution to mix and reach the test section from the tank. Until then, only water flows in the test section. This translates to a higher  $\Delta P$  reading for water flow and immediate reduction in  $\Delta P$  as the polymer solution reaches the test section. This can be observed from each plot showing that initial spike in  $\Delta P$  reading followed by a lower stable value which represents mixing of the polymer solution. At the end of 7 minutes (420 seconds), the polymer is degraded for a set degradation time ( $t_{dg}$ ) to achieve the required %DR, this is the region of the plot that shows a period of zero  $\Delta P$ , since the transducer is isolated during this time. For the first plot of each test section (MDR case), no degradation was performed. Post degradation, the five mass flow values are set (refer to table 1), each running for 6 minutes. This is represented by the following five steps in the  $\Delta P$  readings as seen in each plot.

## B.1 For test section with 1-inch ID

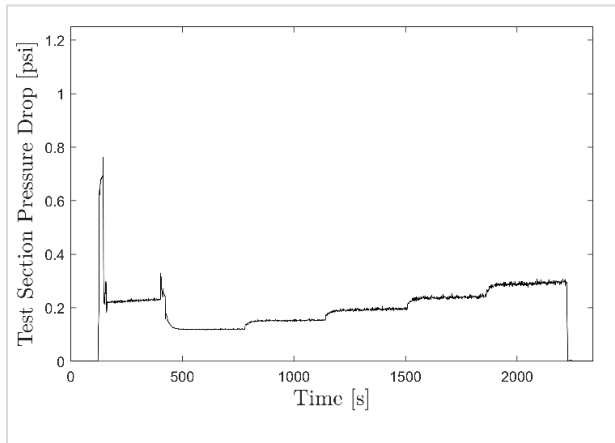


Figure B.1a:  $\Delta P$  versus  $t$  plot for 76% DR.

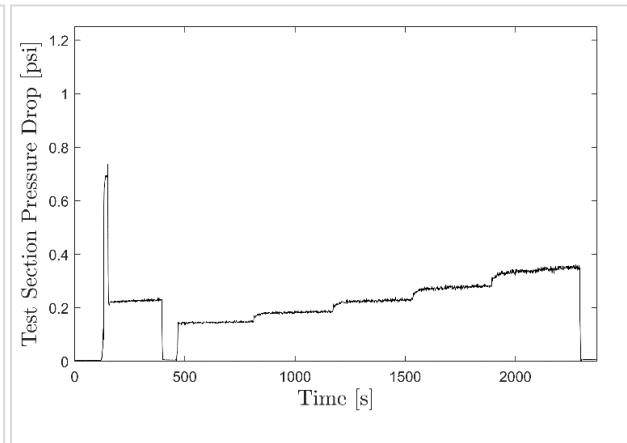


Figure B.1b:  $\Delta P$  versus  $t$  plot for 70% DR.

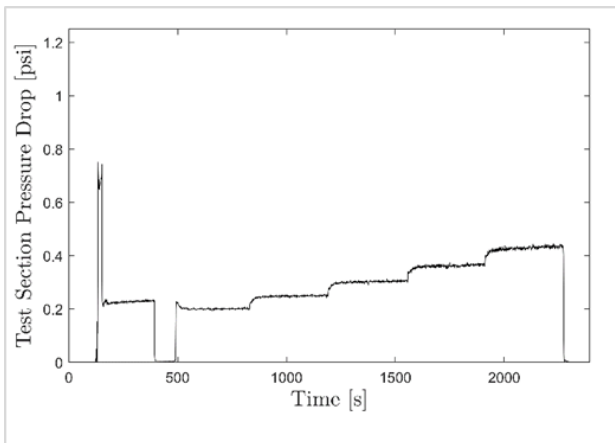


Figure B.1c:  $\Delta P$  versus  $t$  plot for 65% DR.

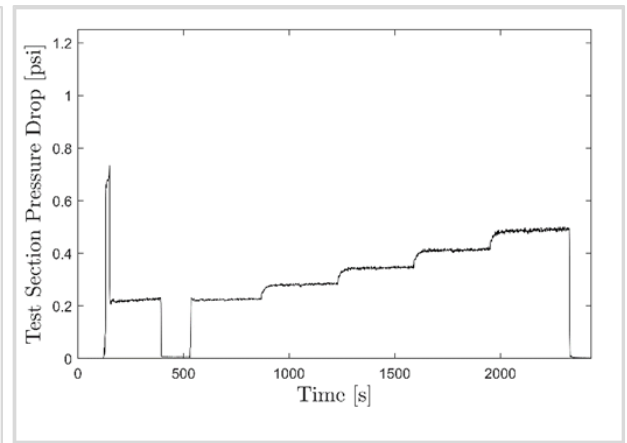


Figure B.1d:  $\Delta P$  versus  $t$  plot for 60% DR.

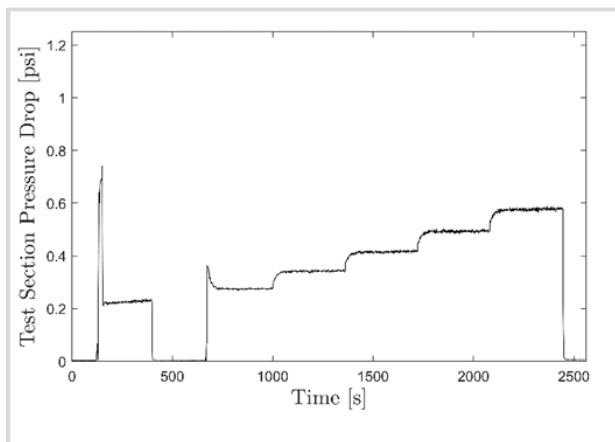


Figure B.1e:  $\Delta P$  versus  $t$  plot for 50% DR.

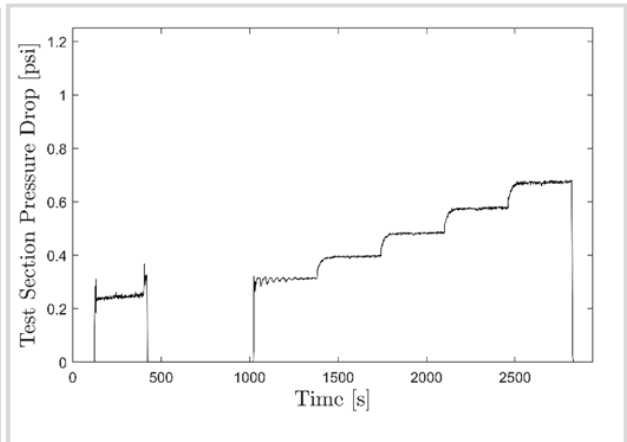


Figure B.1f:  $\Delta P$  versus  $t$  plot for 40% DR.

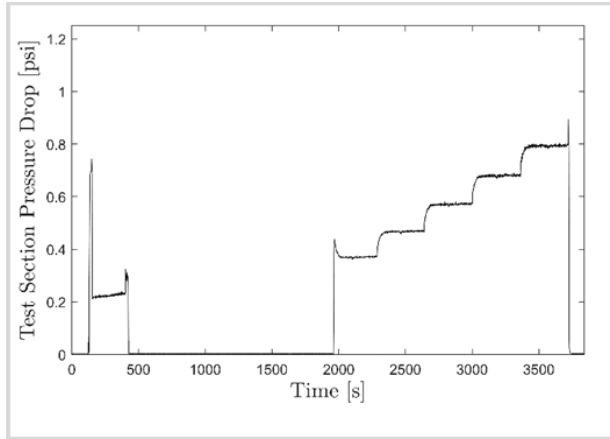


Figure B.1g:  $\Delta P$  versus  $t$  plot for 30% DR.

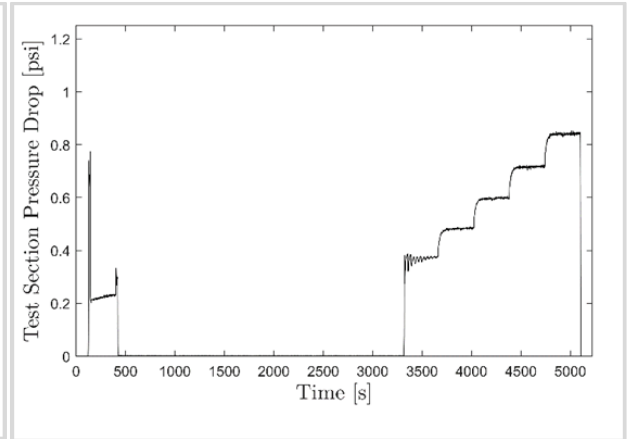


Figure B.1h:  $\Delta P$  versus  $t$  plot for 20%

## B.2 For test section with 1.5-inch ID

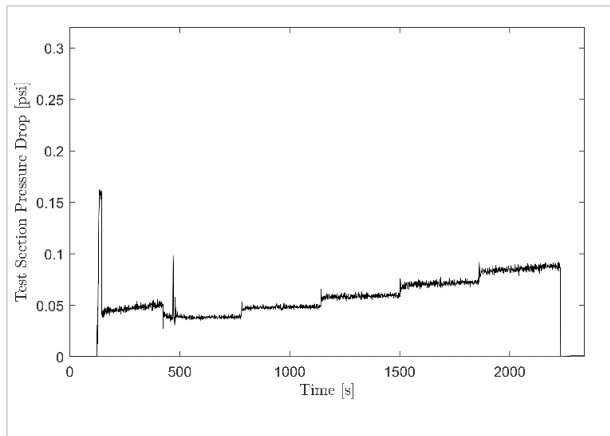


Figure B.2a:  $\Delta P$  versus  $t$  plot for 70% DR.

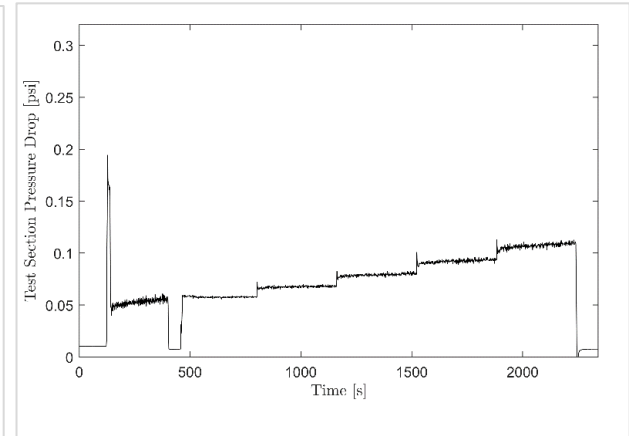


Figure B.2b:  $\Delta P$  versus  $t$  plot for 65% DR.

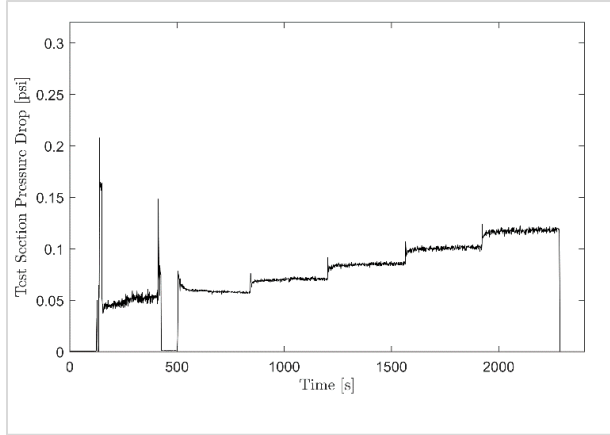


Figure B.2c:  $\Delta P$  versus  $t$  plot for 60% DR.

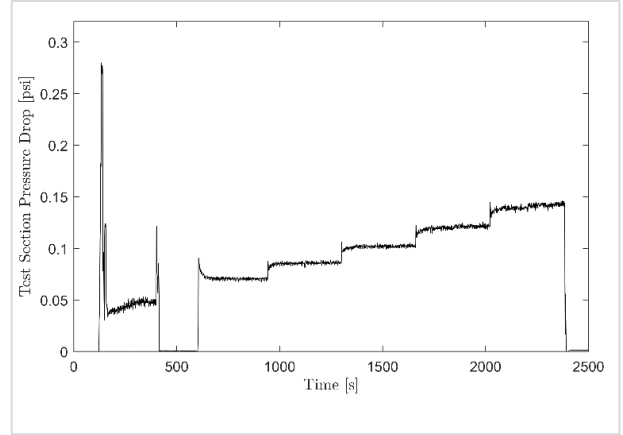


Figure B.2d:  $\Delta P$  versus  $t$  plot for 50% DR.

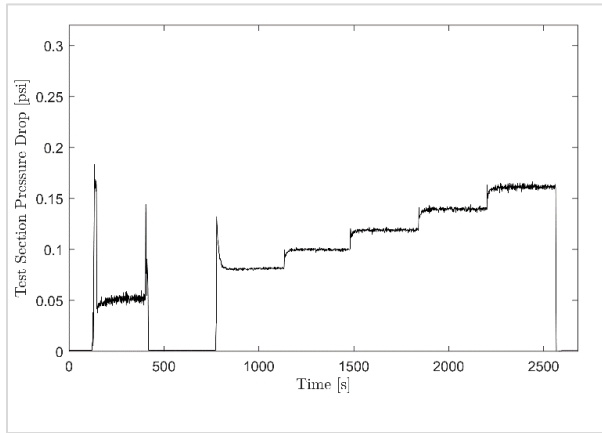


Figure B.2e:  $\Delta P$  versus  $t$  plot for 40% DR.

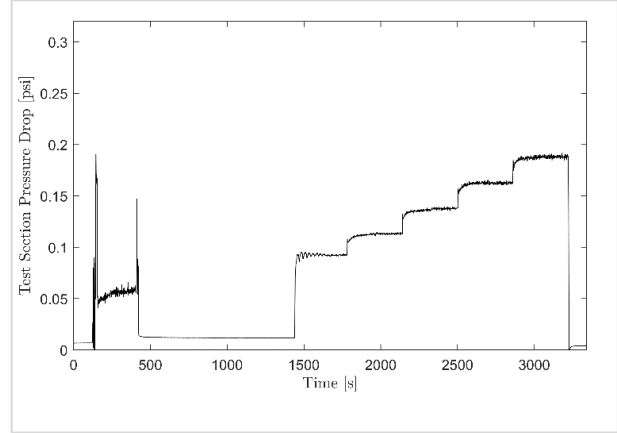


Figure B.2f:  $\Delta P$  versus  $t$  plot for 30% DR.

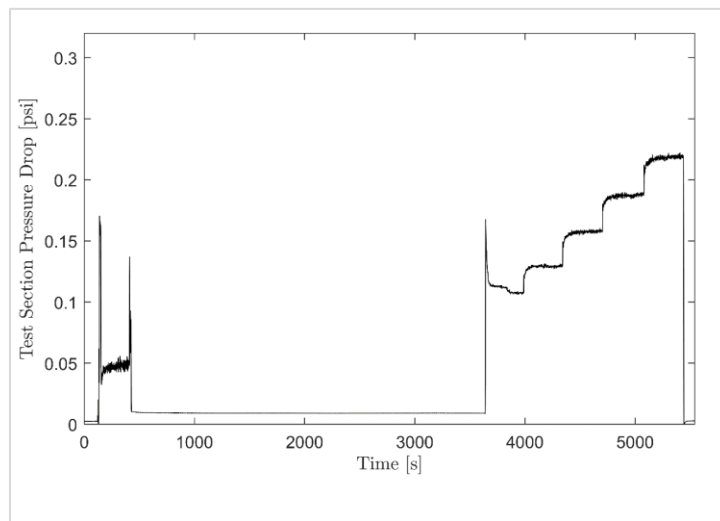


Figure B.2g:  $\Delta P$  versus  $t$  plot for 20% DR.

### B.3 For test section with 2-inch ID

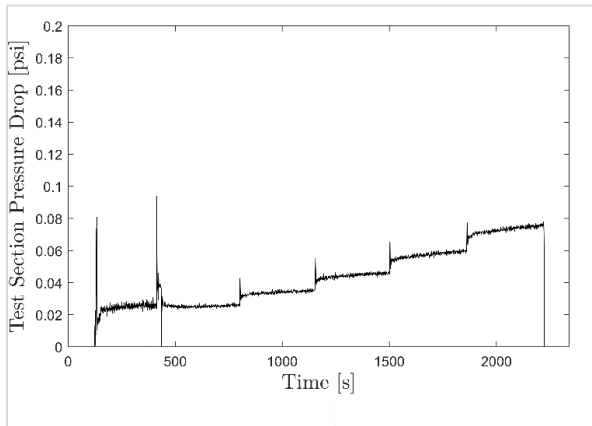


Figure B.3a:  $\Delta P$  versus  $t$  plot for 60% DR.

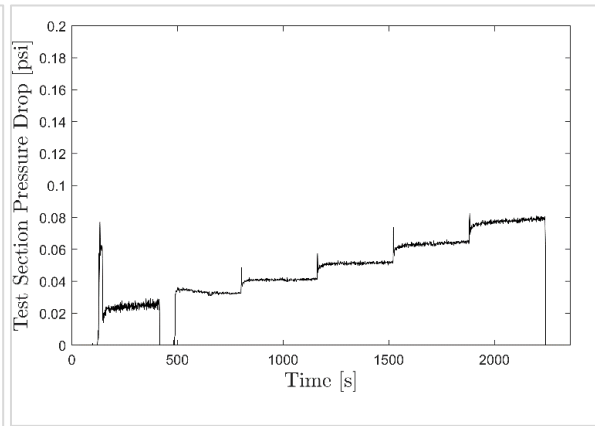


Figure B.3b:  $\Delta P$  versus  $t$  plot for 50% DR.

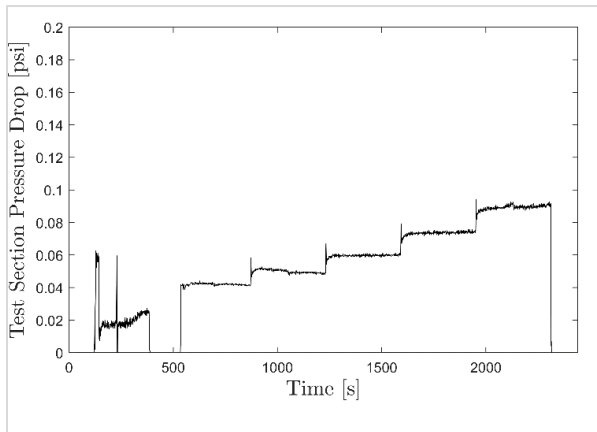


Figure B.3c:  $\Delta P$  versus  $t$  plot for 40% DR.

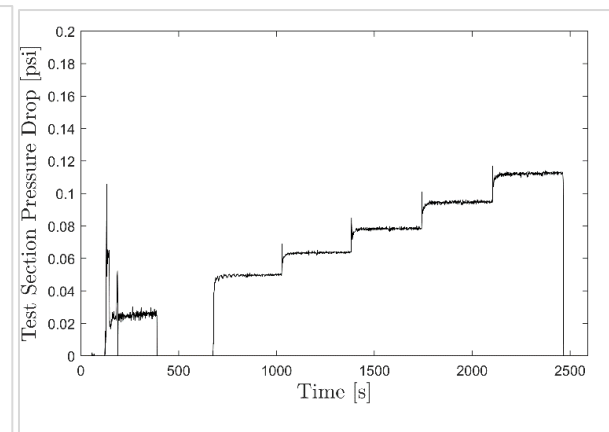


Figure B.3d:  $\Delta P$  versus  $t$  plot for 30% DR.

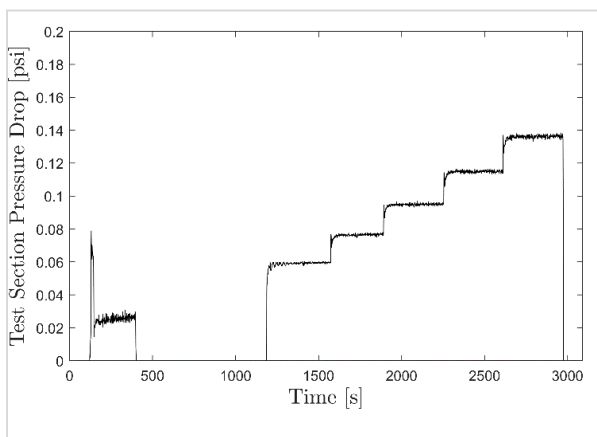


Figure B.3e:  $\Delta P$  versus  $t$  plot for 15% DR.

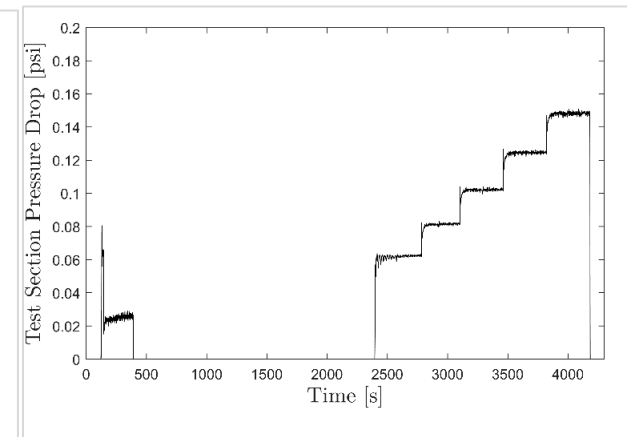


Figure B.3f:  $\Delta P$  versus  $t$  plot for 10% DR.

## Appendix C

### Shear viscosity data

This section lists the data from the shear viscosity measurements as discussed in section 3.5. Each table provides the values for zero-rate viscosity ( $\mu_0$ ), infinite-rate viscosity ( $\mu_\infty$ ), consistency ( $c$ ) and rate index ( $n$ ) for all five  $Re$  (60000, 70000, 80000, 90000, and 100000) for each %DR. The data is presented for all three test sections. This data was used to calculate the shear viscosity ( $\mu_s$ ) of the polymer solution, which was further utilized to obtain  $Re$  value for each sample as detailed in section 3.5.

## C.1 For test section with 1–inch ID

### 76% DR

Data for 1-inch, 76% DR, Re: 60000
zero-rate viscosity: 1.47788e-3 Pa.s
infinite-rate viscosity: 1.16535e-3 Pa.s
consistency: 0.0371144 s
rate index: 0.852253
R <sup>2</sup> : 0.999609

Data for 1-inch, 76% DR, Re: 70000
zero-rate viscosity: 1.43593e-3 Pa.s
infinite-rate viscosity: 1.16585e-3 Pa.s
consistency: 0.0311286 s
rate index: 0.910882
R <sup>2</sup> : 0.999975

Data for 1-inch, 76% DR, Re: 80000
zero-rate viscosity: 1.43767e-3 Pa.s
infinite-rate viscosity: 1.12735e-3 Pa.s
consistency: 0.0373868 s
rate index: 0.746280
R <sup>2</sup> : 0.999882

Data for 1-inch, 76% DR, Re: 90000
zero-rate viscosity: 1.39574e-3 Pa.s
infinite-rate viscosity: 1.15050e-3 Pa.s
consistency: 0.0291223 s
rate index: 0.884987
R <sup>2</sup> : 0.999908

Data for 1-inch, 76% DR, Re: 100000
zero-rate viscosity: 1.37961e-3 Pa.s
infinite-rate viscosity: 1.15221e-3 Pa.s
consistency: 0.0272905 s
rate index: 0.907582
R <sup>2</sup> : 0.999909

### 70% DR

Data for 1-inch, 70% DR, Re: 60000
zero-rate viscosity: 1.45336e-3 Pa.s
infinite-rate viscosity: 1.14247e-3 Pa.s
consistency: 0.0338424 s
rate index: 0.733053
R <sup>2</sup> : 0.999759

Data for 1-inch, 70% DR, Re: 70000
zero-rate viscosity: 1.43556e-3 Pa.s
infinite-rate viscosity: 1.07410e-3 Pa.s
consistency: 0.0242955 s
rate index: 0.606596
R <sup>2</sup> : 0.999044

Data for 1-inch, 70% DR, Re: 80000
zero-rate viscosity: 1.41129e-3 Pa.s
infinite-rate viscosity: 1.14755e-3 Pa.s
consistency: 0.0283743 s
rate index: 0.799593
R <sup>2</sup> : 0.999729

Data for 1-inch, 70% DR, Re: 90000
zero-rate viscosity: 1.34483e-3 Pa.s
infinite-rate viscosity: 1.15559e-3 Pa.s
consistency: 0.0232656 s
rate index: 1.04150
R <sup>2</sup> : 0.999840

Data for 1-inch, 70% DR, Re: 100000
zero-rate viscosity: 1.30772e-3 Pa.s
infinite-rate viscosity: 1.13422e-3 Pa.s
consistency: 0.0224723 s
rate index: 1.03689
R <sup>2</sup> : 0.999773

### 65% DR

Data for 1-inch, 65% DR, Re: 60000
zero-rate viscosity: 1.32995e-3 Pa.s
infinite-rate viscosity: 1.13464e-3 Pa.s
consistency: 0.0224168 s
rate index: 0.901628
R <sup>2</sup> : 0.998197

Data for 1-inch, 65% DR, Re: 70000
zero-rate viscosity: 1.31819e-3 Pa.s
infinite-rate viscosity: 1.15460e-3 Pa.s
consistency: 0.0211985 s
rate index: 1.05122
R <sup>2</sup> : 0.998912

Data for 1-inch, 65% DR, Re: 80000
zero-rate viscosity: 1.31490e-3 Pa.s
infinite-rate viscosity: 1.13439e-3 Pa.s
consistency: 0.0223187 s
rate index: 0.880803
R <sup>2</sup> : 0.996175

Data for 1-inch, 65% DR, Re: 90000
zero-rate viscosity: 1.30039e-3 Pa.s
infinite-rate viscosity: 1.13809e-3 Pa.s
consistency: 0.0222117 s
rate index: 0.950678
R <sup>2</sup> : 0.995660

Data for 1-inch, 65% DR, Re: 100000
zero-rate viscosity: 1.26243e-3 Pa.s
infinite-rate viscosity: 1.14075e-3 Pa.s
consistency: 0.0188817 s
rate index: 1.24593
R <sup>2</sup> : 0.999448



## 60% DR

Data for 1-inch, 60% DR, Re: 60000
zero-rate viscosity: 1.32220e-3 Pa.s
infinite-rate viscosity: 1.11118e-3 Pa.s
consistency: 0.0252207 s
rate index: 0.653243
R <sup>2</sup> : 0.999445

## 50% DR

Data for 1-inch, 50% DR, Re: 60000
zero-rate viscosity: 1.21893e-3 Pa.s
infinite-rate viscosity: 1.14288e-3 Pa.s
consistency: 0.0164962 s
rate index: 1.36994
R <sup>2</sup> : 0.998178

## 40% DR

Data for 1-inch, 40% DR, Re: 60000
zero-rate viscosity: 1.22019e-3 Pa.s
infinite-rate viscosity: 1.09985e-3 Pa.s
consistency: 0.0143782 s
rate index: 0.519139
R <sup>2</sup> : 0.996537

Data for 1-inch, 60% DR, Re: 70000
zero-rate viscosity: 1.28665e-3 Pa.s
infinite-rate viscosity: 1.12037e-3 Pa.s
consistency: 0.0207187 s
rate index: 0.801359
R <sup>2</sup> : 0.999582

Data for 1-inch, 50% DR, Re: 70000
zero-rate viscosity: 1.21072e-3 Pa.s
infinite-rate viscosity: 1.13362e-3 Pa.s
consistency: 0.0164958 s
rate index: 1.24524
R <sup>2</sup> : 0.998450

Data for 1-inch, 40% DR, Re: 70000
zero-rate viscosity: 1.17546e-3 Pa.s
infinite-rate viscosity: 1.10208e-3 Pa.s
consistency: 0.0110345 s
rate index: 0.780116
R <sup>2</sup> : 0.991262

Data for 1-inch, 60% DR, Re: 80000
zero-rate viscosity: 1.27068e-3 Pa.s
infinite-rate viscosity: 1.12582e-3 Pa.s
consistency: 0.0209553 s
rate index: 0.893733
R <sup>2</sup> : 0.999618

Data for 1-inch, 50% DR, Re: 80000
zero-rate viscosity: 1.21229e-3 Pa.s
infinite-rate viscosity: 1.13632e-3 Pa.s
consistency: 0.0158272 s
rate index: 1.20453
R <sup>2</sup> : 0.998342

Data for 1-inch, 40% DR, Re: 80000
zero-rate viscosity: 1.17590e-3 Pa.s
infinite-rate viscosity: 1.12117e-3 Pa.s
consistency: 0.0140380 s
rate index: 1.08432
R <sup>2</sup> : 0.999633

Data for 1-inch, 60% DR, Re: 90000
zero-rate viscosity: 1.26225e-3 Pa.s
infinite-rate viscosity: 1.12465e-3 Pa.s
consistency: 0.0190692 s
rate index: 0.895288
R <sup>2</sup> : 0.999011

Data for 1-inch, 50% DR, Re: 90000
zero-rate viscosity: 1.22044e-3 Pa.s
infinite-rate viscosity: 1.12914e-3 Pa.s
consistency: 0.0171295 s
rate index: 0.936512
R <sup>2</sup> : 0.997968

Data for 1-inch, 40% DR, Re: 90000
zero-rate viscosity: 1.17661e-3 Pa.s
infinite-rate viscosity: 1.13328e-3 Pa.s
consistency: 0.0149413 s
rate index: 1.43389
R <sup>2</sup> : 0.988000

Data for 1-inch, 60% DR, Re: 100000
zero-rate viscosity: 1.24071e-3 Pa.s
infinite-rate viscosity: 1.12811e-3 Pa.s
consistency: 0.0180585 s
rate index: 1.07709
R <sup>2</sup> : 0.999096

Data for 1-inch, 50% DR, Re: 100000
zero-rate viscosity: 1.20837e-3 Pa.s
infinite-rate viscosity: 1.13738e-3 Pa.s
consistency: 0.0162727 s
rate index: 1.19510
R <sup>2</sup> : 0.998970

Data for 1-inch, 40% DR, Re: 100000
zero-rate viscosity: 1.17310e-3 Pa.s
infinite-rate viscosity: 1.12575e-3 Pa.s
consistency: 0.0152374 s
rate index: 1.22032
R <sup>2</sup> : 0.995489

## 30% DR

Data for 1-inch, 30% DR, Re: 60000
zero-rate viscosity: 1.13995e-3 Pa.s
infinite-rate viscosity: 1.12240e-3 Pa.s
consistency: 0.0195278 s
rate index: 1.41203
R <sup>2</sup> : 0.962368

## 20% DR

Data for 1-inch, 20% DR, Re: 60000
zero-rate viscosity: 1.17093e-3 Pa.s
infinite-rate viscosity: 1.11293e-3 Pa.s
consistency: 0.489228 s
rate index: 1.03814
R <sup>2</sup> : 0.947080

Data for 1-inch, 30% DR, Re: 70000
zero-rate viscosity: 1.13935e-3 Pa.s
infinite-rate viscosity: 1.10487e-3 Pa.s
consistency: 0.0352595 s
rate index: 0.660233
R <sup>2</sup> : 0.991625

Data for 1-inch, 20% DR, Re: 70000
zero-rate viscosity: 1.10437e-3 Pa.s
infinite-rate viscosity: 1.09966e-3 Pa.s
consistency: 0.0333496 s
rate index: 3.26449
R <sup>2</sup> : 0.891054

Data for 1-inch, 30% DR, Re: 80000
zero-rate viscosity: 1.12621e-3 Pa.s
infinite-rate viscosity: 1.10770e-3 Pa.s
consistency: 0.0247067 s
rate index: 1.14816
R <sup>2</sup> : 0.997435

Data for 1-inch, 20% DR, Re: 80000
zero-rate viscosity: 1.11281e-3 Pa.s
infinite-rate viscosity: 1.10924e-3 Pa.s
consistency: 0.0281452 s
rate index: 4.63918
R <sup>2</sup> : 0.872457

Data for 1-inch, 30% DR, Re: 90000
zero-rate viscosity: 1.13439e-3 Pa.s
infinite-rate viscosity: 1.11411e-3 Pa.s
consistency: 0.0255277 s
rate index: 0.994692
R <sup>2</sup> : 0.987821

Data for 1-inch, 20% DR, Re: 90000
zero-rate viscosity: 1.11064e-3 Pa.s
infinite-rate viscosity: 1.09978e-3 Pa.s
consistency: 0.0922346 s
rate index: 1.81400
R <sup>2</sup> : 0.917117

Data for 1-inch, 30% DR, Re: 100000
zero-rate viscosity: 1.11598e-3 Pa.s
infinite-rate viscosity: 1.10022e-3 Pa.s
consistency: 0.0204221 s
rate index: 1.57939
R <sup>2</sup> : 0.998471

Data for 1-inch, 20% DR, Re: 100000
zero-rate viscosity: 1.11858e-3 Pa.s
infinite-rate viscosity: 1.10163e-3 Pa.s
consistency: 0.132657 s
rate index: 2.03047
R <sup>2</sup> : 0.942423

## C.2 For test section with 1.5–inch ID

70% DR

Data for 1.5-inch, 70% DR, Re: 60000
zero-rate viscosity: 1.78010e-3 Pa.s
infinite-rate viscosity: 1.20873e-3 Pa.s
consistency: 0.0708401 s
rate index: 0.711454
R <sup>2</sup> : 0.999836

65% DR

Data for 1.5-inch, 65% DR, Re: 60000
zero-rate viscosity: 1.47113e-3 Pa.s
infinite-rate viscosity: 1.17612e-3 Pa.s
consistency: 0.0276905 s
rate index: 0.950123
R <sup>2</sup> : 0.999439

60% DR

Data for 1.5-inch, 60% DR, Re: 60000
zero-rate viscosity: 1.45679e-3 Pa.s
infinite-rate viscosity: 1.16362e-3 Pa.s
consistency: 0.0257490 s
rate index: 0.853403
R <sup>2</sup> : 0.999433

Data for 1.5-inch, 70% DR, Re: 70000
zero-rate viscosity: 1.80153e-3 Pa.s
infinite-rate viscosity: 1.18892e-3 Pa.s
consistency: 0.0814663 s
rate index: 0.639151
R <sup>2</sup> : 0.999051

Data for 1.5-inch, 65% DR, Re: 70000
zero-rate viscosity: 1.46281e-3 Pa.s
infinite-rate viscosity: 1.16685e-3 Pa.s
consistency: 0.0275963 s
rate index: 0.906429
R <sup>2</sup> : 0.999951

Data for 1.5-inch, 60% DR, Re: 70000
zero-rate viscosity: 1.44761e-3 Pa.s
infinite-rate viscosity: 1.17041e-3 Pa.s
consistency: 0.0239175 s
rate index: 0.886445
R <sup>2</sup> : 0.999769

Data for 1.5-inch, 70% DR, Re: 80000
zero-rate viscosity: 1.69759e-3 Pa.s
infinite-rate viscosity: 1.17247e-3 Pa.s
consistency: 0.0571250 s
rate index: 0.663788
R <sup>2</sup> : 0.999729

Data for 1.5-inch, 65% DR, Re: 80000
zero-rate viscosity: 1.44654e-3 Pa.s
infinite-rate viscosity: 1.18384e-3 Pa.s
consistency: 0.0243759 s
rate index: 1.00077
R <sup>2</sup> : 0.999497

Data for 1.5-inch, 60% DR, Re: 80000
zero-rate viscosity: 1.45309e-3 Pa.s
infinite-rate viscosity: 1.14745e-3 Pa.s
consistency: 0.0249090 s
rate index: 0.750873
R <sup>2</sup> : 0.999444

Data for 1.5-inch, 70% DR, Re: 90000
zero-rate viscosity: 1.64037e-3 Pa.s
infinite-rate viscosity: 1.18392e-3 Pa.s
consistency: 0.0478388 s
rate index: 0.736269
R <sup>2</sup> : 0.999424

Data for 1.5-inch, 65% DR, Re: 90000
zero-rate viscosity: 1.43926e-3 Pa.s
infinite-rate viscosity: 1.16639e-3 Pa.s
consistency: 0.0260826 s
rate index: 0.908869
R <sup>2</sup> : 0.999836

Data for 1.5-inch, 60% DR, Re: 90000
zero-rate viscosity: 1.40258e-3 Pa.s
infinite-rate viscosity: 1.18022e-3 Pa.s
consistency: 0.0225398 s
rate index: 1.04575
R <sup>2</sup> : 0.995010

Data for 1.5-inch, 70% DR, Re: 100000
zero-rate viscosity: 1.54960e-3 Pa.s
infinite-rate viscosity: 1.20164e-3 Pa.s
consistency: 0.0334736 s
rate index: 0.899984
R <sup>2</sup> : 0.999895

Data for 1.5-inch, 65% DR, Re: 100000
zero-rate viscosity: 1.41992e-3 Pa.s
infinite-rate viscosity: 1.16463e-3 Pa.s
consistency: 0.0243763 s
rate index: 0.928607
R <sup>2</sup> : 0.999857

Data for 1.5-inch, 60% DR, Re: 100000
zero-rate viscosity: 1.40457e-3 Pa.s
infinite-rate viscosity: 1.14032e-3 Pa.s
consistency: 0.0211343 s
rate index: 0.789359
R <sup>2</sup> : 0.999651

## 50% DR

Data for 1.5-inch, 50% DR, Re: 60000
zero-rate viscosity: 1.35715e-3 Pa.s
infinite-rate viscosity: 1.15350e-3 Pa.s
consistency: 0.0204247 s
rate index: 0.903157
R <sup>2</sup> : 0.996260

## 40% DR

Data for 1.5-inch, 40% DR, Re: 60000
zero-rate viscosity: 1.27905e-3 Pa.s
infinite-rate viscosity: 1.14581e-3 Pa.s
consistency: 0.0157306 s
rate index: 1.00323
R <sup>2</sup> : 0.994968

## 30% DR

Data for 1.5-inch, 30% DR, Re: 60000
zero-rate viscosity: 1.20564e-3 Pa.s
infinite-rate viscosity: 1.14736e-3 Pa.s
consistency: 0.0146037 s
rate index: 1.61385
R <sup>2</sup> : 0.997289

Data for 1.5-inch, 50% DR, Re: 70000
zero-rate viscosity: 1.33841e-3 Pa.s
infinite-rate viscosity: 1.11715e-3 Pa.s
consistency: 0.0180445 s
rate index: 0.767926
R <sup>2</sup> : 0.998926

Data for 1.5-inch, 40% DR, Re: 70000
zero-rate viscosity: 1.27014e-3 Pa.s
infinite-rate viscosity: 1.16483e-3 Pa.s
consistency: 0.0159549 s
rate index: 1.32335
R <sup>2</sup> : 0.998420

Data for 1.5-inch, 30% DR, Re: 70000
zero-rate viscosity: 1.22565e-3 Pa.s
infinite-rate viscosity: 1.14520e-3 Pa.s
consistency: 0.0126141 s
rate index: 1.06566
R <sup>2</sup> : 0.993023

Data for 1.5-inch, 50% DR, Re: 80000
zero-rate viscosity: 1.31094e-3 Pa.s
infinite-rate viscosity: 1.16361e-3 Pa.s
consistency: 0.0197334 s
rate index: 1.26998
R <sup>2</sup> : 0.993929

Data for 1.5-inch, 40% DR, Re: 80000
zero-rate viscosity: 1.29757e-3 Pa.s
infinite-rate viscosity: 1.12037e-3 Pa.s
consistency: 0.0123914 s
rate index: 0.699203
R <sup>2</sup> : 0.994795

Data for 1.5-inch, 30% DR, Re: 80000
zero-rate viscosity: 1.20372e-3 Pa.s
infinite-rate viscosity: 1.13991e-3 Pa.s
consistency: 0.0141781 s
rate index: 1.38662
R <sup>2</sup> : 0.998309

Data for 1.5-inch, 50% DR, Re: 90000
zero-rate viscosity: 1.31656e-3 Pa.s
infinite-rate viscosity: 1.15177e-3 Pa.s
consistency: 0.0183875 s
rate index: 1.05058
R <sup>2</sup> : 0.999826

Data for 1.5-inch, 40% DR, Re: 90000
zero-rate viscosity: 1.25805e-3 Pa.s
infinite-rate viscosity: 1.17280e-3 Pa.s
consistency: 0.0171194 s
rate index: 1.68898
R <sup>2</sup> : 0.974303

Data for 1.5-inch, 30% DR, Re: 90000
zero-rate viscosity: 1.22025e-3 Pa.s
infinite-rate viscosity: 1.12160e-3 Pa.s
consistency: 0.0136724 s
rate index: 0.805431
R <sup>2</sup> : 0.998150

Data for 1.5-inch, 50% DR, Re: 100000
zero-rate viscosity: 1.31686e-3 Pa.s
infinite-rate viscosity: 1.18204e-3 Pa.s
consistency: 0.0178393 s
rate index: 1.34776
R <sup>2</sup> : 0.996007

Data for 1.5-inch, 40% DR, Re: 100000
zero-rate viscosity: 1.26384e-3 Pa.s
infinite-rate viscosity: 1.13514e-3 Pa.s
consistency: 0.0142319 s
rate index: 0.942231
R <sup>2</sup> : 0.997345

Data for 1.5-inch, 30% DR, Re: 100000
zero-rate viscosity: 1.19667e-3 Pa.s
infinite-rate viscosity: 1.13072e-3 Pa.s
consistency: 0.0135764 s
rate index: 1.22993
R <sup>2</sup> : 0.999728

20% DR

Data for 1.5-inch, 20% DR, Re: 60000
zero-rate viscosity: 1.14992e-3 Pa.s
infinite-rate viscosity: 1.12939e-3 Pa.s
consistency: 0.0140900 s
rate index: 1.69378
R <sup>2</sup> : 0.957775

Data for 1.5-inch, 20% DR, Re: 70000
zero-rate viscosity: 1.14943e-3 Pa.s
infinite-rate viscosity: 1.12736e-3 Pa.s
consistency: 0.0155893 s
rate index: 1.52734
R <sup>2</sup> : 0.993572

Data for 1.5-inch, 20% DR, Re: 80000
zero-rate viscosity: 1.14974e-3 Pa.s
infinite-rate viscosity: 1.12568e-3 Pa.s
consistency: 0.0147729 s
rate index: 1.35398
R <sup>2</sup> : 0.993174

Data for 1.5-inch, 20% DR, Re: 90000
zero-rate viscosity: 1.14650e-3 Pa.s
infinite-rate viscosity: 1.12905e-3 Pa.s
consistency: 0.0160059 s
rate index: 1.94179
R <sup>2</sup> : 0.977152

Data for 1.5-inch, 20% DR, Re: 100000
zero-rate viscosity: 1.15575e-3 Pa.s
infinite-rate viscosity: 1.13119e-3 Pa.s
consistency: 0.0140441 s
rate index: 1.27562
R <sup>2</sup> : 0.994392

### C.3 For test section with 2–inch ID

#### 65% DR

Data for 2-inch, 65% DR, Re: 60000
zero-rate viscosity: 1.49059e-3 Pa.s
infinite-rate viscosity: 1.18335e-3 Pa.s
consistency: 0.0335858 s
rate index: 0.901018
R <sup>2</sup> : 0.999888

#### 50% DR

Data for 2-inch, 50% DR, Re: 60000
zero-rate viscosity: 1.43083e-3 Pa.s
infinite-rate viscosity: 1.14956e-3 Pa.s
consistency: 0.0295580 s
rate index: 0.833624
R <sup>2</sup> : 0.999857

#### 40% DR

Data for 2-inch, 40% DR, Re: 60000
zero-rate viscosity: 1.29052e-3 Pa.s
infinite-rate viscosity: 1.15033e-3 Pa.s
consistency: 0.0189633 s
rate index: 1.14746
R <sup>2</sup> : 0.999799

Data for 2-inch, 65% DR, Re: 70000
zero-rate viscosity: 1.40738e-3 Pa.s
infinite-rate viscosity: 1.16764e-3 Pa.s
consistency: 0.0268196 s
rate index: 1.06343
R <sup>2</sup> : 0.999617

Data for 2-inch, 50% DR, Re: 70000
zero-rate viscosity: 1.42125e-3 Pa.s
infinite-rate viscosity: 1.13315e-3 Pa.s
consistency: 0.0316054 s
rate index: 0.774617
R <sup>2</sup> : 0.999749

Data for 2-inch, 40% DR, Re: 70000
zero-rate viscosity: 1.29079e-3 Pa.s
infinite-rate viscosity: 1.13826e-3 Pa.s
consistency: 0.0200980 s
rate index: 0.986483
R <sup>2</sup> : 0.999643

Data for 2-inch, 65% DR, Re: 80000
zero-rate viscosity: 1.42903e-3 Pa.s
infinite-rate viscosity: 1.15162e-3 Pa.s
consistency: 0.0299945 s
rate index: 0.839125
R <sup>2</sup> : 0.999813

Data for 2-inch, 50% DR, Re: 80000
zero-rate viscosity: 1.43543e-3 Pa.s
infinite-rate viscosity: 1.13940e-3 Pa.s
consistency: 0.0311618 s
rate index: 0.720296
R <sup>2</sup> : 0.999620

Data for 2-inch, 40% DR, Re: 80000
zero-rate viscosity: 1.29487e-3 Pa.s
infinite-rate viscosity: 1.13926e-3 Pa.s
consistency: 0.0188249 s
rate index: 0.921381
R <sup>2</sup> : 0.998493

Data for 2-inch, 65% DR, Re: 90000
zero-rate viscosity: 1.40489e-3 Pa.s
infinite-rate viscosity: 1.14281e-3 Pa.s
consistency: 0.0282386 s
rate index: 0.810092
R <sup>2</sup> : 0.999938

Data for 2-inch, 50% DR, Re: 90000
zero-rate viscosity: 1.35563e-3 Pa.s
infinite-rate viscosity: 1.14590e-3 Pa.s
consistency: 0.0231072 s
rate index: 0.950430
R <sup>2</sup> : 0.999776

Data for 2-inch, 40% DR, Re: 90000
zero-rate viscosity: 1.28542e-3 Pa.s
infinite-rate viscosity: 1.13453e-3 Pa.s
consistency: 0.0193912 s
rate index: 0.911003
R <sup>2</sup> : 0.999826

Data for 2-inch, 65% DR, Re: 100000
zero-rate viscosity: 1.35277e-3 Pa.s
infinite-rate viscosity: 1.14682e-3 Pa.s
consistency: 0.0233754 s
rate index: 0.953702
R <sup>2</sup> : 0.999733

Data for 2-inch, 50% DR, Re: 100000
zero-rate viscosity: 1.34767e-3 Pa.s
infinite-rate viscosity: 1.14098e-3 Pa.s
consistency: 0.0232822 s
rate index: 0.899845
R <sup>2</sup> : 0.997840

Data for 2-inch, 40% DR, Re: 100000
zero-rate viscosity: 1.27486e-3 Pa.s
infinite-rate viscosity: 1.13246e-3 Pa.s
consistency: 0.0189322 s
rate index: 0.915976
R <sup>2</sup> : 0.999850

## 30% DR

Data for 2-inch, 30% DR, Re: 60000
zero-rate viscosity: 1.25902e-3 Pa.s
infinite-rate viscosity: 1.11652e-3 Pa.s
consistency: 0.0146857 s
rate index: 0.771238
R <sup>2</sup> : 0.988245

## 20% DR

Data for 2-inch, 20% DR, Re: 60000
zero-rate viscosity: 1.17692e-3 Pa.s
infinite-rate viscosity: 1.12468e-3 Pa.s
consistency: 0.0139004 s
rate index: 1.15686
R <sup>2</sup> : 0.998787

## 10% DR

Data for 2-inch, 10% DR, Re: 60000
zero-rate viscosity: 1.13683e-3 Pa.s
infinite-rate viscosity: 1.10789e-3 Pa.s
consistency: 0.0240053 s
rate index: 0.747201
R <sup>2</sup> : 0.982033

Data for 2-inch, 30% DR, Re: 70000
zero-rate viscosity: 1.22958e-3 Pa.s
infinite-rate viscosity: 1.14019e-3 Pa.s
consistency: 0.0157253 s
rate index: 1.27864
R <sup>2</sup> : 0.999409

Data for 2-inch, 20% DR, Re: 70000
zero-rate viscosity: 1.17688e-3 Pa.s
infinite-rate viscosity: 1.13244e-3 Pa.s
consistency: 0.0138697 s
rate index: 1.33368
R <sup>2</sup> : 0.999548

Data for 2-inch, 10% DR, Re: 70000
zero-rate viscosity: 1.12737e-3 Pa.s
infinite-rate viscosity: 1.10984e-3 Pa.s
consistency: 0.0188864 s
rate index: 1.18383
R <sup>2</sup> : 0.997250

Data for 2-inch, 30% DR, Re: 80000
zero-rate viscosity: 1.21247e-3 Pa.s
infinite-rate viscosity: 1.12295e-3 Pa.s
consistency: 0.0156216 s
rate index: 1.14836
R <sup>2</sup> : 0.998525

Data for 2-inch, 20% DR, Re: 80000
zero-rate viscosity: 1.19307e-3 Pa.s
infinite-rate viscosity: 1.10675e-3 Pa.s
consistency: 0.0193986 s
rate index: 0.639515
R <sup>2</sup> : 0.997646

Data for 2-inch, 10% DR, Re: 80000
zero-rate viscosity: 1.13299e-3 Pa.s
infinite-rate viscosity: 1.12060e-3 Pa.s
consistency: 0.0171093 s
rate index: 1.84523
R <sup>2</sup> : 0.956678

Data for 2-inch, 30% DR, Re: 90000
zero-rate viscosity: 1.21700e-3 Pa.s
infinite-rate viscosity: 1.14172e-3 Pa.s
consistency: 0.0156393 s
rate index: 1.40456
R <sup>2</sup> : 0.999000

Data for 2-inch, 20% DR, Re: 90000
zero-rate viscosity: 1.18492e-3 Pa.s
infinite-rate viscosity: 1.09913e-3 Pa.s
consistency: 0.0140235 s
rate index: 0.585523
R <sup>2</sup> : 0.995541

Data for 2-inch, 10% DR, Re: 90000
zero-rate viscosity: 1.13570e-3 Pa.s
infinite-rate viscosity: 1.10317e-3 Pa.s
consistency: 0.0162314 s
rate index: 0.528652
R <sup>2</sup> : 0.985714

Data for 2-inch, 30% DR, Re: 100000
zero-rate viscosity: 1.20358e-3 Pa.s
infinite-rate viscosity: 1.13526e-3 Pa.s
consistency: 0.0154643 s
rate index: 1.46943
R <sup>2</sup> : 0.998421

Data for 2-inch, 20% DR, Re: 100000
zero-rate viscosity: 1.16876e-3 Pa.s
infinite-rate viscosity: 1.12169e-3 Pa.s
consistency: 0.0149370 s
rate index: 1.09759
R <sup>2</sup> : 0.998125

Data for 2-inch, 10% DR, Re: 100000
zero-rate viscosity: 1.12522e-3 Pa.s
infinite-rate viscosity: 1.11109e-3 Pa.s
consistency: 0.0210032 s
rate index: 1.28382
R <sup>2</sup> : 0.903394

# Appendix D

## Extensional viscosity data

This section presents the plots for the extensional viscosity measurements (detailed in section 3.6), mapping the normalized minimum diameter of the extensional filament ( $D/D_0$ ) versus time ( $t$ ), showing three measurements (represented by color blue, orange and yellow) for each of the five  $Re$  (60000, 70000, 80000, 90000, and 100000) for each %DR. The data is presented for all three test sections. Each plot shows the relaxation time ( $t_r$ ) value calculated using equation 29, for the 3-readings and their average.

### D.1 ( $D/D_0$ ) versus time ( $t$ ) plots for test section with 1-inch ID

#### D.1.1 Plots for 76% DR (data acquisition rate: 4000 fps)

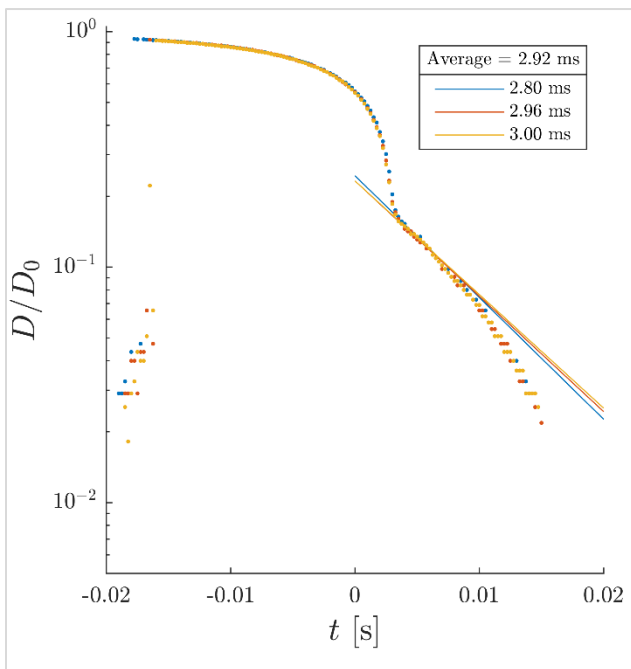


Figure D.1.1a:  $D/D_0$  versus  $t$  plot for 76% DR,  $Re$ : 60000.

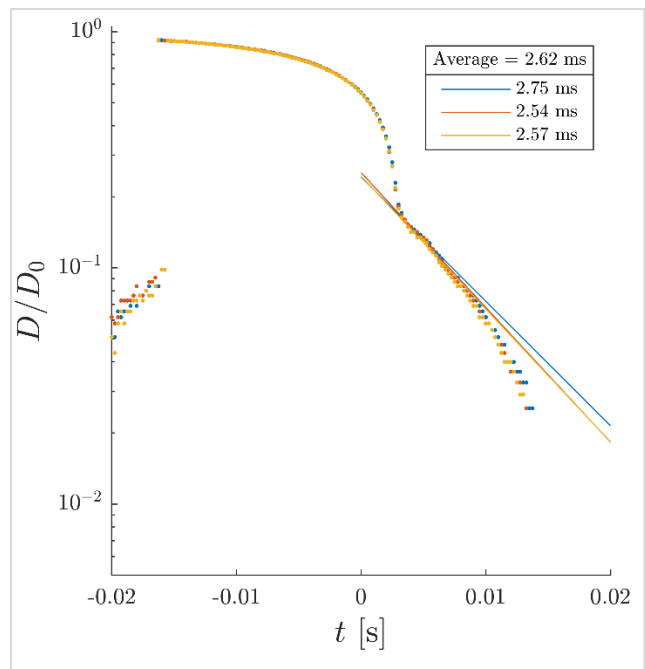


Figure D.1.1b:  $D/D_0$  versus  $t$  plot for 76% DR,  $Re$ : 70000.



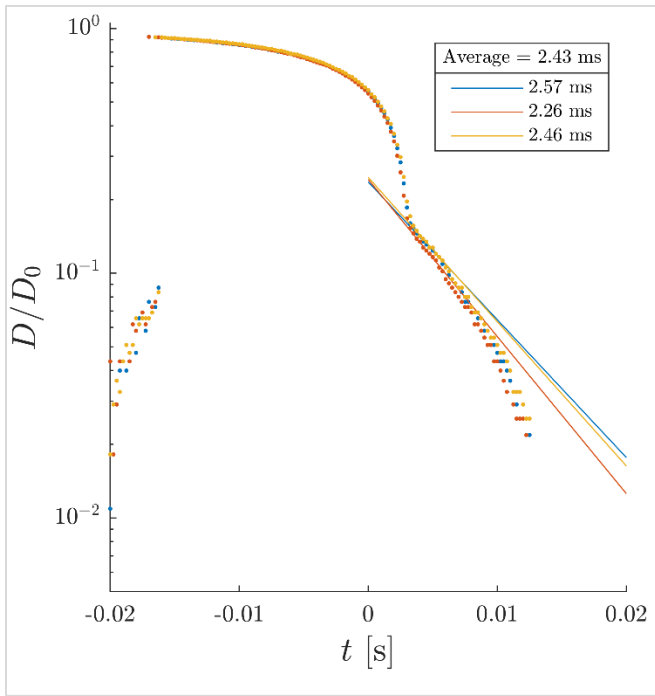


Figure D.1.1c:  $D/D_0$  versus  $t$  plot for 76% DR, Re: 80000.

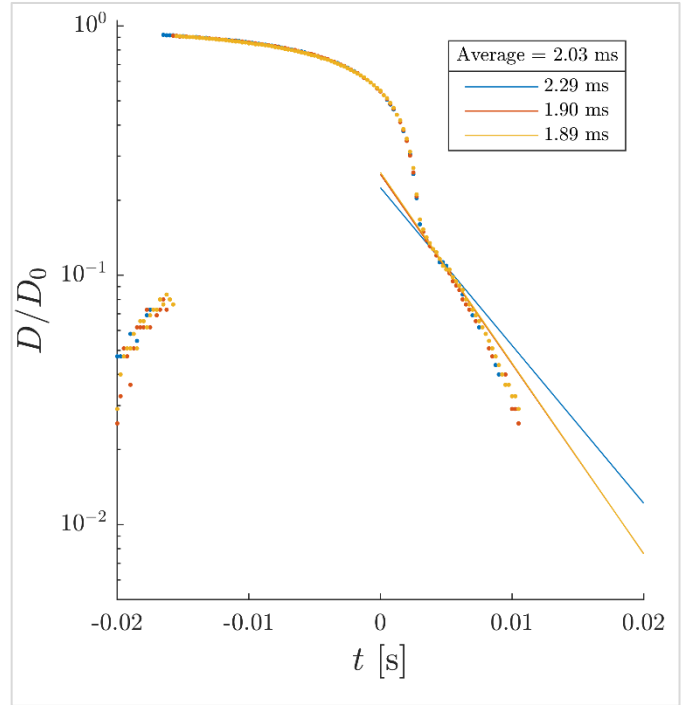


Figure D.1.1d:  $D/D_0$  versus  $t$  plot for 76% DR, Re: 90000.

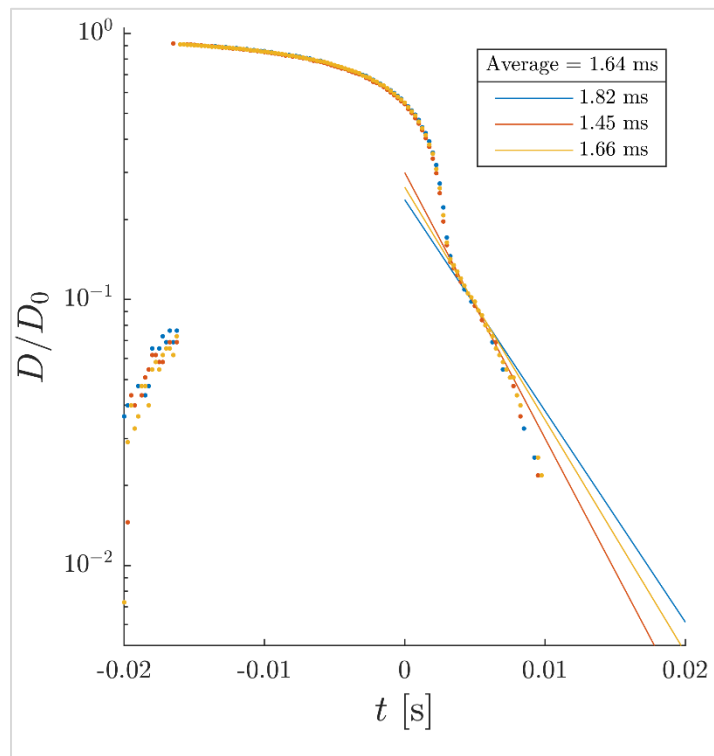


Figure D.1.1e:  $D/D_0$  versus  $t$  plot for 76% DR, Re: 100000.

### D.1.2 Plots for 70% DR (data acquisition rate: 4000 fps)

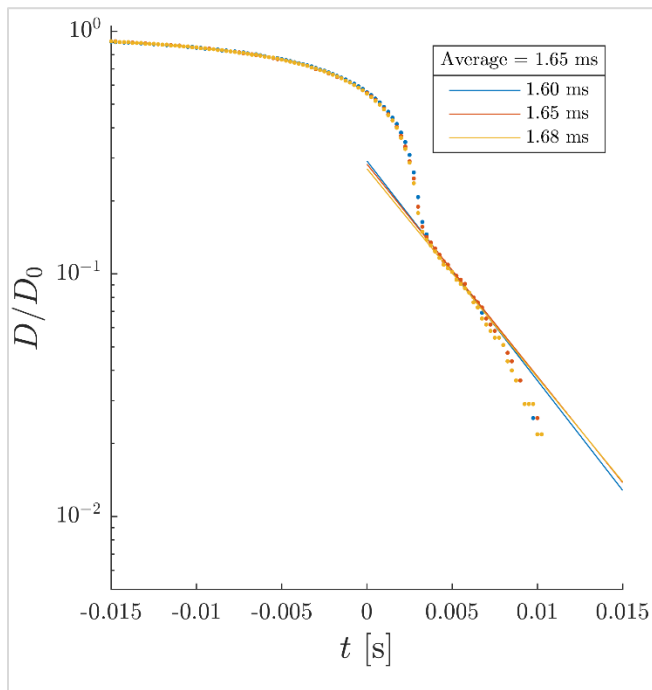


Figure D.1.2a:  $D/D_0$  versus  $t$  plot for 70% DR, Re: 60000.

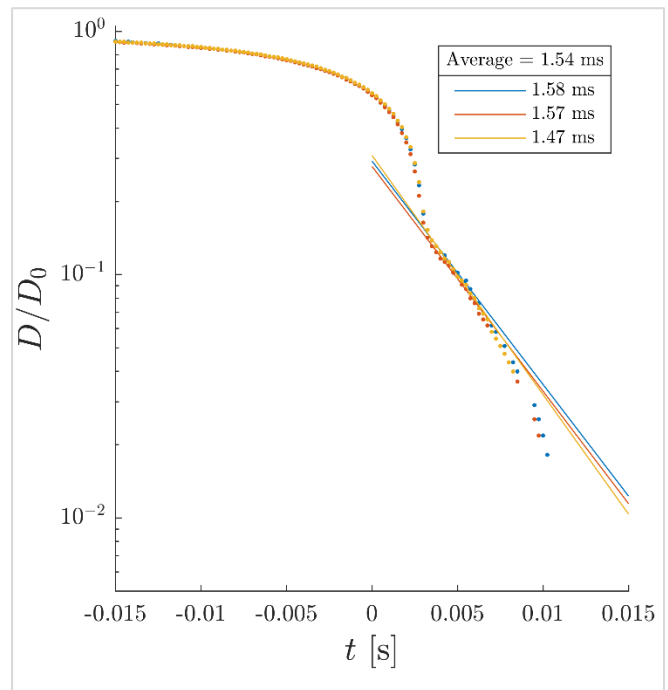


Figure D.1.2b:  $D/D_0$  versus  $t$  plot for 70% DR, Re: 70000.

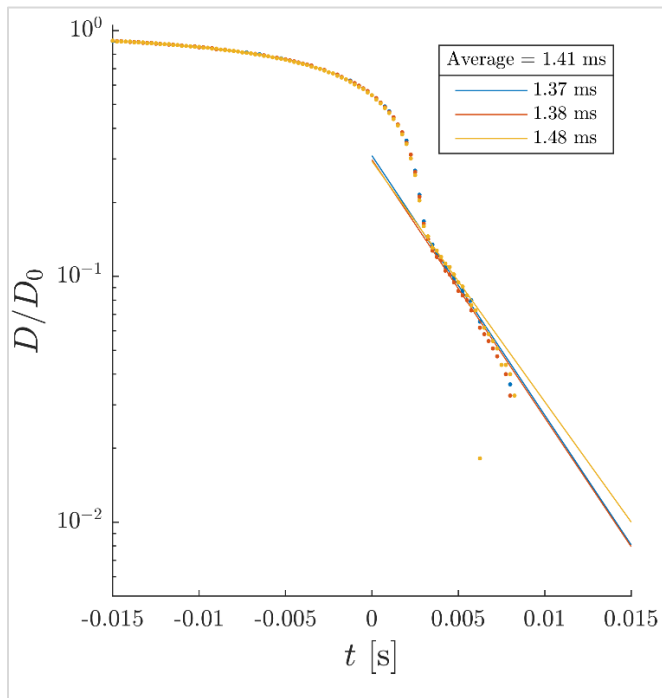


Figure D.1.2c:  $D/D_0$  versus  $t$  plot for 70% DR, Re: 80000.

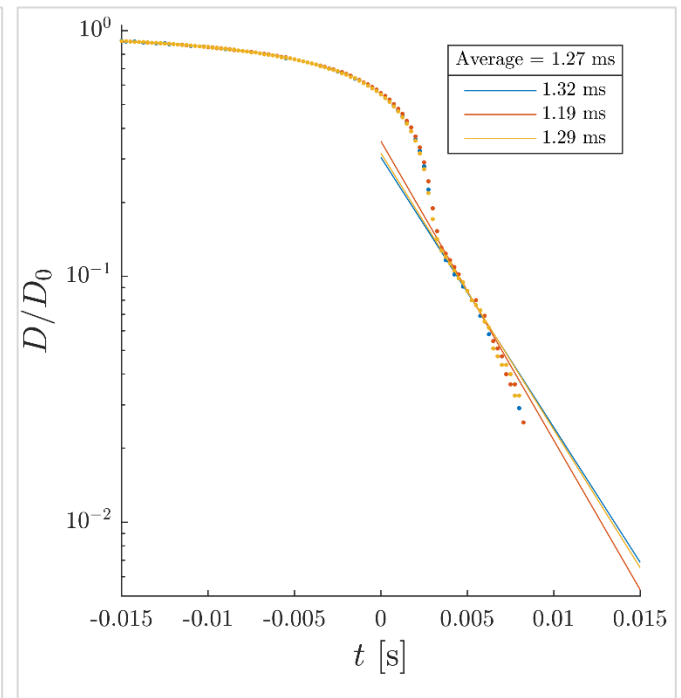


Figure D.1.2d:  $D/D_0$  versus  $t$  plot for 70% DR, Re: 90000.

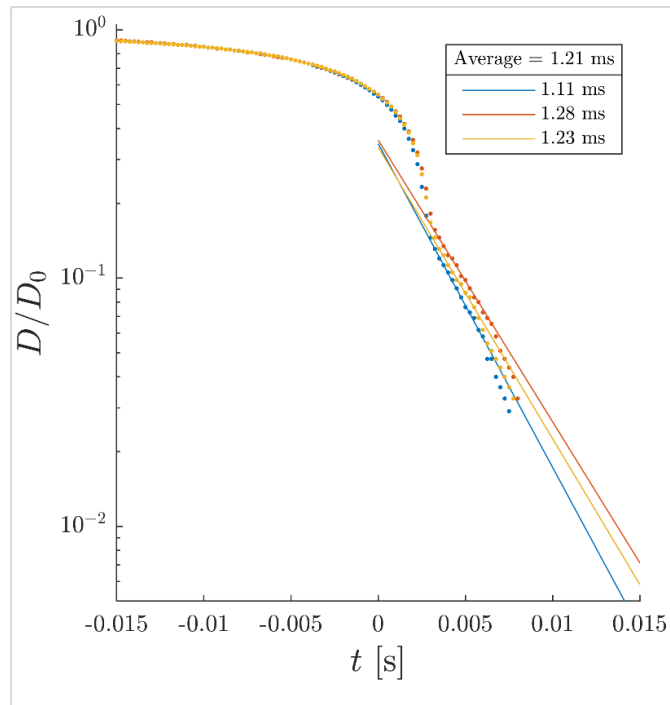


Figure D.1.2e:  $D/D_0$  versus  $t$  plot for 70% DR, Re: 100000.

### D.1.3 Plots for 65% DR (data acquisition rate: 4000 fps)

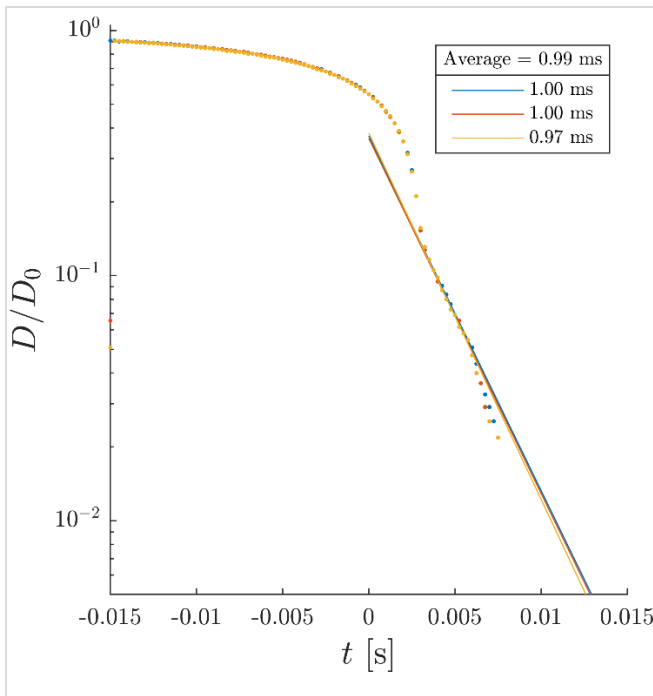


Figure D.1.3a:  $D/D_0$  versus  $t$  plot for 65% DR, Re: 60000.

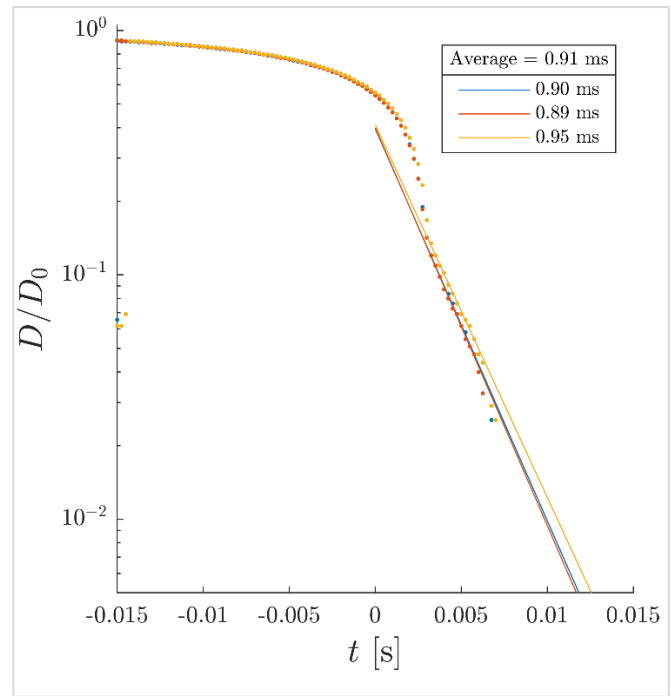


Figure D.1.3b:  $D/D_0$  versus  $t$  plot for 65% DR, Re: 70000.

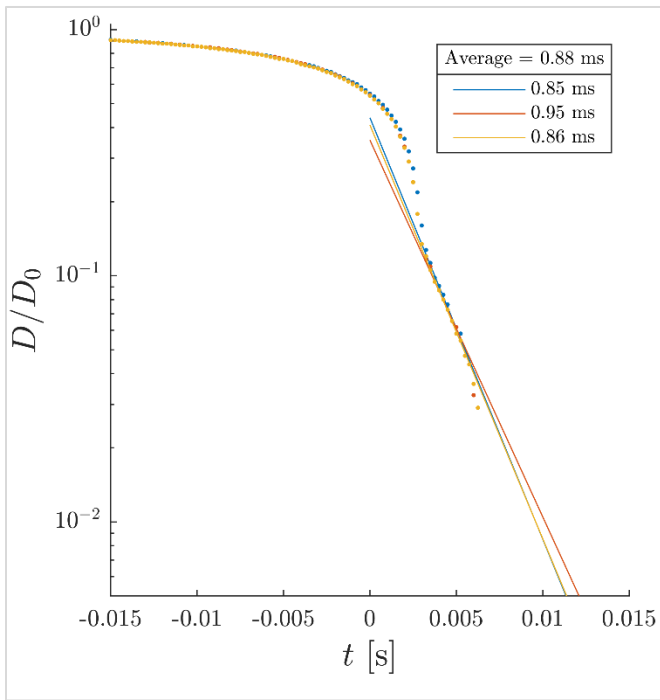


Figure D.1.3c:  $D/D_0$  versus  $t$  plot for 65% DR, Re: 80000.

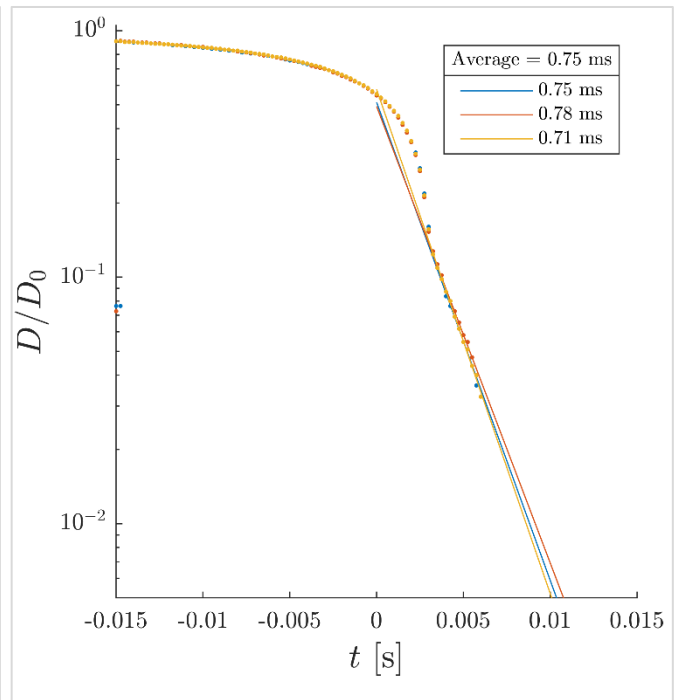


Figure D.1.3d:  $D/D_0$  versus  $t$  plot for 65% DR, Re: 90000.

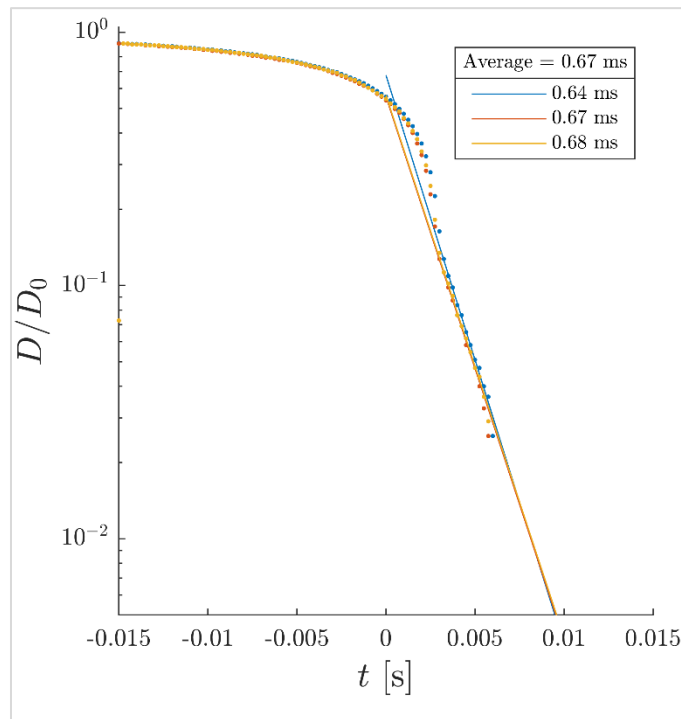


Figure D.1.3e:  $D/D_0$  versus  $t$  plot for 65% DR, Re: 100000.

D.1.4 Plots for 60% DR (data acquisition rate: 4000 fps)

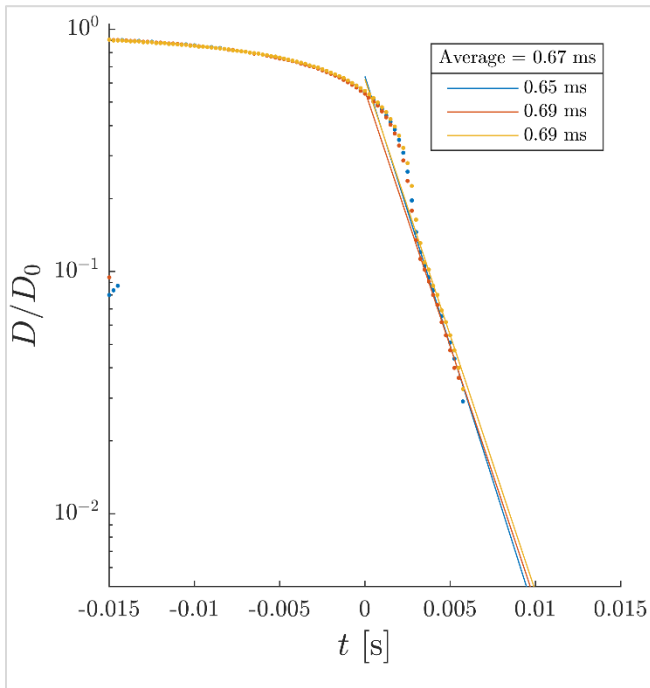


Figure D.1.4a:  $D/D_0$  versus  $t$  plot for 60% DR, Re: 60000.

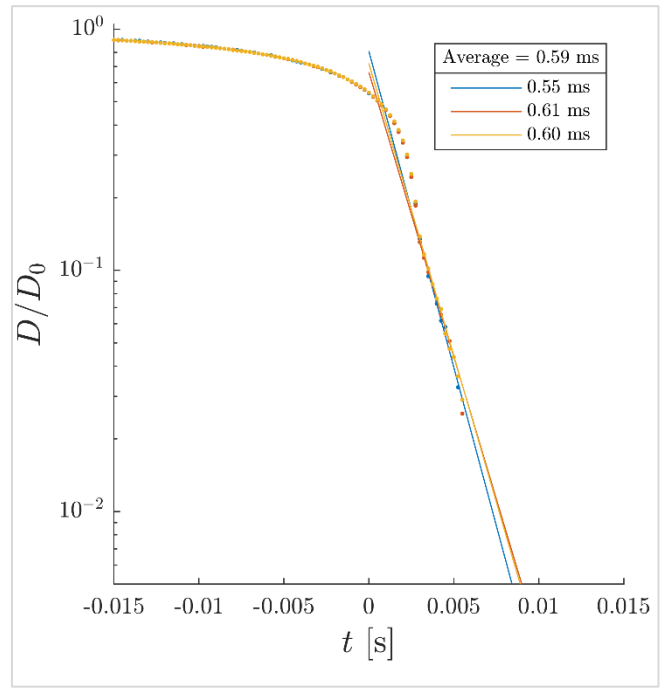


Figure D.1.4b:  $D/D_0$  versus  $t$  plot for 60% DR, Re: 70000.

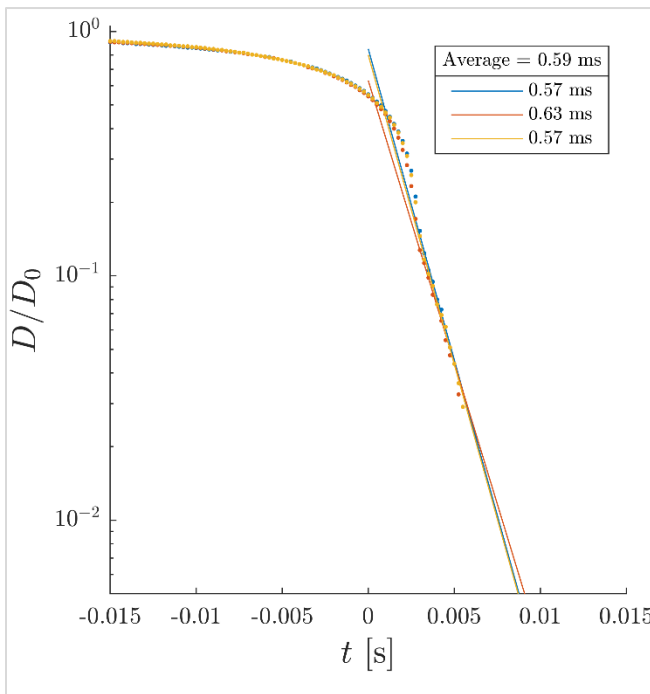


Figure D.1.4c:  $D/D_0$  versus  $t$  plot for 60% DR, Re: 80000.

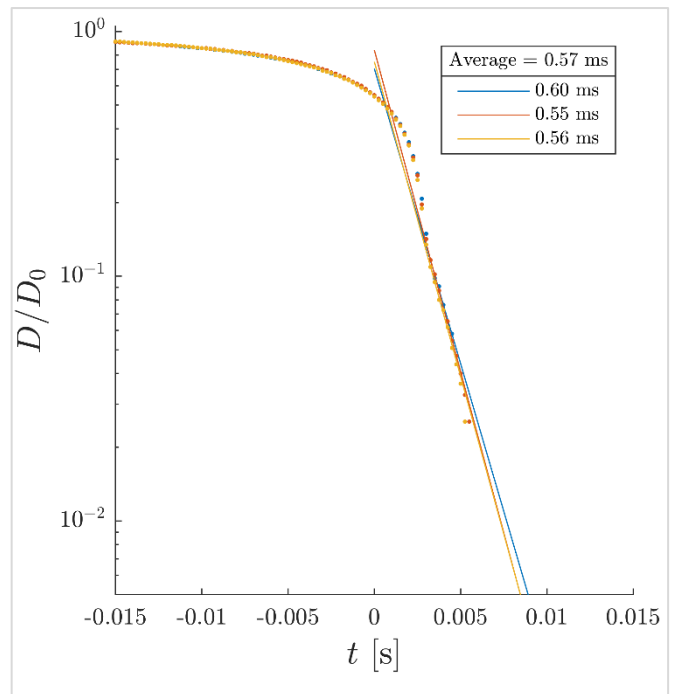


Figure D.1.4d:  $D/D_0$  versus  $t$  plot for 60% DR, Re: 90000.

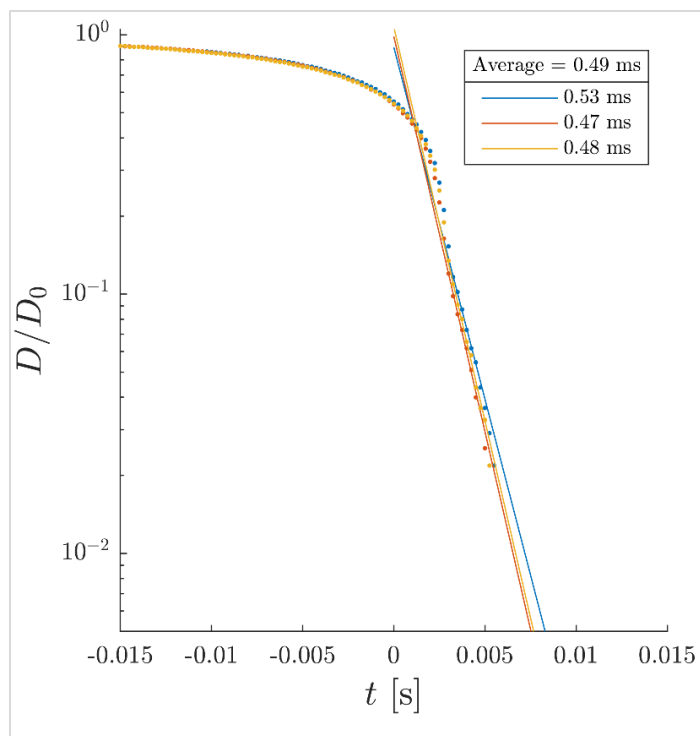


Figure D.1.4e:  $D/D_0$  versus  $t$  plot for 60% DR, Re: 100000.

### D.1.5 Plots for 50% DR (data acquisition rate: 4000 fps)

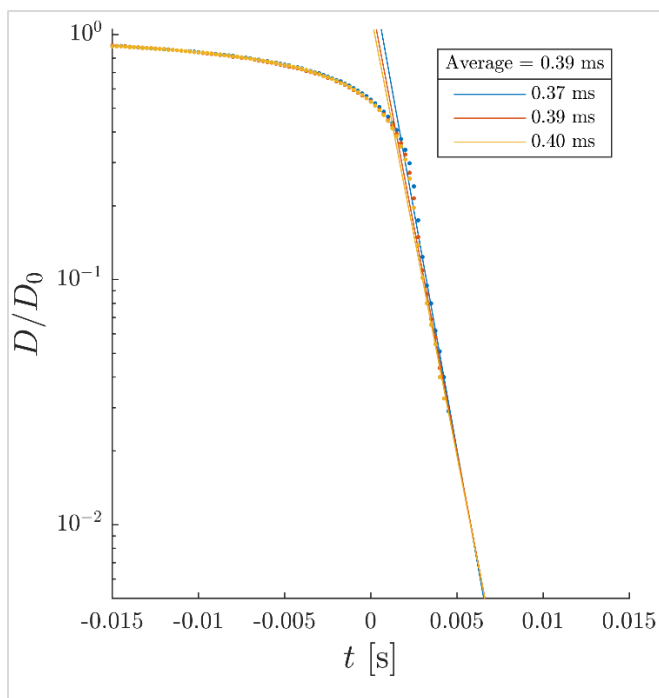


Figure D.1.5a:  $D/D_0$  versus  $t$  plot for 50% DR, Re: 60000.

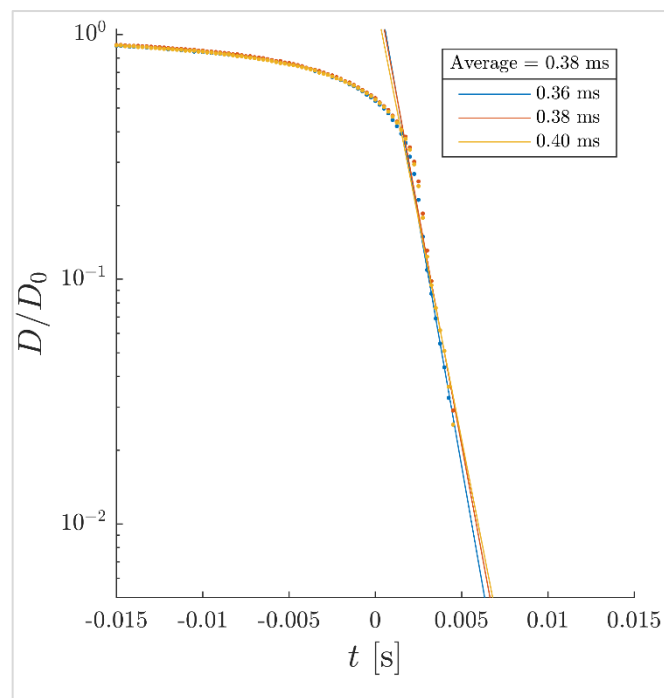


Figure D.1.5b:  $D/D_0$  versus  $t$  plot for 50% DR, Re: 70000.

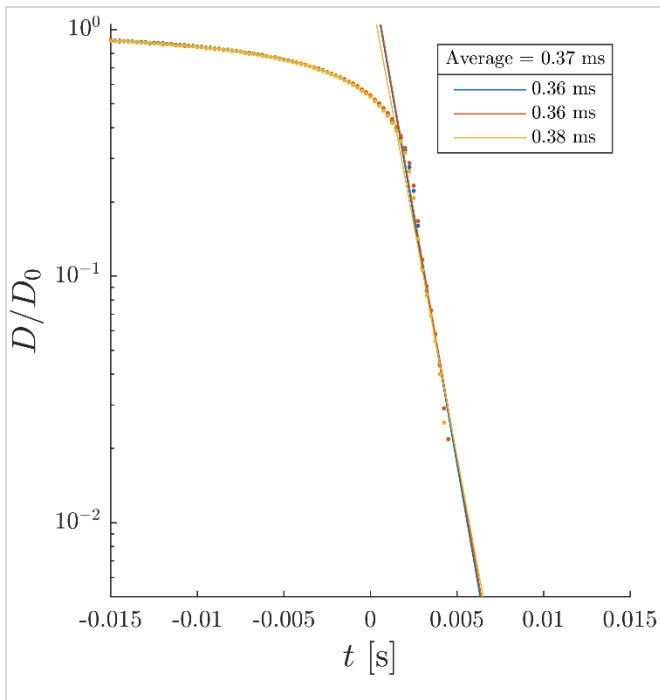


Figure D.1.5c:  $D/D_0$  versus  $t$  plot for 50% DR, Re: 80000.

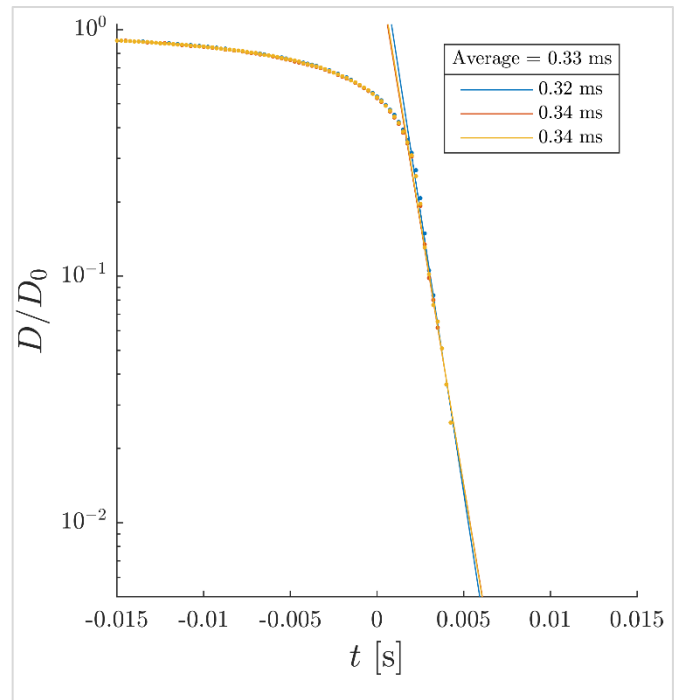


Figure D.1.5d:  $D/D_0$  versus  $t$  plot for 50% DR, Re: 90000.

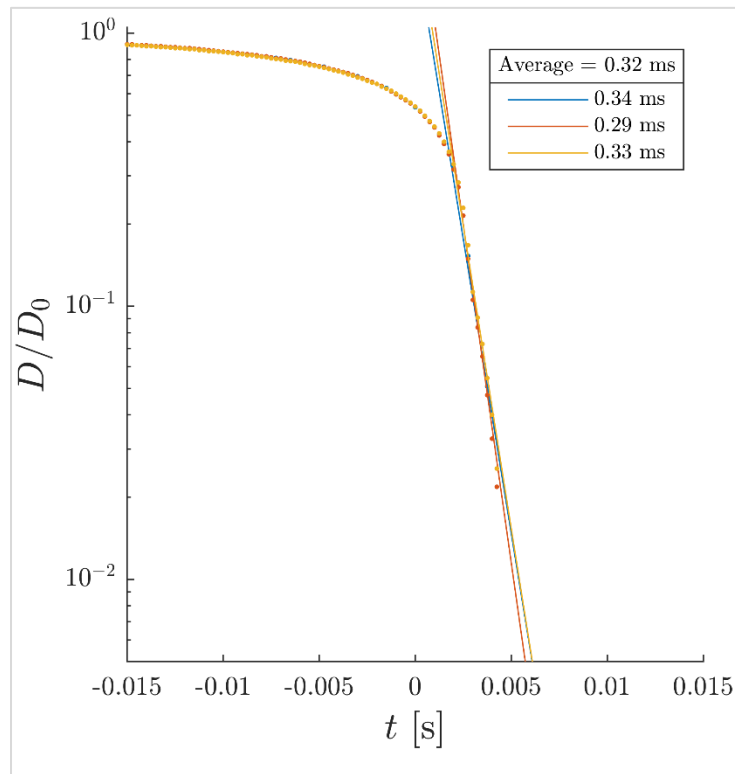


Figure D.1.5e:  $D/D_0$  versus  $t$  plot for 50% DR, Re: 100000.

D.1.6 Plots for 40% DR (data acquisition rate: 9000 fps)

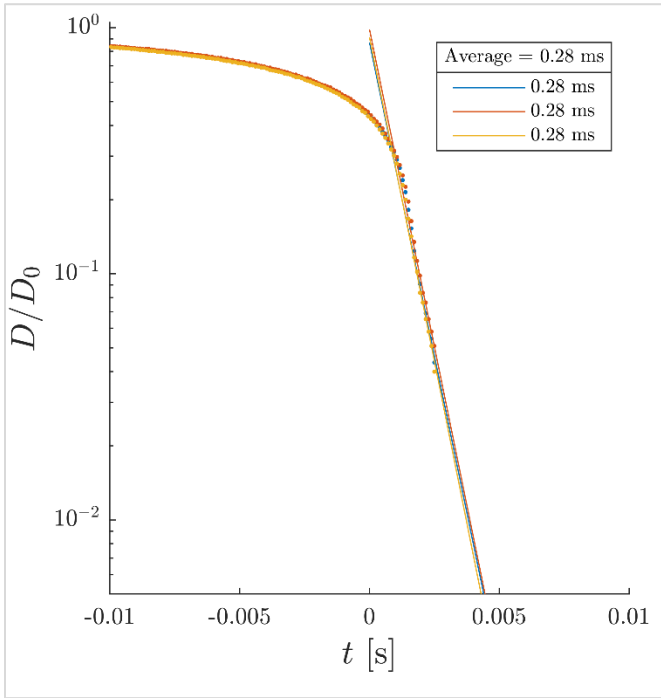


Figure D.1.6a:  $D/D_0$  versus  $t$  plot for 40% DR, Re: 60000.

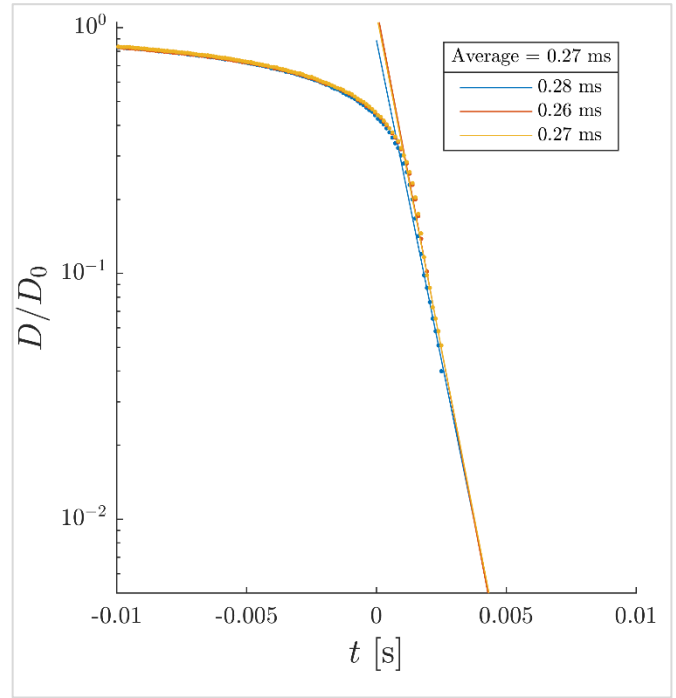


Figure D.1.6b:  $D/D_0$  versus  $t$  plot for 40% DR, Re: 70000.

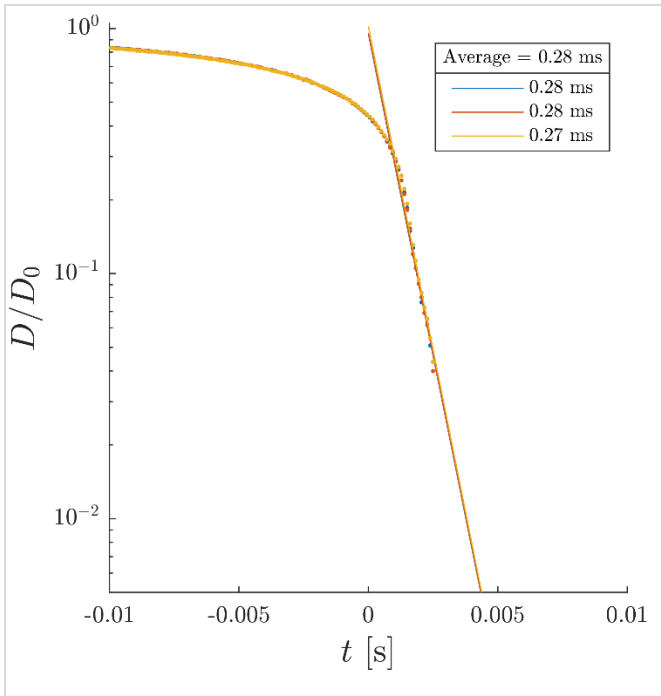


Figure D.1.6c:  $D/D_0$  versus  $t$  plot for 40% DR, Re: 80000.

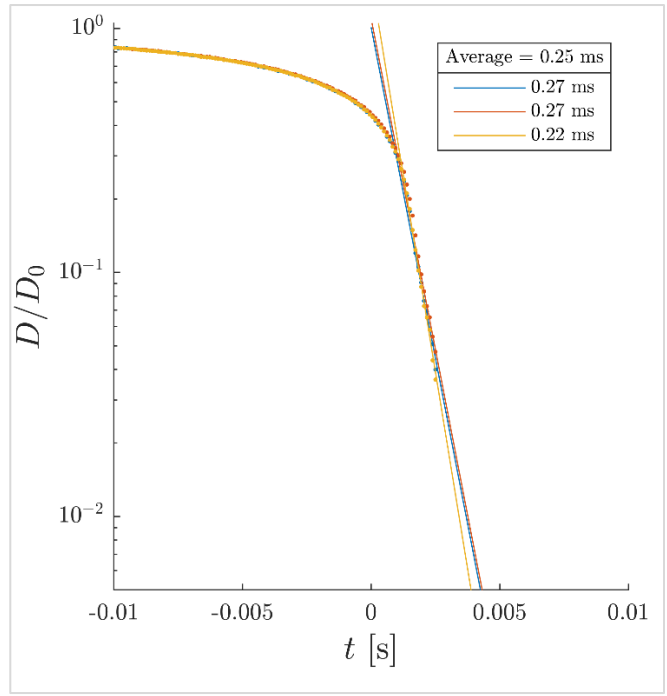


Figure D.1.6d:  $D/D_0$  versus  $t$  plot for 40% DR, Re: 90000.



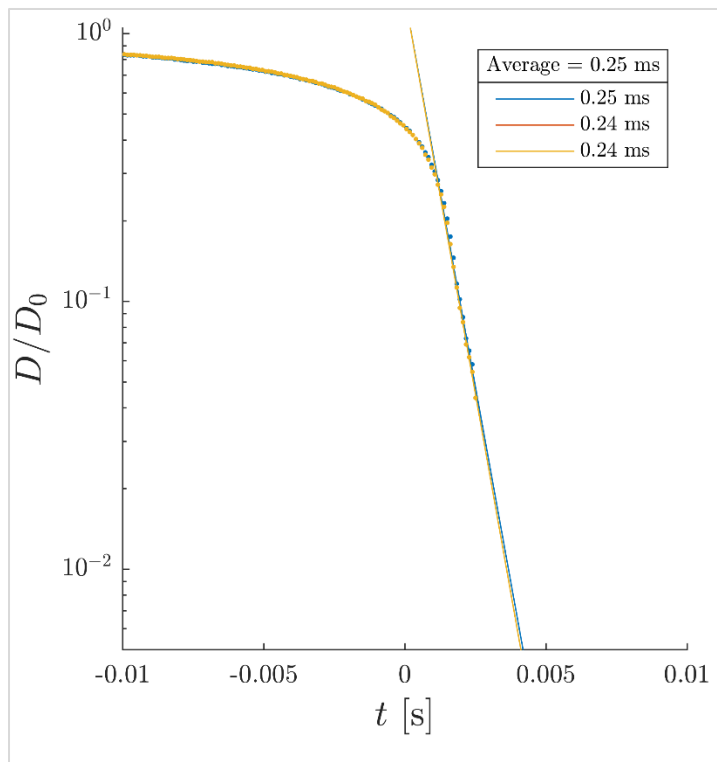


Figure D.1.6e:  $D/D_0$  versus  $t$  plot for 40% DR, Re: 100000.

### D.1.7 Plots for 30% DR (data acquisition rate: 12000 fps)

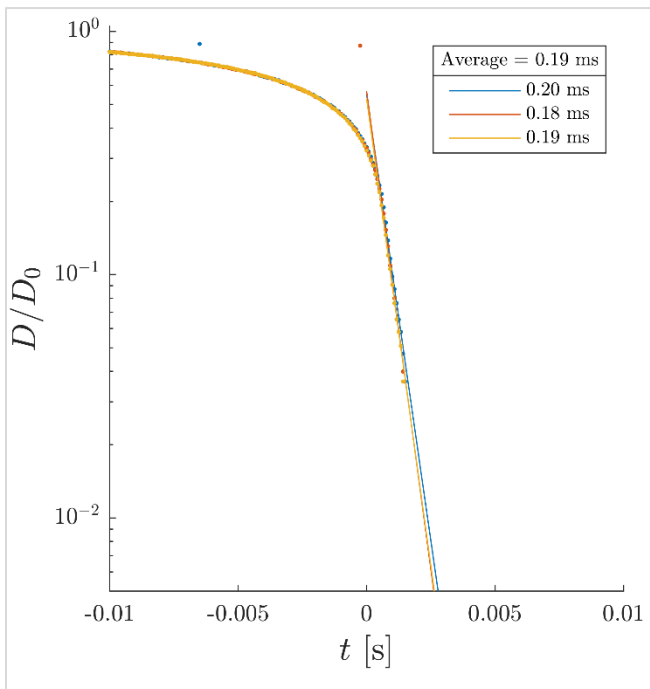


Figure D.1.7a:  $D/D_0$  versus  $t$  plot for 30% DR, Re: 60000.

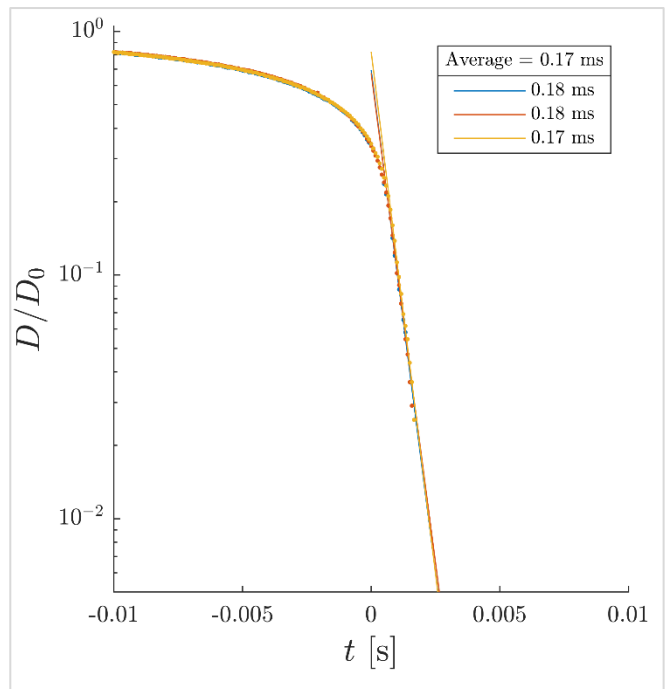


Figure D.1.7b:  $D/D_0$  versus  $t$  plot for 30% DR, Re: 70000.

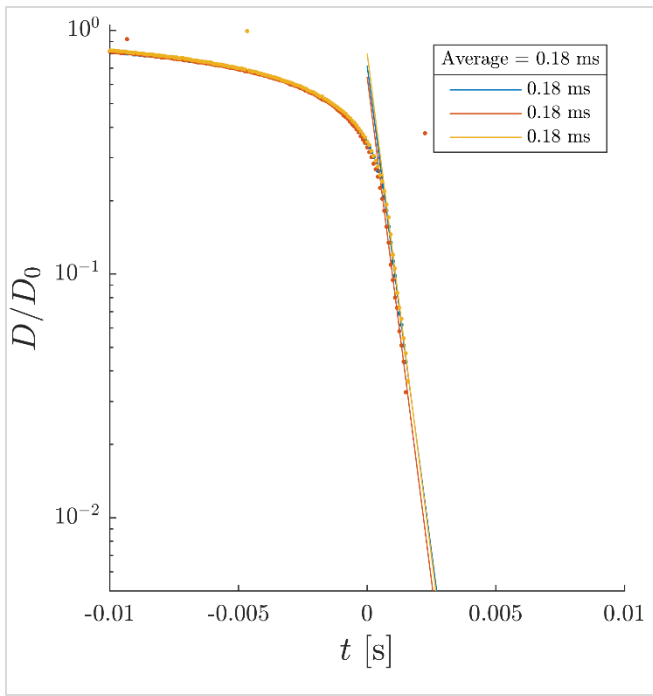


Figure D.1.7c:  $D/D_0$  versus  $t$  plot for 30% DR, Re: 80000.

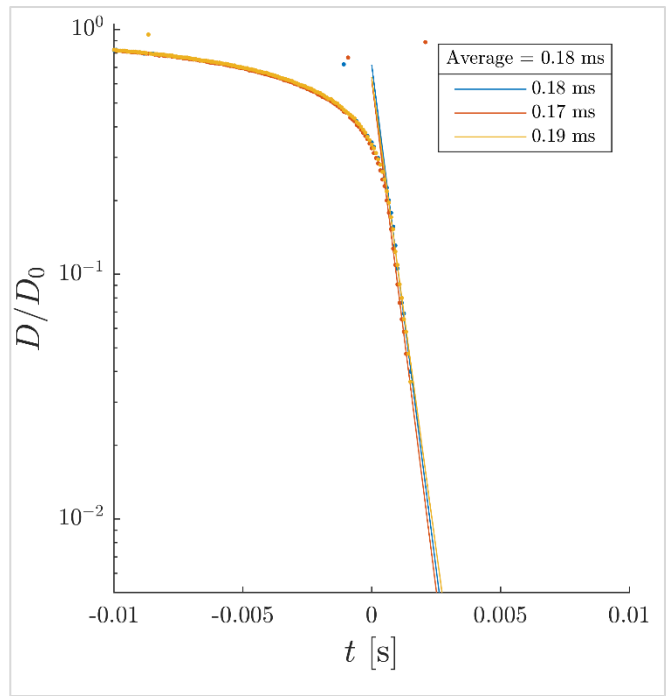


Figure D.1.7d:  $D/D_0$  versus  $t$  plot for 30% DR, Re: 90000.

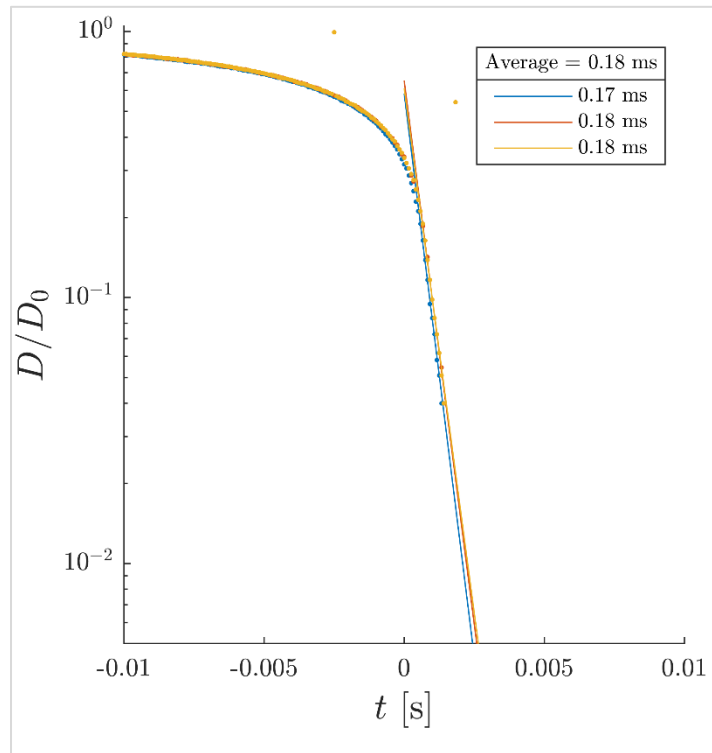


Figure D.1.7e:  $D/D_0$  versus  $t$  plot for 30% DR, Re: 100000.

### D.1.8 Plots for 20% DR (data acquisition rate: 12000 fps)

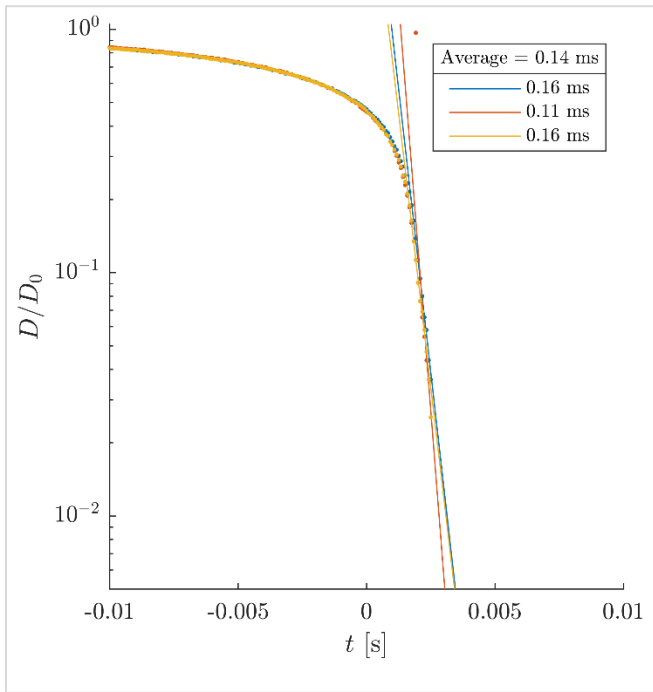


Figure D.1.8a:  $D/D_0$  versus  $t$  plot for 20% DR, Re: 60000.

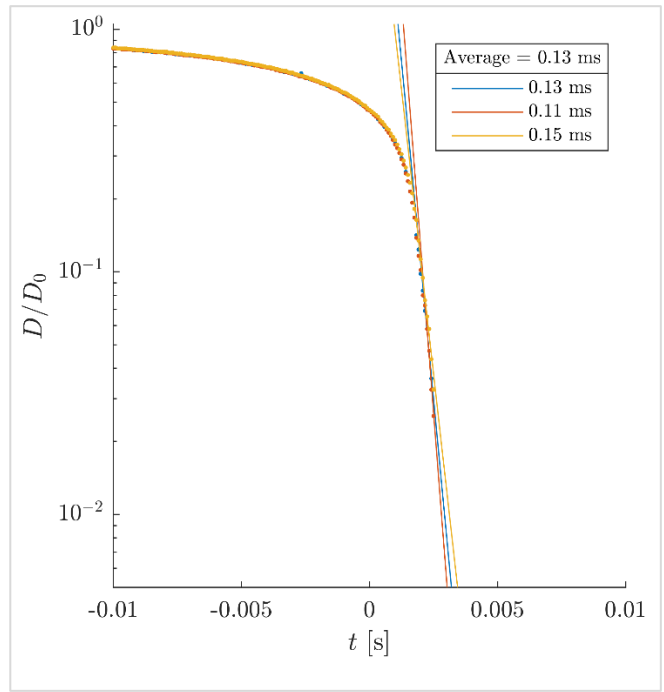


Figure D.1.8b:  $D/D_0$  versus  $t$  plot for 20% DR, Re: 70000.

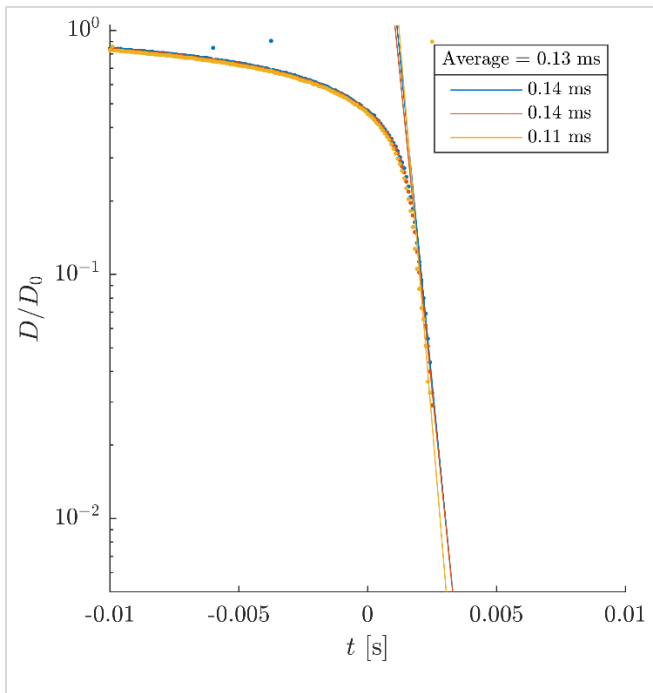


Figure D.1.8c:  $D/D_0$  versus  $t$  plot for 20% DR, Re: 80000.

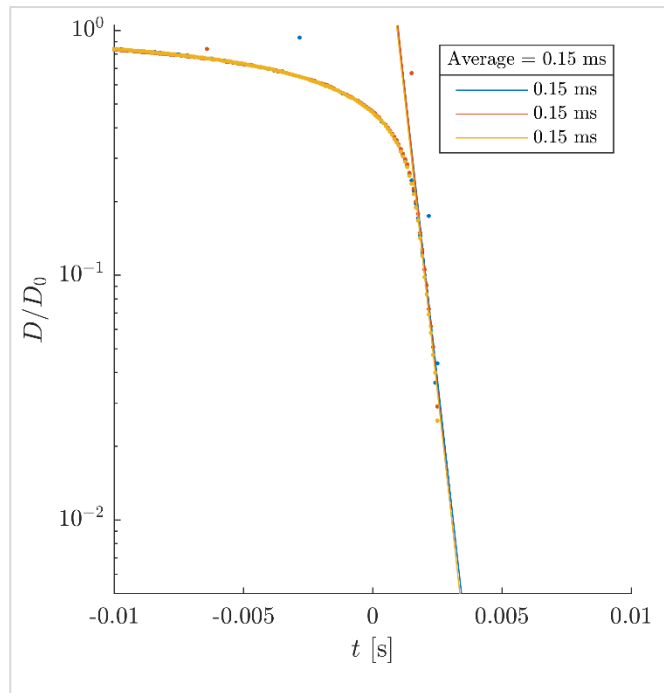


Figure D.1.8d:  $D/D_0$  versus  $t$  plot for 20% DR, Re: 90000.

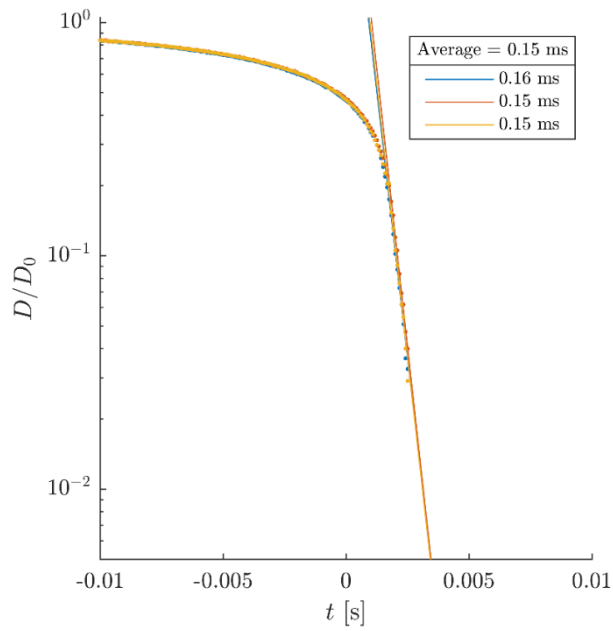


Figure D.1.8e:  $D/D_0$  versus  $t$  plot for 20% DR, Re: 100000.

## D.2 ( $D/D_0$ ) versus time ( $t$ ) plots for test section with 1.5-inch ID

### D.2.1 Plots for 70% DR (data acquisition rate: 4000 fps)

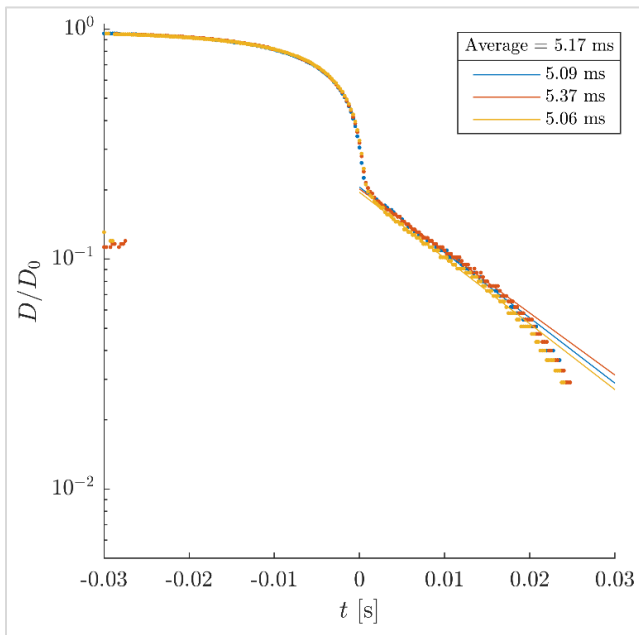


Figure D.2.1a:  $D/D_0$  versus  $t$  plot for 70% DR, Re: 60000.

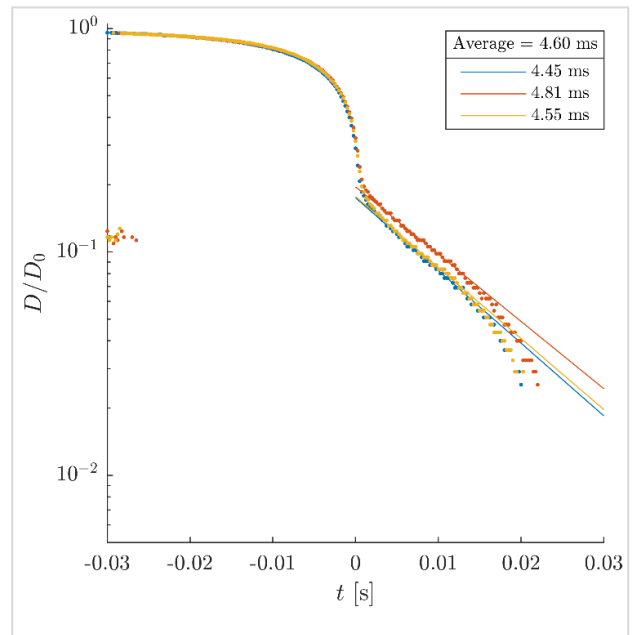


Figure D.2.1b:  $D/D_0$  versus  $t$  plot for 70% DR, Re: 70000.

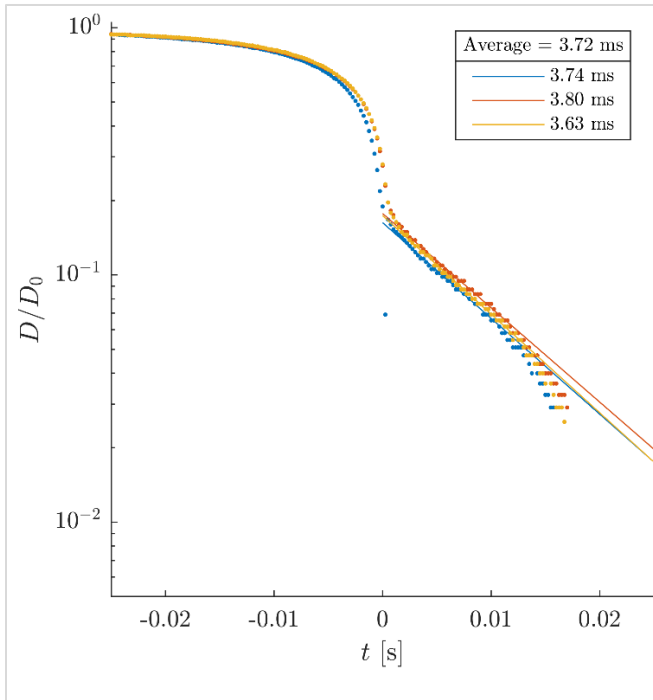


Figure D.2.1c:  $D/D_0$  versus  $t$  plot for 70% DR, Re: 80000.

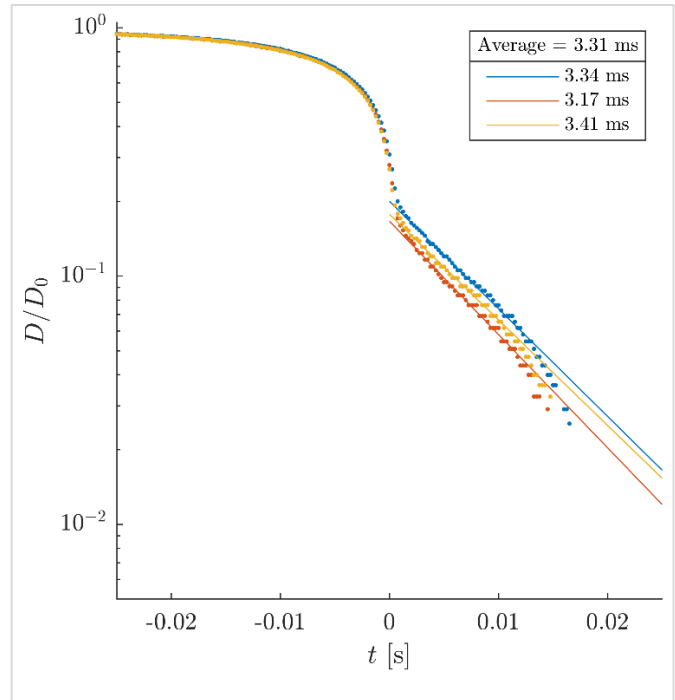


Figure D.2.1d:  $D/D_0$  versus  $t$  plot for 70% DR, Re: 90000.

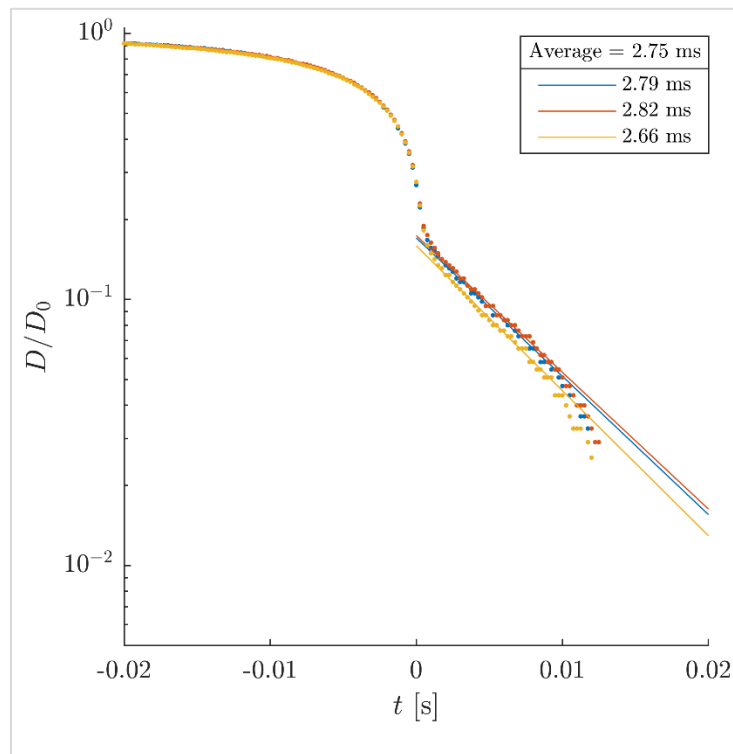


Figure D.2.1e:  $D/D_0$  versus  $t$  plot for 70% DR, Re: 100000.

## D.2.2 Plots for 65% DR (data acquisition rate: 4000 fps)

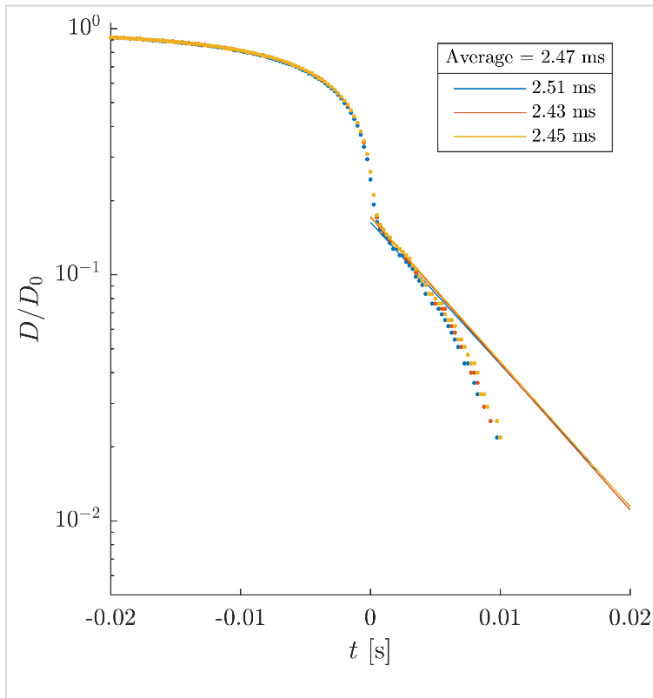


Figure D.2.2a:  $D/D_0$  versus  $t$  plot for 65% DR, Re: 60000.

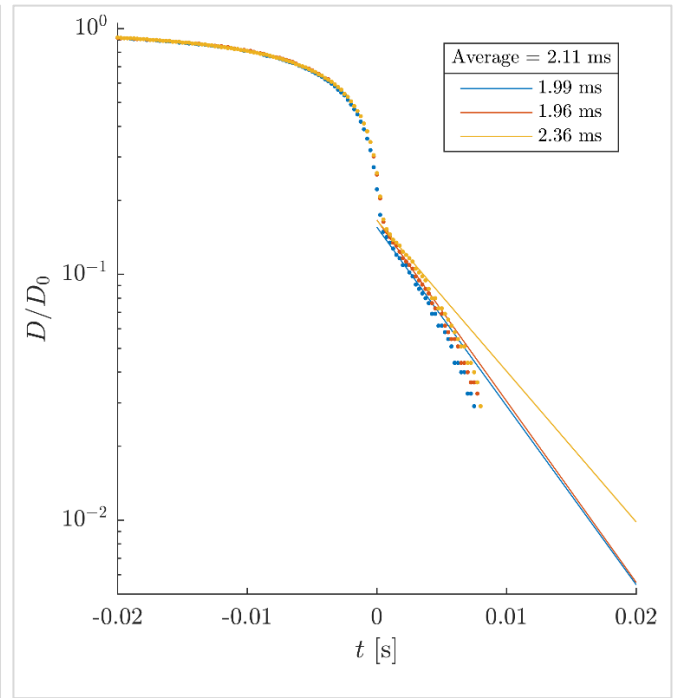


Figure D.2.2b:  $D/D_0$  versus  $t$  plot for 65% DR, Re: 70000.

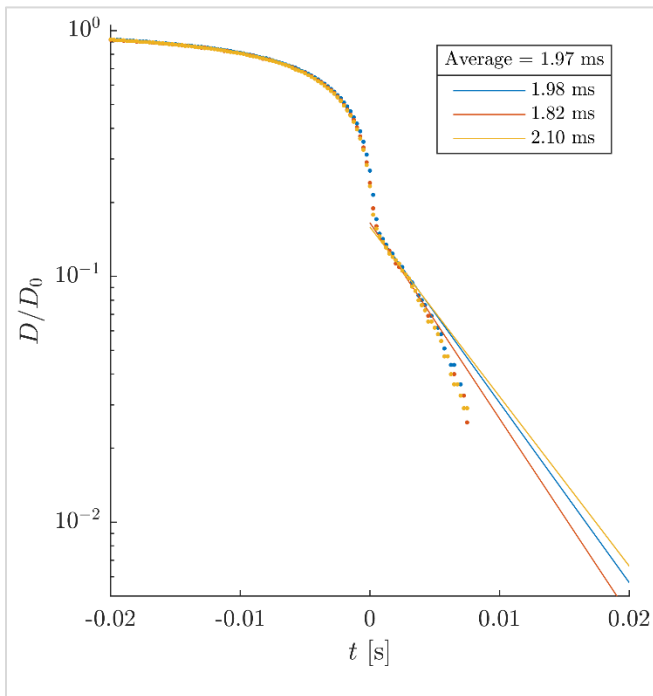


Figure D.2.2c:  $D/D_0$  versus  $t$  plot for 65% DR, Re: 80000.

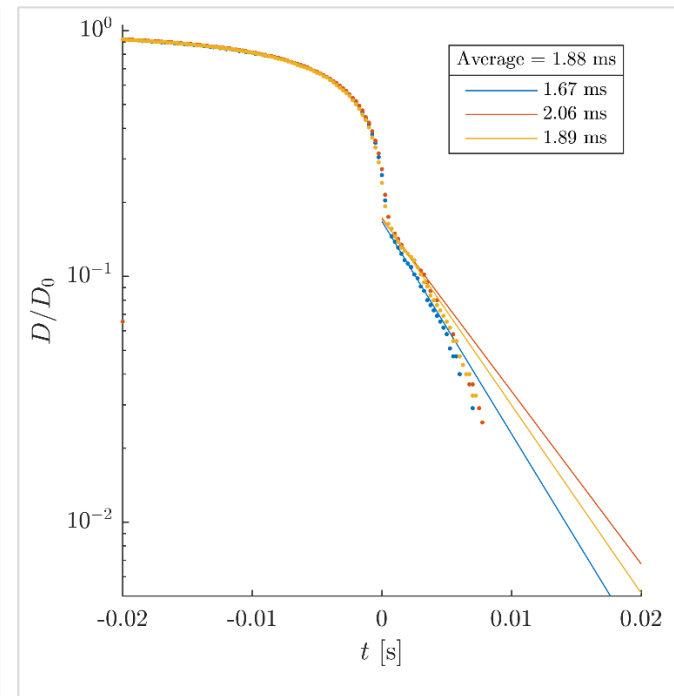


Figure D.2.2d:  $D/D_0$  versus  $t$  plot for 65% DR, Re: 90000.

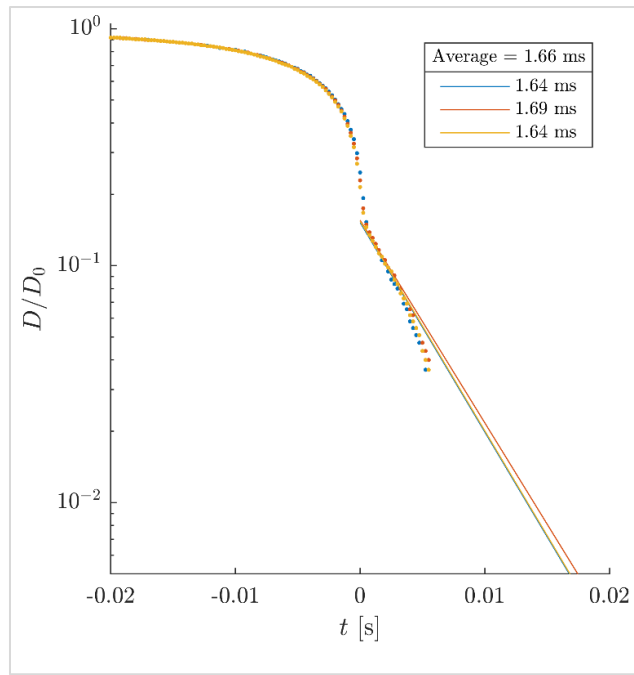


Figure D.2.2e:  $D/D_0$  versus  $t$  plot for 65% DR, Re: 100000.

### D.2.3 Plots for 60% DR (data acquisition rate: 4000 fps)

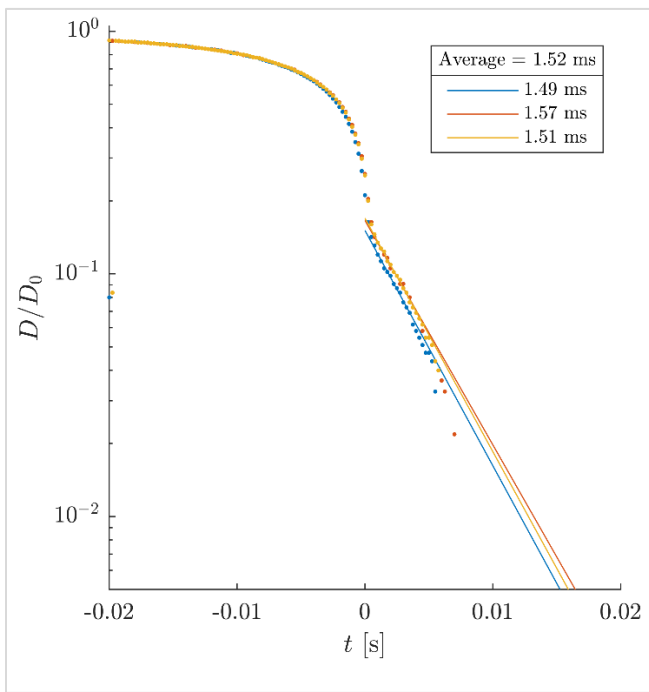


Figure D.2.3a:  $D/D_0$  versus  $t$  plot for 60% DR, Re: 60000.

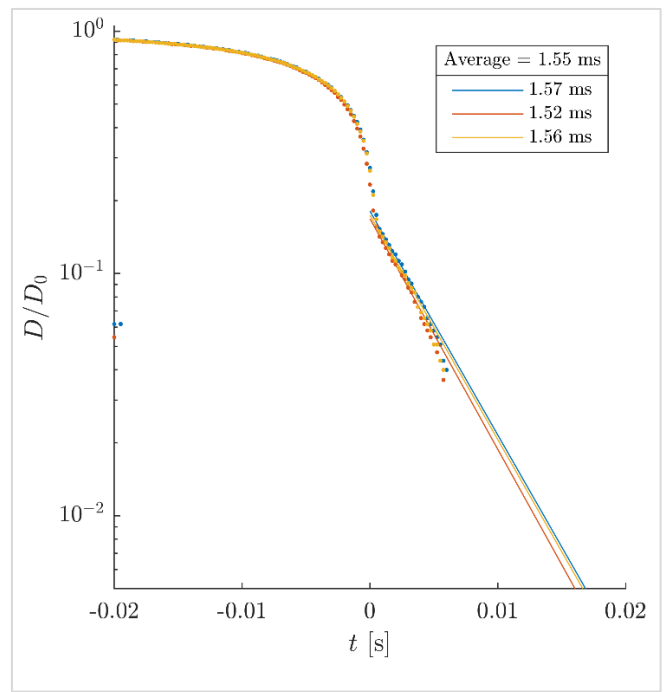


Figure D.2.3b:  $D/D_0$  versus  $t$  plot for 60% DR, Re: 70000.

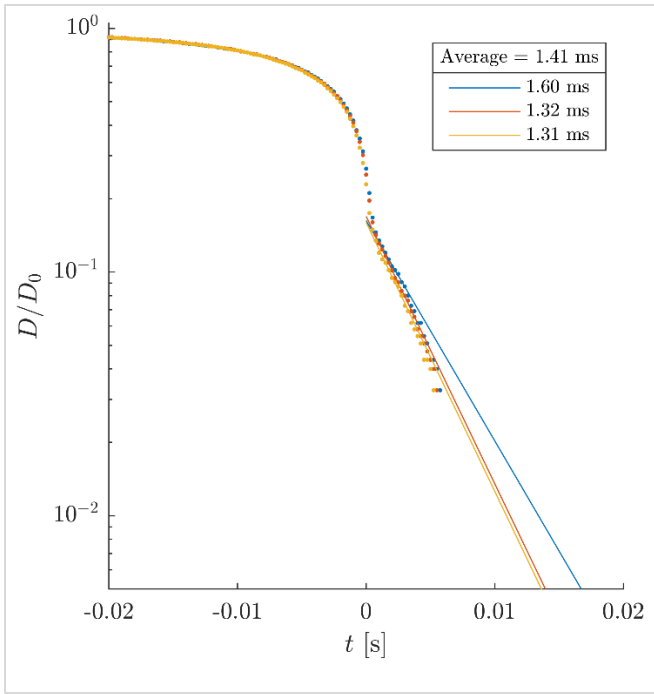


Figure D.2.3c:  $D/D_0$  versus  $t$  plot for 60% DR, Re: 80000.

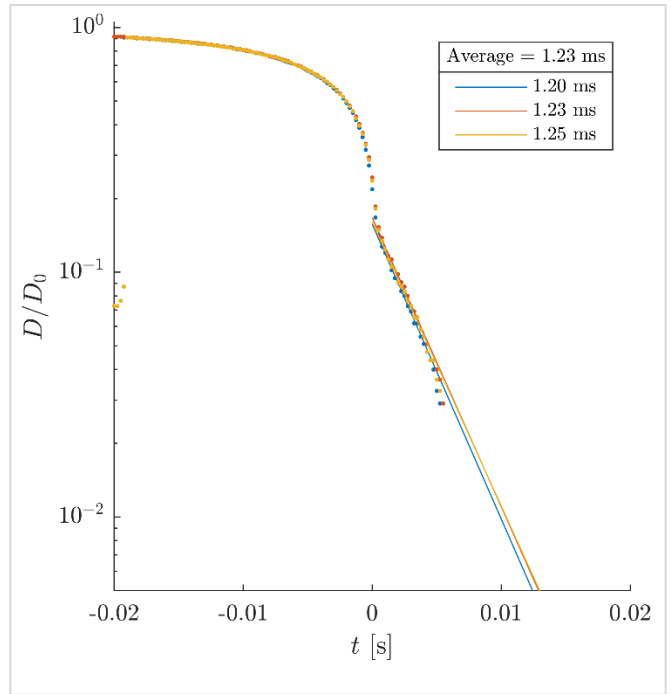


Figure D.2.3d:  $D/D_0$  versus  $t$  plot for 60% DR, Re: 90000.

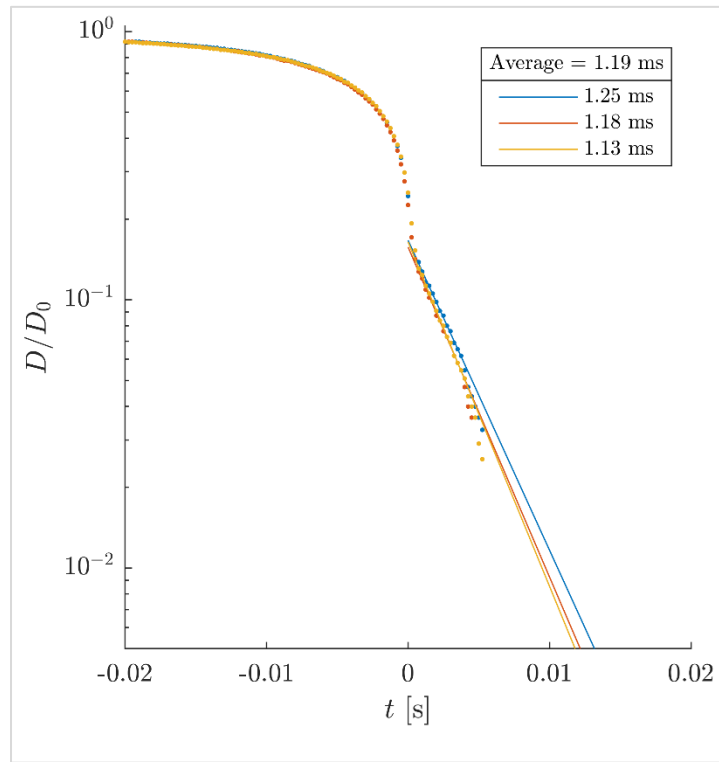


Figure D.2.3e:  $D/D_0$  versus  $t$  plot for 60% DR, Re: 100000.



### D.2.4 Plots for 50% DR (data acquisition rate: 4000 fps)

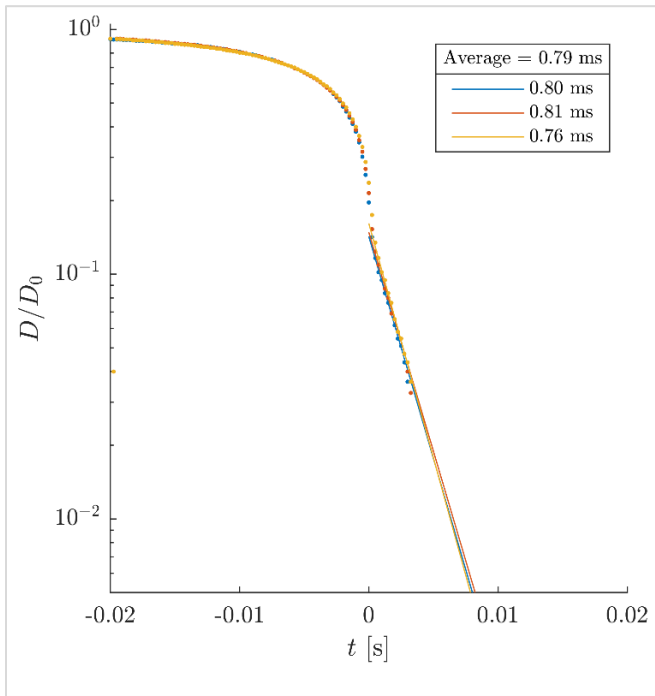


Figure D.2.4a:  $D/D_0$  versus  $t$  plot for 50% DR, Re: 60000.

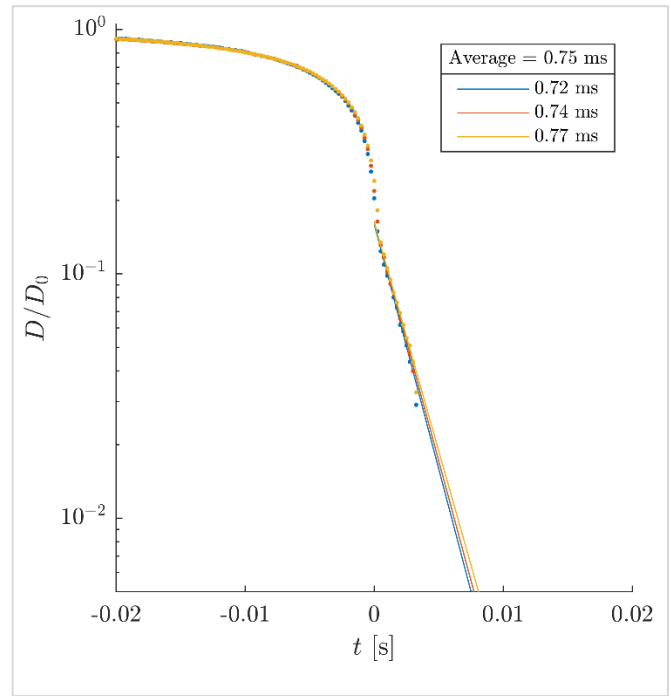


Figure D.2.4b:  $D/D_0$  versus  $t$  plot for 50% DR, Re: 70000.

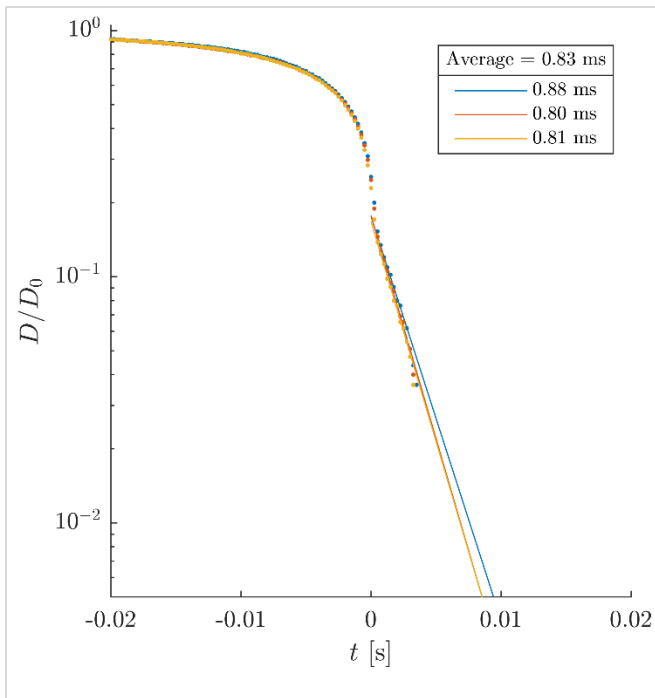


Figure D.2.4c:  $D/D_0$  versus  $t$  plot for 50% DR, Re: 80000.

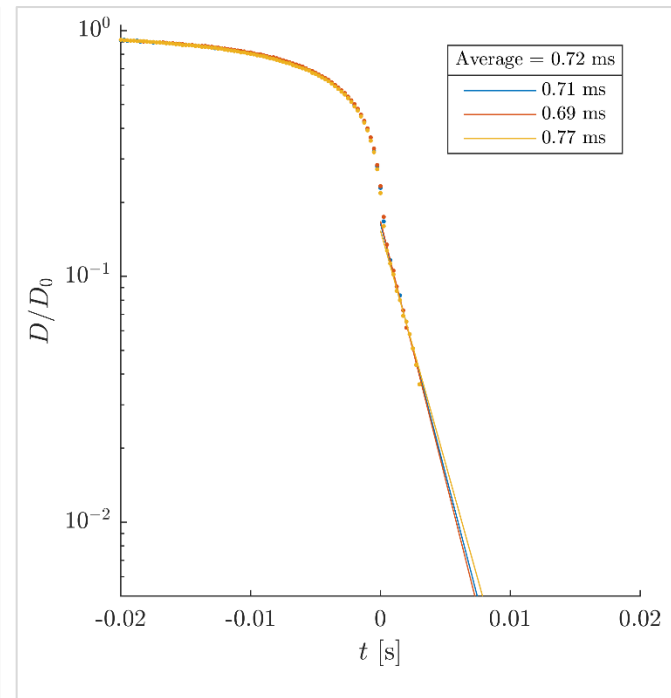


Figure D.2.4d:  $D/D_0$  versus  $t$  plot for 50% DR, Re: 90000.

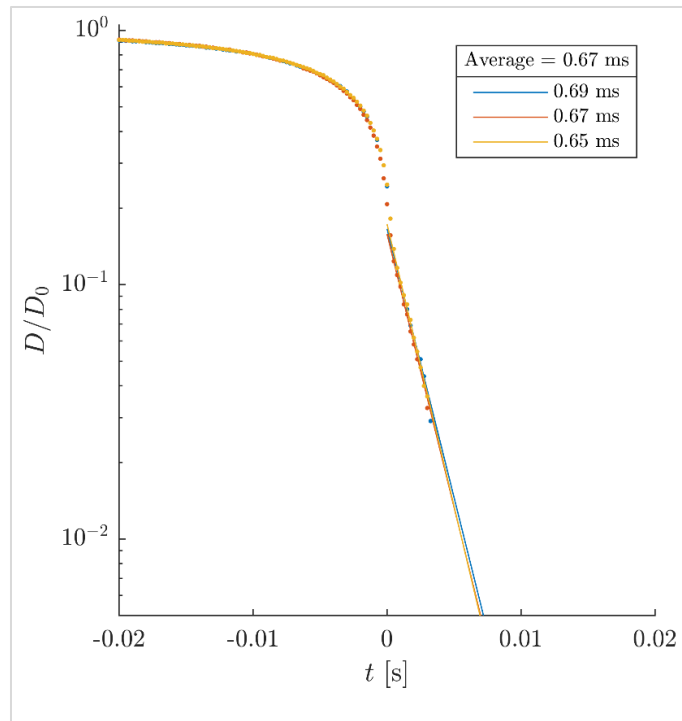


Figure D.2.4e:  $D/D_0$  versus  $t$  plot for 50% DR, Re: 100000.

### D.2.5 Plots for 40% DR (data acquisition rate: 9000 fps)

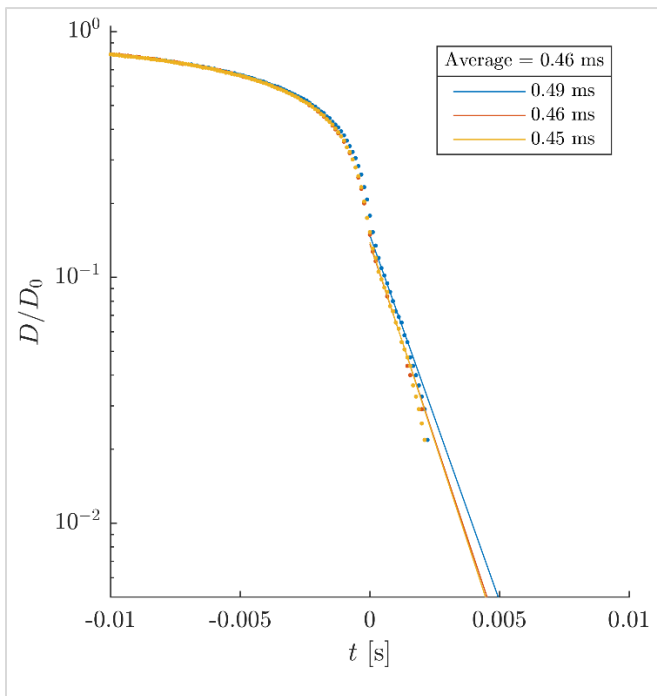


Figure D.2.5a:  $D/D_0$  versus  $t$  plot for 40% DR, Re: 60000.

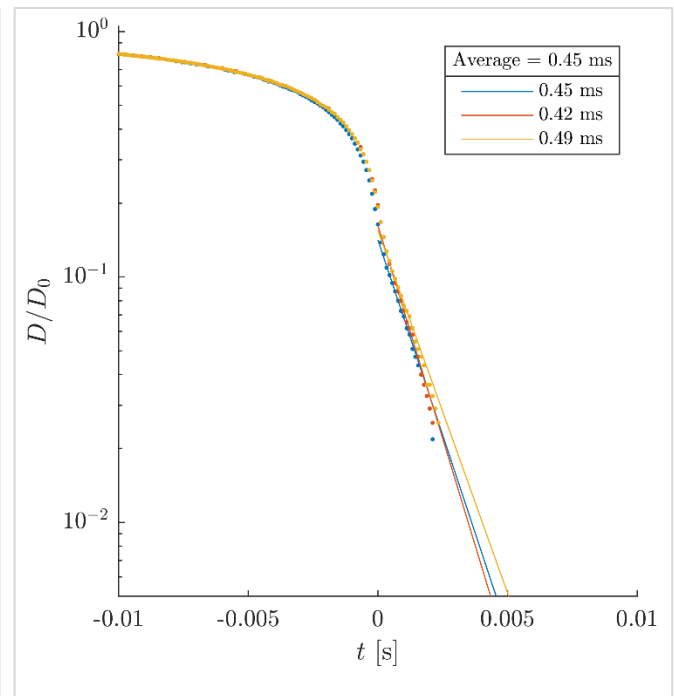


Figure D.2.5b:  $D/D_0$  versus  $t$  plot for 40% DR, Re: 70000.

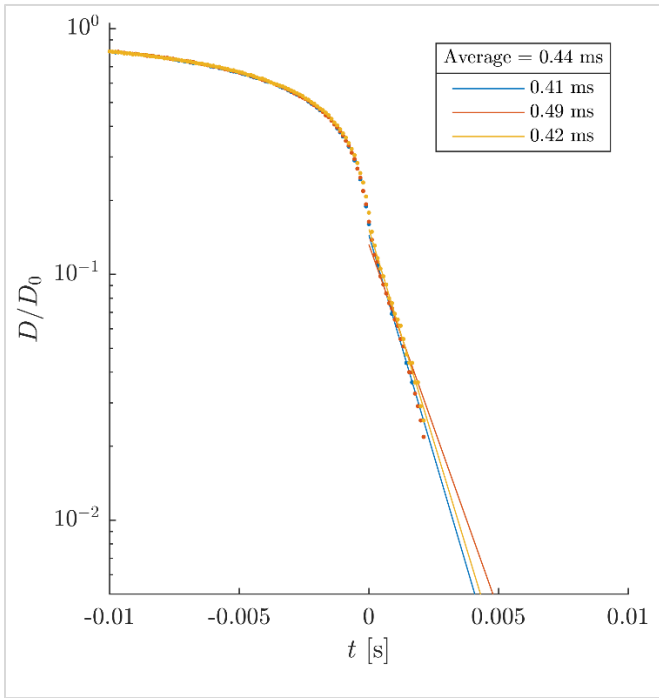


Figure D.2.5c:  $D/D_0$  versus  $t$  plot for 40% DR, Re: 80000.

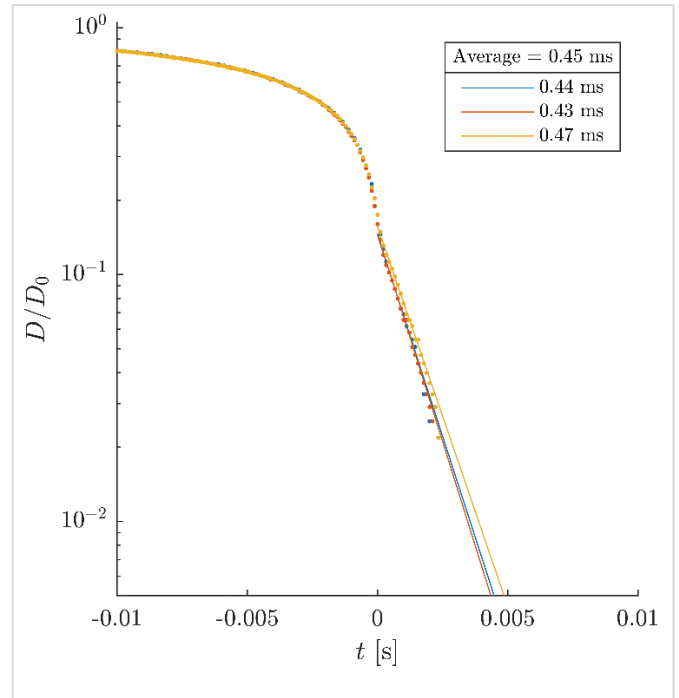


Figure D.2.5d:  $D/D_0$  versus  $t$  plot for 40% DR, Re: 90000.

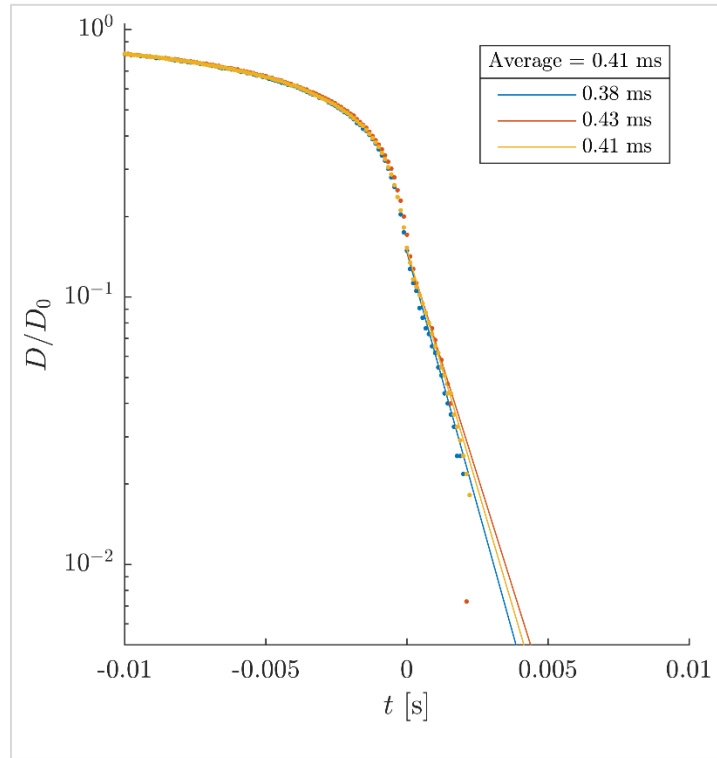


Figure D.2.5e:  $D/D_0$  versus  $t$  plot for 40% DR, Re: 100000.

### D.2.6 Plots for 30% DR (data acquisition rate: 12000 fps)

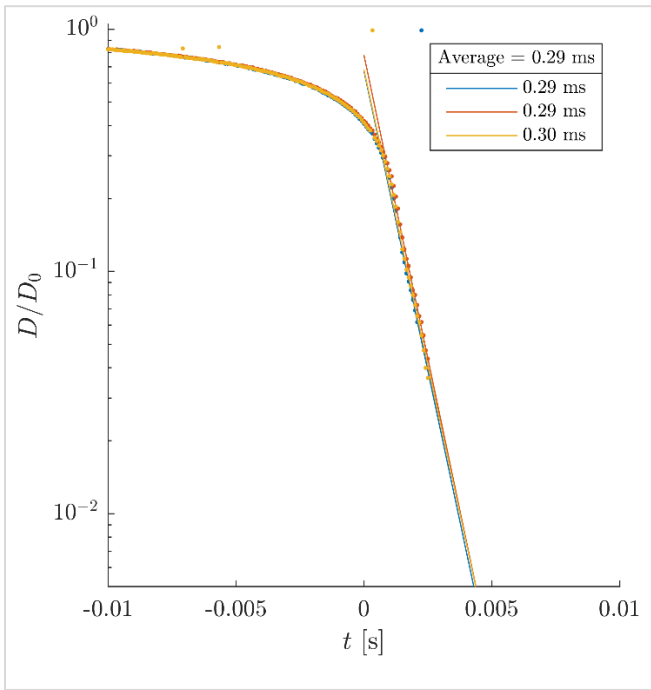


Figure D.2.6a:  $D/D_0$  versus  $t$  plot for 30% DR, Re: 60000.

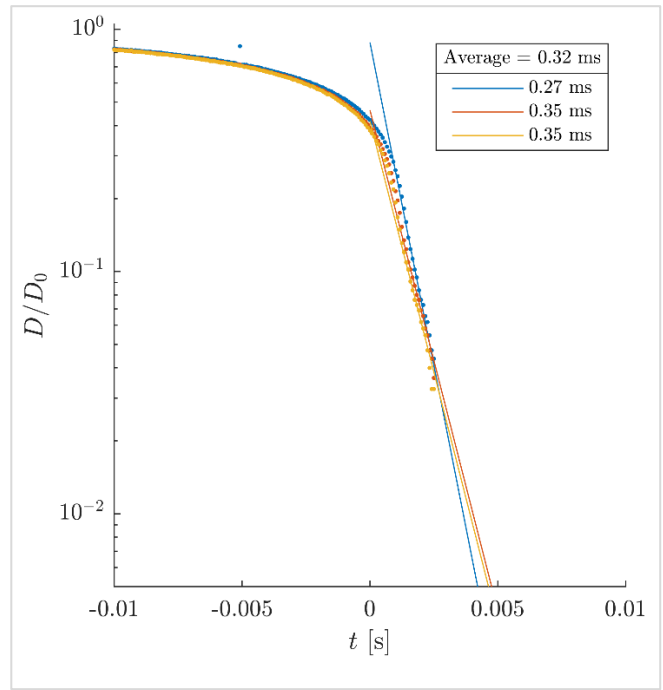


Figure D.2.6b:  $D/D_0$  versus  $t$  plot for 30% DR, Re: 70000.

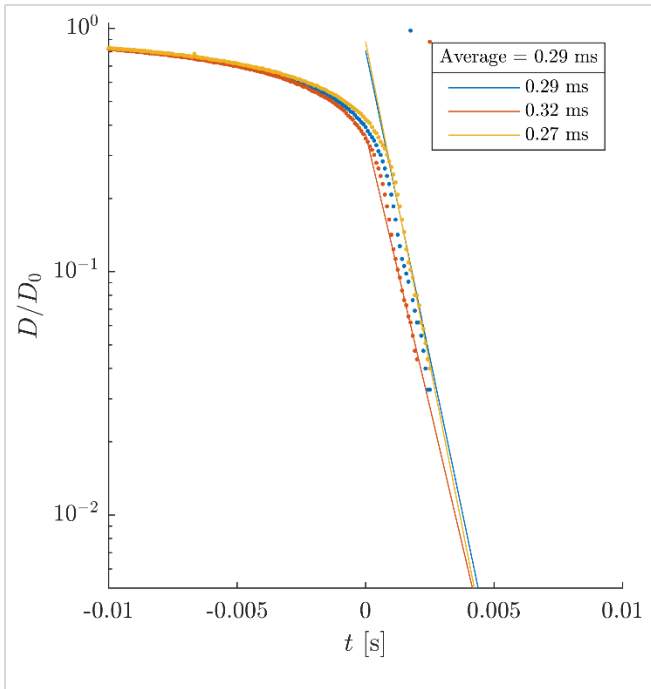


Figure D.2.6c:  $D/D_0$  versus  $t$  plot for 30% DR, Re: 80000.

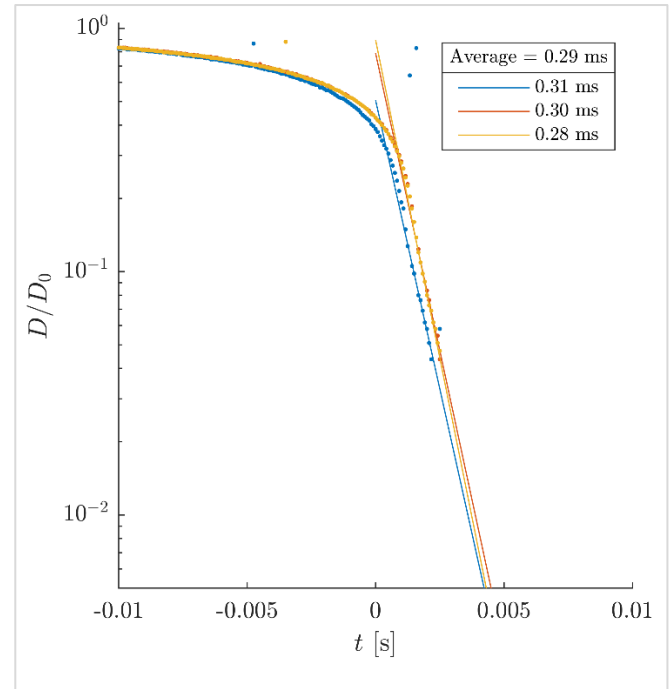


Figure D.2.6d:  $D/D_0$  versus  $t$  plot for 30% DR, Re: 90000.

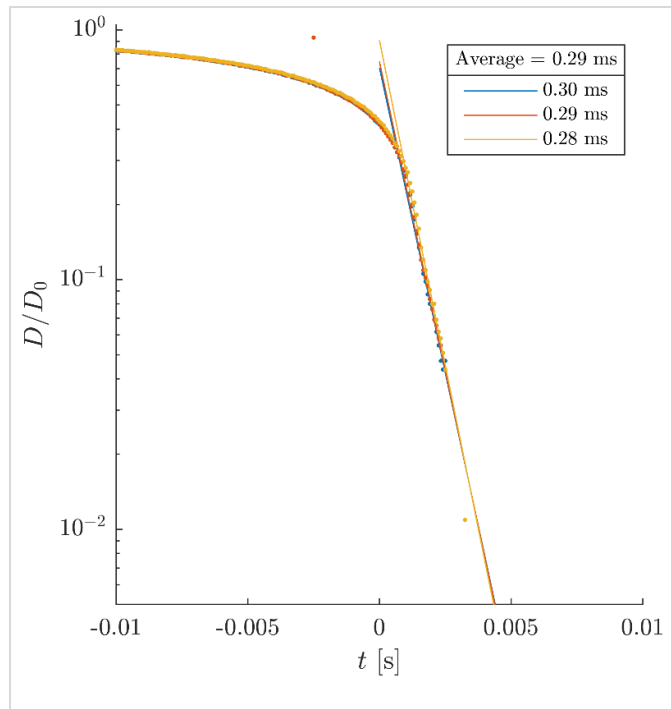


Figure D.2.6e:  $D/D_0$  versus  $t$  plot for 30% DR, Re: 100000.

### D.2.7 Plots for 20% DR (data acquisition rate: 12000 fps)

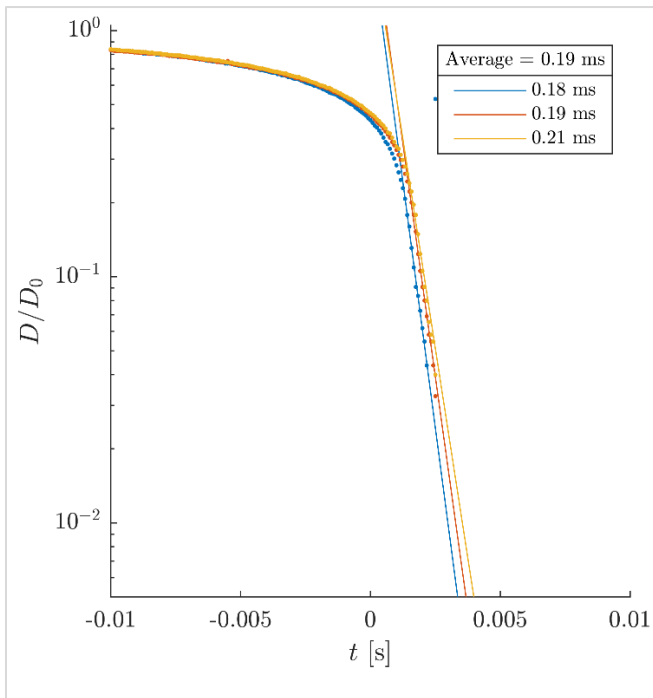


Figure D.2.7a:  $D/D_0$  versus  $t$  plot for 20% DR, Re: 60000.

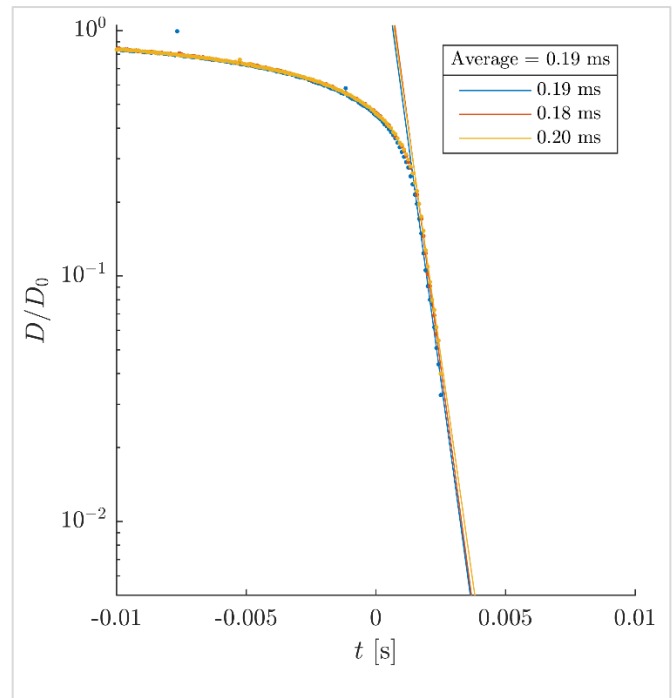


Figure D.2.7b:  $D/D_0$  versus  $t$  plot for 20% DR, Re: 70000.

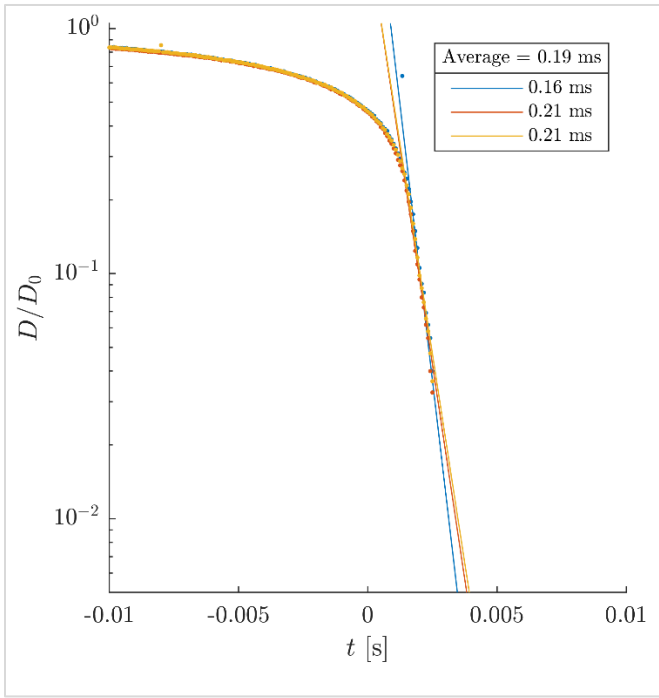


Figure D.2.7c:  $D/D_0$  versus  $t$  plot for 20% DR, Re: 80000.

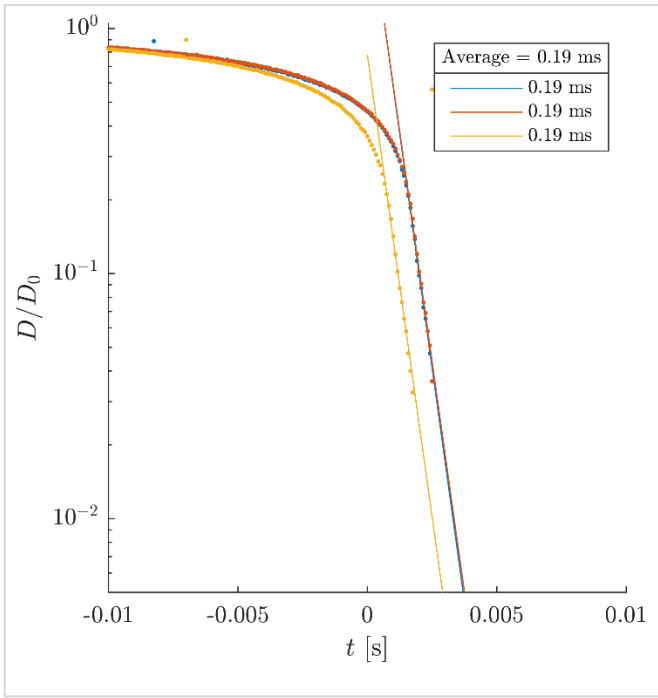


Figure D.2.7d:  $D/D_0$  versus  $t$  plot for 20% DR, Re: 90000.

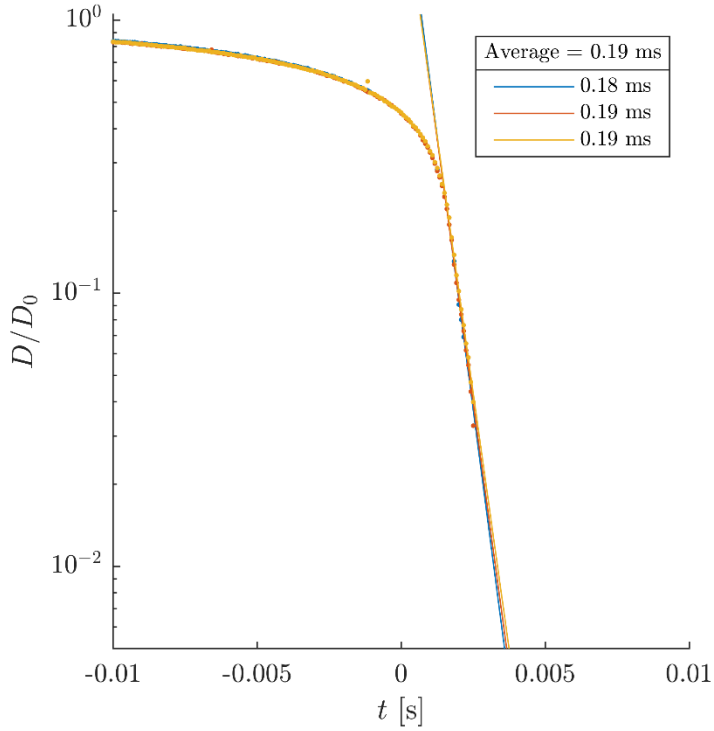


Figure D.2.7e:  $D/D_0$  versus  $t$  plot for 20% DR, Re: 100000.

### D.3 ( $D/D_0$ ) versus time ( $t$ ) plots for test section with 2-inch ID

#### D.3.1 Plots for 60% DR (data acquisition rate: 4000 fps)

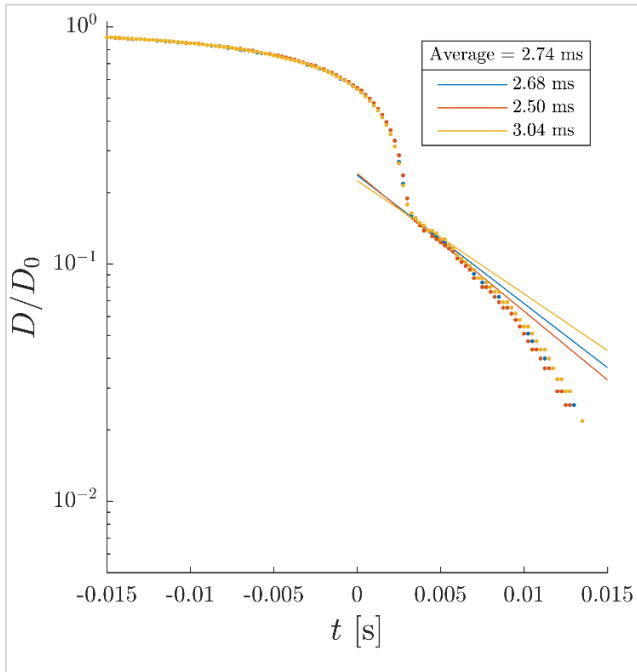


Figure D.3.1a:  $D/D_0$  versus  $t$  plot for 60% DR, Re: 60000.

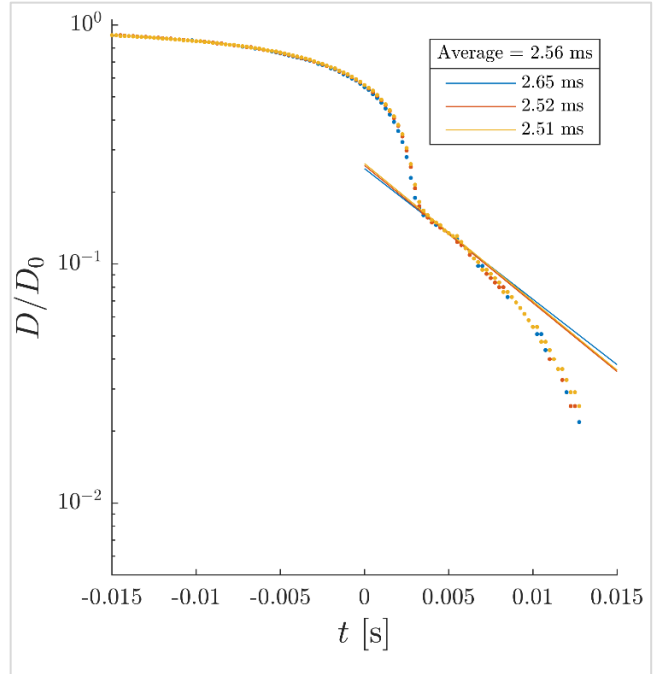


Figure D.3.1b:  $D/D_0$  versus  $t$  plot for 60% DR, Re: 70000.

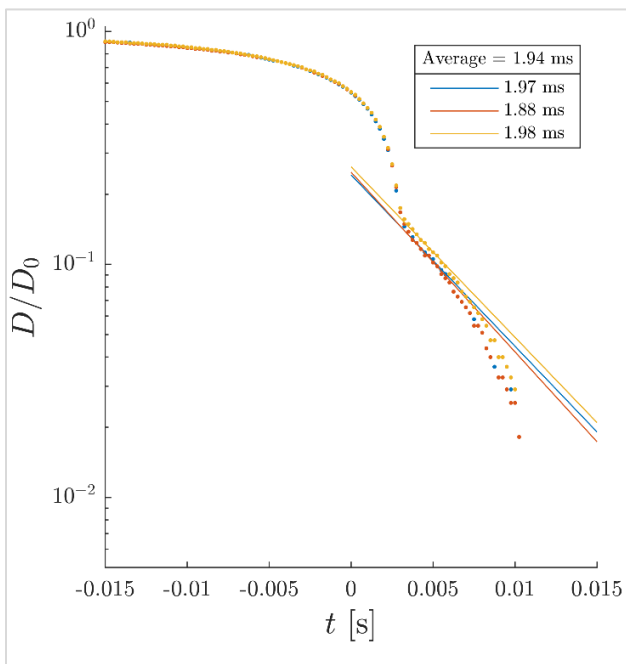


Figure D.3.1c:  $D/D_0$  versus  $t$  plot for 60% DR, Re: 80000.

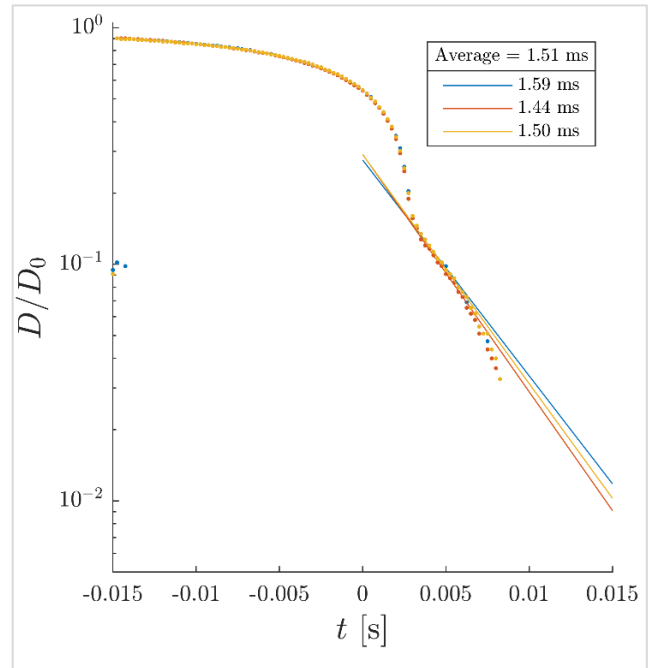


Figure D.3.1d:  $D/D_0$  versus  $t$  plot for 60% DR, Re: 90000.

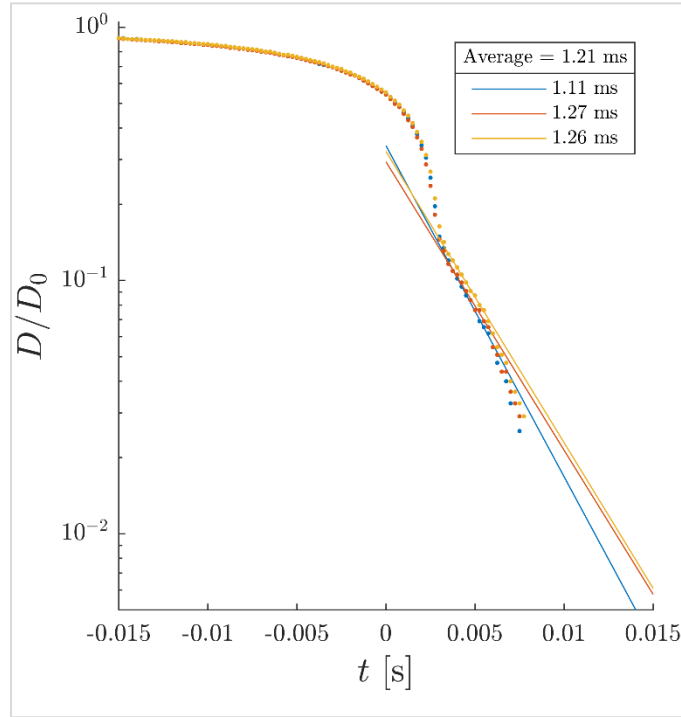


Figure A.4.3.1.c:  $D/D_0$  vs  $t$  plot – 60% DR – Re: 100k (June 28, 2023).

### D.3.2 Plots for 50% DR (data acquisition rate: 4000 fps)

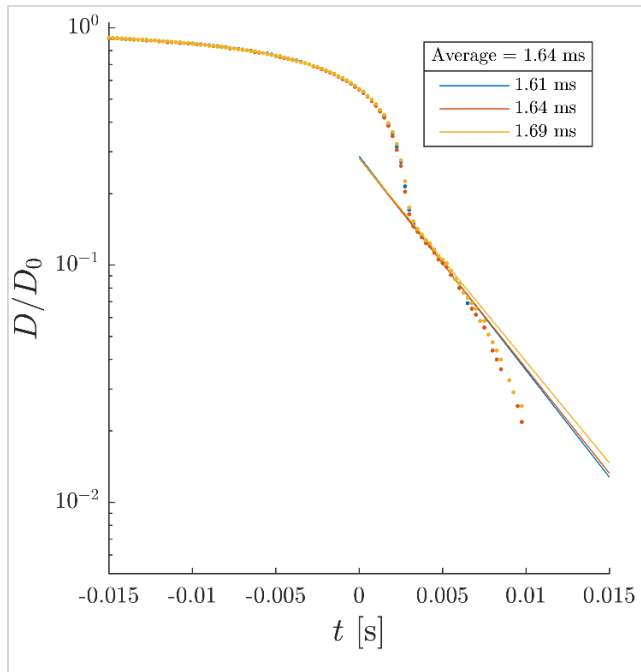


Figure D.3.2a:  $D/D_0$  versus  $t$  plot for 50% DR, Re: 60000.

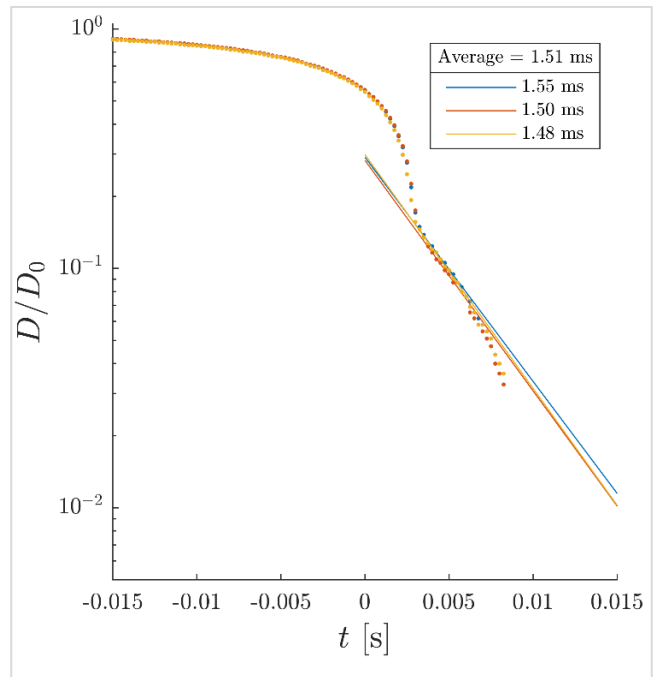


Figure D.3.2b:  $D/D_0$  versus  $t$  plot for 50% DR, Re: 70000.



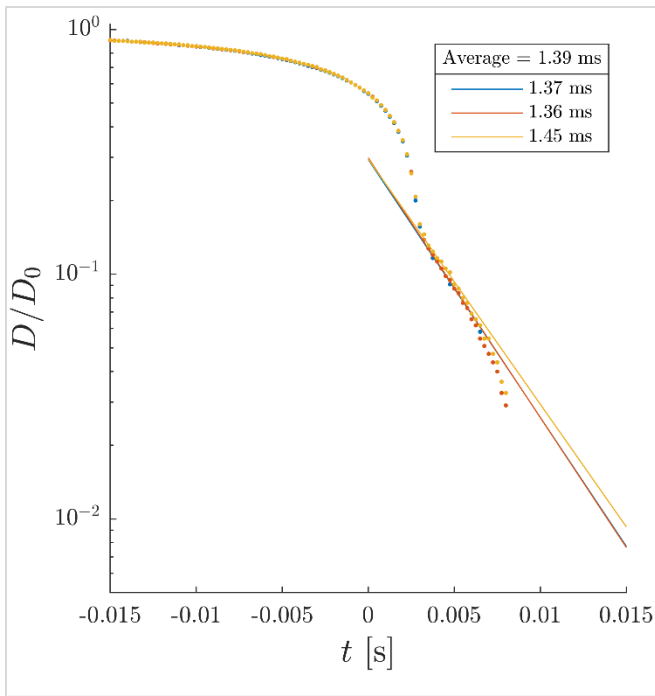


Figure D.3.2c:  $D/D_0$  versus  $t$  plot for 50% DR, Re: 80000.

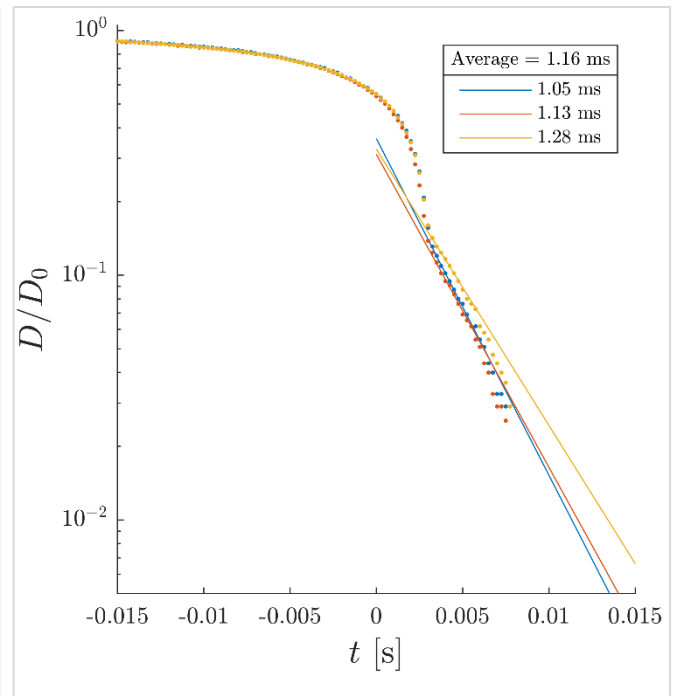


Figure D.3.2d:  $D/D_0$  versus  $t$  plot for 50% DR, Re: 90000.

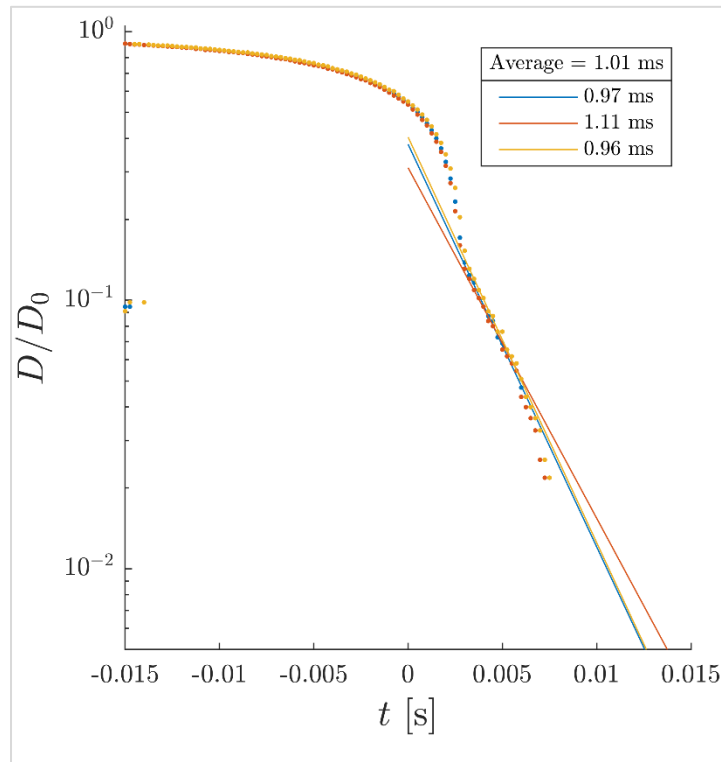


Figure D.3.2e:  $D/D_0$  versus  $t$  plot for 50% DR, Re: 100000.

### D.3.3 Plots for 40% DR (data acquisition rate: 4000 fps)

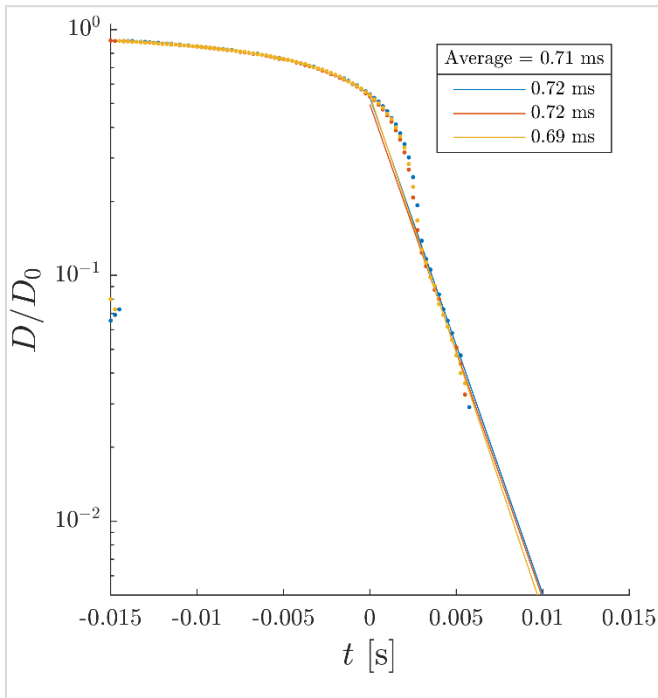


Figure D.3.3a:  $D/D_0$  versus  $t$  plot for 40% DR, Re: 60000.

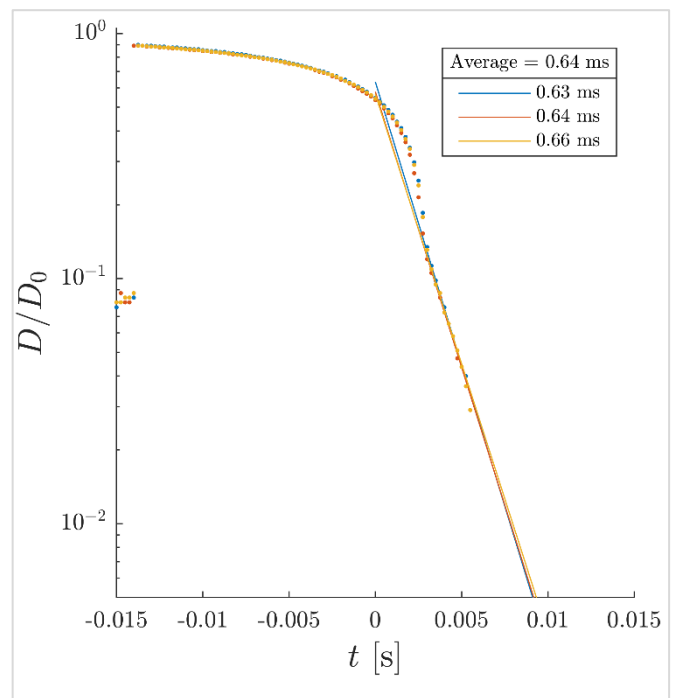


Figure D.3.3b:  $D/D_0$  versus  $t$  plot for 40% DR, Re: 70000.

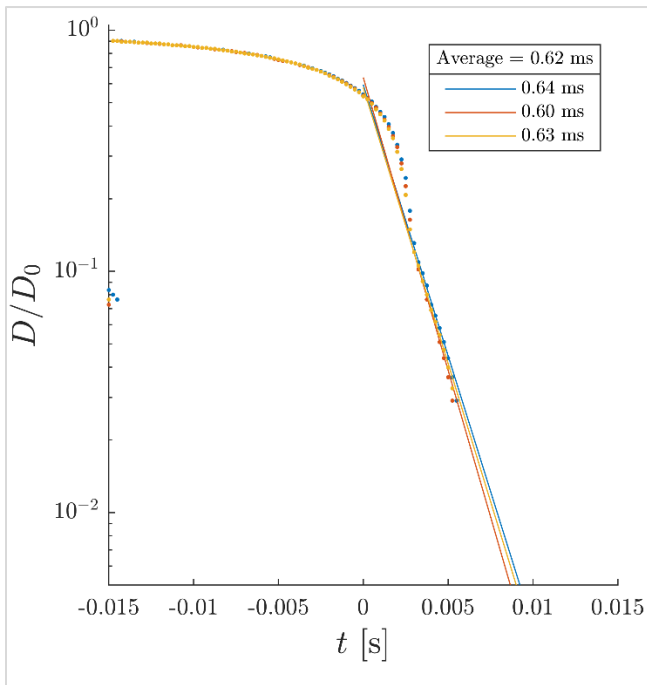


Figure D.3.3c:  $D/D_0$  versus  $t$  plot for 40% DR, Re: 80000.

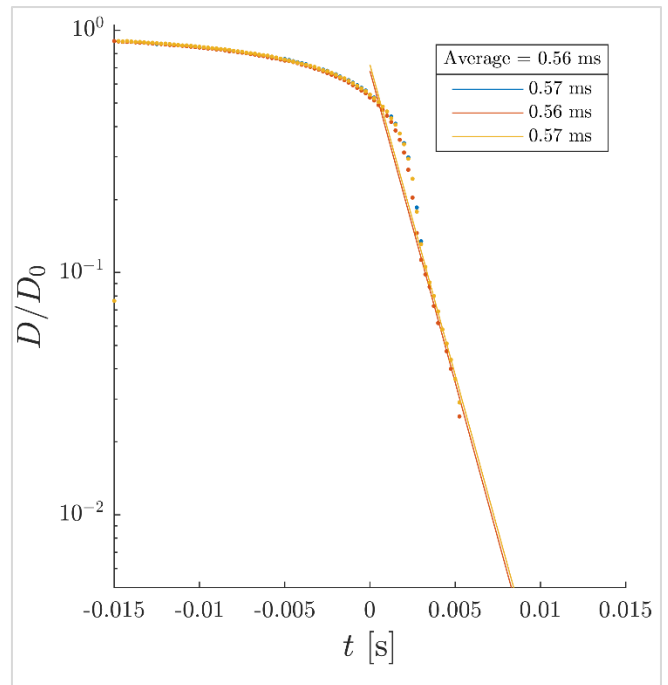


Figure D.3.3d:  $D/D_0$  versus  $t$  plot for 40% DR, Re: 90000.

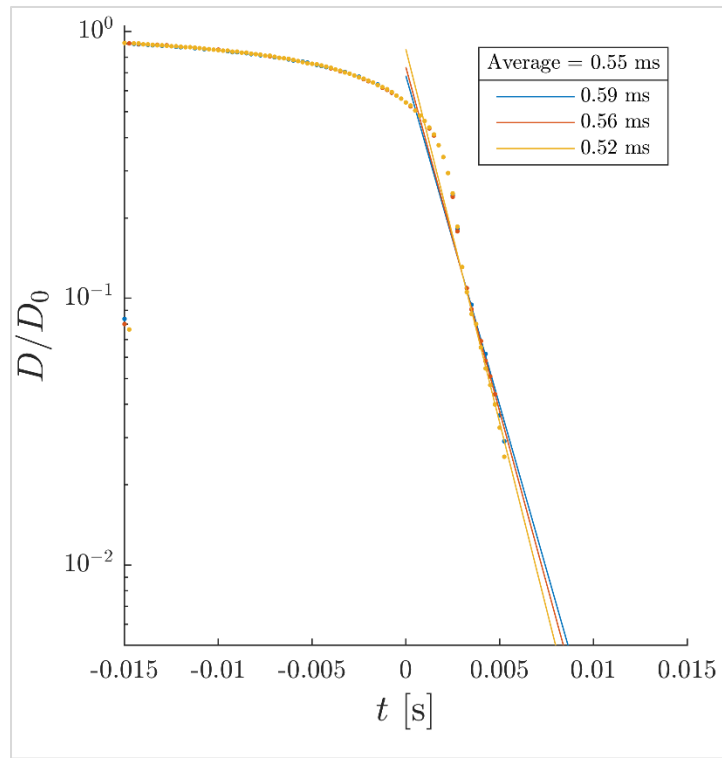


Figure D.3.3e:  $D/D_0$  versus  $t$  plot for 40% DR, Re: 100000.

### D.3.4 Plots for 30% DR (data acquisition rate: 9000 fps)

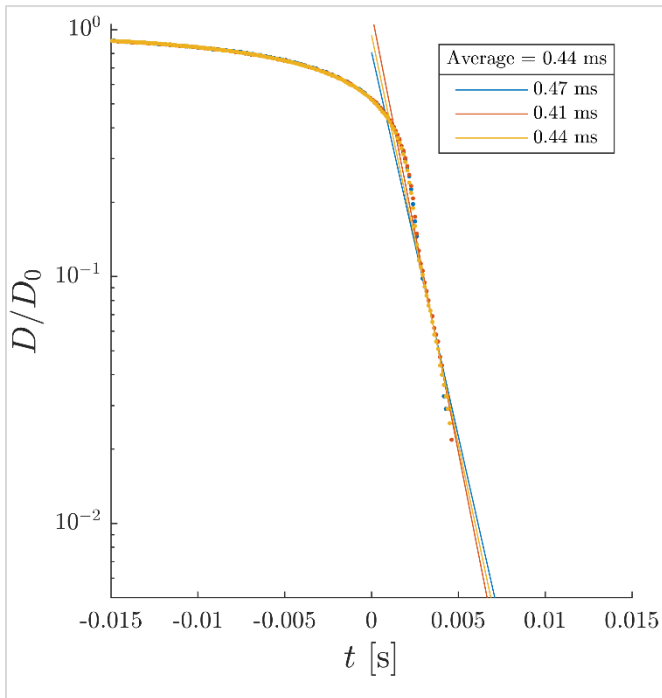


Figure D.3.4a:  $D/D_0$  versus  $t$  plot for 30% DR, Re: 60000.

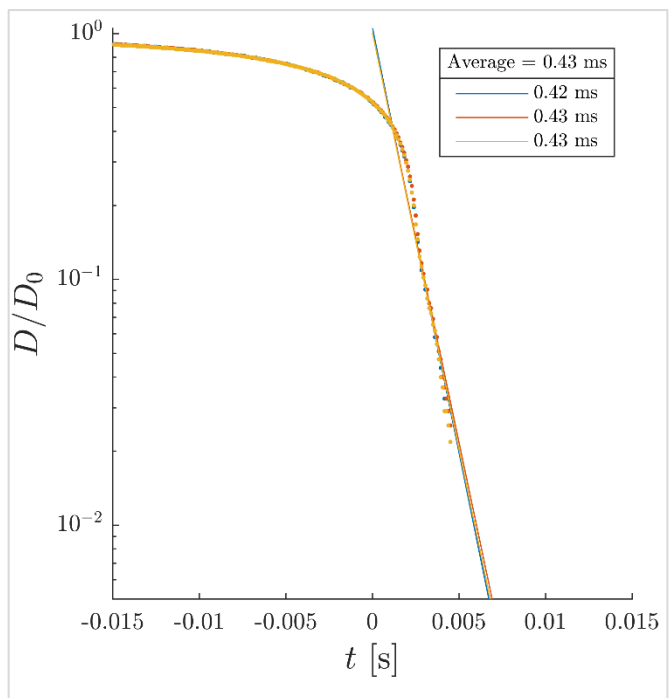


Figure D.3.4b:  $D/D_0$  versus  $t$  plot for 30% DR, Re: 70000.

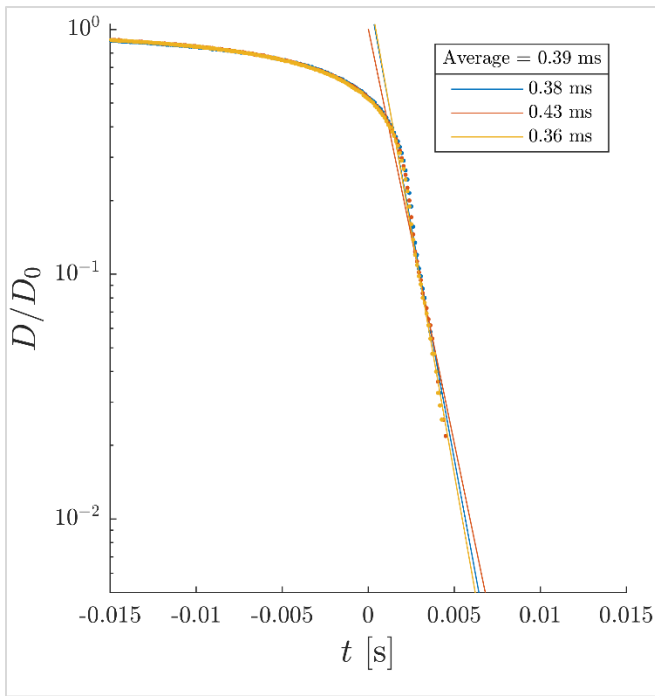


Figure D.3.4c:  $D/D_0$  versus  $t$  plot for 30% DR, Re: 80000.

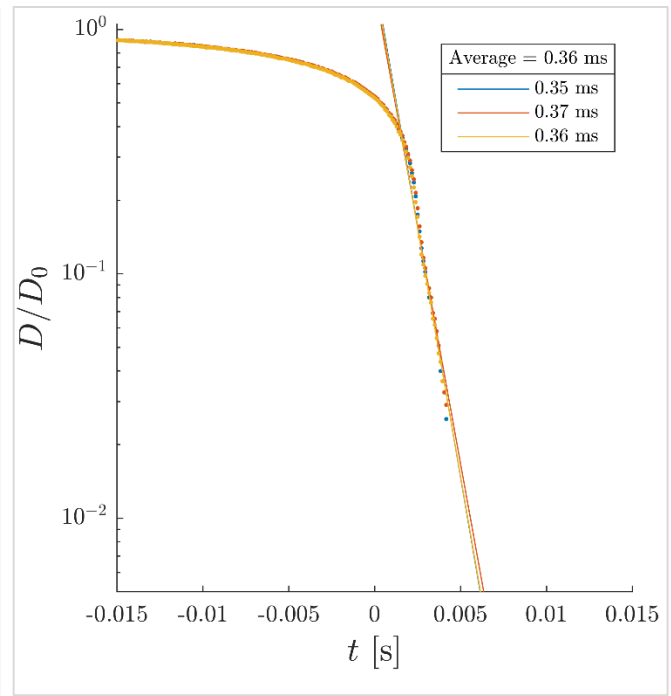


Figure D.3.4d:  $D/D_0$  versus  $t$  plot for 30% DR, Re: 90000.

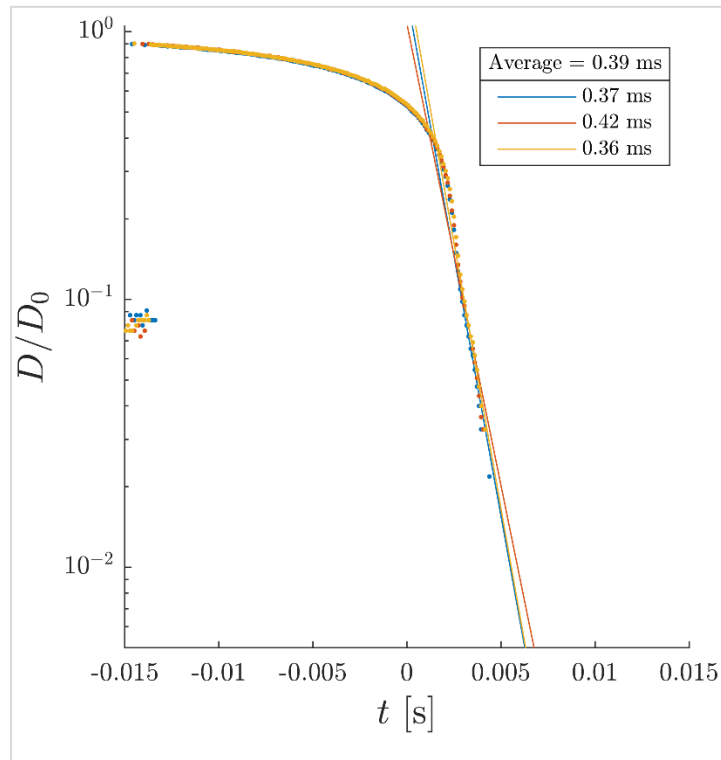


Figure D.3.4e:  $D/D_0$  versus  $t$  plot for 30% DR, Re: 100000.

### D.3.5 Plots for 20% DR (data acquisition rate: 9000 fps)

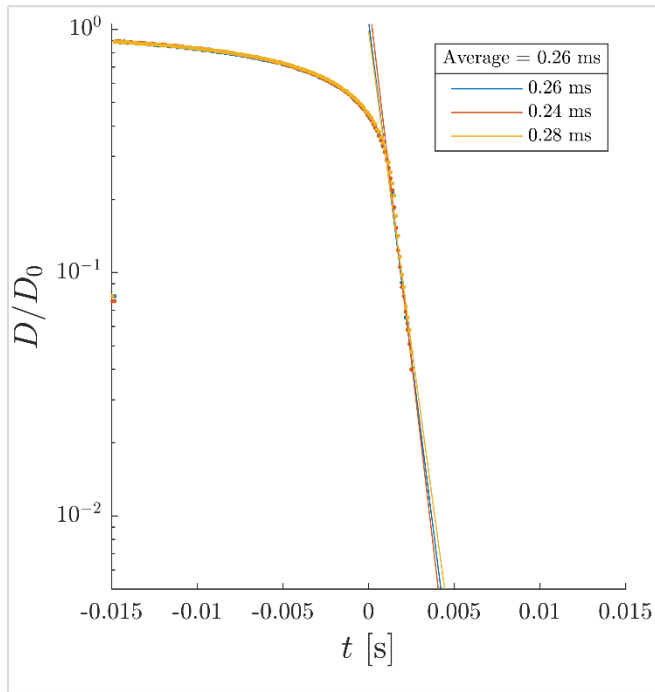


Figure D.3.5a:  $D/D_0$  versus  $t$  plot for 20% DR, Re: 60000.

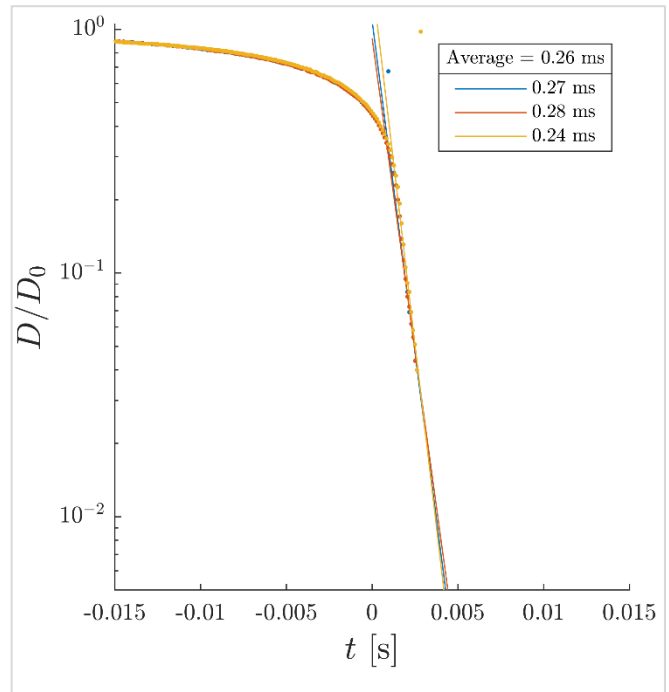


Figure D.3.5b:  $D/D_0$  versus  $t$  plot for 20% DR, Re: 70000.

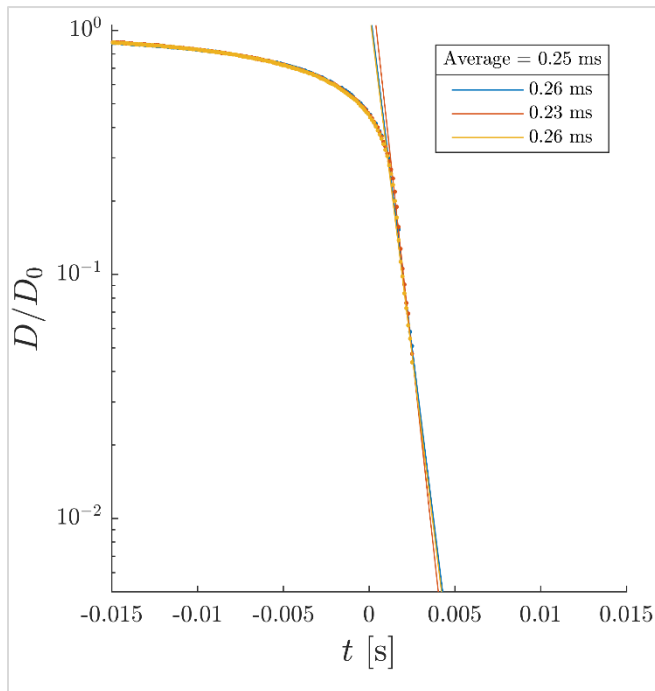


Figure D.3.5c:  $D/D_0$  versus  $t$  plot for 20% DR, Re: 80000.

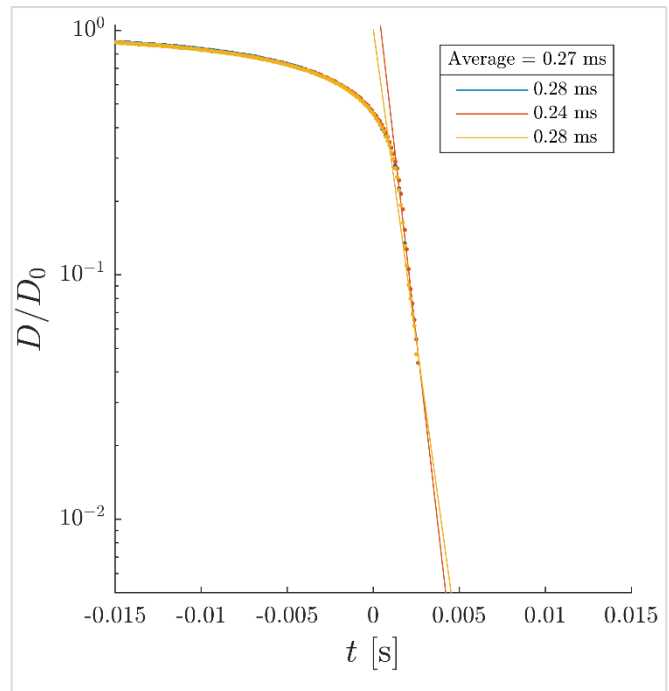


Figure D.3.5d:  $D/D_0$  versus  $t$  plot for 20% DR, Re: 90000.

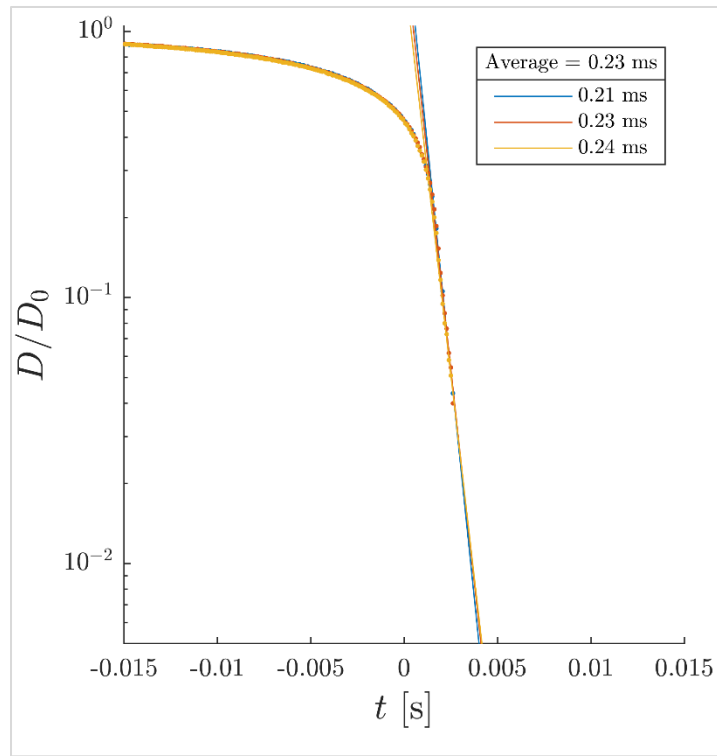


Figure D.3.5e:  $D/D_0$  versus  $t$  plot for 20% DR, Re: 100000.

### D.3.6 Plots for 10% DR (data acquisition rate: 12000 fps)

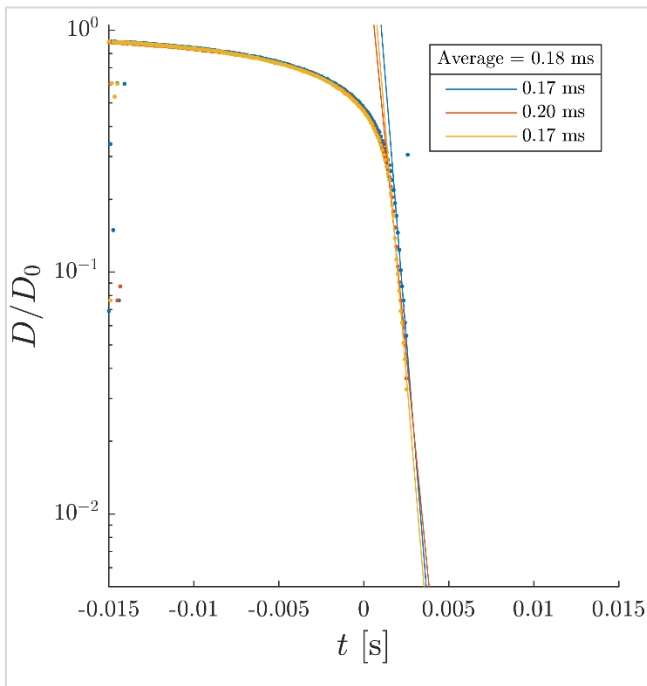


Figure D.3.6a:  $D/D_0$  versus  $t$  plot for 10% DR, Re: 60000.

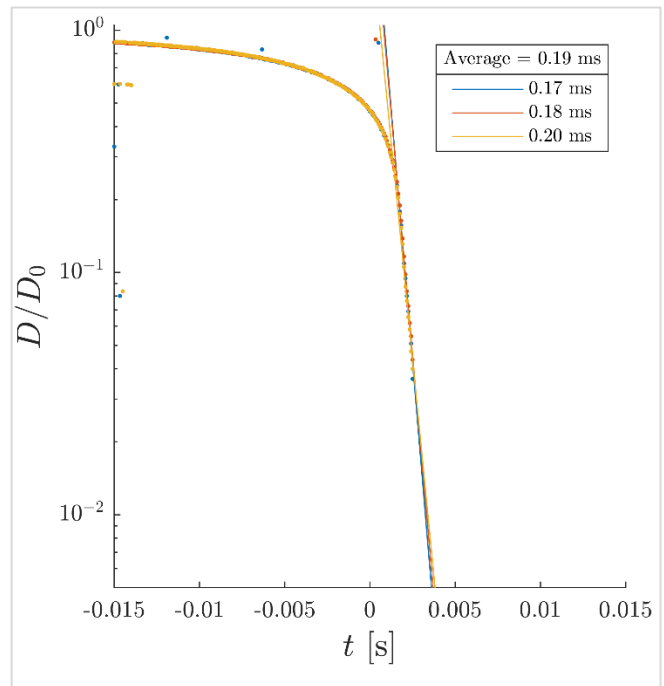


Figure D.3.6b:  $D/D_0$  versus  $t$  plot for 10% DR, Re: 70000.

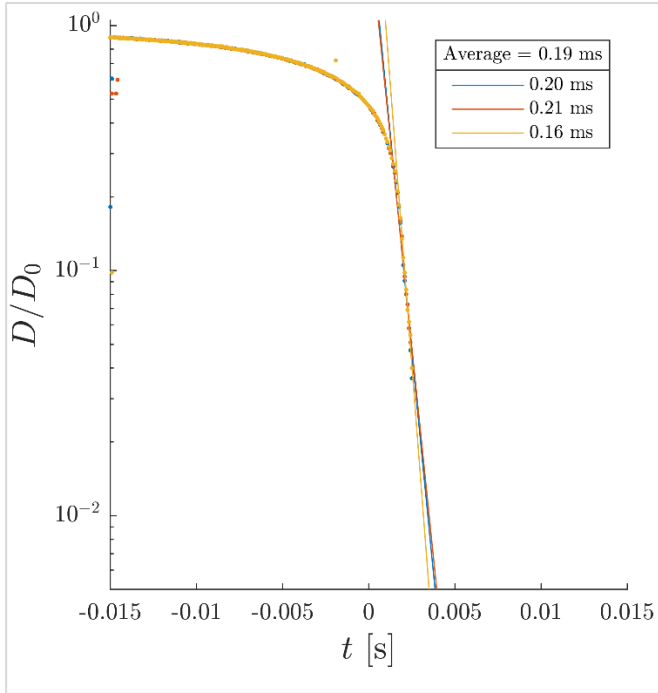


Figure D.3.6c:  $D/D_0$  versus  $t$  plot for 10% DR, Re: 80000.

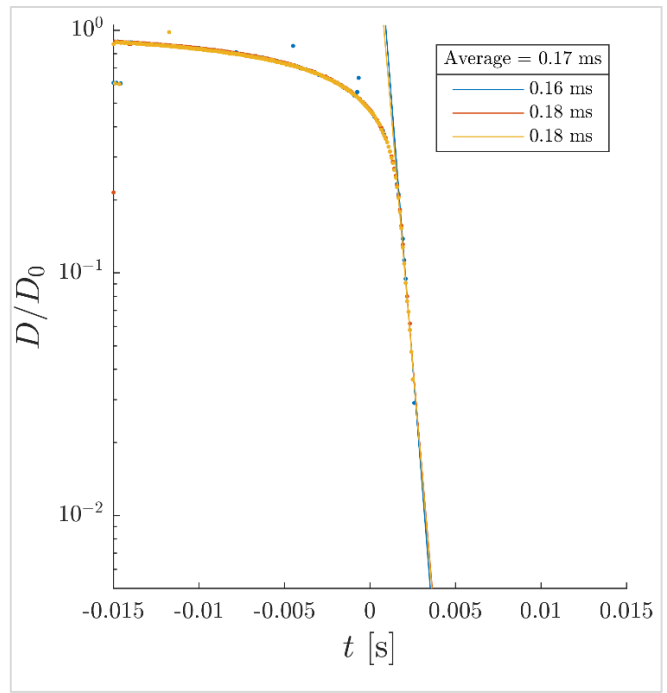


Figure D.3.6d:  $D/D_0$  versus  $t$  plot for 10% DR, Re: 90000.

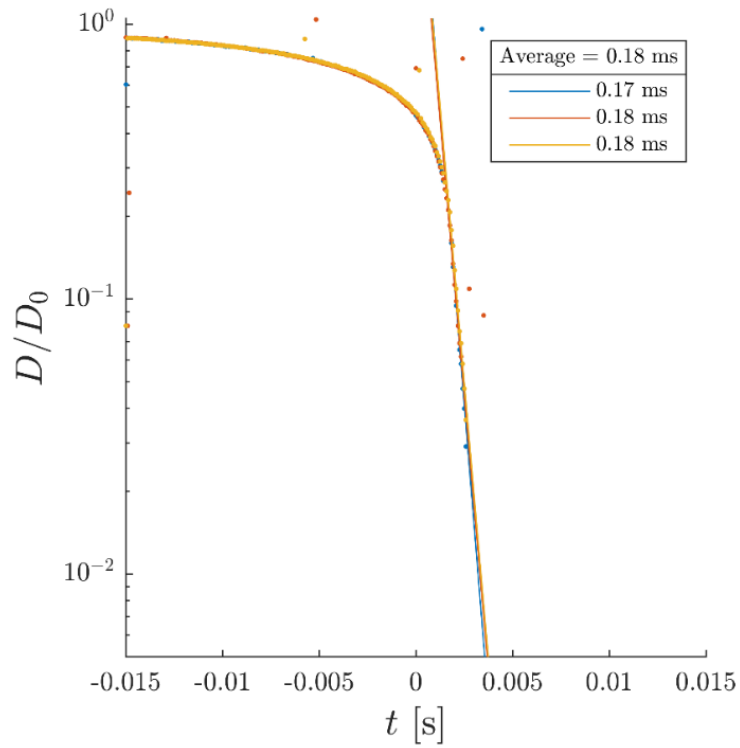


Figure D.3.6e:  $D/D_0$  versus  $t$  plot for 10% DR, Re: 100000.

## Appendix E

# Safe operating procedure for diesel flow loop

Process: diesel flow loop – start up – operation – shut down

Department/faculty: mechanical engineering

Location (room # and building): 3-31, MECE

Supervisor: Sina Ghaemi

Phone #: 780-248-2056

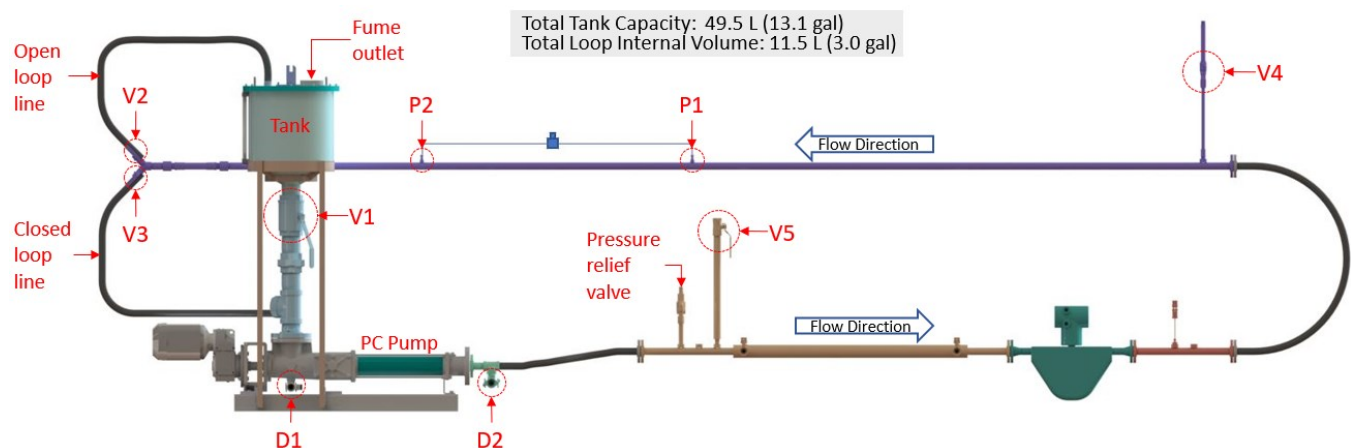
Email: ghaemi@ualberta.ca

Emergency contact: +1 (403) 923-4647 (Satyajit Singh)

After-hours contact: +1 (403) 923-4647 (Satyajit Singh)

### Scope:

This document details the safe operating procedure for the start-up, operation and shut down of the diesel flow loop in MECE 3-31.



### Hazard identification:

1. Diesel may spill while filling up the tank.
2. Diesel may leak from any pipe joint
3. While running the pump if the correct valve configuration is not followed, the system can be over pressurized activating the pressure relief valve, this may damage the pump and/or compromise any joints.
4. A spark can be a fire hazard if any electrical equipment is not grounded.



5. Diesel fumes can cause irritation if not properly ventilated.
6. Running the pump empty can cause internal damage and unsafe working conditions.

### Control/protective measures:

- 1.1. Use the 5-gallon portable diesel can with spill protection to fill the tank.
- 1.2. In case of spill, use the diesel compatible spill kit available and accessible in the lab.
- 2.1. The entire loop teak test was performed with compressed air prior to filling the loop for the first time.
- 2.2. Metal spill trays (2) are present and are in correct position to ensure spill containment.
- 3.1. The below show valve configuration must be followed for each type of operation.

Operation	Filling tank		Filling loop		Open loop run		Closed loop run		Draining loop		Pressurized drain		
Valve Configuration	Valve	Open / Closed	Valve	Open / Closed	Valve	Open / Closed	Valve	Open / Closed	Valve	Open / Closed	Valve	Open / Closed	
	V1	CLOSED	V1	OPEN	V1	OPEN	V1	CLOSED	V1	OPEN	V1	CLOSED	
	V2	CLOSED	V2	OPEN	V2	OPEN	V2	CLOSED	V2	OPEN	V2	CLOSED	
	V3	CLOSED	V3	OPEN	V3	CLOSED	V3	OPEN	V3	OPEN	V3	OPEN	
	V4	CLOSED	V4	OPEN	V4	CLOSED	V4	CLOSED	V4	OPEN	V4	OPEN	
	V5	CLOSED	V5	CLOSED	V5	CLOSED	V5	CLOSED	V5	CLOSED	V5	CLOSED	
	D1	CLOSED	D1	CLOSED	D1	CLOSED	D1	CLOSED	D1	OPEN	D1	OPEN	
	D2	CLOSED	D2	CLOSED	D2	CLOSED	D2	CLOSED	D2	OPEN	D2	OPEN	
	P1	CLOSED	P1	CLOSED	P1	CLOSED	P1	CLOSED	P1	CLOSED	P1	CLOSED	
	P2	CLOSED	P2	CLOSED	P2	CLOSED	P2	CLOSED	P2	CLOSED	P2	CLOSED	
	VFD Status	OFF		OFF		ON		ON		OFF		OFF	

- 3.2. Ensure the pressure relief valve exit pipe is securely placed into the splash proof, diesel compatible container provided.
4. All electrical equipment and metal framing are properly grounded.
5. Proper ventilation with a correct flow rate is ensured at any place where diesel is exposed to the environment.
6. Pump must never run empty. Refer to point 4.1 for VFD status to follow for different operations.

### Tools, materials, equipment, and PPE:

1. Safety glasses.
2. Lab coat (only while filling and draining the loop).
3. Nitrile gloves (only while filling and draining the loop).

### Emergency procedures:

1. In case of small fire (size of a trash bin), Use the fire extinguisher, refer to appendix E.1 for procedure.
2. In case of bigger fire, STOP operations, pull the alarm and evacuate, refer to appendix E.1 for procedure.
3. In case of a small spill or leak, STOP pump immediately and use the diesel spill kit to contain it.
4. In case of larger spills, refer to appendix E.2 for hazardous spill response procedure.
5. In case of over pressurization and activation of pressure relief valve.
  - 5.1 Stop the pump immediately.
  - 5.2 Ensure no spill around the pressure relief valve, if there is spill follow step 3 or 4.
  - 5.3 Verify the loop to check for leaks from any other location.
  - 5.4 Verify that correct valve configuration is followed.
  - 5.5 If leak is observed, drain loop safely and completely, then perform root cause analysis.

## Step by step procedure

### Filling the loop:

1. Ensure all personals are wearing the required PPE.
2. Ensure all valves are closed prior to filling the tank.
3. Use proper height ladder / step stool to manually fill the tank through the fume outlet port.
4. Ensure correct volume by monitoring the sight gauge on the tank.
5. Replace the exhaust duct over the fume outlet once the tank is filled.
6. Ensure the valve configuration for filling the loop as mentioned above in the following order:  
V4→V2→V3→V1.
7. After gravity assisted fill is completed, set open loop valve configuration by closing V3 then closing V4 (V1 and V2 must be open).
8. Turn ON the VFD and start the pump at 8 Hz to let the open loop line get filled with diesel.
9. Now ensuring V1 and V2 are open, open V3 intermittently and close to flush the close loop line.
10. Now the flow can be adjusted by VFD to de-air the system.

### Draining the loop:

1. Ensure VFD is OFF.
2. Attach the two drain-hoses to their respective drain port and place the steel pan under it.
3. Ensuring the hose ends are securely placed in the drain barrel. Then set the valve configuration to drain.
4. Now let the loop drain by gravity. Leave it for 10 minutes.
5. Once gravity drain is complete, set the valve configuration to closed loop.
6. Attach the compressed air hose to the inlet above V4.
7. Ensure the pressure regulator is set at 20 PSI.
8. Now, open V4 for 30 seconds to pressurize the loop at 20 PSI, then close V4
9. With the loop under pressure, open D1 releasing the pressure along with the remaining fluid into the barrel. Once de-pressurized, close D1.
10. Repeat step 8, followed by opening D2, releasing the pressure along with the remaining fluid into the barrel. Once de-pressurized, close D2.
11. Repeat steps 8, 9, and 10 two more times with a 10-minute gap between each attempt to let the fluid settle down.
12. Once drain completes, set to close loop valve configuration and remove the two drain hoses carefully dripping any leftover diesel in the steel pan.
13. Empty the pan in the barrel and secure the hose and pan at their designated location.
14. Move the diesel barrel to the fuel room safely.

Prepared By: Satyajit Singh

Date: 17<sup>th</sup> September 2023

Approved by (supervisor): Dr. Sina Ghaemi

Date:

## WHAT TO DO

# IN CASE OF FIRE

### IF YOU DISCOVER A FIRE

- Extinguish the fire if it is safe to do so.
- If you cannot extinguish it:
  - Close all doors to prevent the spread of fire and smoke.
  - Pull the manual fire alarm near the marked fire exit.
  - Evacuate to the building muster point.
- Call 911 and then 780-492-5050.

### IF YOU HEAR AN ALARM

- Evacuate the building immediately via the closest exits.
- DO NOT USE ELEVATORS.
- Report to the muster point.

### IF YOUR EXIT IS BLOCKED

- Try another exit.
- If both exits are unsafe, stay in an area away from smoke or flame and call 911 and then 780-492-5050.

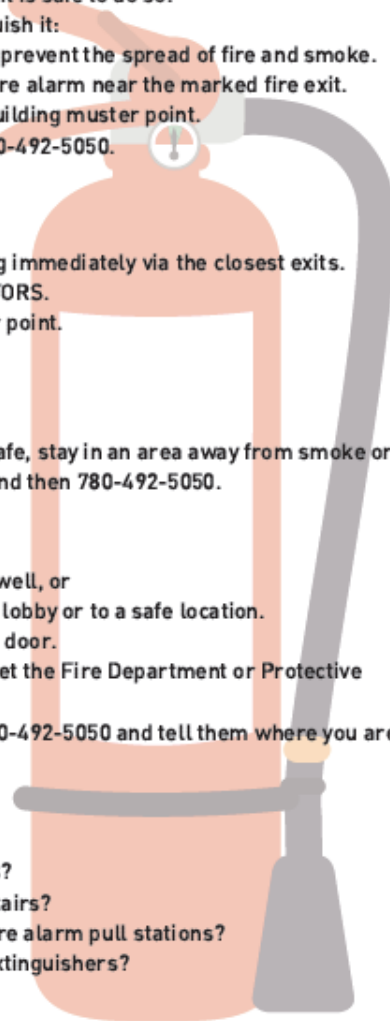
### IF YOU ARE IN A WHEELCHAIR OR OTHERWISE MOBILITY IMPAIRED

- Move to an exit stairwell, or
- Move to the elevator lobby or to a safe location.
- If possible, close the door.
- Send a runner to meet the Fire Department or Protective Services, or
- Call 911 and then 780-492-5050 and tell them where you are.

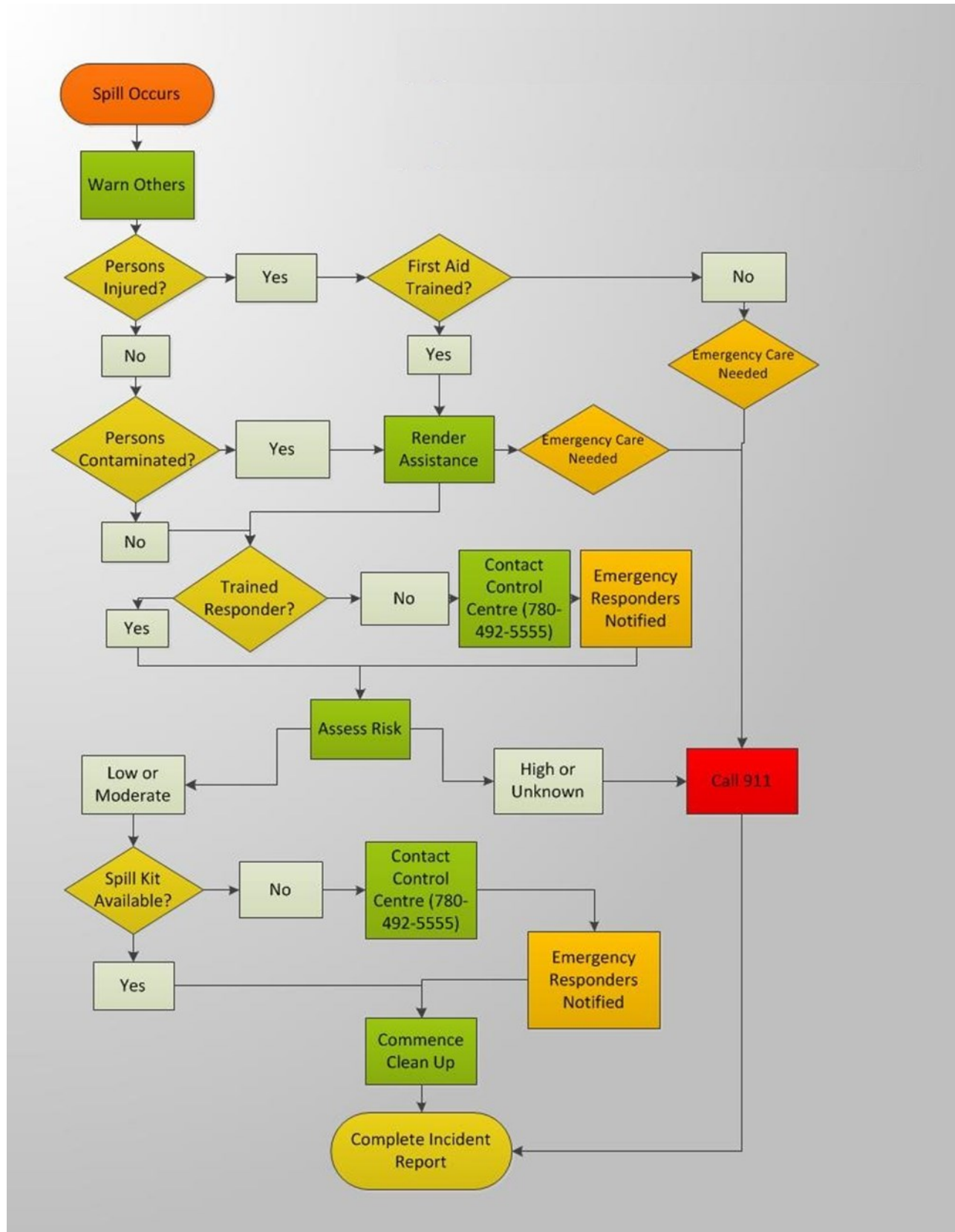
### KNOW YOUR EMERGENCY PLAN AND PRACTICE IT

- Where are your exits?
- Where are the exit stairs?
- Where are manual fire alarm pull stations?
- Where are the fire extinguishers?

***All fires can be deadly! After you get out, stay out!***



## Appendix – E.2



# Appendix F

## NETZSCH PC pump drawing and curve.

This section presents the engineering drawing for the NM038 model pump-motor assembly, and the pump curve as provided by the pump supplier NETZSCH Canada, Inc.

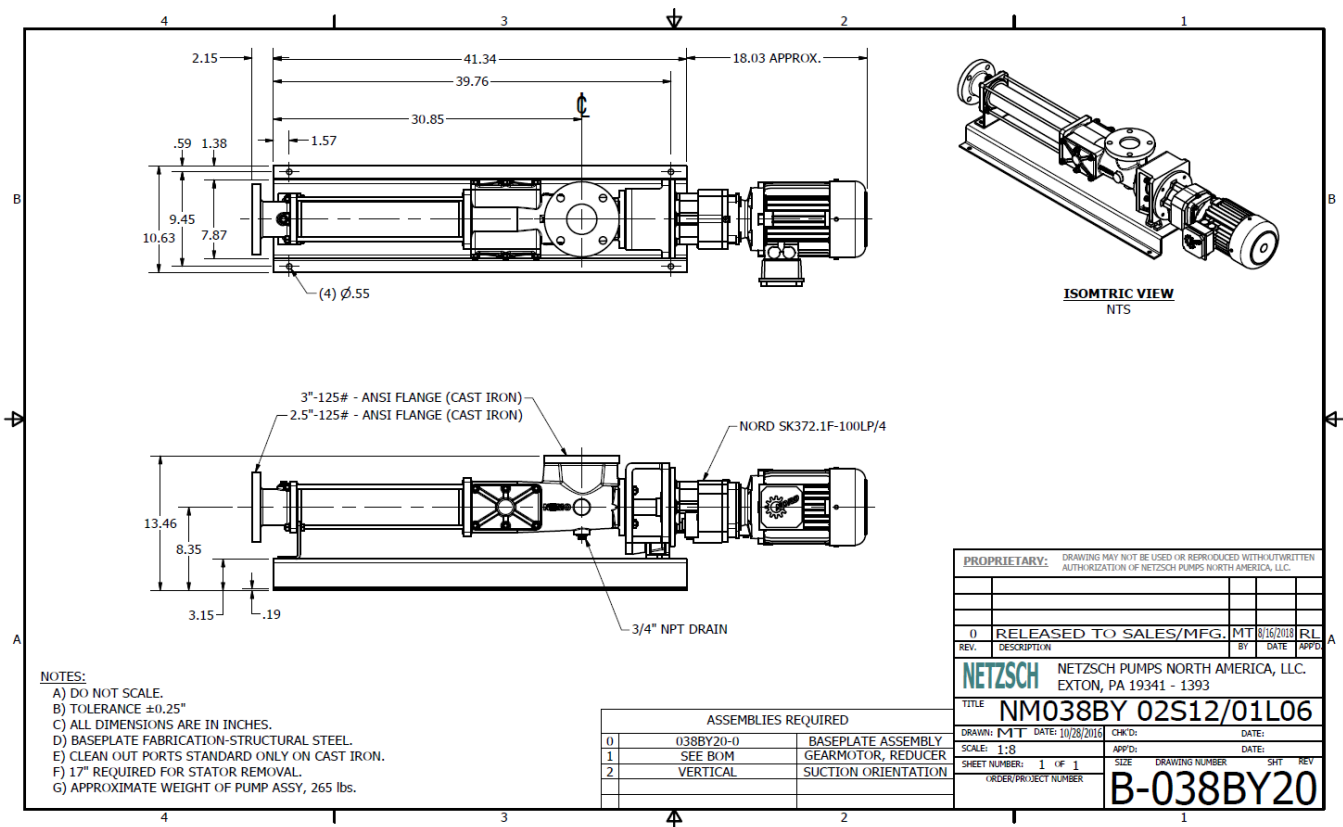
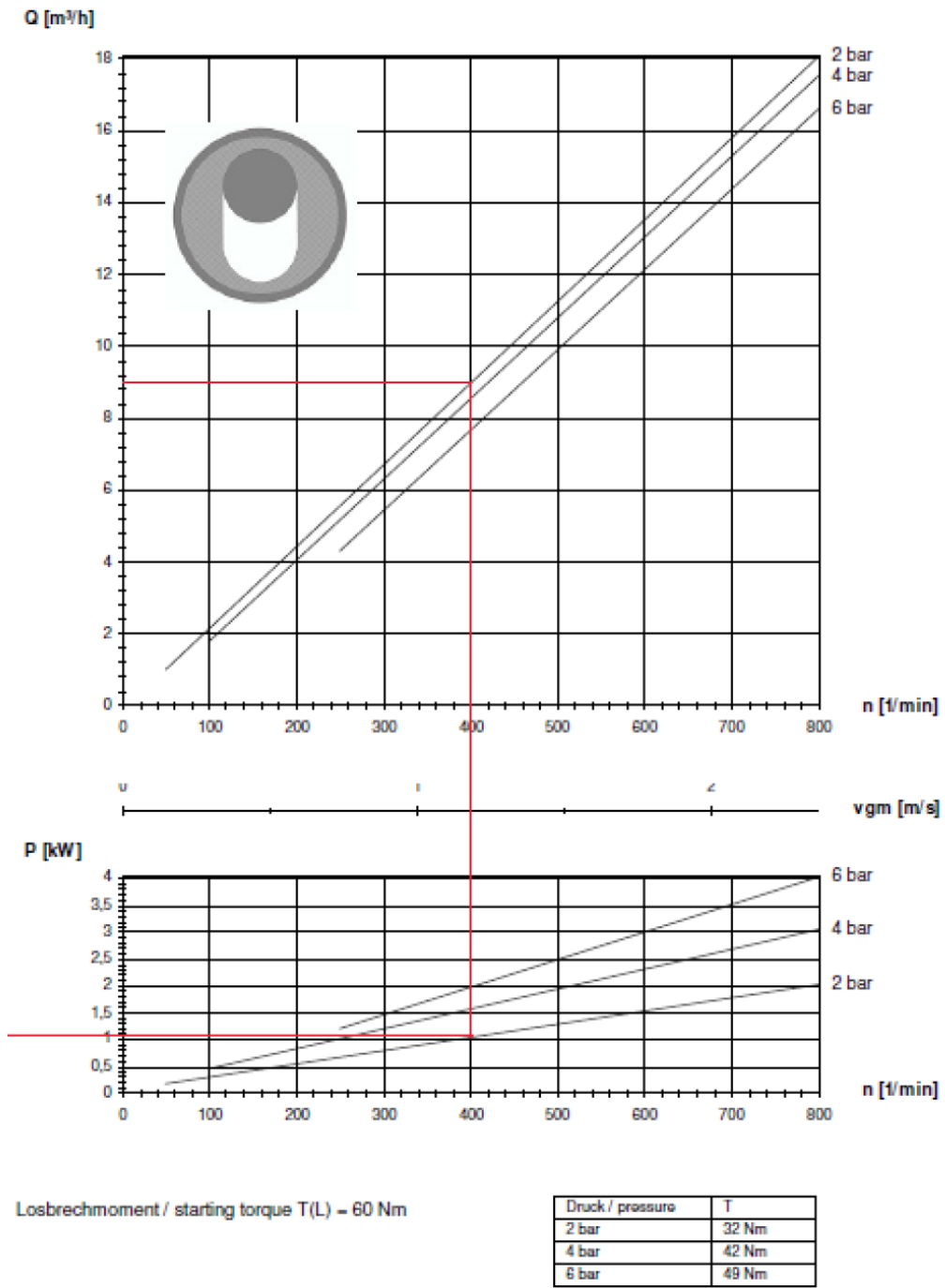


Figure F1: Engineering drawing for NM038 model pump-motor assembly provided by NETZSCH Canada, Inc.



Gültigkeit für Wasser (1 cP) bei 20 °C. Toleranzen nach VDMA 24284 (+10%/-5%).  
 Valid for water (1 cP) at 20 °C (70 °F). Tolerances are in accordance with VDMA 24284 (+10%/-5%).

[www.netzsch-pumpen.de](http://www.netzsch-pumpen.de)

Figure F1: Pump curve for NM038 model pump-motor assembly provided by NETZSCH Canada, Inc.